Investigating the Effects of Fluid Flow and Consequent Porosity and Permeability Changes through an Artificially Fractured Carbonate Geothermal System

Rebecca Daniella Morgan

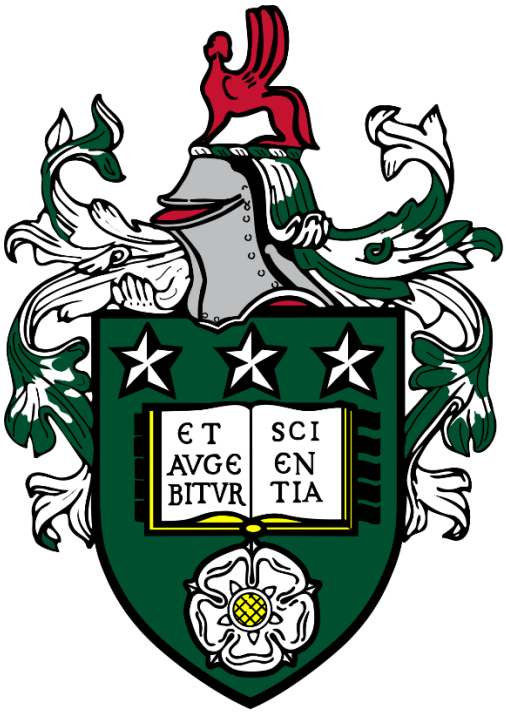

Submitted in accordance with the requirements for the degree of Master's by Research

University of Leeds

School of Earth and Environment

February 2022

Word count: 40,960

Declaration

The candidate confirms that the work submitted is her own and that appropriate credit has been given where reference has been made to the work of others.

Acknowledgements

I would like to thank my supervisor's Professor Sandra Piazolo and Professor Quentin Fisher, who gave me the opportunity to undertake this project and provided me with support and encouragement throughout. Thank you for teaching me so much in such a short space of time and for both inspiring me with your work and attitudes toward research.

The laboratory and experimental work would not have been possible without Samuel Allshorn and Dr. Carlos Grattoni. Thank you for spending a great deal of time teaching me and helping me throughout my entire degree, particularly Sam. Thank you for being patient and enabling me to understand things thoroughly, whilst teaching me how to use laboratory equipment. I am extremely grateful for all of your help throughout the degree. A huge thanks also goes to John Wyn Williams for preparing multiple thin sections and for showing me how to prepare samples myself. A huge thank you to Richard Walshaw who taught me how to carbon coat samples and also how to use the TESCAN microscope to undertake SEM analysis. Thank you for being patient and letting me spend multiple sessions using the microscope.

A massive thank you to Eliot Eaton for supporting me, for all the helpful discussions and for helping me to understand the programming language of Python. Thank you to my family for loving and supporting me throughout my degree, I couldn't have done it without you.

Abstract

In a geothermal system, understanding how the permeability of carbonate host rocks develops overtime is a key parameter in the efficiency of geothermal energy production. This study contributes to pre-existing research into the longevity of fluid flow and how this may change as a result of potential precipitation-dissolution reactions, concentrating on geothermal systems. Here, the results of laboratory experiments to study long-term fluid flow changes through artificially fractured carbonates in a simulated geothermal system, with a focus on potential dissolution-precipitation reactions, are presented. Three main variables were monitored, including: comparing limestone and dolomite samples, studying the effects of temperatures up to 80°C, and comparing the effects of closed-loop and open-loop systems. Overall findings generally showed a decrease in the permeability of the limestone and dolomite samples throughout the experiment. Despite this, the micro-structural, CT scan and water sample results for many limestone and dolomite samples suggested an increase in dissolution throughout the experiment, generally showing a positive correlation with temperature. The cause of the occurrence of both an increase in dissolution, yet decline in permeability is discussed, with evidence of small grains blocking the pore throats of larger grains in the SEM images. The implications of a decrease in permeability in the carbonate host rock, as suggested by the laboratory experiments, would imply a reduction in the long-term efficiency of a geothermal system in a natural setting.

Table of Contents

Figures

4.30.1-4.30.4	68	Backscatter-Electron (BSE) images taken between 300-400μm of the host rock from Dolostone core samples initial, B5, B4 and B3, located in the open-loop experiment
4.31.1a-4.31.2b	70	CT scan image of limestone sample B (ambient) showing an image slide, taken from approximately the centre of the core sample, before and after the closed-loop experiment
4.32.1a-4.32.2b	71	CT scan image of limestone sample A (80°C) showing an image slide, taken from approximately the centre of the core sample, before and after the closed-loop experiment
4.33.1a-4.33.2b	72	CT scan image of limestone sample D (40°C) showing an image slide, taken from approximately the centre of the core sample, before and after the closed-loop experiment
4.34.1a-4.34.2b	73	CT scan image of dolostone sample B6 (ambient) showing an image slide, taken from approximately the centre of the core sample, before and after the closed-loop experiment
4.35.1a-4.35.2b	74	CT scan image of dolostone sample B2 (80°C) showing an image slide, taken from approximately the centre of the core sample, before and after the closed-loop experiment
4.36.1a-4.36.2b	75	CT scan image of dolostone sample B1 (40°C) showing an image slide, taken from approximately the centre of the core sample, before and after the closed-loop experiment
4.37.1a-4.37.2b	76	CT scan image of limestone sample C (ambient) showing an image slide, taken from approximately the centre of the core sample, before and after the open-loop experiment
4.38.1a-4.38.2b	77	CT scan image of limestone sample F (80°C) showing an image slide, taken from approximately the centre of the core sample, before and after the open-loop experiment
4.39.1a-4.39.2b	78	CT scan image of limestone sample E (40°C) showing an image slide, taken from approximately the centre of the core sample, before and after the open-loop experiment
4.40.1a-4.40.2b	79	CT scan image of dolostone sample B5 (ambient) showing an image slide, taken from approximately the centre of the core sample, before and after the open-loop experiment
4.41.1a-4.41.2b	80	CT scan image of dolostone sample B4 (80°C) showing an image slide, taken from approximately the centre of the core sample, before and after the open-loop experiment
4.42.1a-4.42.2b	81	CT scan image of dolostone sample B3 (40°C) showing an image slide, taken from approximately the centre of the core sample, before and after the open-loop experiment
4.43	83	Graph to show the Mg-concentration of the fluid travelling through the Limestone core samples B (ambient), A (80°C) and D (40°C), respectively, throughout the closed-loop experiment (made using Python)
4.44	83	Graph to show the Mg-concentration of the fluid travelling through the Limestone core samples C (ambient), F (80°C) and E (40°C), respectively, throughout the open-loop experiment (made using Python)
4.45	84	Graph to show the Ca-concentration of the fluid travelling through the Limestone core samples B (ambient), A (80°C) and D (40°C), respectively, throughout the closed-loop experiment (made using Python)
4.46	84	Graph to show the Ca-concentration of the fluid travelling through the Limestone core samples C (ambient), F (80°C) and E (40°C), respectively, throughout the open-loop experiment (made using Python)
4.47	85	Graph to show the Mg-concentration of the fluid travelling through the Dolostone core samples B6 (ambient), B2 (80°C) and B1 (40°C), respectively, throughout the closed-loop experiment (made using Python)4.48
4.48	85	Graph to show the Mg-concentration of the fluid travelling through the Dolostone core samples B5 (ambient), B4 (80°C) and B3 (40°C), respectively, throughout the open-loop experiment (made using Python)
4.49	86	Graph to show the Ca-concentration of the fluid travelling through the Dolostone core samples B6 (ambient), B2 (80°C) and B1 (40°C), respectively, throughout the closed-loop experiment (made using Python)
4.50	86	Graph to show the Ca-concentration of the fluid travelling through the Dolostone core samples B5 (ambient), B4 (80°C) and B3 (40°C), respectively, throughout the open-loop experiment (made using Python)
4.51	87	Graph to show the permeability of the limestone core samples B (ambient), A (80°C) and D (40°C), throughout the closed-loop experiment
4.52	88	Graph to show the permeability of the limestone core samples C (ambient), F (80°C) and E (40°C), throughout the open-loop experiment (made using Python)
4.53	88	Graph to show the permeability of the dolostone core samples B6 (ambient), B2 (80°C) and B1 (40°C), throughout the closed-loop experiment
4.54	89	Graph to show the permeability of the dolostone core samples B5 (ambient), B4 (80°C) and B3 (40°C), throughout the open-loop experiment (made using Python)
4.55	90	Graph to show the pressure changes for the Limestone (line 1), in pressure gauges 1A – 1F, throughout the duration of the closed-loop experiment
4.56	91	Graph to show the pressure changes for the Limestone (line 1), in pressure gauge 1F (the downstream of core holder three within the 40°C oven), throughout the duration of the closed-loop experiment (made using Python)
4.57	91	Residue left on the filter paper from the upstream (1A) of the first core holder in limestone (line one)
4.58	92	Graph to show the pressure changes for the Dolostone (line 2), in pressure gauges 2A – 2F, throughout the duration of the closed-loop experiment
4.59	92	Graph to show the pressure changes for the Dolostone (line 2), in pressure gauge 2F (the downstream of core holder three within the 40°C oven), throughout the duration of the closed-loop experiment (made using Python)
4.60	93	Graph to show the pressure changes for the Limestone (line 1), in pressure gauges 1A – 1F, throughout the duration of the open-loop experiment (made using Python)
4.61	93	Graph to show the pressure changes for the Dolostone (line 2), in pressure gauges 2A – 2F, throughout the duration of the open-loop experiment (made using Python)
5.1.1	102	Graph to show the Aztec grain analysis undertaken on dolostone sample B2. The composition appears to consist of calcium carbonate, suggesting a limestone composition
5.1.2	115	Chemical composition of the mineral evident in a grain, inside the fracture, in dolostone sample B5, located in the ambient core holder in the open-loop experiment
5.1.3	115	Chemical composition of the mineral evident outside the fracture in dolostone sample B5, located in the ambient core holder in the open-loop experiment

Tables

Equations

1. Introduction

This dissertation aims to further understand fluid pathway processes in carbonate geothermal energy systems. Experiments have been undertaken to compare how limestones and dolostone samples, subject to varying temperatures between approximately 25°C and 80°C, react to percolating water in a closed-loop and open-loop system. The experiments will focus on dissolution precipitation reaction changes and how they may affect the porosity and permeability of the samples. Three major comparisons will be made: (1) between the limestone and dolostone samples, (2) between three core holders subject to different temperatures of 25°C, 40°C and 80°C and finally, (3) between the closed-loop and open-loop systems. SEM images, CT scans, water sampling (monitoring magnesium and calcium levels in the percolating water), permeability measurements and pressure monitoring of the system has been used to analyse the results. Overall, the aim of this dissertation is to identify porosity and permeability changes within the limestone and dolostone samples to further understand the potential changes occurring within a carbonate geothermal system at shallow depths. It will also aim to outline the self-designed experimental method used and highlight what may be improved for future references.

2. Literature Review

2.1 Geothermal Energy

2.1.1 Importance of Geothermal Energy

The effects of global warming on the planet are prevalent and devastating (UNEP, 2018). The UNEP Emissions Gap Report 2018 states that 'if the emissions gap is not closed by 2030, it is extremely unlikely that the 2°C temperature goal can still be achieved'. As we move towards a NetZERO future, it is more important than ever to push forward decarbonisation energy methods (UNEP, 2018; Rybach, 2003). The rapid growth in demand for oil and gas energy production in the 20th and 21st centuries have resulted in environmental decline and a major contribution to a warming planet (Mikhaylov, 2020). In many locations, geothermal energy provides the potential to meet energy demands, whilst producing lower greenhouse gas emissions than pre-existing methods (Rybach, 2003). The current known environmental impacts from geothermal energy appear controllable, if not negligible (Rybach, 2003). The potential of geothermal energy appears promising; being a predictable, reliable and sustainable energy source for future generations (Rybach, 2003).

2.1.2 What is Geothermal Energy?

Geothermal energy is remnant heat from the formation of the planet (4.5 billion years ago) and movement of heat transfer from a molten metal core, alongside radioactive decay of naturally occurring isotopes (Glassley, 2014; Johnston et al. 2011). Modern technologies are now able to capture such naturally occurring heat and use it to generate sustainable geothermal energy production (Rybach, 2003 and 2007; Barbier, 2002; Mburu, 2009; Glassley, 2014; Boden, 2016 and 2017). Geothermal energy provides a renewable energy with manageable resource depletion and little to negligible environmental impacts, depending on the type of geothermal energy plant (Glassley, 2014; Rybach, 2003). Geothermal systems are characterised by temperature-depth relationships (T-D profile), whereby typically the temperature increases with geothermal gradient (Ziagos et al. 1986).

Naturally fractured geothermal reservoirs are recognised as the ideal scenario for potential geothermal energy production (Van Oversteeg et al. 2014). However, many systems with geothermal energy potential lack sufficient fracture pathways and interconnectivity of pathways to contribute to a viable geothermal system (Huenges, 2016). Induced fractures have been enabled by recent technology and impermeable systems can potentially be accessed via chemical, hydraulic or thermal simulation, resulting in what's known as an enhanced geothermal system (Huenges, 2016). Issues

involved in this process include the closing of fractures, after being opened, due to high pressures at depth or from fluid chemical reactions (Huenges, 2016).

Understanding the stress and temperatures at the depth the geothermal reservoir is located and their effects is crucial to determine the long-term sustainability of the geothermal system (Michie et al. 2021). Deformation mechanisms at this depth result in structural features in the carbonates, which consequently affects the porosity and permeability, and thus the potential of geothermal energy (Michie et al. 2021; Goldscheider et al. 2010).

2.1.3 Geothermal Resources

Fridleifsson et al. (2008) divide exploitable geothermal systems into two groups: (1) high-temperature fields (> 180°C) and (2) low-temperature fields (< 180°C). High-temperature fields are classified by volcanic or magmatic activity and are restricted to certain geological locations (Fridleifsson et al. 2008). Low-temperature fields can be separated into four types, including resources related to; (1) deep circulation of meteoric water along pathways, (2) deep high permeability rocks (at hydrostatic pressure), (3) geo-pressured resources in high-porosity rocks (pressures exceeding hydrostatic pressure) and (d) hot dry low-porosity rocks (Fridleifsson et al. 2008). Please note, most systems portray intermediate characteristics and the aforementioned 'four types' are end members (Fridleifsson et al. 2008). The experiments undertaken throughout this thesis relate to low-temperature fields (< 180°C), most likely the deep circulation of meteoric water along pathways.

2.1.4 Geothermal Utilisation

There are three main ways geothermal energy can be used, including (1) to generate power, (2) as a direct use and (3) geothermal heat pumps (geo-exchange) (Boden, 2017). The first relates to producing electricity and requires the highest temperatures, usually >100°C (Boden, 2017). High temperatures mean the access to this energy is restricted to specific geologically favourable areas, such as along plate boundaries and volcanic areas (Boden, 2017). There are currently three main methods for electricity generation, including: (1) dry steam, (2) flash steam, and (3) binary cycle (Fridleifsson et al. 2008; Barbier, 2002). Dry steam is the use of hot steam from the ground to directly turn the turbine (Barbier, 2002; Fridleifsson et al. 2002). Flash steam methods consist of rising hot, high-pressured water leading to a pressure drop which produces steam to directly turn the turbine (Barbier, 2002). Finally, binary cycle plants use deep, hot fluids to bypass and therefore heat a secondary fluid (often

with a lower boiling point) which then becomes vapour to turn the turbine (Barbier, 2002; Fridleifsson et al. 2008). Binary cycle plants require geothermal fluids at lower temperatures (74 – 170 °C), making them a popular option (Fridleifsson et al. 2008). Binary cycle plants are found to produce essentially no emissions, making them a popular environmental option, as the only emission is steam (National Geographic, 2021). In electricity production, whether it be dry steam, flash steam or binary cycle, the geothermal fluids require high porosity and permeability in the rock to enable fluid movement to become naturally heated and consequently captured (Fridleifsson et al. 2008). Direct use relates to the heating and cooling of buildings, thermal baths, desalination and agricultural applications and temperatures needed for this are typically 50-100°C (Boden, 2017; Mburu, 2009; Fridleifsson et al. 2008). The final is geothermal heat pumps, also a form of direct use, whereby heat is deposited in the ground in the summer months and removed in winter months, therefore, reducing heat waste in the summer (Boden, 2017). Geo-exchange is extremely efficient and not geologically restricted (Boden, 2017).

Naturally fractured geothermal reservoirs are recognised as the ideal scenario for potential geothermal energy production (Van Oversteeg et al. 2014). However, many systems with geothermal energy potential lack sufficient fracture pathways and interconnectivity of pathways to contribute to a viable geothermal system (Huenges, 2016). Induced fractures have been enabled by recent technology and impermeable systems can potentially be accessed via chemical, hydraulic or thermal simulation, resulting in what's known as an enhanced geothermal system (Huenges, 2016). Issues involved in this process include the closing of fractures, after being opened, due to high pressures at depth or from fluid chemical reactions (Huenges, 2016). The experiment undertaken in this thesis consists of the artificial fracturing of samples. However, the artificial fractures were created by cutting the core sample in half, whereas this is not viable at depth, therefore in a geothermal system at depth, induced fractures are often created from chemical, hydraulic or thermal simulation (Huenges, 2016).

Any geothermal system that produces less fluid than the natural discharge can be considered fully renewable, despite such rates being limited and often not economically viable (Rybach, 2003; Stefansson, 2000). Overproduction may result in the depletion of resources, leading to geothermal systems becoming unsustainable (Rybach, 2003). Reservoir depletion may be tackled with managed production rates that consider resource characteristics such as reservoir size and recharge rates (Rybach, 2007). Many schemes have also begun re-injecting reservoirs to restore the fluid and maintain pressure (Rybach, 2003). A problem encountered from re-injection may be cooling of large

areas of the reservoir (Rybach, 2003). Higher injection rates may be required due to higher temperatures of the injected water, ascribed to lower viscosity (Su et al. 2018; Zhou et al. 2007; Wang, 2014).

When a production well captures geothermal fluid, isotherms are diverted to form a heat sink and heat flow is captured (Figure 2.1) (Rybach, 2003 and 2007). Once production ceases, an influx of heat and fluid naturally restore pressure and temperature gradients (Rybach, 2003 and 2007).

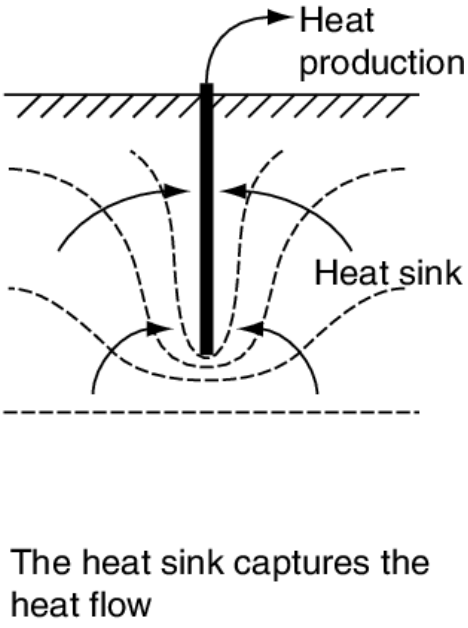

Figure 2.1: Schematic diagram showing geothermal extraction forming a heat sink to capture heat flow (taken from Rybach, 2007).

2.1.5 Potential of Geothermal Energy

A particularly positive example of how geothermal energy can be economically viable, whilst supporting mass populations is in Iceland (Mikhaylov, 2020). By 2016, Iceland has gone 100% renewable with around 25% from geothermal energy (Mikhaylov, 2020). In the 1960's the Icelandic government established anti-change climate fund policies to develop the knowledge of geothermal energy (Mikhaylov, 2020; Amini and Reinhart, 2011; Bansal et al, 2013).

2.2 Dissolution, Porosity and Permeability

In most geothermal systems, high porosity and permeability is required to enable fluid flow, unless fractures are purposefully induced (Huenges, 2016). It is widely known that geothermal fluids, interacting with the carbonate host rock to create dissolution-precipitation reactions, may lead to porosity and/or permeability changes in a geothermal reservoir (Ledésert et al. 2010; André et al. 2010). Min et al. (2016) states that the dissolution of carbonates may lead to either increases in the matrix type pores, enhancing the porosity of the host rock, or fracture type pores, enhancing the permeability. Bai et al. (2019) states that calcium carbonate precipitation is more likely to occur at lower pressures, for example at a wellbore within a system.

André et al. (2010) researched the enhanced geothermal system in Soultz-sous-Forêts, France, looking at the circulation of fractured fluids through a deep granitic reservoir with a sedimentary cover. The research studied fluid-host rock chemical reactions and whether this affected porosity and/or permeability (André et al. 2010). The study used FRACHEM, the developed thermo-hydraulic-chemical coupled computer code to predict changes in this specific geothermal system (André et al. 2010). The results identify dissolution increases porosity close to the well, where the reaction is largely dominated by carbonates due to being highly reactive (André et al. 2010). The average initial porosity of the fractured area was 10% (André et al. 2010). Once fluid circulation began this increased to 13.5-14% in the first 10 metres after 1,000 days due to dissolution of carbonate grains (André et al. 2010). From 1,000 to 1,800 days the porosity then slightly decreases from 13.5-14% to 12.5-13% due to precipitation (André et al. 2010). The study identifies a modelled relationship between porosity and permeability; therefore, they observe the same trend for permeability (André et al. 2010). André et al's (2010) study can be compared to the experiments presented in this thesis, due to observing fluid-rock interactions affecting porosity and permeability of a geothermal system. Porosity appears to increase with more dissolution, proving these reactions are affecting the porosity. This is significant to the longevity of an enhanced geothermal reservoir.

Ling et al (2014), suggests that strong dissolution leads to high porosity and pores with large diameters. This makes the rock become lower in tensile strength and the grains become prone to breaking under tectonic stress.

2.2.1 Dissolution of Carbonate Rocks

Carbonate systems typically have low porosity and portray complex pore structures (Garing et al. 2015; Siena et al. 2014). Experiments portray that the carbonate dissolution leading to porosity increase shows a positive correlation with permeability increase (Garing et al. 2015). Particularly, if the fluid is highly reactive it may lead to even more carbonate dissolution (Garing et al. 2015). In carbonates, generally, permeability increases from (1) an increase in pore-conduit hydraulic radius, (2) a decrease in tortuosity (measure of deviation from a straight line), and (3) pore network connectivity increase (Garing et al. 2015). The relationship between porosity and permeability will vary due to hydrodynamic/chemical conditions and initial heterogeneity of pore spaces (Garing et al. 2015).

Geothermal systems comprising of hydrothermal fluids provide for highly reactive environments, thus leading to potential precipitation and/or dissolution reactions between the fluid-rock interface (Garing et al. 2015; Appelo and Postma 1993; Moore 2001; Noiriel et al. 2009; Luquot and Gouze 2009). These consequent reactions may affect the longevity of a geothermal system by altering the porosity and permeability of the carbonate host rocks (Garing et al. 2015). Dissolution of carbonate rocks typically result in an increase in both porosity and permeability (Garing et al. 2015). Garing et al. 2015 used both experiments and models to understand dissolution controls on carbonates (Garing et al. 2015). The fluid comprised of deionized water, which in relation to calcite is undersaturated, and a positive correlation was discovered when CO_2 was added to the fluid to increase the dissolution of calcite (Garing et al. 2015). The dissolution is dependent on multiple factors such as (1) how undersaturated is the fluid, (2) composition of fluid and host rock, (3) grain shape and size affecting the tortuosity (Garing et al. 2015). For example, if the fluid is undersaturated, the surrounding rock will dissolve and may potentially lead to increased porosity and/or permeability (Garing et al. 2015). In some instances, grains or particles may detach and migrate in the flow without complete dissolution, then deposit in pore throats or block passageways, thus decreasing the overall permeability depending on the relationship with the porosity (Garing et al. 2015). Mangane et al. (2013) inferred such grain or particle detachment, migration and accumulation processes using X-ray microtomography (XRMT) (Mangane et al. 2013). The study showed overall permeability decrease and porosity increase due to the blocking of flow pathways within pore spaces and macroporosity areas, increasing tortuosity, and decreasing sample-scale effective hydraulic radius (Garing et al. 2015). Within a geothermal system, an overall decrease in flow permeability may affect the long-term sustainability of a geothermal energy plant.

Facets can be identified in micro-structural work and related to the dissolution of the rock (Snyder and Doherty, 2007). Facets appear as right-angled grain edges, suggesting the mineral has been affected by dissolution (Snyder and Doherty, 2007). Dissolution can often be revealed by increasing facets in micro-structural work (Snyder and Doherty, 2007).

2.2.2 Solubility of Calcium Carbonate

There have been many studies on the dissolution of carbonates, particularly calcite (Morse, 2018). The solubility of calcite is shown to be a function of many variables including temperature, hydrogen ion activity, pH of the fluid, salinity, particle size and other factors (Wood, 1986; Goldscheider et al 2010; Shih et al. 2000; Singurindy et al. 2004).

Shih et al. 2000 identifies how calcite dissolution rates are a strong effect of particle size. Kirstein et al. (2016) undertook dissolution experiments on a micritic carbonate sample, a sparitic limestone sample and a dolostone sample, to understand the temperature dependency between 5 to 25°C. The sparitic limestone appeared to comprise of larger grains with a fine matrix. It was observed that the fine grains were firstly dissolved, leaving behind the larger calcite grains, resulting in secondary porosity from gaps and channels between the larger grains, thus increasing permeability and connectivity of the sample.

Extensive previous research has been undertaken on the solubility of calcite, showing the solubility of calcite decreases with increasing temperature (Goldscheider et al. 2010; Morse et al. 2007; Plummer and Wigley (1976); Plummer et al. (1978); Kirstein et al. 2016). Goldscheider et al. (2010) identifies 'retrograde solubility' and highlights that in a closed-loop system, the solubility of calcite increases with decreasing temperature (Figure 2.2). The paper also identifies that in an open system, the escape of CO_2 by pressure release can result in calcite precipitation (Goldscheider et al. 2010). One issue with many of the research is that it is based on pure calcite and does not account for the host rock of either limestone or dolostone and potential impurities.

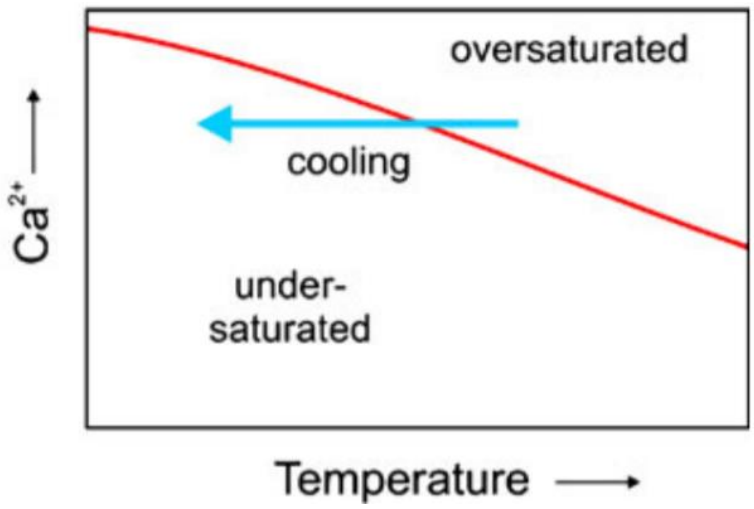

Figure 2.2: A graph to show the retrograde solubility of calcite in a closed system, according to Goldscheider et al. 2010. The calcite solubility increases with decreasing temperature (Figure taken from Goldscheider et al. 2010).

However, Wood (1986) shows a speciation diagram for calcite-water between the temperature range 0-200°C, which identifies calcite solubility to initially increase with increasing temperature (prograde), until approximately 125°C, after which the solubility begins to decrease with increasing temperature (retrograde) (figure 2.3) (Wood, 1986). The calculations made by Wood (1986) suggest that the solubility of calcite might not always be retrograde, yet, prograde at lower temperatures in closed systems and under conditions of intrinsic PCO_2.

Wood (1986) calculates the solubility of calcite in an open system, whereby the entire system shows retrograde calcite solubility versus temperature. However, the experiment is undertaken with relatively high imposed CO_2 values on the system (Wood, 1986).

Comparing the work from Wood (1986), Goldscheider et al. (2010), Plummer and Wigley (1976), Plummer et al. (1978), Kirstein et al. (2016) and many more, the take-away is that generally for pure calcite: (1) increasing water temperature decreases the amount of equilibrium dissolved CO_2 and leads to calcite precipitation (2) decreasing water temperature increases the amount of CO_2 dissolved and leads to calcite dissolution (3) increasing the pressure of CO_2 gas in a system causes calcite to dissolve (4) decreasing the pressure of CO_2 gas in a system causes calcite to precipitate. However, Wood (1986) suggests that in a closed system at lower temperatures calcite dissolution increases until 125°C, following this calcite dissolution decreases with increasing temperature.

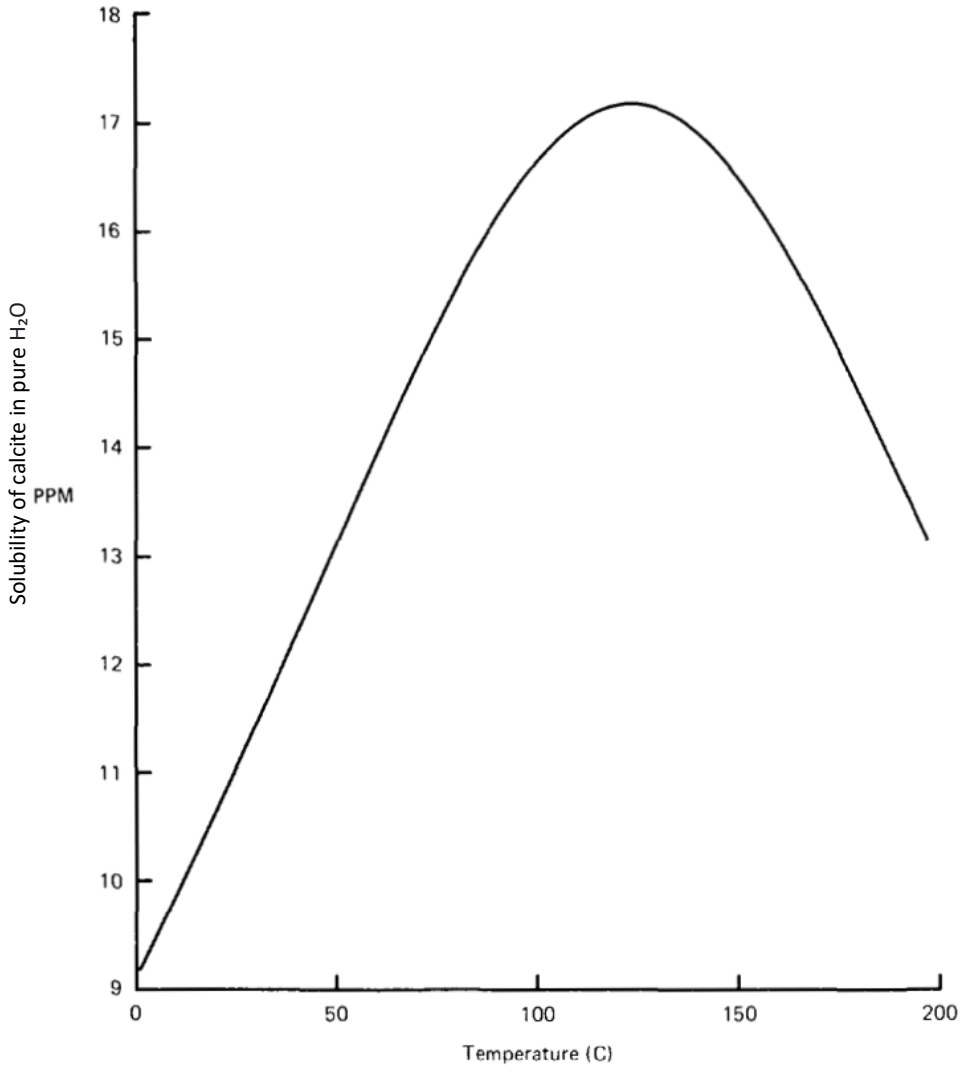

Figure 2.3: Diagram shows solubility of Calcite in pure H_2O in a closed system, between temperature range 0-200°C, showing solubility curve to prograde until 125°C, when the curve begins to retrograde. Partial pressure of CO_2 variable is dependent on equilibria in the system (Wood, 1986).

2.2.3 Geothermal Potential of Limestone

Due to limestones typically comprising of efficient porosity and permeability, they often show good geothermal potential (Garing et al. 2015). Geothermal fluids can typically percolate through limestone to become heated, essential for geothermal energy (Garing et al. 2015). Limestone often consists of karsts, fractures and vugs from dissolution at the Earth's surface which typically result in a high permeability (Romanov et al. 2003)

2.2.4 Dolostone Dissolution Kinetics

The composition of limestone is primarily composed of calcium carbonate, with a chemical formula of $CaCO_3$, however, the composition of dolostone is primarily composed of the mineral dolomite, with a chemical formula of $MgCO_3$ - $CaCO_3$ due to dolostone comprising of a magnesium component. (Warren, 2000).

Zhang et al. (2007) studied the dissolution kinetic of dolomite over a temperature range from 25 – 250°C in water. Three particle size samples of 18-35 mesh, 35-60 mesh and 60-80 mesh were studied; the dissolution rates were shown to be dependent on the difference in grain-sizes (Zhang et al. 2007). For the smaller sample of 20-40 mesh, the release of both Ca and Mg ions to solution rate showed to increase with the increase in temperature until 200°C and then decrease with an increase in temperature (Zhang et al. 2007). For the samples 40-60 mesh and 60-80 mesh the maximum dissolution rate occurs at 100°C in the sample (Zhang et al. 2007). The data shows that for low temperature (25-100°C) dissolution of dolomite in water there appears to be an increase in dissolution with increased temperatures at lower temperatures up to 200°C. With an increase in grain size, dissolution continues to increase with increasing temperature but to a lower temperature of 100°C. This is similar to Wood (1986)'s argument that at lower temperatures calcite dissolution increases with temperature until approximately 125°C. Zhang et al. (2007) argues that the dolomite grain size determines the temperature at which the dissolution of dolomite switches from increasing with increasing temperature, to decreasing with increasing temperature.

Morse et al. 2007 however disagrees from Zhang et al. (2007) and reinforces the previous research by Goldscheider et al. 2010, Morse et al. 2007, Plummer and Wigley (1976), Plummer et al. (1978) and Kirstein et al. 2016 which state that the solubility of calcite decreases with increasing temperature. When studying magnesium calcite (dolomite), the temperature also determines the dissolution rate of dolomite. The temperature effects on magnesium calcite precipitation were explored in Mucci (2007) and when the precipitation of magnesium calcite was plotted against temperature, there appeared to be a positive correlation. However, it should be noted that the aforementioned experiment was undertaken using seawater, with a different salinity to the tap water used in the experiment.

Morse (2018) highlights that dolomite, compared to calcite, has been found to be relatively unreactive. From experiments and analysis, dolomite shows a lower dissolution rate (by approximately a factor of 3 to 60) than limestone (Liu et al. 2005).

Kirstein et al. (2016) show that the increase in temperature mainly shows a decrease in limestone and dolomite solubility. The research showed that due to having large fracture spacing and slower dissolution kinetics, the dissolution of dolomite was much slower than the limestone dissolution (Kirstein et al. 2016). Min et al. (2016) studied limestone and dolomite dissolution rates, with the effect of temperature and pressure, within an open-continuous flow system. The results showed that under conditions between 30°C and 5 MPa to 187°C and 60 MPa, with the increase in temperature and pressure, the dissolution of limestone and dolomite both decrease (Min et al. 2016). Dolomite dissolution appeared to decrease continuously and steadily with a dissolution rate of approximately 20% by the end of the experiment (Min et al. 2016). Firstly, limestone dissolution appeared to decrease slowly, then quickly, then slowly again until becoming steadier, with a dissolution rate of approximately 50% by the end of the experiment (Min et al. 2016). This portrays that the dissolution of limestone was still higher than that of dolomite under the same conditions. However, alongside studying the effects of increasing temperatures, the study focuses on the effects of increasing pressures, which is not relevant for the experiments undertaken in this dissertation.

2.2.5 Geothermal Potential of Dolostone

Dolostones appear to be a good geothermal reservoir, due to comprising of up to 50% of carbonate geothermal reservoirs globally (Warren, 2000). This may be due to their high porosity and permeability, and likely comprising of fractures (Warren, 2000).

Dolostone appears a good host rock; in North America 80% of oil and gas reservoirs are found to be in dolostones and globally dolostones are found in up to 50% of carbonate reservoirs (Warren, 2000). Typically, oil and gas reservoirs require similar features to a geothermal reservoir including high porosity and permeabilities, often from geological structures such as faults (Warren, 2000). Warren, 2000 states that excellent hydrocarbon reservoirs are found in dolostones with well-developed intercrystalline porosity, typically associated with evaporites (Warren, 2000).

Dolostone can form in a variety of ways including: from primary precipitation, diagenetic replacement and finally as a hydrothermal and/or metamorphic phase (Warren, 2000). For dolostone to form there must be (1) permeability and (2) a required supply of Mg (Warren, 2000). Dolomite is a metastable mineral, meaning later formed, more stable, crystals may repeatedly replace early formed crystals during burial and metamorphism (Warren, 2000). This occurs due to the partial/complete dissolution of crystals (Warren, 2000). This cycle of dissolution and re-precipitation can hold or produce porosity and permeability to further depths, and therefore higher temperatures, than that of limestone (Warren, 2000). The re-occurring dissolution-reprecipitation favours retention of intergranular porosities, therefore dolostones often result in a suitable reservoir for hydrocarbons and fluids (Warren, 2000). However, dolostone evolves with space and time due to changing conditions due to burial, pressure, temperature and changes in fluid chemistry, which consequently re-sets the rocks chemical and porosity (Warren, 2000). Therefore, dolostones may show changes in chemistry or porosity multiple times during the overall burial history (Warren, 2000).

Saller et al. (2011) studied how likely the partial dolomitization of a Pennsylvanian limestone in the Reinecke field in west Texas effected reservoir quality and performance (Saller et al. 2011). The Reinecke reservoir shows approximately 25% dolomite of which is shown to form diagenetically late (Saller et al., 2011). The study found that the dolostones had a lower porosity but higher permeability than surrounding limestone, thus providing pathways for hot fluid (Figure 2.4) (Saller et al. 2011). The reason for high permeability in this study is due to fractures, vugs and larger intercrystalline pores which resulted from coarse crystalline dolomite (Saller et al, 2011). The overall porosity of the researched Reinecke dolomite reduced by roughly 3% due to the dolomitization of limestone, with a five times horizontal and thirty times vertical increase of the permeability (Saller et al. 2011). Major finds from this paper concluded that hydrothermal dolomitization has largely affected the dominantly limestone reservoir.

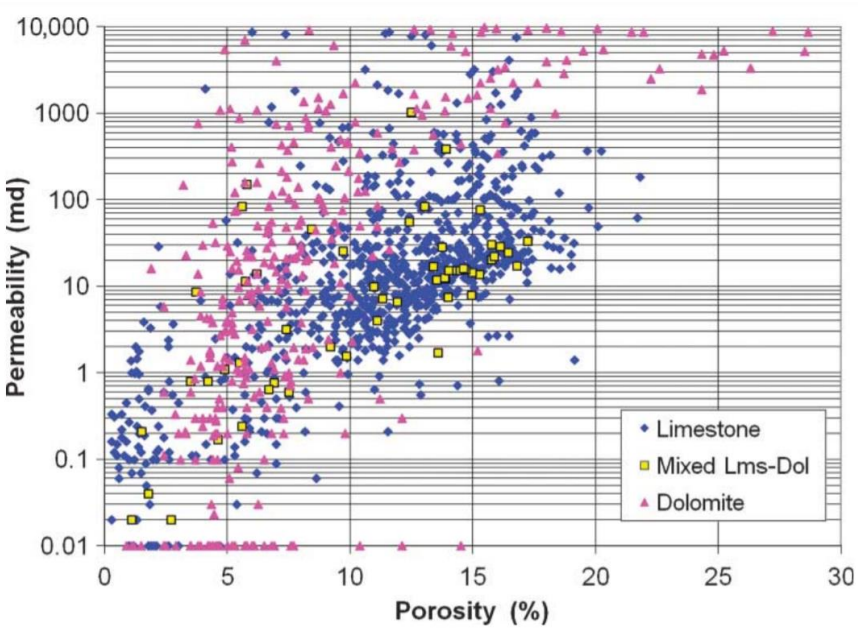

Figure 2.4: Plot of the porosity vs horizontal permeability between Reinecke limestones and dolostones in the south dome (taken from Saller et al. 2011). The dolostones show lower porosity and higher permeabilities.

2.2.6 Saturation levels

Experimental studies have shown that calcite dissolution rates drop to low levels when calcite saturation in the meteoric water exceed 75% (Figure 2.5) (Goldscheider et al. 2010; Plummer and Wigley, 1976; Plummer et al. 1978).

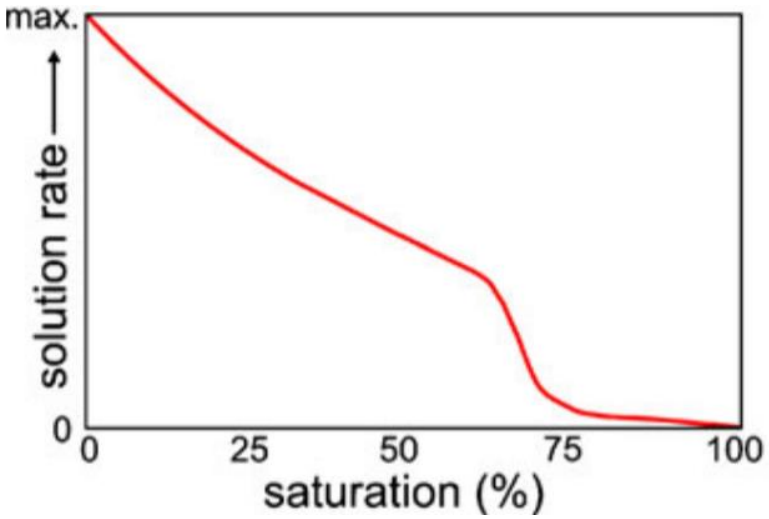

Figure 2.5: A graph to show the dissolution kinetics of calcite. When calcite saturation exceeds 75% the dissolution rates drop to low levels (Figure taken from Goldscheider et al. 2010).

2.3 Fractures, Porosity and Permeability

Fractures provide a pathway for fluids to store and migrate in reservoirs, making them favourable in geothermal energy systems (Zambrano et al. 2019). Understanding their behaviour is therefore essential to identify whether a geothermal system is viable (Zambrano et al. 2019). Modelling and laboratory-experiments provide excellent insight into fracture and geothermal fluid interaction in a natural setting (Zambrano et al. 2019).

Fractures are important in determining fluid flow, as they can act as conduits, barriers or neither (Michie et al. 2021; Cooke et al. 2018; Smeraglia et al. 2021). An excellent understanding of fault zone behaviour and the porosity and permeability properties is essential in determining the behaviour of low-temperature hydrothermal fluids in deep geothermal systems (Smeraglia et al. 2021). Carbonates are often low-porosity rocks and therefore fault zones, particularly the well-connected faults generally found within the damage zones, may support hydrothermal fluid flow (Smeraglia et al. 2021).

The presence of natural or induced fractures, may allow for a non-porous host rock, with geothermal potential, to become a viable energy system (Goldscheider et al. 2010). The presence of fractures and conduits increases the porosity and permeability of the host rock and, therefore, the efficiency of a geothermal system (Goldscheider et al. 2010). On a larger scale, faults often act as a pathway for fluids, portraying different zones of deformation in the surrounding rock, due to stress accommodation from the faulting (Figure 2.6) (Michie, 2021). It should be noted that fault architecture is often not homogenous, therefore the fault zone may vary from localized conduits and baffles, to dual conduits-barriers or distributed conduits (Michie, 2021 & Caine et al, 1996). Extensive studies have been undertaken on fluid flow in siliclastic fault rocks and until recently, there has been little research on carbonates (Michie, 2021). The permeability of faults is determined by multiple factors, for example, lithology of the host rock, stress, time and petrophysical and mechanical properties (Michie, 2021).

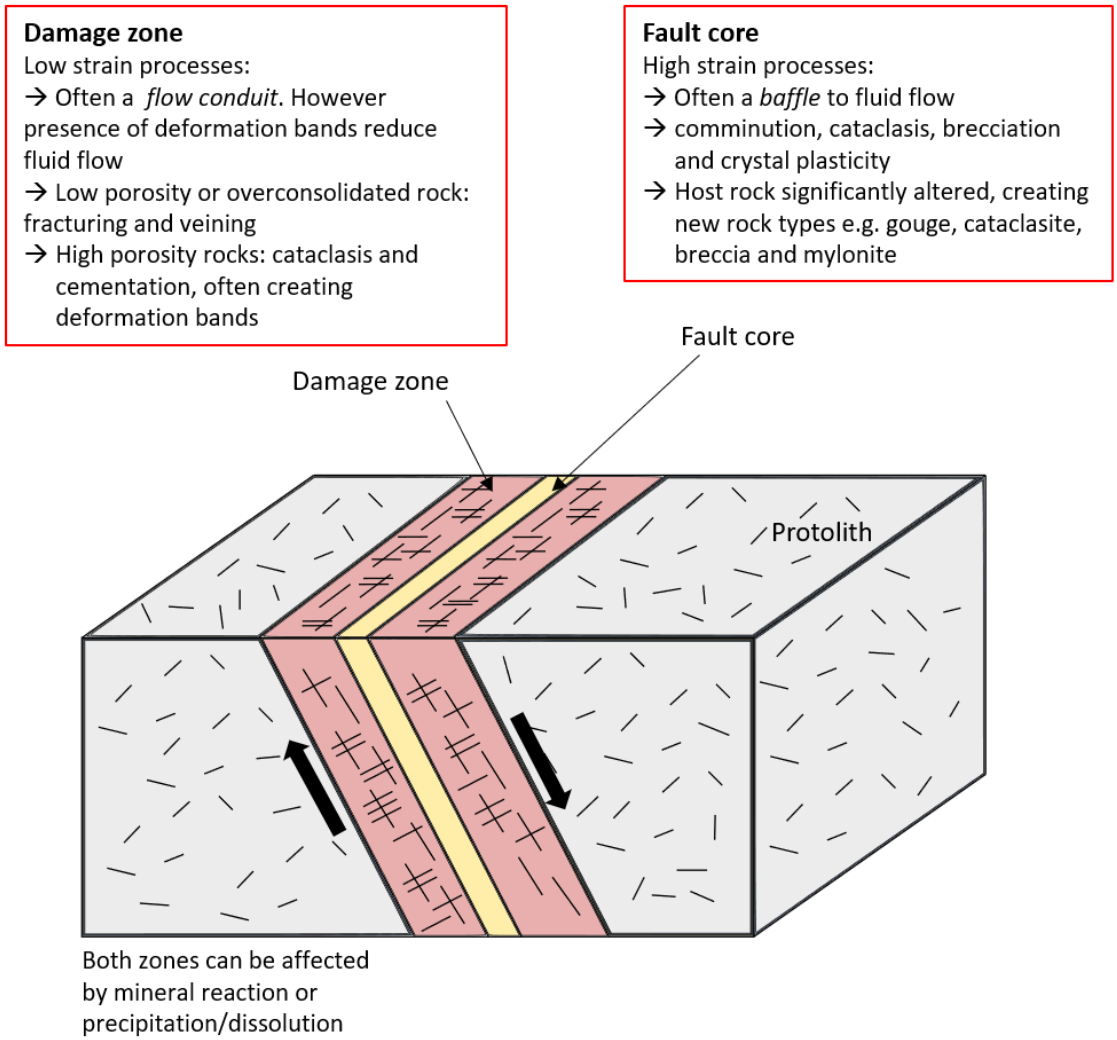

Figure 2.6: Schematic drawing of a fault zone, which comprises of a fault core and damage zone. The area surrounding the fault zone is the protolith. (Modelled after Johri et al. 2014. Information taken from Michie, 2021).

2.3.1 Fractures as a Barrier

Fractures may not always act as a conduit to fluid flow, as sometimes they appear to act as a barrier, or have no impact on fluid flow (Fisher et al. 2001; Fisher et al. 2003) (Engelder, 1974; Fisher and Knipe, 1998; Gibson, 1998; Watts, 1987). Fisher et al. (2001) found that fault permeabilities are controlled by clay distribution, stress and temperature histories occurring pre-, syn- and post-deformation (Fisher et al. 2001). This might also be estimated based on the behaviour of faults such as strike and throw, thickness and depth of reservoir (mainly oil but perhaps applicable to fluid flow) and net-to-gross ratio (Fisher et al. 2001; Knott, 1993). Due to fault zone structures being extremely complex it is difficult to determine fluid flow properties for fault structures (Fisher et al. 2001; Foxford et al. 1998). Despite

this, fault structural analysis may help to predict fault fluid flow behaviour and properties (Fisher et al. 2001).

Fluid flow properties of faults have generally been less studied in carbonate rocks, with the majority of research done on siliclastic rocks (Fisher et al. 2003). It has previously been argued active faults act as conduits, and those which are critically stressed appear to act as a barrier (Fisher et al. 2003; Barton et al. 1995).

2.4 Deformation Bands

Deformation bands in porous sedimentary rocks are often fault-related strain features (Lubiniecki, 2019). During burial, compaction of sediments leads to pore-space collapse, due to accommodation of strain (Fossen, 2007). Cataclasis usually occurs through pressure solution in carbonates (Lubiniecki, 2019). Despite the lack of research in carbonate-hosted deformation bands, research has been more prevalent in the recent years (Lubiniecki et al 2019, Kaminskaite et al 2019, Tondi et al 2006, Antonellini et al 2014, Micarelli et al 2006). Cataclasis and cementation in deformation bands have been proven to reduce overall porosity and permeability in porous carbonates in previous studies (Zambrano et al. 2018). Alternatively, pressure dissolution and faulting has shown to result in interconnected channels in deformation bands and therefore increase in permeability (Zambrano et al. 2018).

3. Experimental Method

3.1 Aim of the Experiment

The experiments are designed to monitor porosity and permeability changes in the core samples, and identify whether the artificial fracture remains a conduit for flow or becomes a barrier. Significant attention will be drawn towards any changes in porosity and permeability, fluid-rock chemical interactions and micro-structural changes. It will be interesting to see whether there is a change in porosity and permeability, and whether this will affect the efficiency of fluid flow through the system. As previously mentioned in the literature review, the importance of porosity and permeability in a geothermal system is key to allow geothermal fluids to flow (Huenges, 2016).

The experiment has been set up to further understand the processes involved with transporting fluids through carbonate rocks in geothermal systems. The experiment will compare two different carbonate rocks, limestone and dolostone, to compare if one is more ideal than the other when looking for geothermal systems. The experiment will identify if there are dissolution-precipitation reactions occurring within the carbonate rock. Variable conditions have been set-up to try to replicate an injection closed-loop geothermal system, whereby fluid is injected into the natural earth, heated until it eventually rises and used for energy (Huenges, 2016). The fluid starts at room temperature (to replicate initial injection), then to 80°C (to replicate deep percolation) and then finally to 40°C (to replicate the rising of the heated fluids to the surface. Section 3.4 explains the experiment methodology in further detail.

The experiments will attempt to analyse the following questions:

- What will happen to a geothermal system under variable conditions such as different carbonate composition, temperature and whether the system is closed-loop or open-loop?
- Will the porosity and permeability change in the system, and will it become more or less efficient?
- How will the limestone and dolostone react differently in the system?
- What will the difference between closed-loop and open-loop be?
- How will the temperature effect the rate of dissolution and precipitation?
- How much dissolution-precipitation may occur?

The experiment was designed to understand how fluids in a geothermal system react with the host rock and pre-existing fractures, and whether the fractures retain their shape, become bigger (due to dissolution) or smaller (due to precipitation).

3.2 Samples

Carbonate samples were cored from limestone and dolostone blocks, which were approximately 0.5m x 0.5m in size. Six limestone and six dolostone core samples were made. The dolostone samples were collected from Smaws Quarry, Tadcaster, North Yorkshire, United Kingdom. The limestone samples were collected from Stoney Middleton, Derbyshire, United Kingdom. Table 1 highlights the labelling system used for the limestone and dolostone core samples. The limestone core samples were labelled A, B, C, D, E and F. The dolostone core samples were labelled B1, B2, B3, B4, B5 and B6. The volume (cm^3) of each core was calculated and are highlighted in Table 2 and Table 3 below.

LIMESTONE CORE SAMPLES	DOLOSTONE CORE SAMPLES
A	B1
B	B2
C	B3
D	B4
E	B5
F	B6

Table 1: Labelling system used for the limestone and dolostone core samples throughout the experiment. The limestone core samples were labelled A, B, C, D, E and F. The dolostone core samples were labelled B1, B2, B3, B4, B5 and B6.

LIMESTONE CORE SAMPLE	CORE SAMPLE VOLUME (cm^3)
A	55.11
B	57.61
C	54.69
D	55.74
E	60.48
F	56.17

Table 2: Volume measurements (cm^3) of the limestone core samples.

DOLOSTONE CORE SAMPLE	CORE SAMPLE VOLUME (cm^3)
B1	48.71
B2	49.92
B3	50.12
B4	47.75
B5	47.68
B6	61.07

Table 3: Volume measurements (cm^3) of the dolostone core samples.

3.3 Rock Descriptions

The limestone samples were collected near Stoney Middleton in the Peak District. The limestone is called the 'Monsal Dale Limestone Formation', which is part of the larger 'Peak Limestone Group' (British Geological Survey, 2021). The sample consists of light to medium grey, well-rounded, well-sorted, finely grained limestone. The BGS date this rock in the late-Carboniferous, approximately 330 million years ago (British Geological Survey, 2021).

The dolostone samples were collected from Smaws Quarry in Tadcaster. The dolostone is known as the 'Cadeby Formation', which is part of the 'Zechstein Group' (British Geological Survey, 2021). The samples consist of pale yellowy-brown, well-rounded, well-sorted, fine-medium grained dolomite. There appears to be black, well-rounded, evenly distributed, medium grained inclusions. The BGS date this rock as being formed at the end of the Permian, approximately 260 million years ago (British Geological Survey, 2021).

3.4 Experiment Methodology

Two self-designed fluid flow experiments were created and undertaken, a closed-loop system and an open-loop system. The fluid used was un-equilibrated tap water. The first experiment replicated a closed-loop system, whereby the fluid ran in a loop throughout the experiment. The second experiment reflected an open-loop system, whereby the fluid was not recycled throughout the experiment and was discarded after the 40°C and final core holder. The closed-loop experiment began on 23/07/2021 and ended on 01/09/2021, lasting just less than six weeks. The open-loop experiment began on 13/09/2021 and ended on 25/10/2021, lasting six weeks. In both experiments, there was a limestone line (line one) and a dolostone line (line two). Each line consists of three core holders, an ambient temperature core holder, an 80°C core holder and a 40°C core holder. Each core holder consists of an upstream and downstream pressure gauge. Before entering the ovens, the fluid is heated to the respective temperature, for example, the fluid is heated up to 80°C before entering the 80°C oven and cooled to 40°C before entering the 40°C oven. This is to make sure the temperature of the fluid isn't different to the actual temperature of the ovens. Fluid was pumped at a constant rate of 0.4rpm (revolutions per minute) through the limestone and dolostone samples. Figure 3.1 and Figure 3.2 shows the experiment set-up for both the closed-loop and open-loop experiments, including: position of each core holder, line one and line two, direction of fluid flow, water sample valve location, pressure gauge location and the labels given to each when analysing data. The limestone core samples were labelled from A – F and the dolostone core samples were labelled from

B1 – B6. Figure 3.3 and Figure 3.4 portrays which limestone and dolostone sample was placed in each core holder. Refer back to the aforementioned figures in this paragraph throughout the results and discussion section to enable ease of understanding the nomenclature. Refer to figures 3.5a, 3.5b, 3.5c and 3.5d to see photos of the experiment setup.

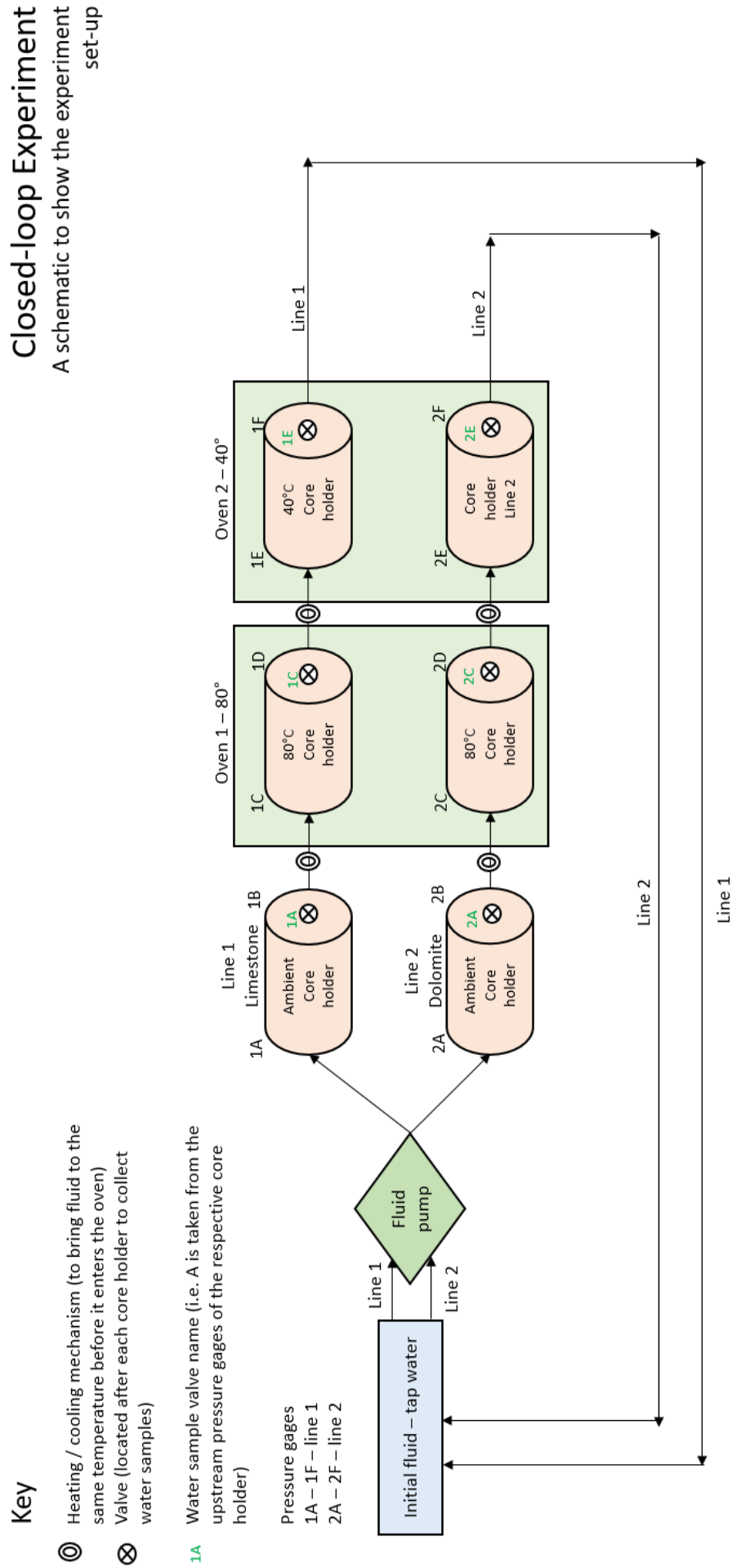

Figure 3.1: A schematic diagram of the closed-loop experiment.

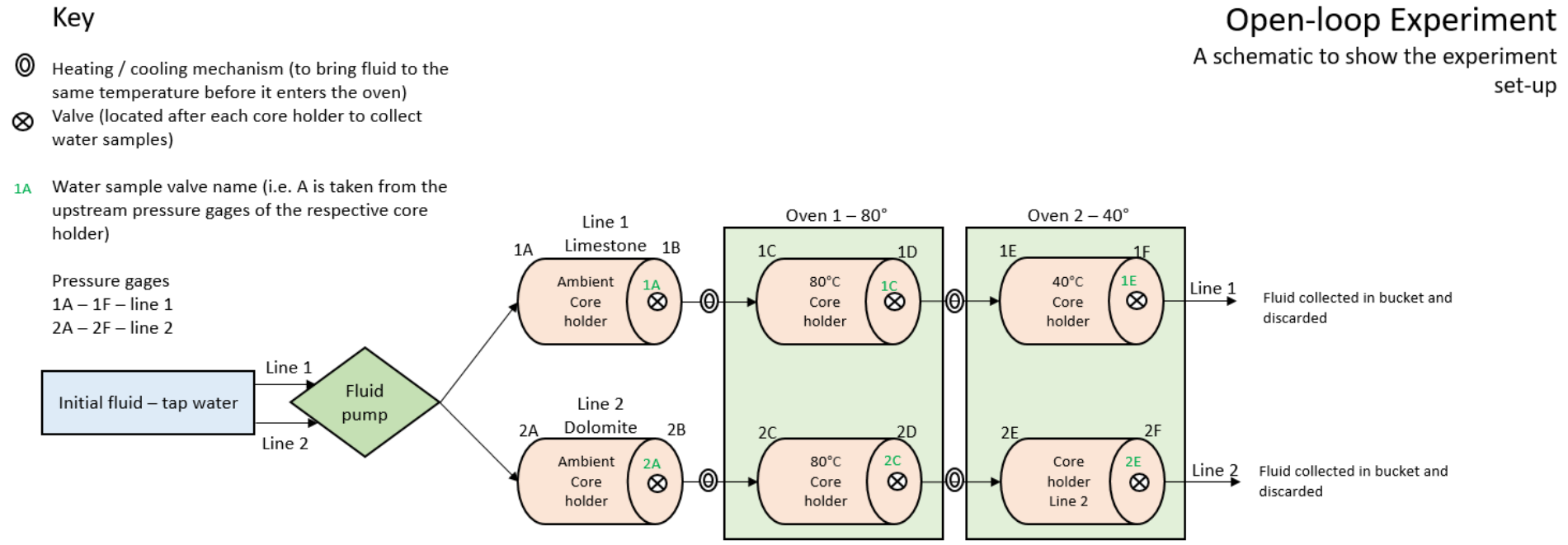

Figure 3.2: A schematic diagram of the open-loop experiment.

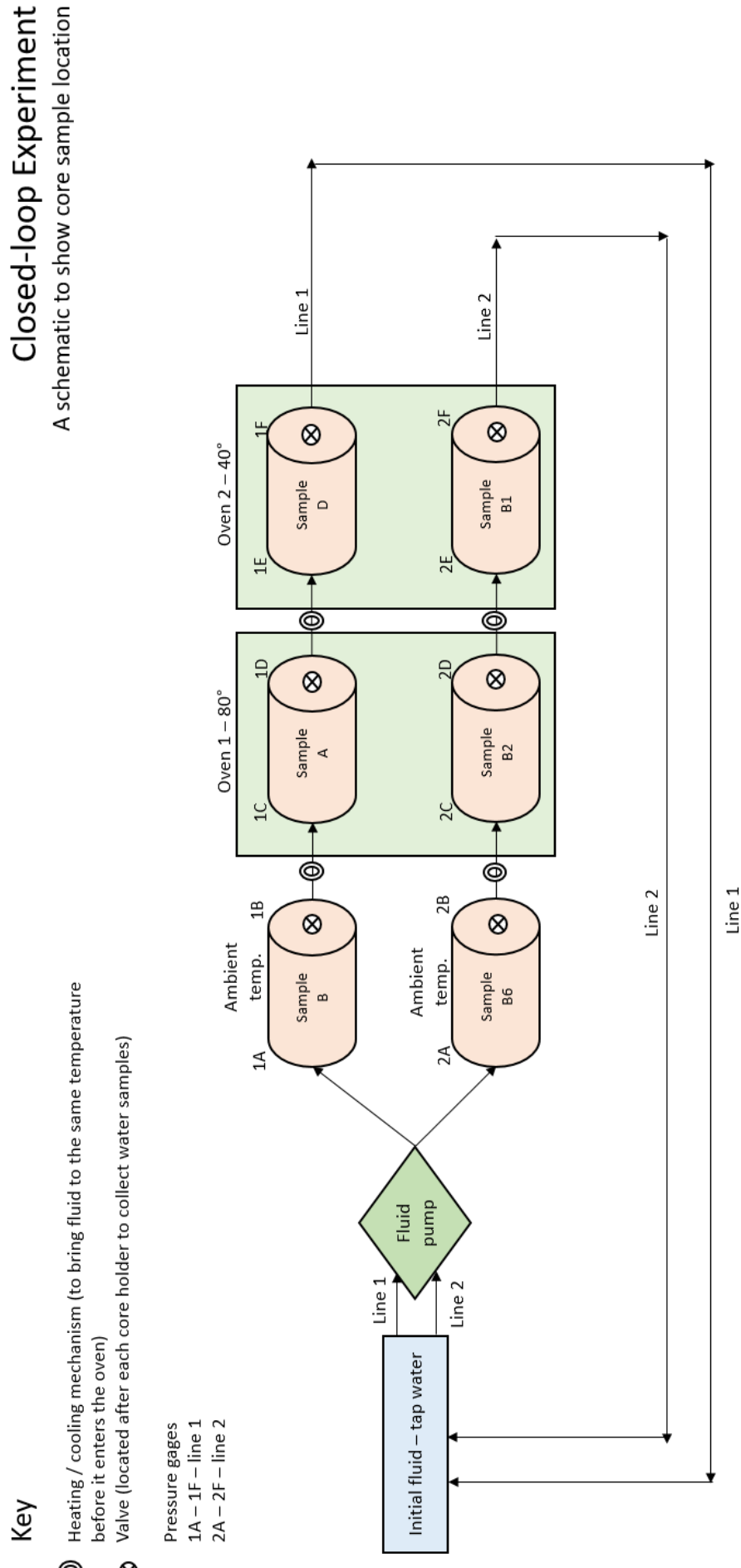

Figure 3.3: A schematic diagram of the closed-loop experiment, showing the location of limestone and dolostone core samples throughout the experiment.

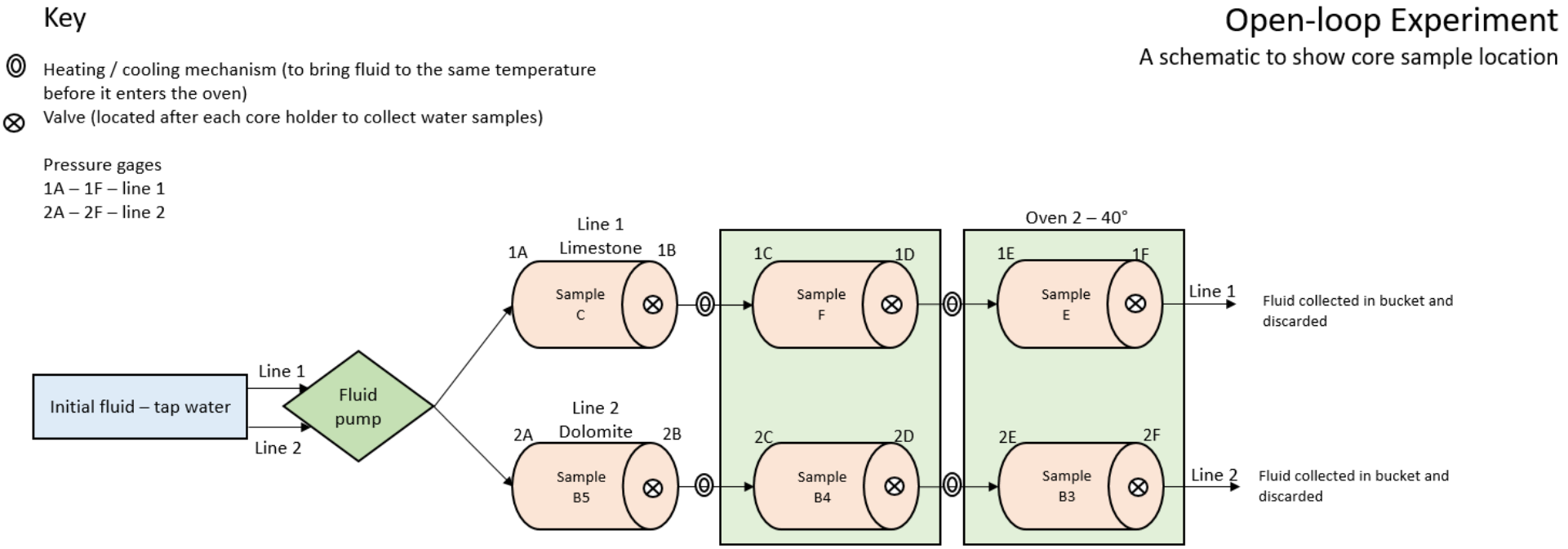

Figure 3.4: A schematic diagram of the open-loop experiment, showing the location of limestone and dolostone core samples throughout the experiment.

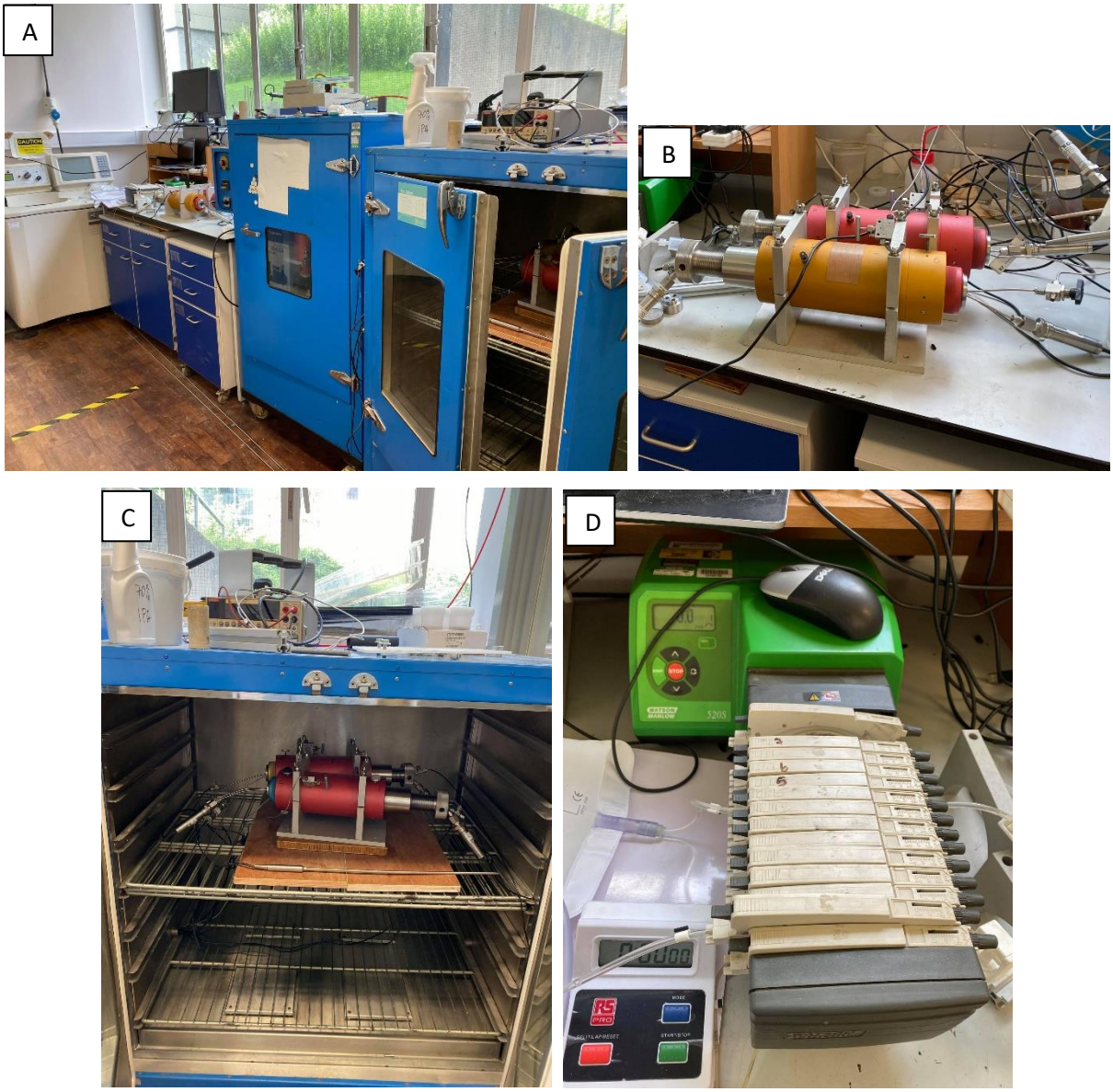

Figures 3.5a, 3.5b, 3.5c and 3.5d: Photos of the experiment setup. (a) The ambient core holders (far left), the 80°C oven (middle) and the 40°C oven (far right), (b) The ambient core holders with red as line one (limestone) and orange as line two (dolostone). (c) The core holders located inside the 40°C oven. (d) The pump to determine flow.

Twelve core samples were prepared, six limestone and six dolostone samples. Porosity was determined for each core sample using the helium method (explained in detail later). Steady-state liquid permeability measurements were taken of the pre-fractured dolostone samples. An issue during data collection meant the permeability values for dolostone samples B5, B4 and B3 taken pre-fracturing were unfortunately lost. However, we presume the values wouldn't have been too dissimilar from samples B6, B2 and B1. Gas pulse decay permeability measurements were taken from the pre-fractured limestone samples, due to having a porosity too low for steady-state liquid permeability (explained in detail later). The samples were CT-scanned before fracturing to identify their internal structure.

3.5 Sample Preparation Pre-Experiment

Six limestone and six dolostone core samples were prepared. The samples were cut vertically and approximately central. This is to replicate a natural fracture, despite the likelihood of a fracture being so parallel in a natural setting being low. The samples were then saturated. Limestone from the same starting block as the samples was crushed into powder between 200-250 microns. The powder was in-filled into the fracture to keep the fracture open, whilst enabling a fluid flow pathway and providing a medium for the fluid to potentially react with. The powder was infilled by being placed into a rectangular dish and frozen, with one half of the previously saturated limestone core sample sitting on top of the powder, whilst the other half was also frozen (figure 3.6). Once frozen, the samples were placed together with the frozen powder in the middle. This was then placed in a plastic tube which was heated to mould around the sample, holding the samples in place whilst melting (figure 3.7). Filter paper was placed at either end to stop any loose grains from falling out whilst un-freezing. The complete sample was then placed in a compressor to compact the core sample. The samples were CT-scanned again after being compressed and then saturated. A final permeability measurement was taken of the samples before being loaded into their respective core holders and ready to start the experiment. The same was done with dolostone. Figure 3.8 portrays a flow chart showing the stages of the core sample preparation.

Figure 3.6: Picture of the preparation of the saturated limestone sample A before being frozen. Crushed limestone grains between 200 and 250 microns were placed into a rectangular dish. One half of the limestone core sample was placed on top so that the grains would freeze to the sample. The other half was frozen. Once the halves were frozen, they were placed together in a plastic tube which was heated and consequently moulded to the sample to hold it together.

Figure 3.7: Picture of limestone sample A held together by a plastic tube, which was heated and therefore, moulded to hold the sample together.

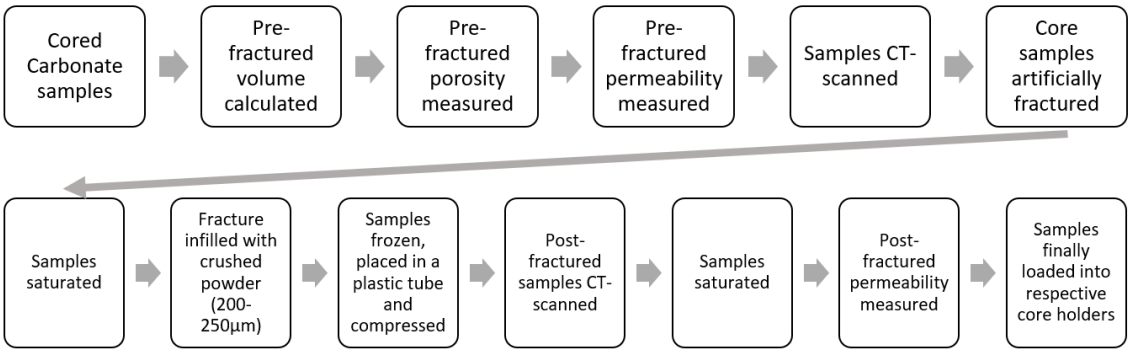

Figure 3.8: A flow chart showing the stages of the core sample preparation.

Carbonates are often naturally fractured and may not require artificial fracturing. However, due to time constraints of the experiments, artificial fracturing was necessary to allow the fluid to pass through the rock quickly enough to provide results within the timescale of the experiments. In a real geothermal system, an artificial reservoir or enhanced geothermal system (EGS) may be created, whereby artificial hydro-fractures are created from pumping high pressurized water into the host rock (Mohais et al. 2011). This enables for fractures to form and become interconnected, creating a previously low permeability system to a high permeability system (Phillips, 1991; Christopher et al. 1978; Mohais et al. 2011).

After the experiment, the samples were CT-scanned and prepared for thin section analysis with resin impregnation. Originally the plan was to impregnate either end of the samples with resin, however in some samples the grains had been removed or fallen out at the end of the core. Therefore, half the samples were impregnated with blue resin, with the sample orientated with its long axis horizontal and the fracture vertical to capture more grains. After the resin had set, the sample was cut along the boundary between the impregnated and non-impregnated section. Three polished sections were prepared from the impregnated part, one parallel to the axis of the sample and two from either end perpendicular to the axis of the sample (making sure the particles were apparent). The non-impregnated area was split along the fracture and used for secondary electron imaging. Thin section and scanning electron microscopy (SEM) analysis was undertaking on the limestone and dolostone samples.

3.6 Sample Selection

The core samples were chosen for each experiment so that each experiment consisted of a mixture of less permeable and more permeable samples. Figures 3.9 and 3.10 portray which core samples were chosen for each experiment (relate to previous figures 3.1, 3.2, 3.3 and 3.4).

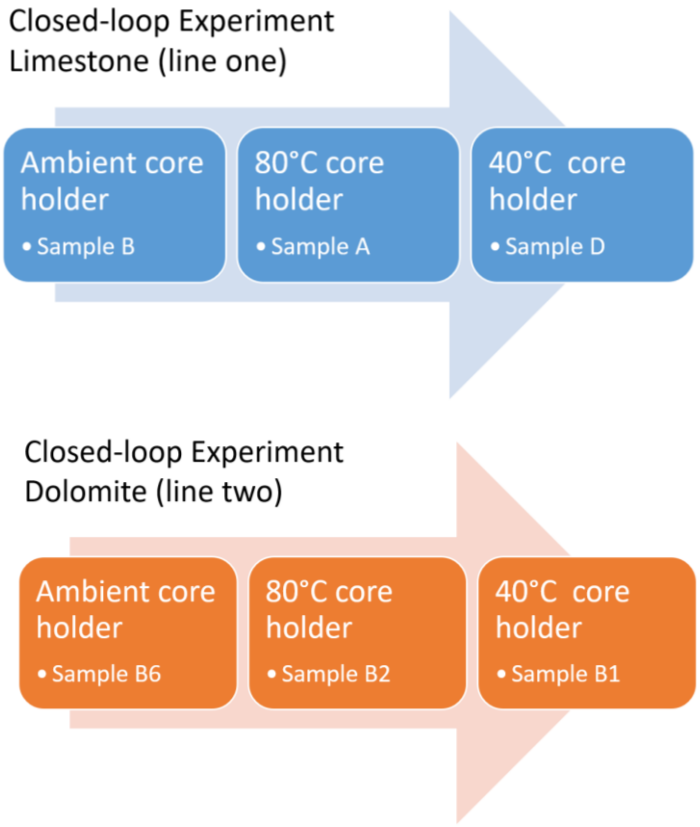

Figure 3.9: Flow chart showing the limestone and dolostone samples chosen for the closed-loop experiment.

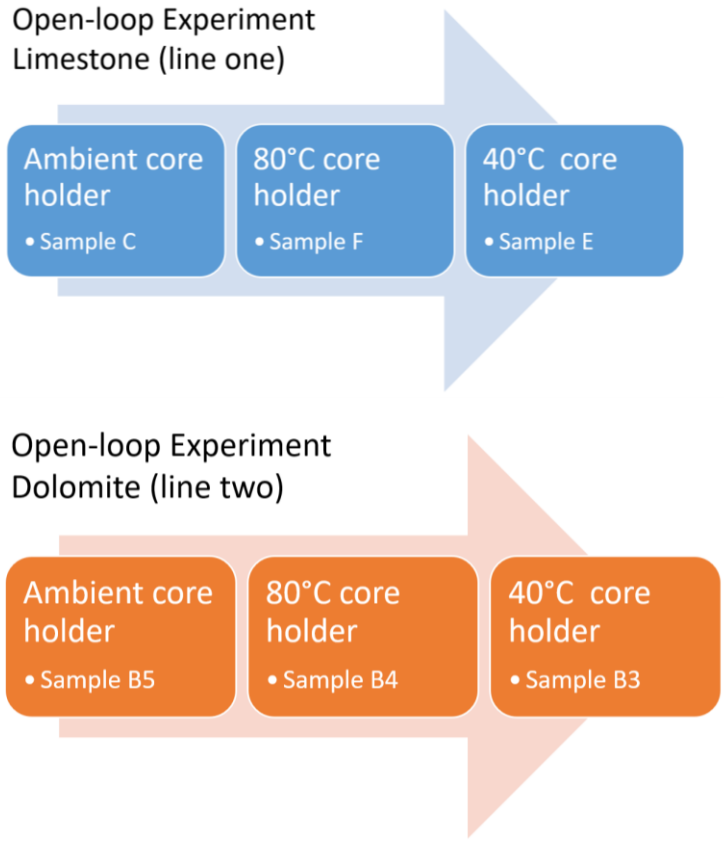

Figure 3.10: Flow chart showing the limestone and dolostone samples chosen for the open-loop experiment.

3.7 Porosity Measurements

Helium porosity measurements were taken from all twelve samples before the experiment. Samples were dried before the measurements were taken. The test equipment comprises a modified twin-cell helium porosimeter, which determines the overall grain volume (McPhee et al. 2015).

Helium gas enters a sample chamber with a sample and a known volume (V_1). The analysis works by pressurising the initial sample cell (P_1 = approx. 15psi), followed by expansion into a reference chamber. The expanding pressure enters a reference chamber with an understood volume (V_2). The pressure after expansion into the second chamber is P_2. The grain volume is determined from a solid volume vs. P_1/P_2. The solid volume was a standard steel cylinder with a known volume. The grain volume is calculated using Boyle's Law, which states that 'for an ideal gas assuming constant temperature, the product of pressure and volume in a closed system remains constant' (McPhee et al. 2015) (equation 1):

$$V_1/V_2 = P_2/P_1 \quad [1]$$

Once the grain volume is calculated, it can be subtracted from the bulk volume, leaving pore volume and thus porosity. See Table 4 and Table 5 below for the carbonate sample porosity data (McPhee et al. 2015).

LIMESTONE CORE SAMPLE	CORE SAMPLE POROSITY (%)
A	1.15%
B	0.57%
C	0.22%
D	0.25%
E	0.36%
F	0.66%

Table 4: Porosity measurements (%) of the limestone core samples.

DOLOSTONE CORE SAMPLE	CORE SAMPLE POROSITY (%)
B1	19.30%
B2	20.64%
B3	22.45%
B4	18.49%
B5	28.12%
B6	29.33%

Table 5: Porosity measurements (%) of the dolostone core samples.

3.8 Permeability Measurements

Permeability measurements were taken of the limestone and dolostone samples pre-fracturing (pre-experiment), post-fracturing (pre-experiment) and throughout the experiment.

Prior to fracturing, the limestone and dolostone permeabilities had to be measured differently, due to the limestone host having a permeability that was too low for steady-state liquid permeability measurements. Following fracturing, all samples had permeabilities high enough for steady-state liquid permeability measurements and so this was the method used for the limestone and dolostone. Before the first closed-loop experiment, each limestone and dolostone sample used in this experiment (B, A and D and B6, B2 and B1) was placed into the same core holder, one after another, and the steady-state liquid permeability measurements were undertaken. Each sample was then removed and placed into their respective core holder for the experiment. However, several problems occurred using this method including:

- Upon removal of the core samples from the core holder, some of the core samples were slightly knocked, therefore, some grains inside the fracture were lost from the edge of the sample or the make-up of the grains and fracture were altered. Due to this, some samples were ruined and had to be re-made, costing days of work due to the samples having to be re-frozen.
- This method was time consuming due to only using one of the core holders to measure the steady-state liquid permeability. This method took approximately one to two hours each and only a maximum of three samples could be measured per day.

Due to the problems raised above, for the open-loop experiment, it was decided the steady-state liquid permeabilities would not be done before the experiment. Instead, permeability measurements were taken on the first day of the experiment. This method assumes that there is little alteration in the permeability on the first day of the experiment, despite fluid flow and heat. This proved to be an easier method, as all the samples could be placed into their respective core holders for the experiment, therefore meaning no samples were ruined and time was saved. However, if one was wanting to be extremely accurate in the permeability methods and to make sure absolutely no change to the permeability of the sample was made, they may want to use the original, albeit time-consuming, method.

3.8.1 Steady-state Liquid Permeability Measurements

Steady-state liquid permeability measurements were taken of the dolostone samples pre-fracturing, all the dolostone and limestone samples post-fracturing and throughout the experiment. The samples were saturated in water before being loaded into a core holder and confined to a pressure of approximately 1500 psi. A HPLC (constant rate) pump was used to vary the flow rate throughout the permeability test. An upstream and downstream pressure gauge is located either side of the core holder. Darcy's law is then used to determine liquid permeability (equation 2):

$$k = \frac{Q\mu L}{A(P_1 - P_2)} \quad [2]$$

Whereby flow rate = Q, differential pressure = $(P_1 - P_2)$, viscosity μ, length of sample = L, cross-sectional area = A and permeability = k.

3.8.2 Gas Pulse Decay Permeability

Gas pulse decay permeability measurements were taken of the limestone samples pre-fracturing due to having a porosity too low to undertake steady-state liquid permeability. The 'Klinkenberg Effect' was used due to being an important method of calculating low-permeability rocks. Unlike liquid flow (where there is a zero-velocity layer at the pore walls), the interaction between the sample pore walls and gas molecules enable the gas to move in the direction of flow (McPhee et al. 2015). At lower mean pressures, the gas molecules will collide less and more gas slippage occurs and therefore, gas permeability increases (McPhee et al. 2015). At higher mean pressures, due to being closer together, the gas molecules experience more friction against pore walls and therefore, the measured gas permeability decreases (McPhee et al. 2015). In low permeability samples, the pore spaces have a small radius and the gas slippage effects increase (McPhee et al. 2015). However, in high permeability samples with larger pore radii, this appears less significant (McPhee et al. 2015). Therefore, in low permeability samples, the method of calculating permeability, by gas slippage effects, is extremely significant and proved to be the most effective method to calculate the permeability of the limestone samples prior to them being fractured (McPhee et al. 2015).

The 'Klinkenberg Effect' was used to calculate the gas permeabilities of the limestone samples. Klinkenberg (1941) argued 'that if measurements could be made at infinite gas pressure, then the gas permeabilities measured at infinite pressure would be equivalent to the permeability to a non-reactive

liquid' (McPhee et al. 2015). Therefore, meaning the Klinkenberg permeability at infinite mean pressure will always remain the same, no matter the gas or mean pressure used (McPhee et al. 2015). Klinkenberg identified a way to find the equivalent liquid permeability (McPhee et al. 2015). Steady-state gas permeabilities are measured at a number of recorded mean pressures (McPhee et al. 2015). Gas permeability results are plotted against the inverse mean pressure, ideally falling on a straight line (McPhee et al. 2015). The intercept of the linear regression line gives the Klinkenberg number. The Klinkenberg permeability for each core sample can be then calculated using (equation 3):

$$k_g = k_l\left(1 + \frac{b}{P_m}\right) \quad [3]$$

where k_g is the gas permeability (mD), k_l is the Klinkenberg permeability (mD), b is the constant for a particular gas in a given rock type (psi) and P_m is the mean pressure (psi).

b can be calculated from the linear regression line slope using (equation 4):

$$b = \frac{mP_m}{k_l} \quad [4]$$

where m is calculated from the slope and P_m is the mean pressure.

Figure 3.10 shows an example of a Klinkenberg plot taken from limestone sample A. Where the linear regression line is shown to intercept the y-axis is known as the Klinkenberg number. The values were plotted for all six limestone samples: A, B, C, D, E and F and the gas permeability values were calculated as an average using the Klinkenberg effect equations above (equations 3 and 4).

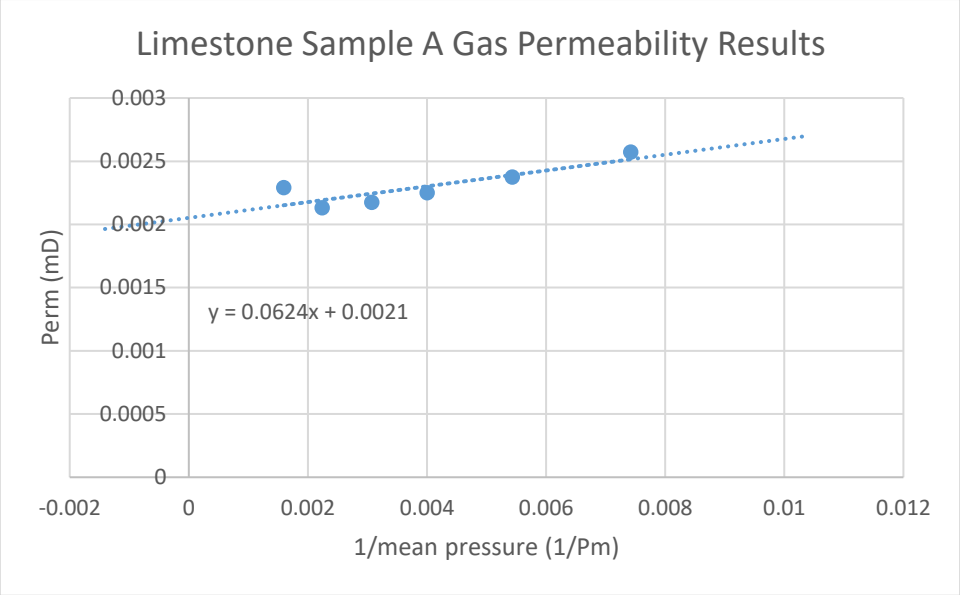

Figure 3.11: Example of a Klinkenberg plot taken from limestone sample A from the closed-loop experimen.

In Figure 3.11, the equation can be seen for the linear regression line as follows (equation 5):

$$y = mx + c \quad [5]$$

where m represents the value of the slope and c represents the Klinkenberg number.

Post-fracturing, all of the limestone and dolostone permeabilities could be measured using the steady-state liquid permeability measurements. This is due to the limestone permeability increasing enough to use this method. Table 6 portrays the permeability values acquired for the limestone and dolostone, taken pre-fracturing and post-fracturing of the core samples. The range of permeabilities evident in the samples post-fracturing is expected, due to the grains in the fracture sitting differently in each core sample. There may be some error in the steady-state liquid permeability measurements, due to the pressures varying throughout the system. It is unclear as to how much this error affects the final data.

Sample	Pre-fractured Permeability Range (mD)	Post-fractured Permeability Range (mD)
Limestone	0.04 – 0.07	3.04 – 23.80
Dolostone	0.22 – 1.30	1.68 – 14.31

Table 6: Limestone and Dolostone permeability ranges (mD) taken pre-fracturing and post-fracturing.

3.8.3 Steady-state Liquid Permeability Measurements Taken Throughout the Experiment

Steady-state liquid permeabilities were taken throughout the experiment. Data was collected when taking the water samples, calculating the amount of fluid collected and the time taken to collect the fluid, along with pressure data. This information was later used to calculate the permeability of the samples throughout. It is to be noted that the permeabilities throughout the experiment were calculated using the flow rate data from the water sample valve located after the 40°C core holder only (water sample valve 1E and 2E) (see figures 3.1 and 3.2) and applied to the samples located in both the ambient and 80°C core holders. This is because the 40°C core holder is located at the end of the experiment and once the system is opened it affects the equilibrium and potentially fluid flow. Water sample valves 1E and 2E were located at the end of the experiment and when water samples were taken, they were the first to be opened. Water samples were taken progressively backwards during the experiment, sampling fluid from water valves 1E and 2E first, followed by water valves 1C and 2C and finally water valves 1A and 2A, therefore, not to affect the pressure further down the system. So, for example, the limestone located in line one comprises of core holders in the order of, ambient core holder → 80°C core holder → 40°C core holder, therefore all the permeabilities calculated for the samples in these three core holders are calculated using the water sample data from the 40°C core holder (see figures 3.1 and 3.2).

3.9 Water Sampling Method

The magnesium and calcium concentrations in the fluid percolating through the samples were measured throughout the experiments. The aim was to determine whether the fluid was reacting with the samples by releasing magnesium and/or calcium to solution from the limestone and dolostone samples. Fluid sampling occurred every hour for five hours on the first day of the experiment to understand the initial fluid processes occurring. Sampling continued for every day to every two days after this due to the logistics of having someone sample every hour for five to six weeks.

In order to sample the water, samples are collected in small plastic tubes. Starting from the last valve (water valves 1E and 2E) to the first valve (water valves 1A and 2A), in order to stop the valve before having to re-equilibrate if it was the other way (figure 3.1 and figure 3.2). Two samples are collected at once from line one (limestone) and two (dolostone). Firstly, the sample number is written on the tube. Then the weight of the empty tube is measured. The sample is then taken whilst being timed. The upstream and downstream pressures (psi) are measured during the sampling. Once the sample is taken, the weight of the tube is measured again with the sample. Using this alongside the time taken

to measure the sample, a permeability can be calculated. After this, hydrochloric acid is added to the tube to react with the water sample, so the magnesium and calcium concentrations are preserved. Finally, the tube, water sample and the acid are weighed to calculate the amount of acid added. Before the fluid samples were sent off to be analysed, the water sample and hydrochloric acid is diluted with de-ionised water due to sampling practicalities. The water samples are then sent for analysis to determine magnesium and calcium concentrations.

When taking the water samples, they have been labelled as such: 1A1, 2A1, 1C1, 2C1, 1E1, 2E1 (first batch of samples). The first number refers to the line which the sample is on. The letter related to the upstream label of the core holder which the sample is taken, so the only numbers used for the water samples are A, C and E (A is the upstream and B is the downstream of the first ambient core holder, and so on). The last number relates to the number of samples taken, so this increases with number of samples taken e.g. sample 1 = 1A1, sample 2 = 1A2, and so on.

3.10 Problems and Suggestions for Future Improvements

3.10.1 Temperature Limitations

The initial plan of the experiment was to heat the fluid and samples to 90°C and 130°C to reach higher temperatures that are typically found in a geothermal system. However, the core holders in the laboratory were only able to heat to a maximum of 80°C and consequently, it was decided a low-temperature system would be simulated instead. To further improve on the research, it would be good to have access to core holders that can heat the core sample above 80°C. Wood (1986) states that 125°C in a closed system, is the point where the relationship between calcite solubility and temperature goes from being prograde to retrograde, therefore it would be interesting to test what happens at temperatures above 125°C.

3.10.2 Precipitation into the Pipes

Residue was discovered in the clear plastic tubes after the experiment. In the future it may be worth weighing the pipes before and after the experiment to determine how much precipitation, if any, has occurred inside the pipework.

3.10.3 Disadvantages of Using Powder to Infill the Artificial Fracture

It may be argued that it is not realistic to use powder to infill the artificial fractures in the core samples. In a natural setting, it would be unlikely to find a fracture perfectly infilled with material of a specific grain-size. Also, typically in faults there would be rough edges, breccia and cataclasis, alongside other factors which is not accounted for in the experiment (Michie, 2021).

Problems arose when the core samples were fractured, frozen and the fractures were in-filled with grains. Due to the samples being frozen, preparation of the samples had to be undertaken quickly and accurately. Whilst making the samples, grains would often un-freeze and fall out or break apart, meaning they had to be re-made. This sometimes happened after they had been saturated, CT-scanned and their permeabilities had been taken. Therefore, if the sample was re-made, they would have to be re-saturated, CT-scanned and have their permeability taken again. This would often push work back by a few days due to having to re-freeze and re-prepare the samples.

Often times, after the permeability measurements were taken, some grains seemed to have slightly moved or shifted, which may affect the final permeability of the core. Initially the plan was to use honey to glue the grains together, which would then be flushed away once the core was held together in a plastic sleeve. The decision to freeze the grains and samples together was decided as likely the most effective and easy method, due to the honey method being complicated to flush the honey out.

3.10.4 Water Sampling and Pressure

Every time a water valve is opened when a water sample is taken, the pressure readings recorded a sudden drop (removed from the pressure graphs and explained later). This must be accounted for when analysing the final pressure results and must not be mistaken for something that has occurred because of the experiment.

3.10.5 Pressure Gauge Limitations

During the experiment, some of the pressure gauges had to be changed due to having a maximum pressure limit which was exceeded by the pressures in the system. Therefore, some pressure gauges were replaced mid-experiment and may have disrupted some of the pressure readings.

3.10.6 Changing the Experiment Variables

There are multiple different variations and endless possibilities to test in a potential system. For example, which rocks are situated alongside, above or below others, and different temperature gradients. Given more time, it would be interesting to see what would happen if these experiments ran for longer. Four to six weeks is not that long in geological history, so, albeit impractical, it would be interesting to see what would happen after months, even years.

4. *Results*

4.1 Micro-structural Results

Micro-structural analysis was undertaken on the samples post-experiment (Figures 4.1, 4.2, 4.3 and 4.4). Thin sections were made from the closed-loop experiment and open-loop experiment. Samples were taken from either: the upstream (top) of the core sample, the downstream (bottom) of the core sample, or from a long axis through the middle of the core sample. Figure 4.5 portrays the location of the core sample the thin section was taken when referring to upstream, downstream and long-axis. When undertaking the analysis, the long-axis section was the preferred sample to use, due to the ends of the core sample being more prone to grains falling out during sample preparation. Scanning Electron Microscope (SEM) analysis was undertaken on the thin sections. Analysis was undertaken using the TESCAN SEM microscope, in which Secondary Electron (SE) and Backscatter-Electron (BSE) images were produced. Secondary electron imaging focuses on topography, which is not relevant for the focus of this study. Therefore, BSE imaging was used, which focuses on composition and enables for clear grain images. Aztec grain analysis, a software used to identify grain and measure grain size, was undertaken on the BSE images to identify exact composition of grains. Refer back to figures 3.1–3.4 to understand the location of the limestone and dolostone samples and core holders, with their respective temperatures, referred to throughout this section. All SEM images relate to the limestone and dolostone samples post-experiment, unless stated otherwise. In some sections, initial pre-experiment limestone and dolostone samples will be included to enable comparison between the SEM images. It is to be noted that the micro-structure varies throughout the samples and the SEM images provide a snapshot of one location within the core samples.

Figure 4.1: Photo of Limestone and Dolostone core samples after the closed-loop experiment. Limestone samples B, A and D and Dolostone samples B6, B2 and B1.

Figure 4.2: Limestone sample D and Dolostone sample B1 (closed-loop). Dolostone sample B1 was cut in half due to thinking there was an issue with the sample blocking fluid flow. This was discovered as a leak and nothing to do with the sample. This is discussed later in section 4.5.

Figure 4.3: Photo of Limestone and Dolostone core samples after the open-loop experiment. Limestone samples C, F and E and Dolostone samples B5, B4 and B3.

Figure 4.4: Photo of Limestone and Dolostone core samples after the open-loop experiment. Limestone samples C, F and E and Dolostone samples B5, B4 and B3.

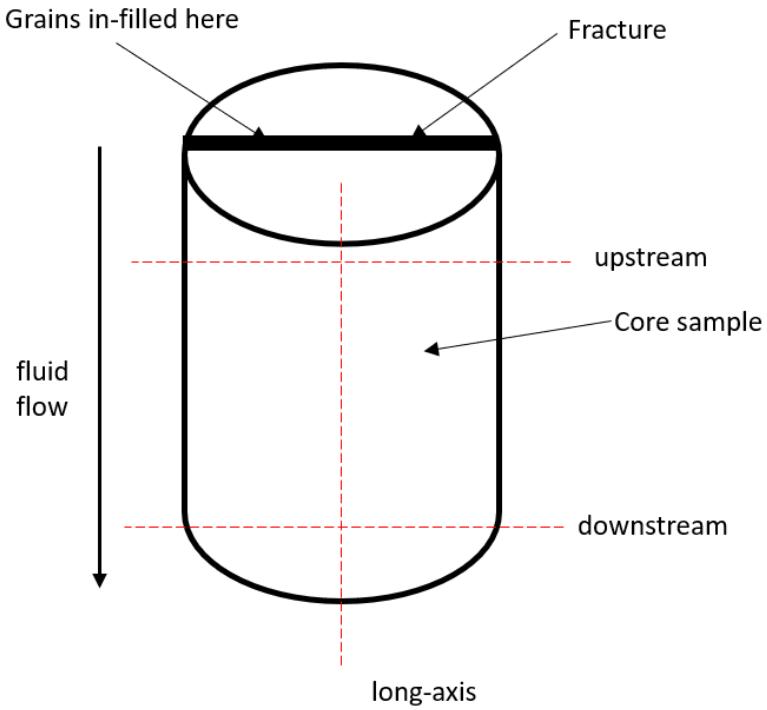

Figure 4.5: Schematic to show the location of the thin section samples along the core sample when referring to upstream, downstream and long-axis.

4.1.1 Limestone Samples: Closed-loop Experiment

Limestone samples B, A and D were located in line one in the closed-loop experiment. Sample B was located in the ambient core holder, sample A was located in the 80°C core holder and sample D was located in the 40°C core holder respectively. An image from each core holder, of similar magnitude, has been selected to aid the ease of comparison between the samples.

Figure 4.6.1, 4.6.2 and 4.6.3: Backscatter-Electron (BSE) images taken of the fracture from Limestone core samples B, A and D, located in the closed-loop experiment. All photographs are taken from the long-axis section. (1) Sample B was located in the ambient core holder, (2) sample A was located in the 80°C core holder and (3) sample D was located in the 40°C core holder. The white grains represent the limestone. The black areas represent porosity.

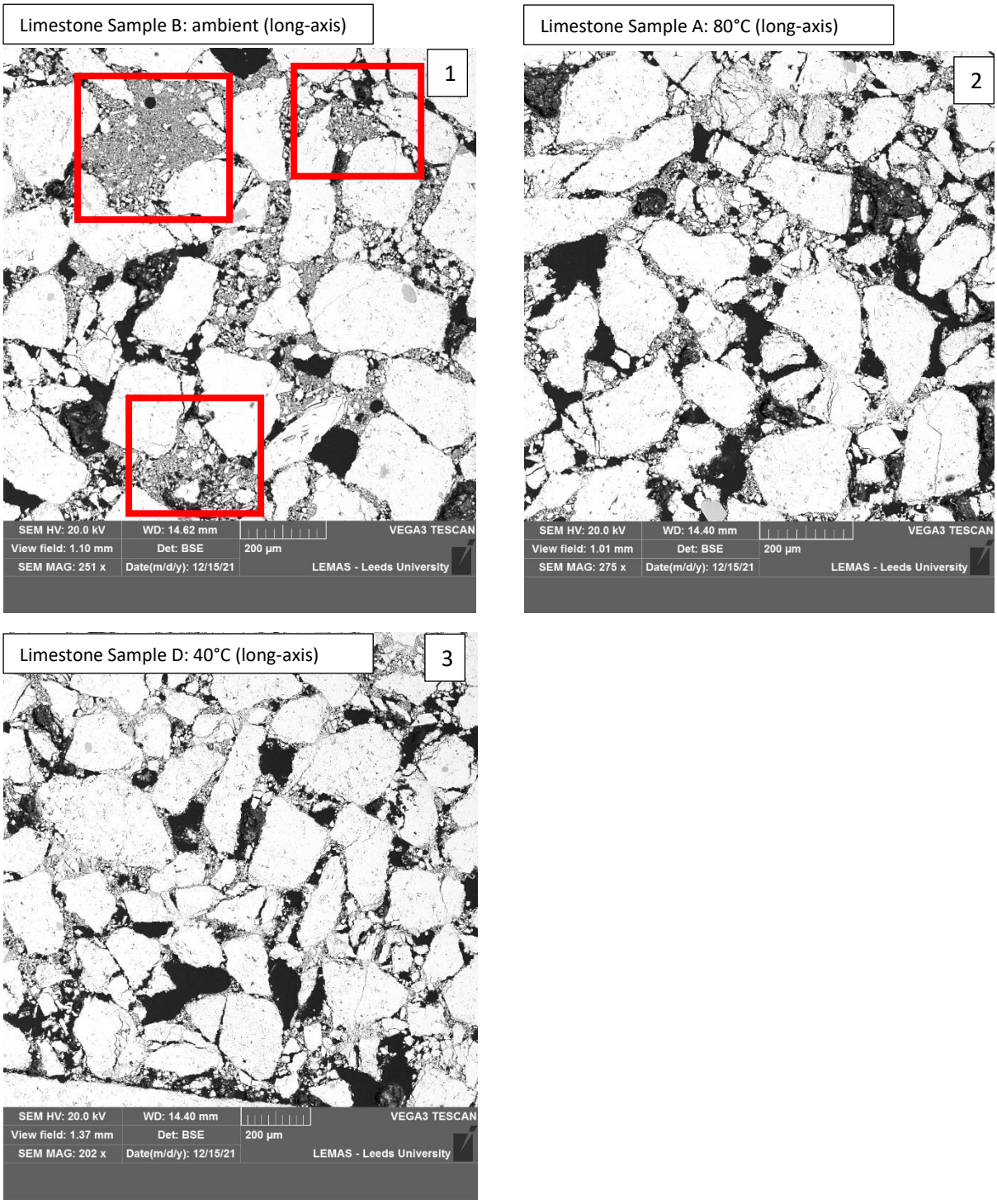

Figure 4.7.1, 4.7.2 and 4.7.3: Backscatter-Electron (BSE) images taken of the grains within the fracture from Limestone core samples B, A and D, located in the closed-loop experiment. All photographs are taken from the long-axis section. Tne red boxes in figure 4.7.1 highlight areas of small-grain accumulation in the pore spaces in the sample. (1) Sample B was located in the ambient core holder, (2) sample A was located in the 80°C core holder and (3) sample D was located in the 40°C core holder. The white grains represent the limestone. The black areas represent porosity.

Figures 4.6.1 – 4.6.3 show the limestone fracture in samples B (ambient), A (80°C) and D (40°C). The dark areas represent the pore spaces within the sample. The grains within the fracture are apparent

in the SEM images and are shown at a higher magnitude in figures 4.7.1 – 4.7.3. The grains were sieved to approximately 200-250µm before being placed in the fracture. Generally, the images show the fracture in all three samples comprising of significant pore spaces and interconnected pores. Therefore, assuming the fracture appears to be the preferential fluid pathway through the samples. The grains within the fractures appear to be angular to sub-angular (Figures 4.6.1 – 4.6.3; 4.7.1 – 4.7.3).

Figures 4.7.1 – 4.7.3 shows all three samples comprising of multiple pockets of small grains (approximately less than 5µm) in-between the larger, obvious grains. Particularly, Limestone sample B (ambient) appears to show a significant amount of these small pockets of grains in comparison to A and D (Figure 4.7.1). In samples A and D many of these small grains appear to cumulate in the 'pore throats' of the grains. These small grains are thought to have occurred from the crushing of larger grains, due to there being a constant pressure of approximately 1500 psi throughout the experiment. Figures 4.8.1 – 4.8.3 and Figures 4.9.1 and 4.9.2 shows evidence of fracture grains being crushed and the breakdown of the fracture boundary edge from the constant pressure state of the system. This will be addressed in further detail in the discussion.

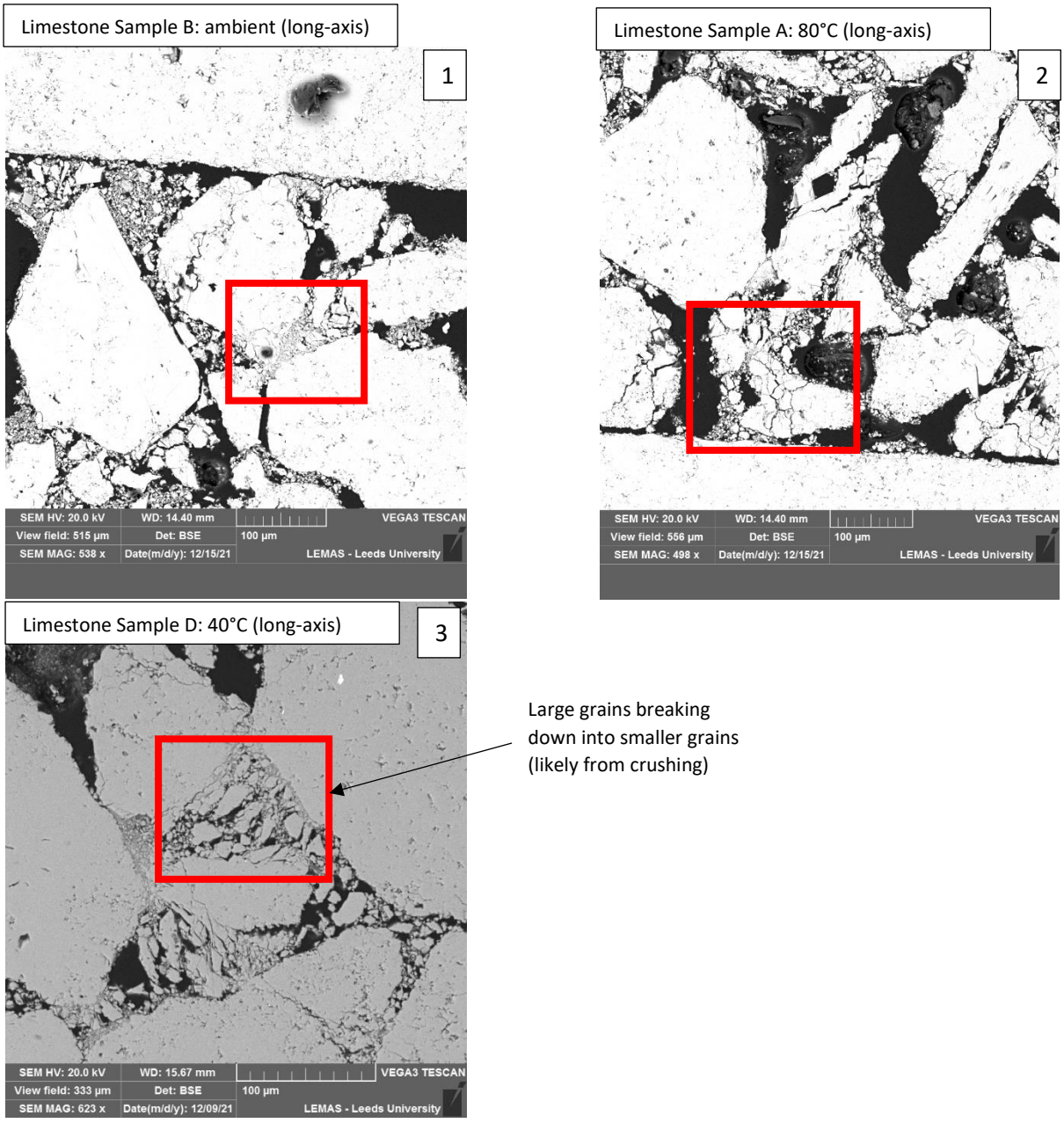

Figure 4.8.1, 4.8.2 and 4.8.3: Backscatter-Electron (BSE) images taken of the grains within the fracture from Limestone core samples B, A and D, located in the closed-loop experiment. All photographs are taken from the long-axis section. Red boxes highlight the areas of large grains breaking down into small grains. (1) Sample B was located in the ambient core holder, (2) sample A was located in the 80°C core holder and (3) sample D was located in the 40°C core holder. The white and grey grains represent the limestone. The black areas represent porosity.

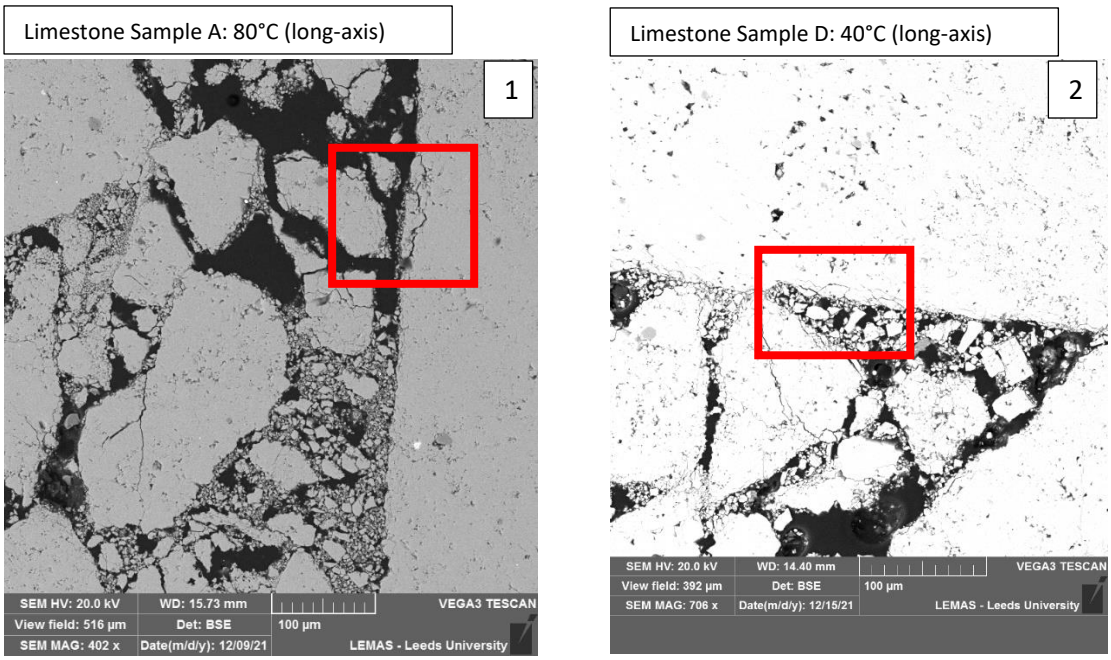

Figure 4.9.1 and 4.9.2: Backscatter-Electron (BSE) images taken of the fracture boundary from Limestone core samples B, A and D, located in the closed-loop experiment. All photographs are taken from the long-axis section. Red boxes highlight the areas of the boundary edge breaking down into small grains. (1) Sample A was located in the 80°C core holder and (2) sample D was located in the 40°C core holder. The white and grey grains represent the limestone. The black areas represent porosity.

Figures 4.10.1 – 4.10.4 show the porosity of the host rock with a scale of between 1-2mm. Figures 4.11.1 – 4.11.4 show the porosity of the host rock with a scale of between 500-600µm. The dark areas on the images represent the pore spaces. The initial limestone images have been included to enable comparison before and after the experiment. It is worth noting some black dots may be resin remnants from the preparation of the thin sections, however it is likely not of significance when analysing the images unless it is otherwise stated.

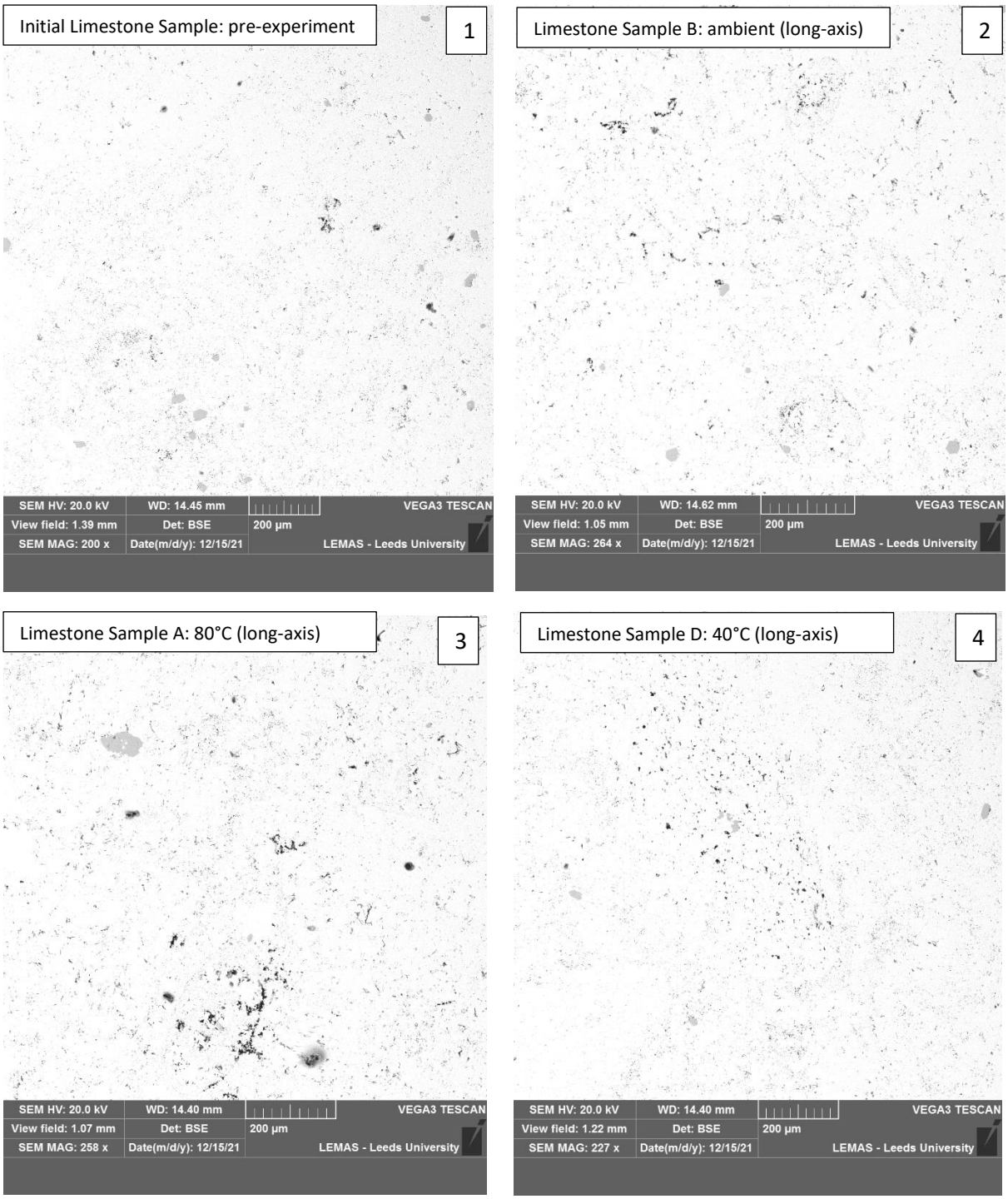

Figure 4.10.1, 4.10.2, 4.10.3 and 4.10.4: Backscatter-Electron (BSE) images taken between 1-2mm of the host rock from Limestone core samples initial, B, A and D, located in the closed-loop experiment. All photographs are taken from the long-axis section. (1) Initial limestone sample was taken pre-experiment, (2) sample B was located in the ambient core holder, (3) sample A was located in the 80°C core holder and (4) sample D was located in the 40°C core holder. The white grains represent the limestone. The black areas represent porosity.

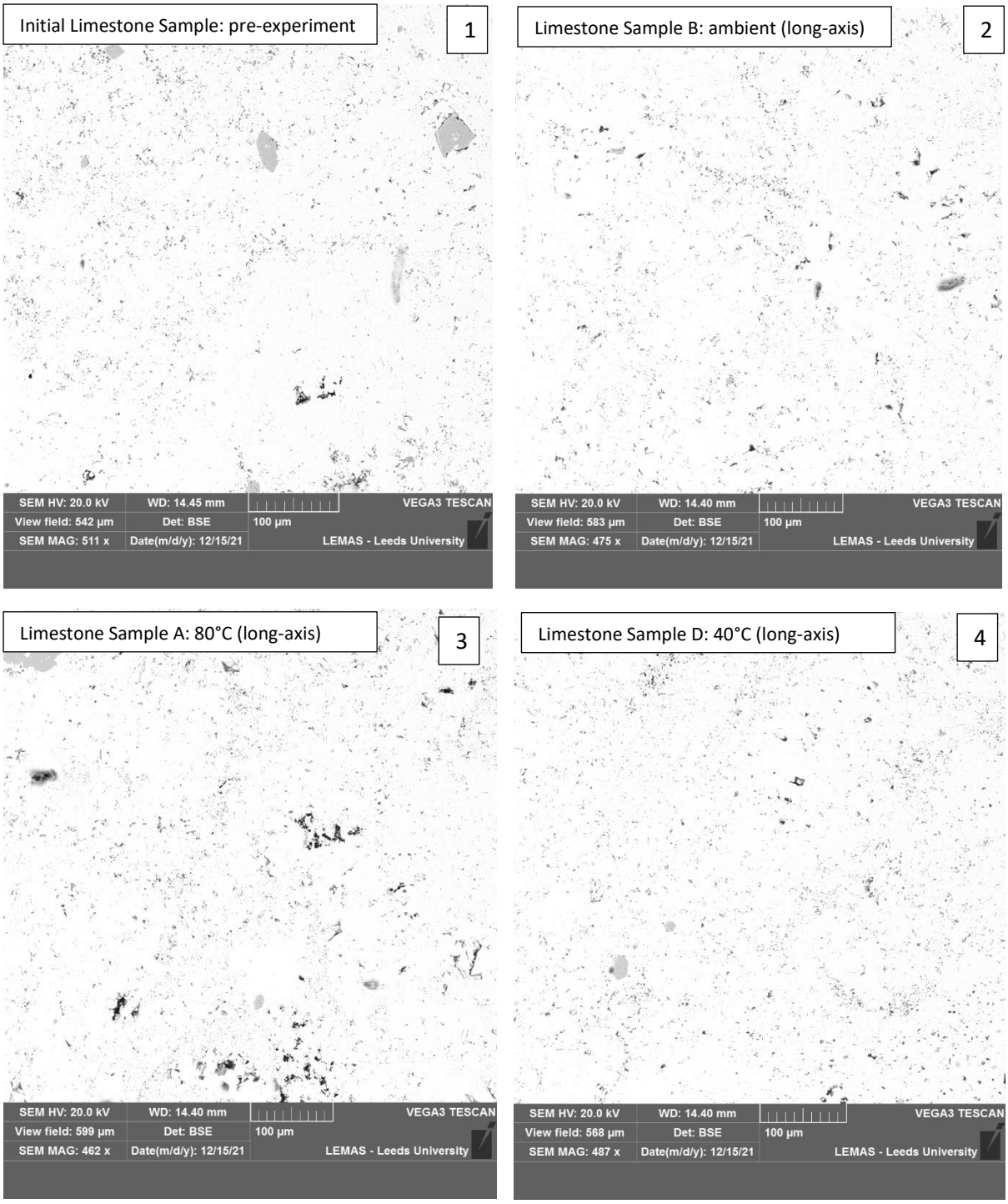

Figure 4.11.1, 4.11.2, 4.11.3 and 4.11.4: Backscatter-Electron (BSE) images taken between 500-600µm of the host rock from Limestone core samples initial, B, A and D, located in the closed-loop experiment. All photographs are taken from the long-axis section. (1) Initial limestone sample was taken pre-experiment, (2) sample B was located in the ambient core holder, (3) sample A was located in the 80°C core holder and (4) sample D was located in the 40°C core holder. The white grains represent the limestone. The black areas represent porosity.

4.1.2 Dolostone Samples: Closed-loop Experiment

Dolostone samples B6, B2 and B1 were situated in line two in the closed-loop experiment. Sample B6 was located in the ambient core holder, sample B2 was located in the 80°C core holder and sample B1 was located in the 40°C core holder respectively. An image from each core holder, of similar magnitude, has been selected to aid the ease of comparison between the samples.

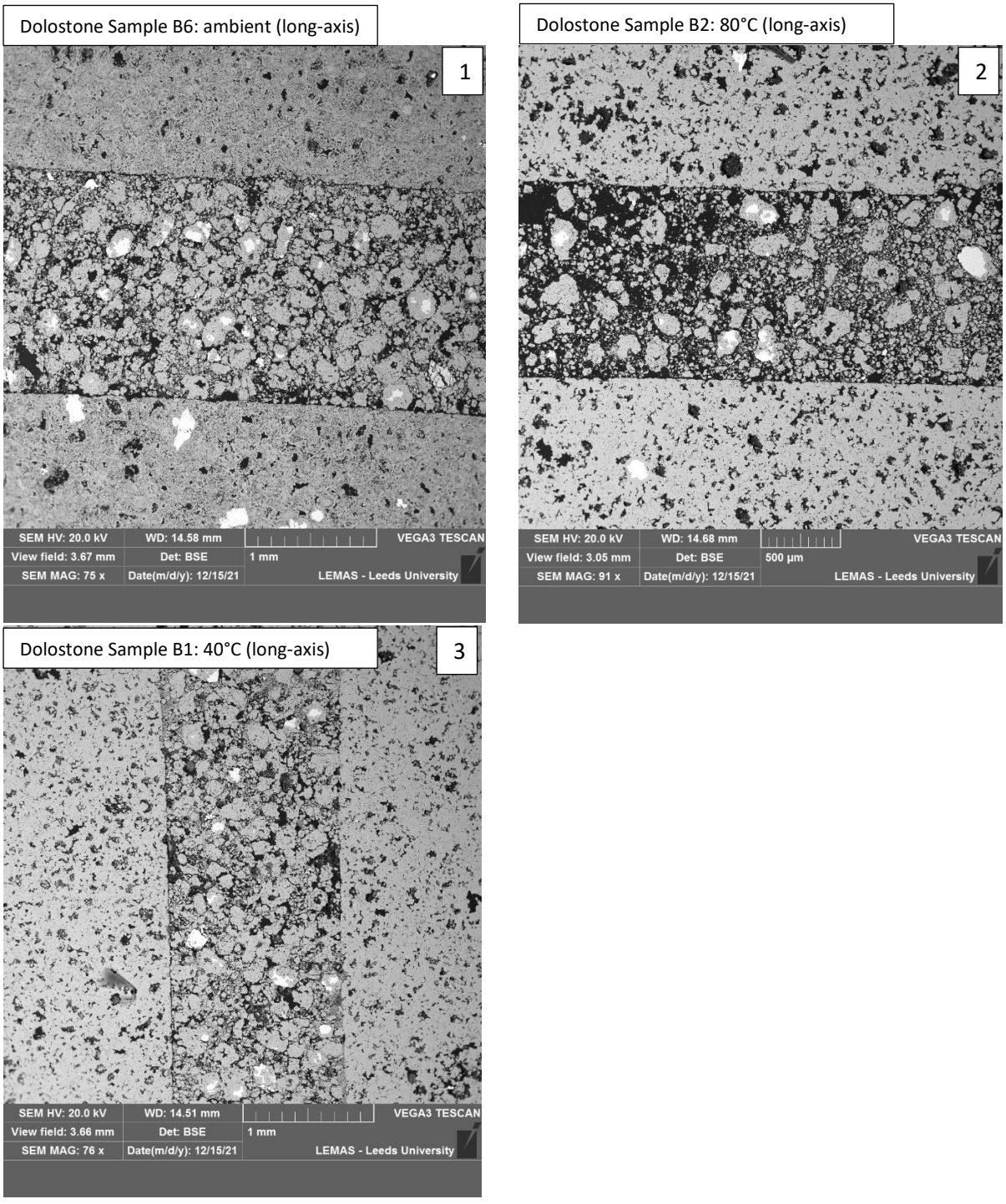

Figure 4.12.1, 4.12.2 and 4.12.3: Backscatter-Electron (BSE) images taken of the fracture from Dolostone core samples B6, B2 and B1, located in the closed-loop experiment. All photographs are taken from the long-axis section. (1) sample B6 was located in the ambient core holder, (2) sample B2 was located in the 80°C core holder and (3) sample B1 was located in the

40°C core holder. The grey grains represent dolomite. The white grains represent the limestone inclusions. The black areas represent porosity.

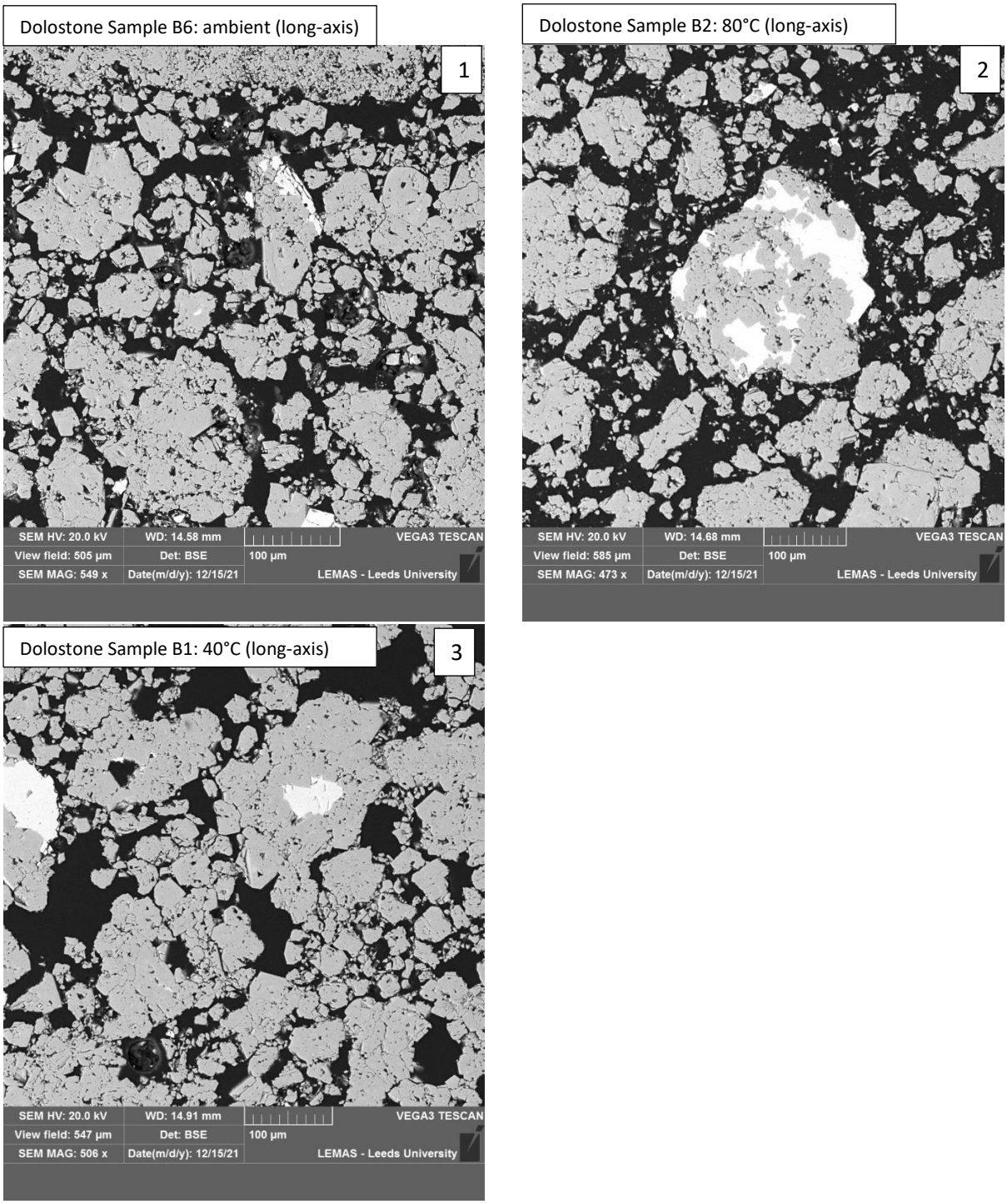

Figure 4.13.1, 4.13.2 and 4.13.3: Backscatter-Electron (BSE) images taken of the grains within the fracture from Dolostone core samples B6, B2 and B1, located in the closed-loop experiment. All photographs are taken from the long-axis section. (1) sample B6 was located in the ambient core holder, (2) sample B2 was located in the 80°C core holder and (3) sample B1 was located in the 40°C core holder. The grey grains represent dolomite. The white grains represent the limestone inclusions. The black areas represent porosity.

Figures 4.12.1 – 4.12.3 show the dolostone fracture in samples B6 (ambient), B2 (80°C) and B1 (40°C). Similar to the limestone, the grains were sieved to approximately 200-250µm before being placed inside the fracture. Overall, the dolostone SEM images portray a high volume of pores and interconnected pores inside the fracture, providing a likely pathway for the fluid during the experiment. On initial inspection, the dolostone appears different to the limestone. The grains inside the fracture appear to be angular to sub-rounded (Figures 4.13.1 – 4.13.3). It should be noted that a natural fracture occurred across the short-axis, half-way down sample B2 (80°C) during the experiment, therefore, some grains within the fracture may have been lost (Figures 4.14 and 4.15). It is thought the natural fracture likely occurred due to the pressure in the system.

Figure 4.14: Photograph of Dolostone Sample B2 after the closed-loop experiment. An evident natural fracture has occurred during the experiment and was discovered after removal of the sample.

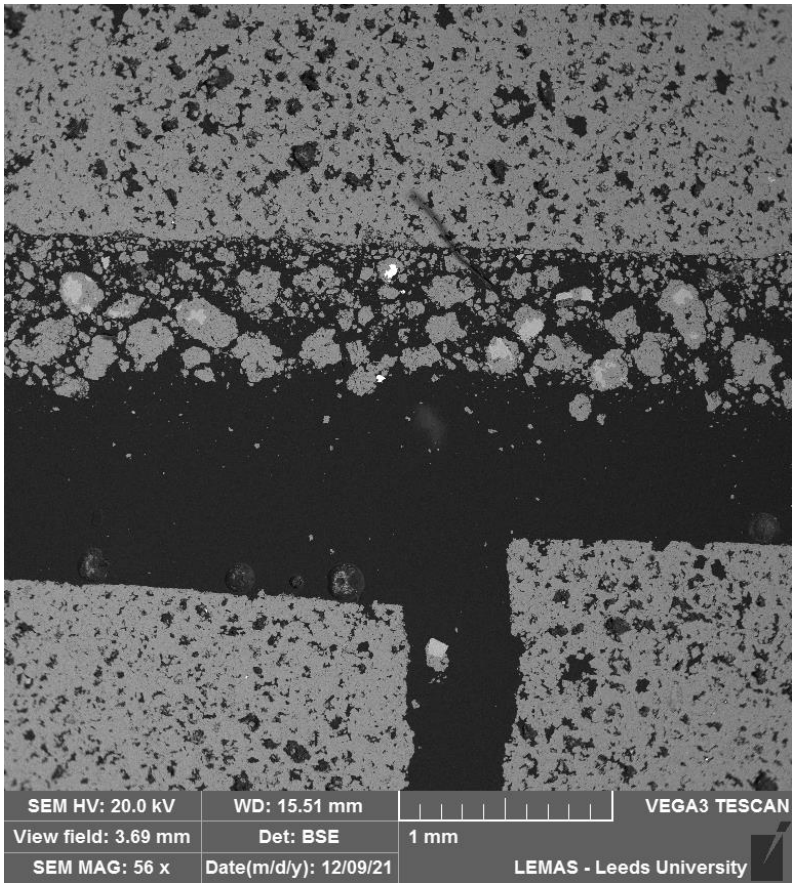

Figure 4.15: SEM image of Dolostone Sample B2 after the closed-loop experiment. An evident natural fracture has occurred during the experiment and was discovered after removal of the sample. The grey grains represent dolomite. The white grains represent the limestone inclusions. The black areas represent porosity.

Figures 4.12.1 – 4.12.3 shows the grey dolostone, black pore spaces and a white to pale grey mineral. Energy-Dispersive Spectroscopy (EDS) analysis was undertaken to determine the composition of this mineral and is discussed in the later section 5.1. The inclusions are also evident in the initial host rock samples pre-experiment (figure 4.17.1).

Figure 4.13.1 – 4.13.3 portrays SEM images of the grains within the fracture at a higher magnitude. Overall, the grains (grey) and pore spaces (black) can be seen clearly here.

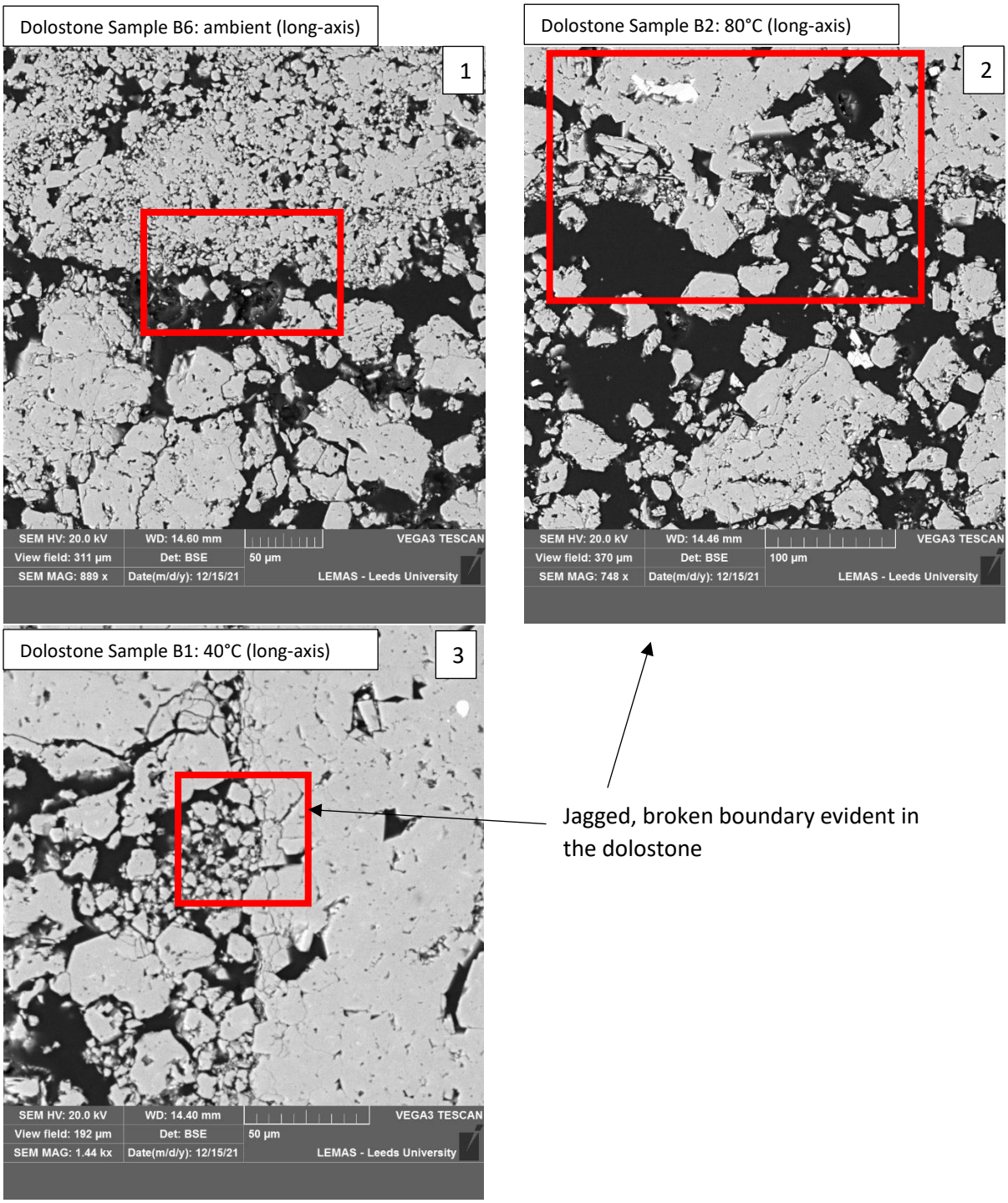

Figure 4.16.1, 4.16.2 and 4.16.3: Backscatter-Electron (BSE) images taken of the fracture boundary from Dolostone core samples B6, B2 and B1, located in the closed-loop experiment. All photographs are taken from the long-axis section. (1) sample B6 was located in the ambient core holder, (2) sample B2 was located in the 80°C core holder and (3) sample B1 was located in the 40°C core holder. The grey grains represent dolomite. The white grains represent the limestone inclusions. The black areas represent porosity.

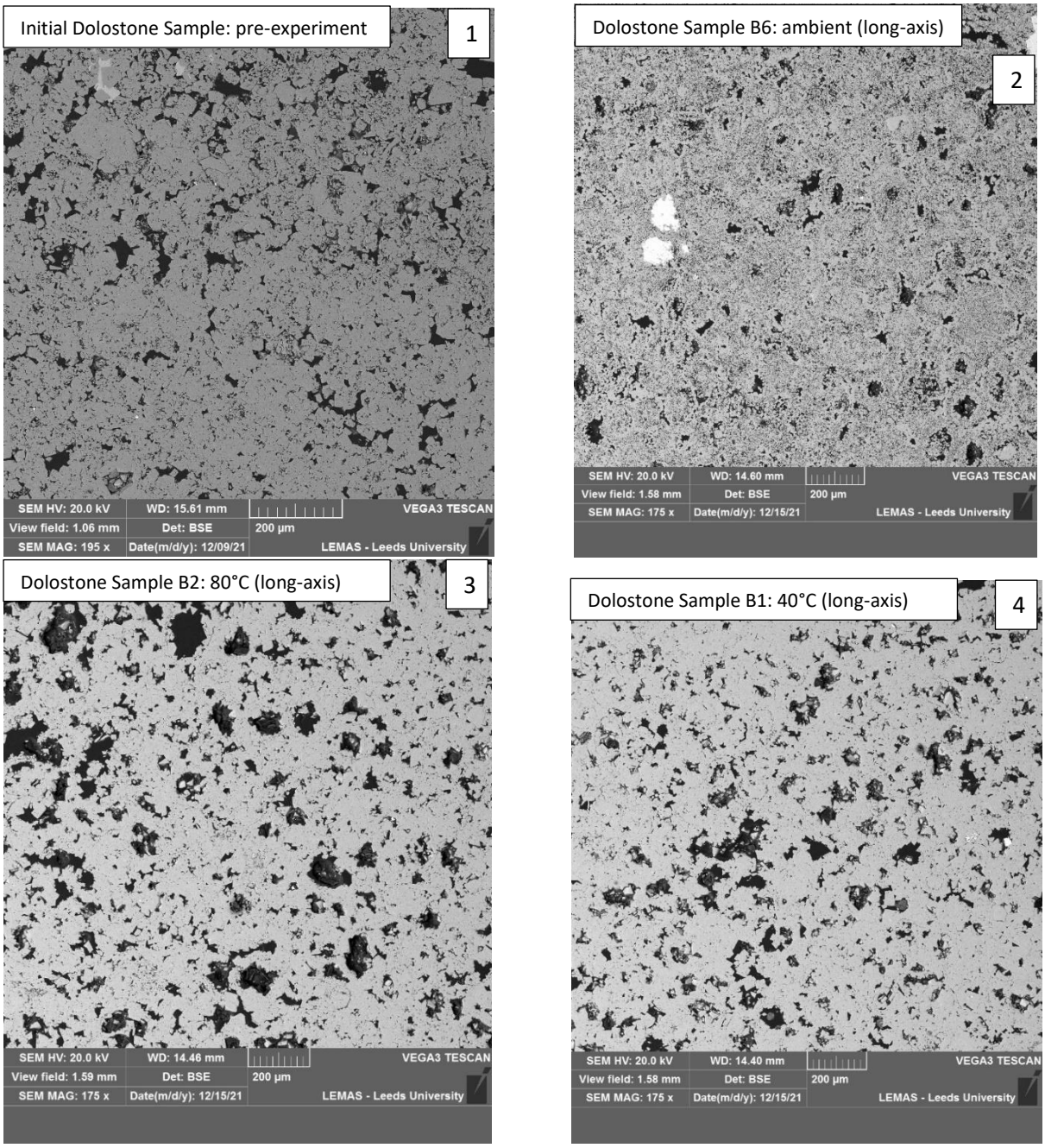

Figure 4.17.1, 4.17.2, 4.17.3 and 4.17.4: Backscatter-Electron (BSE) images taken between 1-2mm of the host rock from Dolostone core samples B6, B2 and B1, located in the closed-loop experiment. All photographs are taken from the long-axis section. (1) Initial dolostone host rock sample pre-experiment (2) sample B6 was located in the ambient core holder, (3) sample B2 was located in the 80°C core holder and (4) sample B1 was located in the 40°C core holder. The grey grains represent dolomite. The white grains represent the limestone inclusions. The black areas represent porosity.

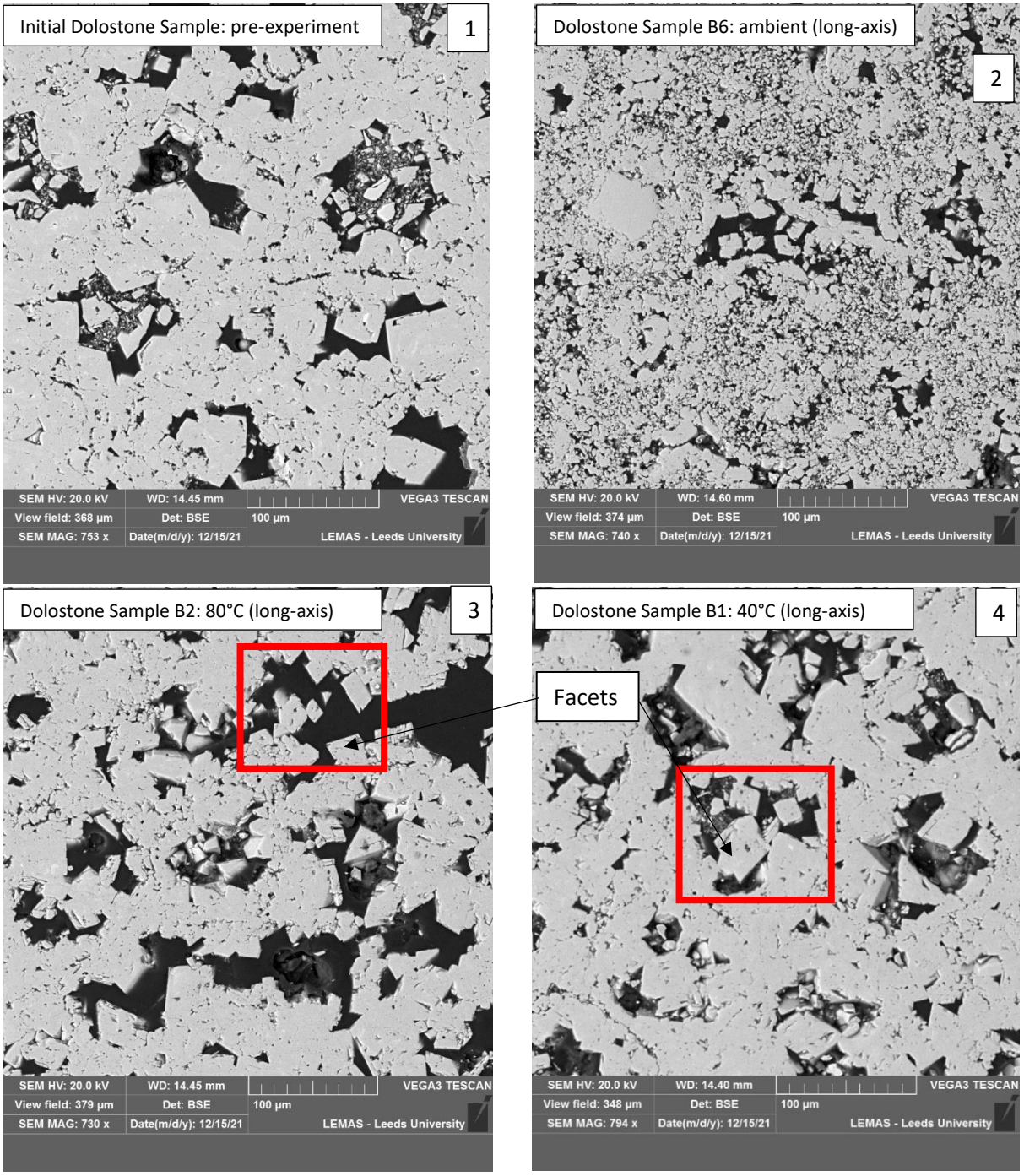

Figure 4.18.1, 4.18.2, 4.18.3 and 4.18.4: Backscatter-Electron (BSE) images taken between 300-400µm of the host rock from Dolostone core samples B6, B2 and B1, located in the closed-loop experiment. All photographs are taken from the long-axis section. (1) Initial dolostone host rock sample pre-experiment (2) sample B6 was located in the ambient core holder, (3) sample B2 was located in the 80°C core holder and (4) sample B1 was located in the 40°C core holder. The grey grains represent dolomite. The white grains represent the limestone inclusions. The black areas represent porosity.

Figures 4.16.1 – 4.16.3 portray the fracture-host boundary in the dolostone samples. The boundary between the fracture and the host rock appears generally more jagged and wavey in comparison to the limestone fracture-host boundary (see previously figures 4.9.1 – 4.9.2).

Figures 4.17.1 – 4.17.4 and 4.18.1 – 4.18.4 portray the host rock in the initial dolostone (pre-experiment), samples B6 (ambient), B2 (80°C) and B1 (40°C) at a magnitude of 1-2mm and 300-400µm, respectively. There are obvious and abundant pores in all dolostone samples in the SEM images.

4.1.3 Limestone Samples: Open-loop Experiment

Limestone samples C, F and E were located in line one in the open-loop experiment. Sample C was located in the ambient core holder, sample F was located in the 80°C core holder and sample E was located in the 40°C core holder respectively.

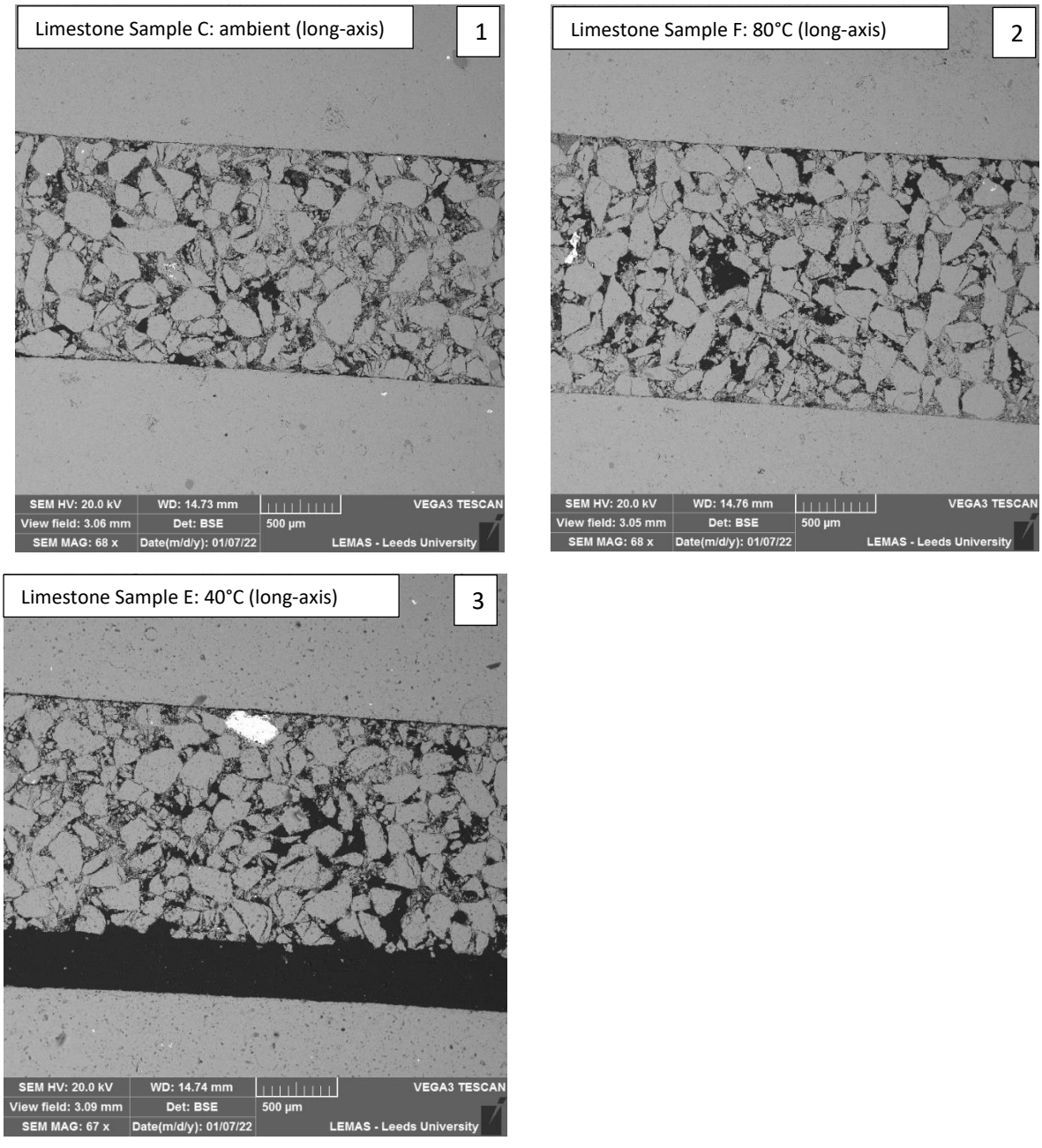

Figure 4.19.1, 4.19.2 and 4.19.3: Backscatter-Electron (BSE) images taken of the fracture from Limestone core samples C, F and E, located in the open-loop experiment. All photographs are taken from the long-axis section. (1) Sample C was located in the ambient core holder, (2) sample F was located in the 80°C core holder and (3) sample E was located in the 40°C core holder. The grey grains represent limestone. The rare white grains represent an un-identified mineral inclusion. The black areas represent porosity.

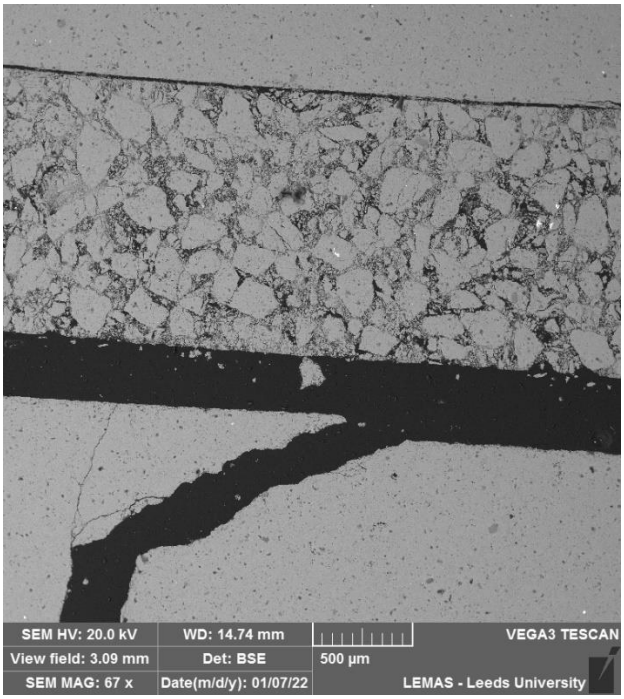

Figure 4.20: SEM image of Limestone Sample E after the open-loop experiment. An evident natural fracture has occurred during the experiment and was discovered after removal of the sample. The grey grains represent limestone. The black areas represent porosity.

Figures 4.19.1 – 4.19.4 portray SEM images of the fractures within the limestone samples C (ambient), F (80°C) and E (40°C), located in the open-loop experiment. Figure 4.19.3 portrays sample E (40°C) with a large gap of grains evident at the bottom of the fracture. Figure 4.20 portrays a natural fracture in sample E (40°C) that was evident post-experiment. It is believed the fracture formed sometime during the experiment, likely due to pressure, and therefore, grains have likely escaped and fallen out the sample. The photographs of the SEM image are likely upside down, therefore explaining why the remaining grains don't appear to have fallen into the evident gap in the fracture. There may also have been further grain-loss during the removal of the sample from the experiment and/or during thin section preparation after the experiment. Sample E (40°C) appears to portray a high number of dark spots in comparison to the other two samples (figures 4.19.1 – 4.19.3; 4.21.1 – 4.21.3; 4.22.1 – 4.22.3). It is believed many of these dark areas are not from potential dissolution creating new pore spaces, but remnants of the resin used to coat the samples to aid with preparation of thin sections. The resin was only meant to cover half the sample; however, the resin potentially infiltrated sample E (40°C) more than samples C (ambient) and F (80°C), resulting in comparatively dark areas evident.

Figures 4.21.1 – 4.21.4 portray SEM images taken at higher magnitude of the grains within the fractures from the limestone samples C (ambient), F (80°C) and E (40°C), located in the open-loop experiment. Figures 4.22.1 – 4.22.2 portray the fracture-host boundary in the limestone samples.

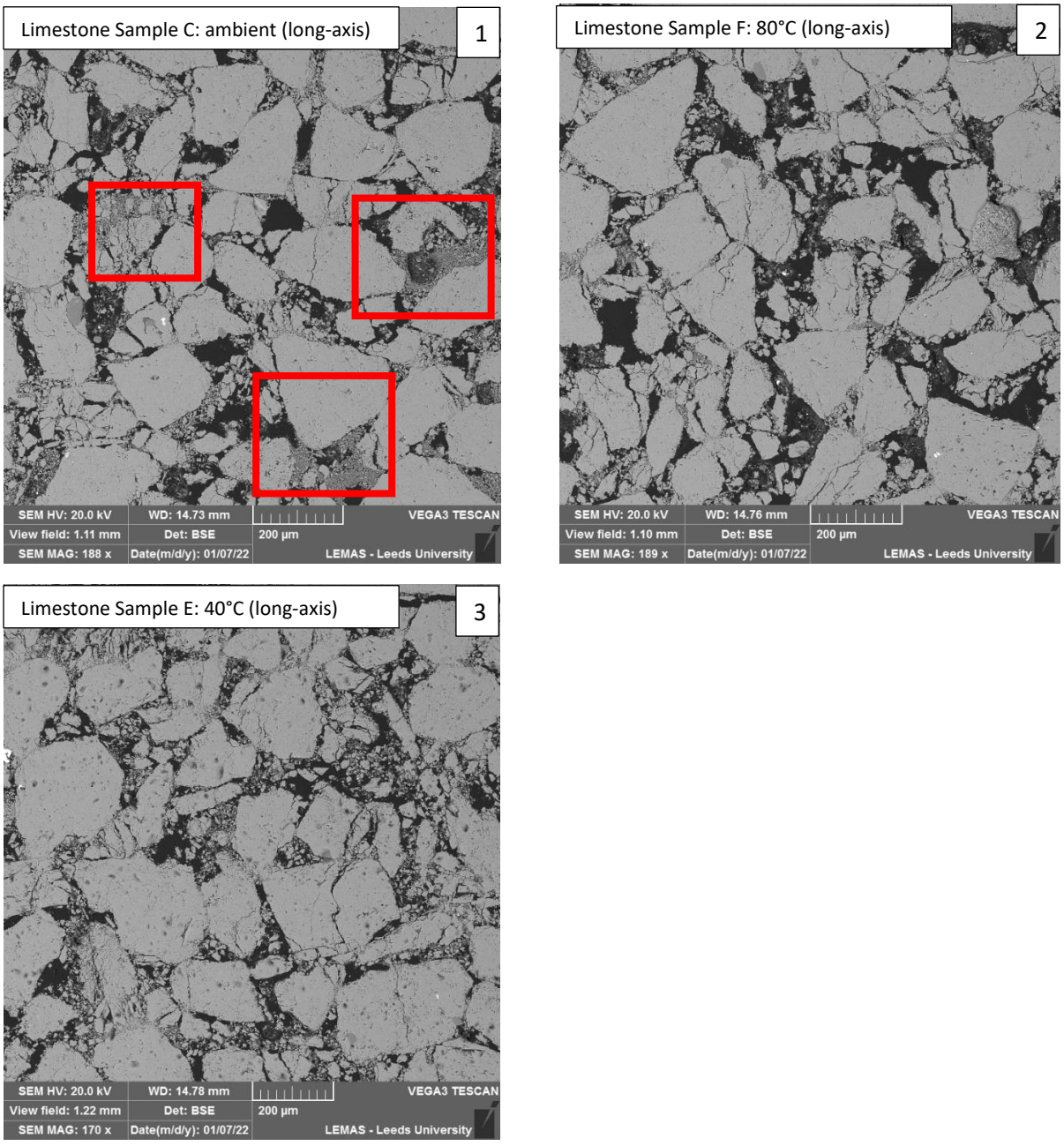

Figure 4.21.1, 4.21.2 and 4.21.3: Backscatter-Electron (BSE) images taken of the grains within the fracture from Limestone core samples C, F and E, located in the open-loop experiment. All photographs are taken from the long-axis section. The red boxes in figure 4.21.1 higlight areas of small-grain accumulation in the pore spaces in the sample. (1) Sample C was located in the ambient core holder, (2) sample F was located in the 80°C core holder and (3) sample E was located in the 40°C core holder. The grey grains represent limestone. The black areas represent porosity.

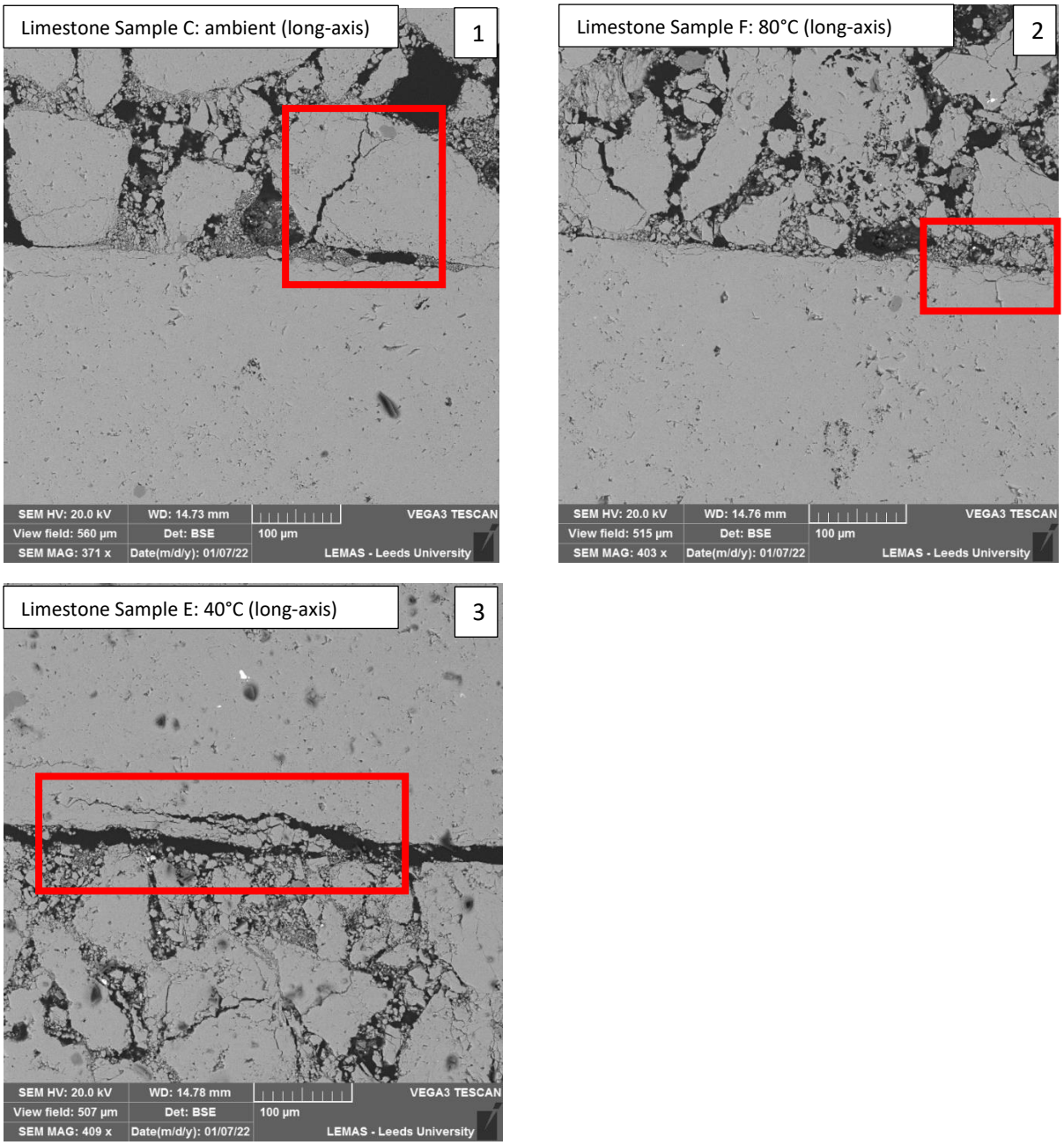

Figure 4.22.1, 4.22.2 and 4.22.3: Backscatter-Electron (BSE) images taken of the fracture boundary from Limestone core samples C, F and E, located in the open-loop experiment. All photographs are taken from the long-axis section. Red boxes highlight the areas of the boundary edge breaking down into small grains. (1) Sample C was located in the ambient core holder, (2) sample F was located in the 80°C core holder and (3) sample E was located in the 40°C core holder. The grey grains represent limestone. The black areas represent porosity.

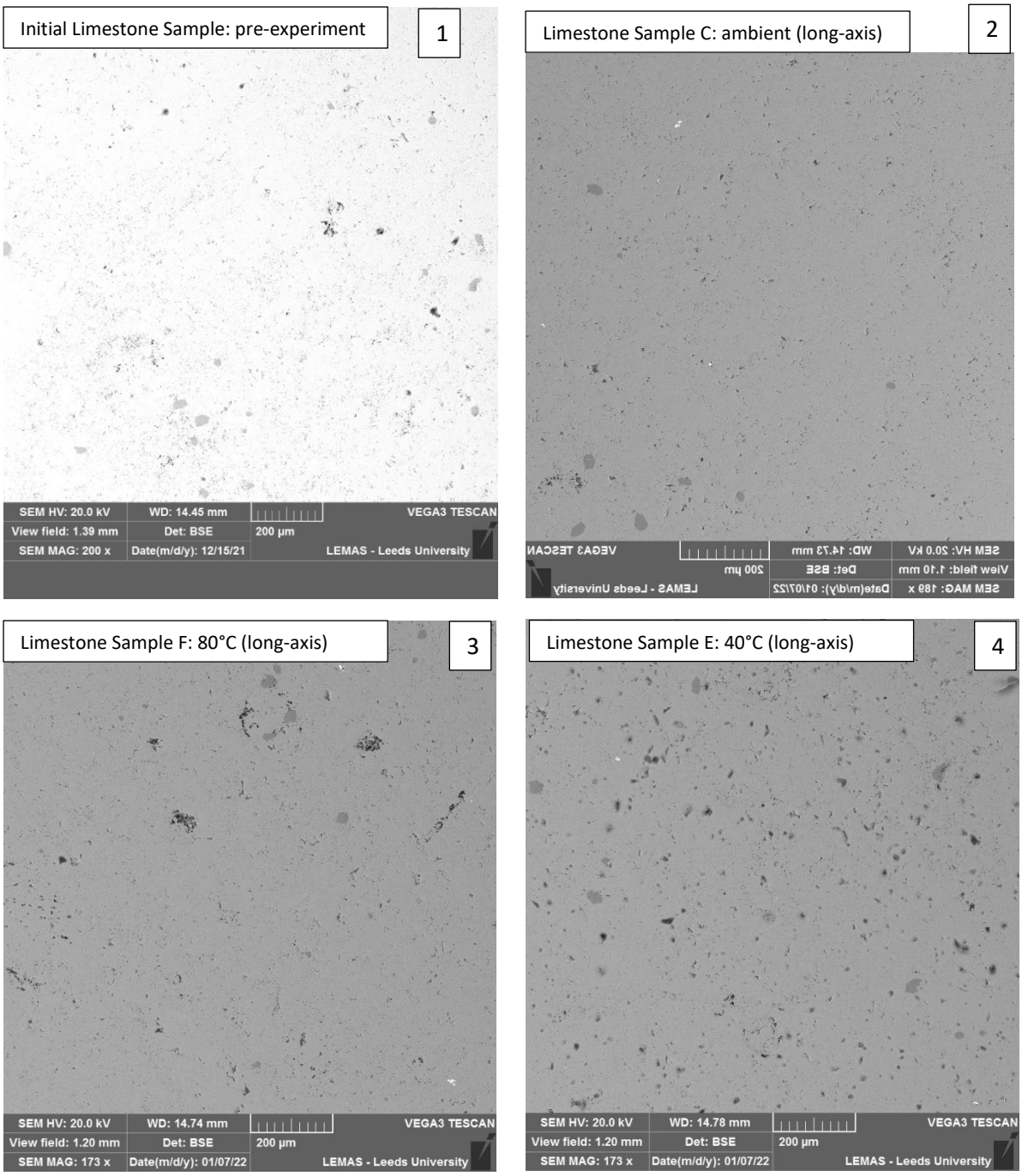

Figure 4.23.1, 4.23.2, 4.23.3 and 4.23.4: Backscatter-Electron (BSE) images taken between 1-2mm of the host rock from Limestone core samples initial, C, F and E, located in the open-loop experiment. All photographs are taken from the long-axis section. (1) Initial limestone sample was taken pre-experiment, (2) sample C was located in the ambient core holder, (3) sample F was located in the 80°C core holder and (4) sample E was located in the 40°C core holder. The grey grains represent limestone. The black areas represent porosity.

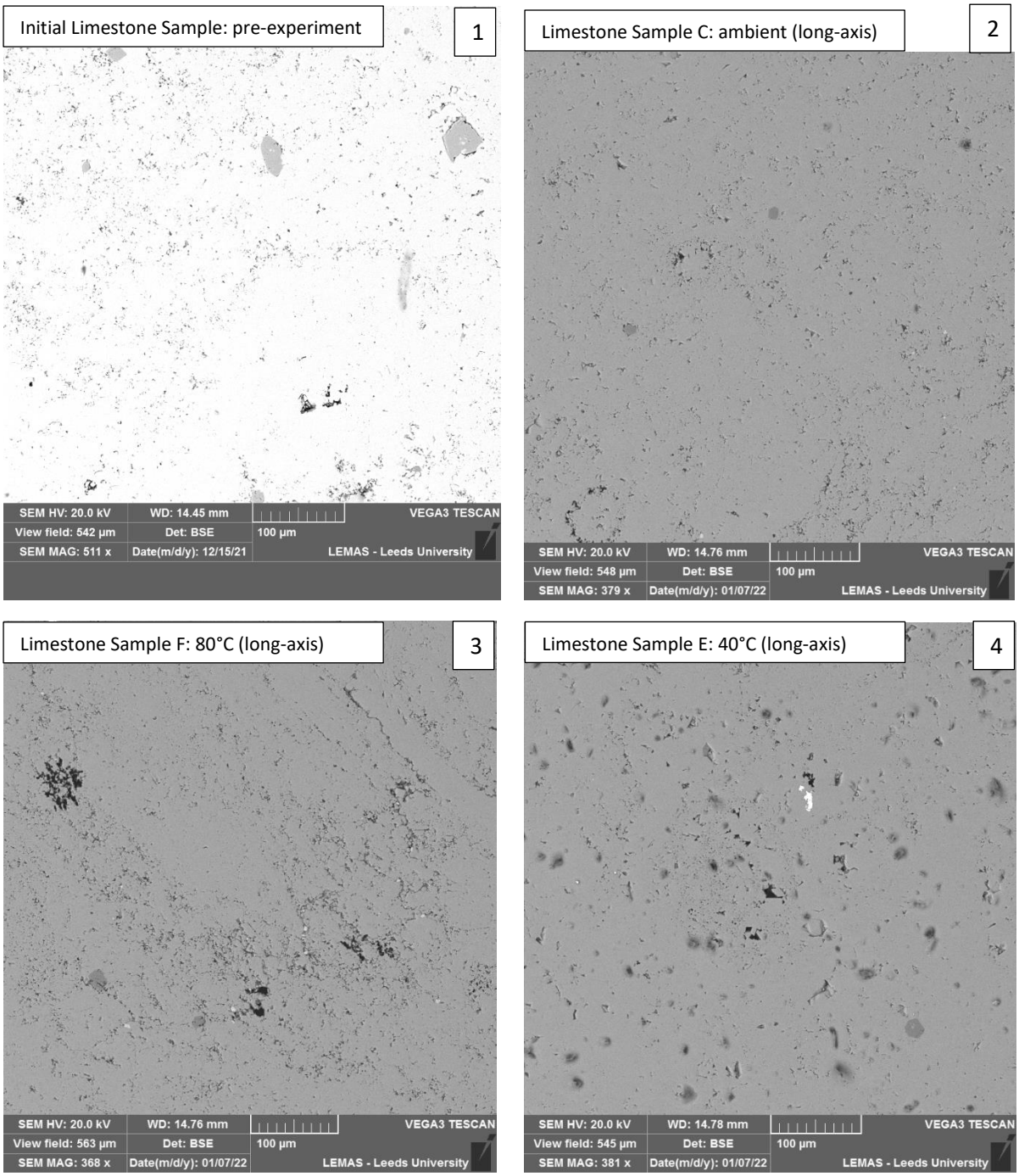

Figure 4.24.1, 4.24.2, 4.24.3 and 4.24.4: Backscatter-Electron (BSE) images taken between 500-600µm of the host rock from Limestone core samples initial, C, F and E, located in the open-loop experiment. All photographs are taken from the long-axis section. (1) Initial limestone sample was taken pre-experiment, (2) sample C was located in the ambient core holder, (3) sample F was located in the 80°C core holder and (4) sample E was located in the 40°C core holder. The grey grains represent limestone. The black areas represent porosity.

Figures 4.23.1 – 4.23.4 show the porosity of the host rock in the limestone, during the open-loop experiment, with a scale of between 1-2mm. Figures 4.24.1 – 4.24.4 show the porosity of the host rock in the limestone, with a scale of between 500-600µm. As previously mentioned above, it is believed many of the dark spots evident in the host rock of sample E (40°C) are remnants from the

resin used to prepare sample E (40°C) to be made into a thin section (figures 4.23.1 – 4.23.4; 4.24.1 – 4.24.4).

4.1.4 Dolostone Samples: Open-loop Experiment

Dolostone samples B5, B4 and B3 were situated in line two in the open-loop experiment. Sample B5 was located in the ambient core holder, sample B4 was located in the 80°C core holder and sample B3 was located in the 40°C core holder respectively.

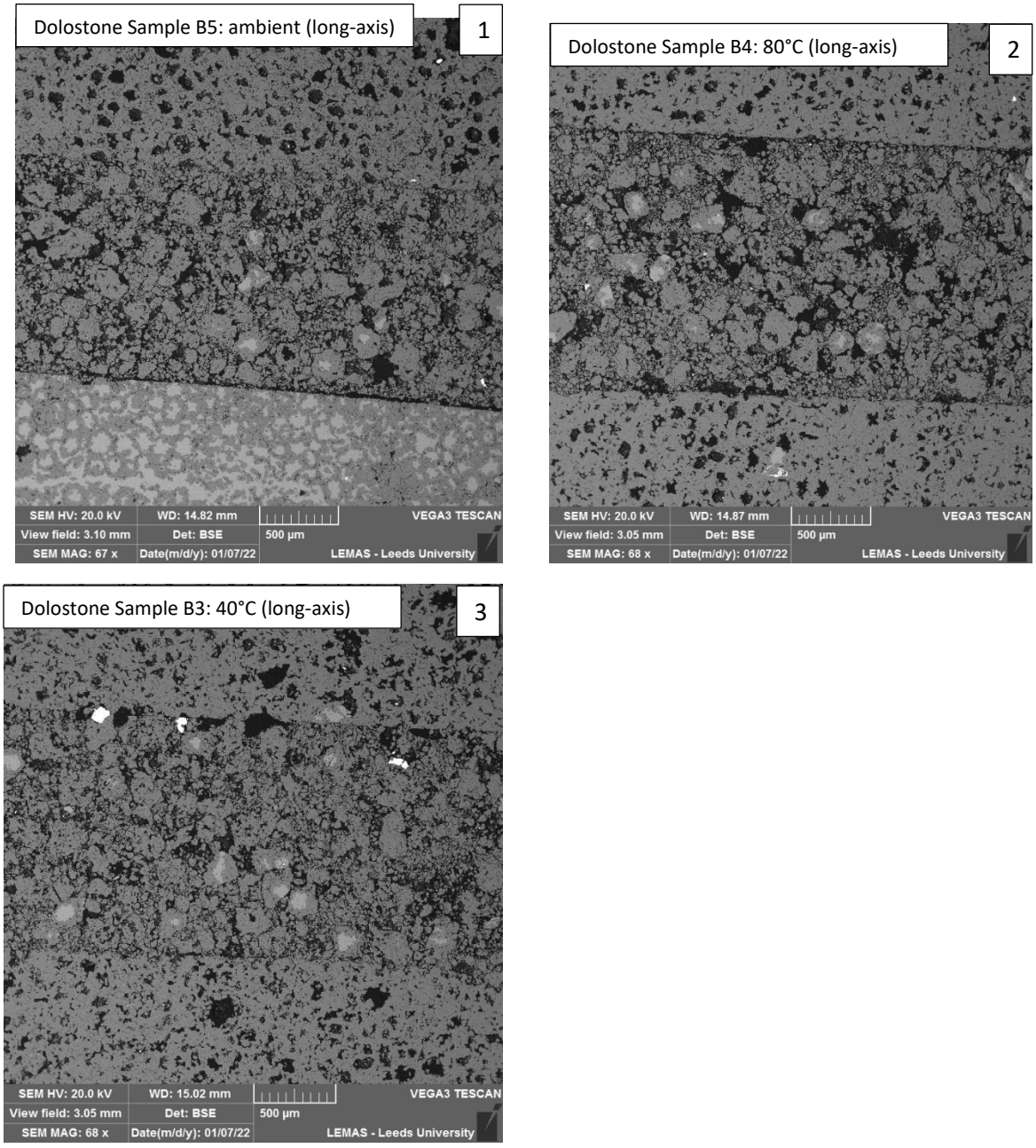

Figure 4.25.1, 4.25.2 and 4.25.3: Backscatter-Electron (BSE) images taken of the fracture from Dolostone core samples B5, B4 and B3, located in the open-loop experiment. All photographs are taken from the long-axis section. (1) Sample B5 was

located in the ambient core holder, (2) sample B4 was located in the 80°C core holder and (3) sample B3 was located in the 40°C core holder. The dark grey grains represent dolomite. The pale grey grains represent limestone inclusions. The black areas represent porosity.

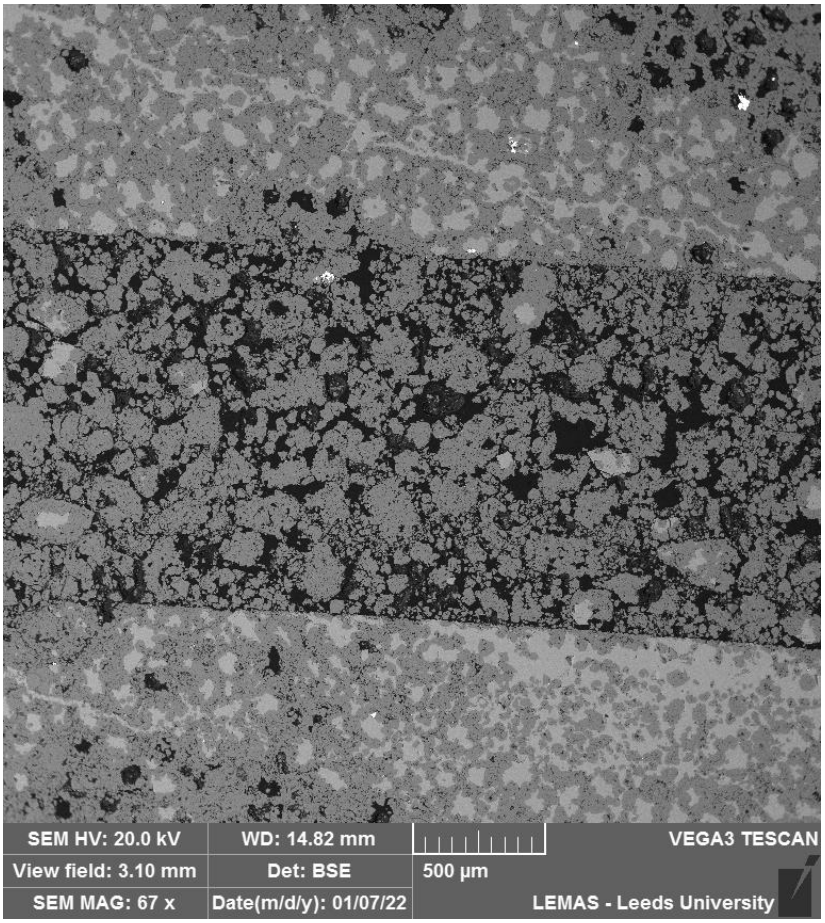

Figure 4.26: SEM image of Dolostone Sample B5 after the open-loop experiment. Ca-rich inclusions are evident surrounding the fracture. The dark grey grains represent dolomite. The pale grey grains represent limestone inclusions. The black areas represent porosity.

Figures 4.25.1 – 4.25.3 portray SEM images of the dolostone samples B5 (ambient), B4 (80°C) and B3 (40°C), after the open-loop experiment. Figure 4.26 portrays sample B5 (ambient) due to having an unusual amount of the Ca-rich inclusion surrounding the fracture. Figures 4.27.1 – 4.27.3 portray SEM images, with a higher magnitude, of the grains within the fracture in the dolostone samples. Figures 4.28.1 – 4.28.3 portray the fracture-host boundary in the dolostone samples, taken after the open-loop experiment.

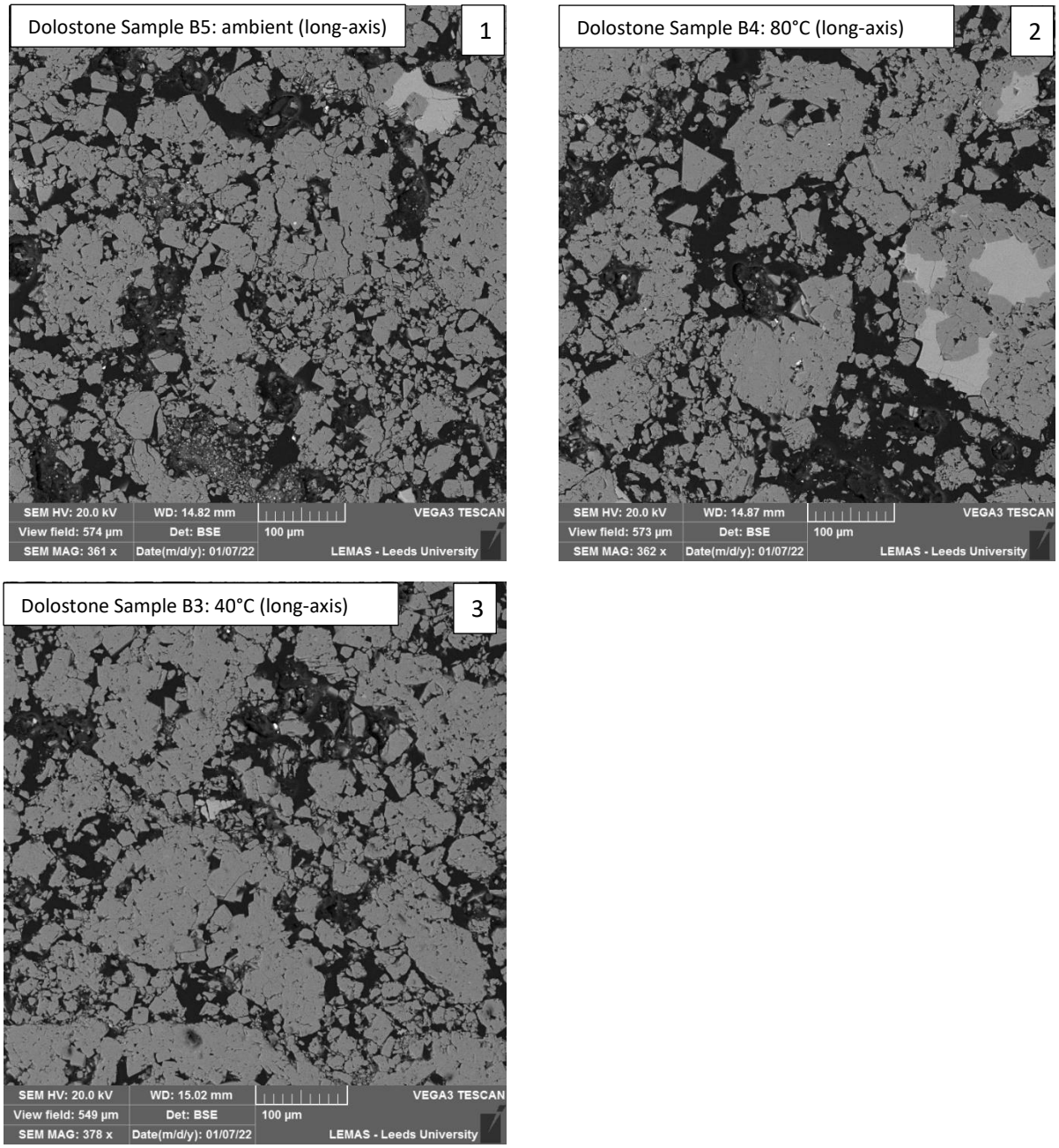

Figure 4.27.1, 4.27.2 and 4.27.3: Backscatter-Electron (BSE) images taken of the grains within the fracture from Dolostone core samples B5, B4 and B3, located in the open-loop experiment. All photographs are taken from the long-axis section. (1) Sample B5 was located in the ambient core holder, (2) sample B4 was located in the 80°C core holder and (3) sample B3 was located in the 40°C core holder. The dark grey grains represent dolomite. The pale grey grains represent limestone inclusions. The black areas represent porosity.

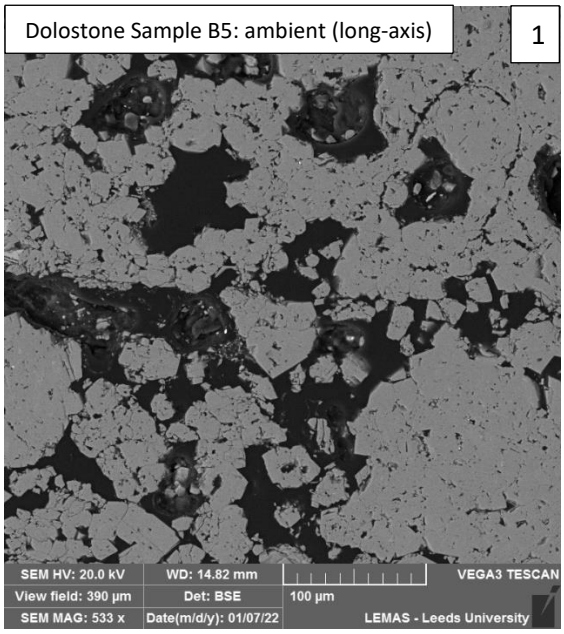

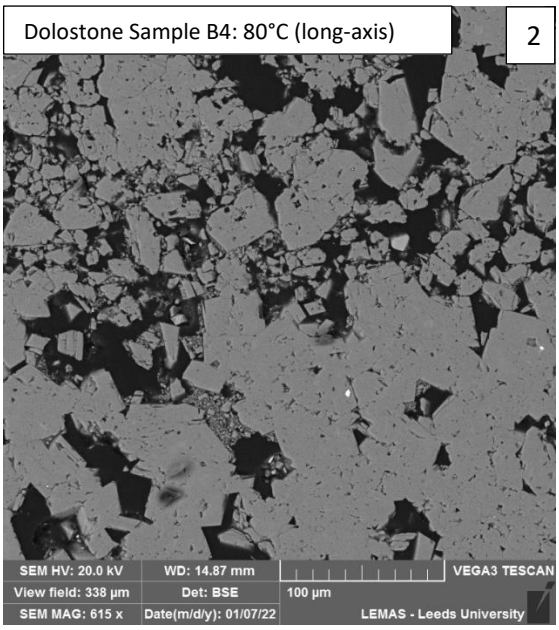

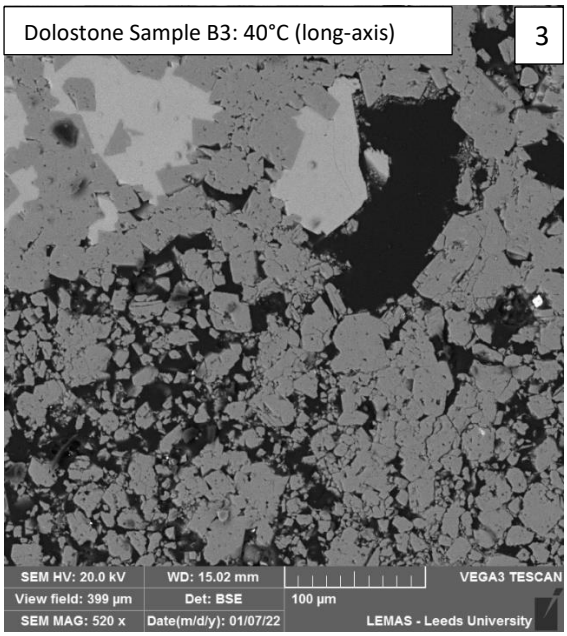

Figure 4.28.1, 4.28.2 and 4.28.3: Backscatter-Electron (BSE) images taken of the fracture boundary from Dolostone core samples B5, B4 and B3, located in the open-loop experiment. All photographs are taken from the long-axis section. (1) Sample B5 was located in the ambient core holder, (2) sample B4 was located in the 80°C core holder and (3) sample B3 was located in the 40°C core holder. The dark grey grains represent dolomite. The pale grey grains represent limestone inclusions. The black areas represent porosity.

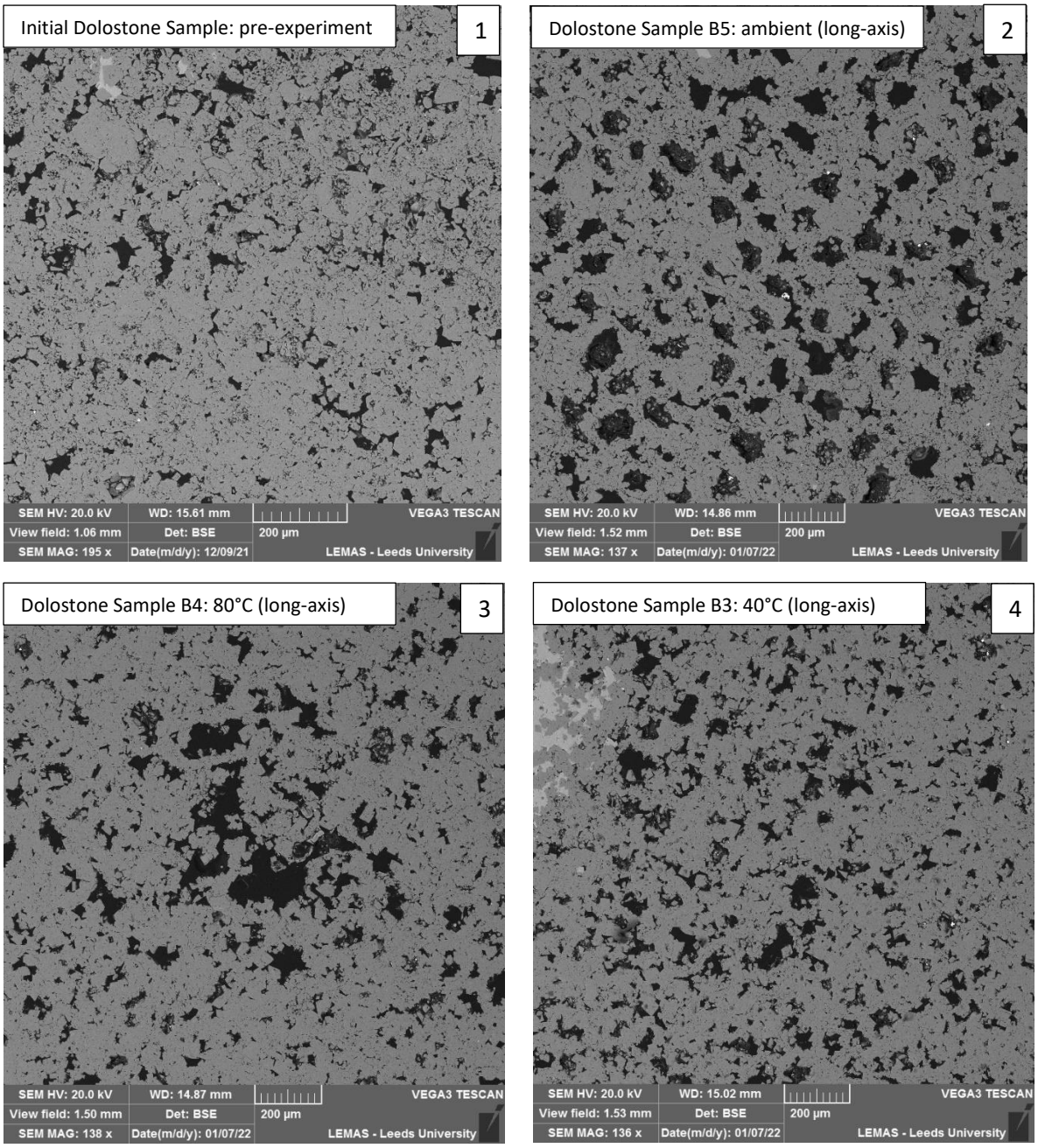

Figure 4.29.1, 4.29.2, 4.29.3 and 4.29.4: Backscatter-Electron (BSE) images taken between 1-2mm of the host rock from Dolostone core samples initial, B5, B4 and B3, located in the open-loop experiment. All photographs are taken from the long-axis section. (1) Initial limestone sample was taken pre-experiment, (2) sample B5 was located in the ambient core holder, (3) sample B4 was located in the 80°C core holder and (4) sample B3 was located in the 40°C core holder. The dark grey grains represent dolomite. The pale grey grains represent limestone inclusions. The black areas represent porosity.

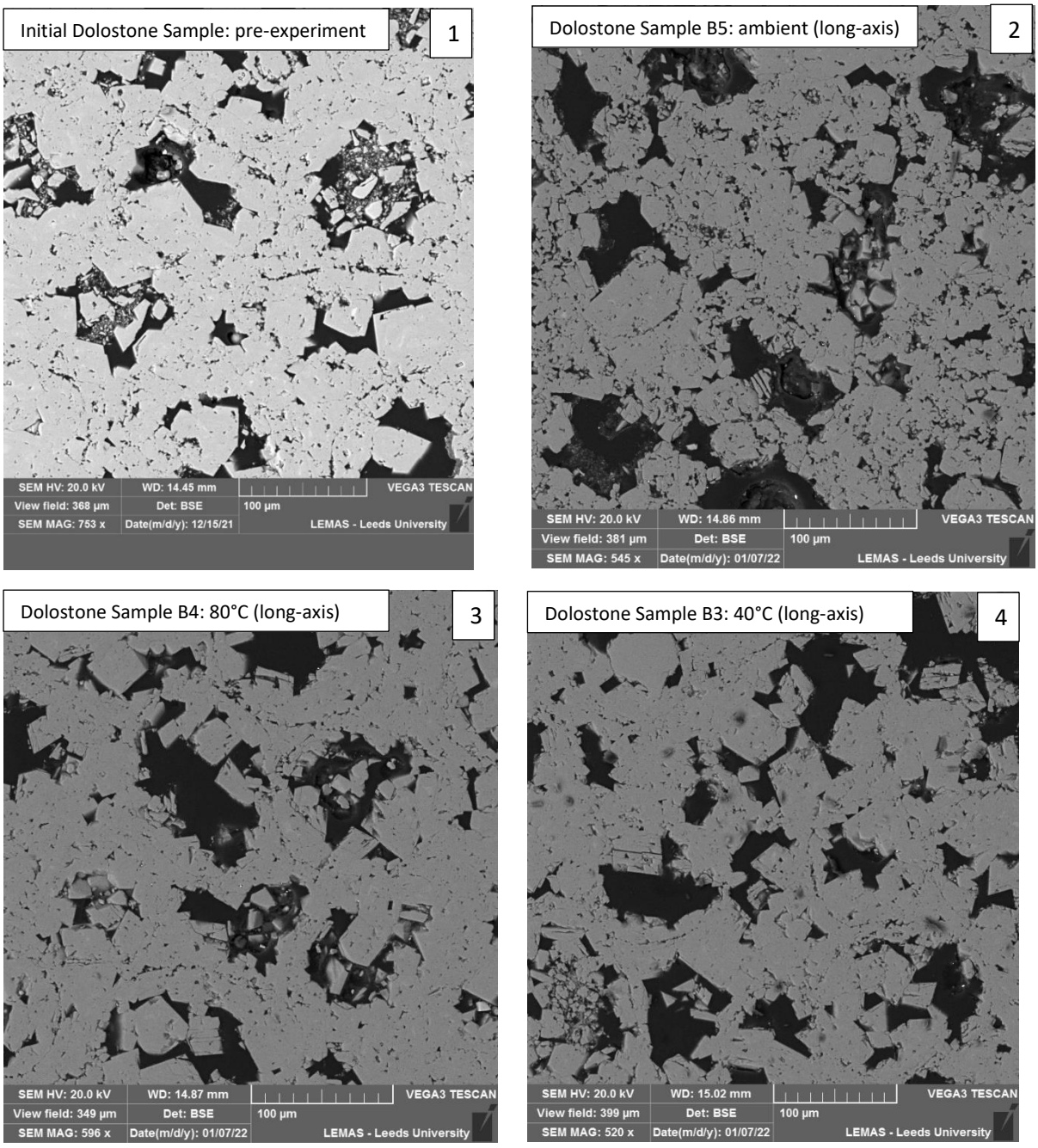

Figure 4.30.1, 4.30.2, 4.30.3 and 4.30.4: Backscatter-Electron (BSE) images taken between 300-400µm of the host rock from Dolostone core samples initial, B5, B4 and B3, located in the open-loop experiment. All photographs are taken from the long-axis section. (1) Initial limestone sample was taken pre-experiment, (2) sample B5 was located in the ambient core holder, (3) sample B4 was located in the 80°C core holder and (4) sample B3 was located in the 40°C core holder. The dark grey grains represent dolomite. The pale grey grains represent limestone inclusions. The black areas represent porosity.

Figures 4.29.1 – 4.29.4 show the porosity of the host rock of the dolostone samples, during the open-loop experiment, with a scale of between 1-2mm. Figures 4.30.1 – 4.30.4 show the porosity of the host rock in the dolostone samples, with a scale of between 500-600µm. The SEM images presented during this section will be discussed in section 5.

4.2 CT Scan Results

The limestone and dolostone samples were CT scanned pre-experiment; before and after being fractured, and post-experiment. To capture the core sample, the CT scanner captures multiple image slides to portray an entire core. The images below have been selected from approximately the centre of the core sample, to avoid images showing loss of grains from the edge of the core sample. The images have undergone ImageJ analysis, whereby a cross-section, perpendicular to the fracture, has been taken to determine the number of grains present inside the artificial fracture in the sample (Schneider et al. 2012). The ImageJ analysis works by displaying a two-dimensional graph based on the grey-scale intensity of the pixels in the image (Ferreira and Rasband 2012). Comparing the number of grains in the fracture is key to understand the porosity and permeability changes within the samples. Depending on whether there has been dissolution or precipitation in the fracture, will determine the amount of space there is for fluid to flow. If the fracture appears to be more cemented after the experiment, it is possible precipitation occurred within the fracture, therefore reducing the permeability. Therefore, the CT scan images will enable for the comparison of the fracture permeability, before and after the experiment. When comparing the CT scan images, an image has been selected of the core samples from before and after the closed-loop or open-loop experiment. The slide numbers may not appear to align with one another before and after the experiment, however this is due to slide numbers changing depending on; (1) whether they were scanned with a metal end-piece (as the core samples located in the 80°C oven required longer sleeves and therefore, metal end-pieces) or (2) whether they were scanned alongside another core sample. One issue that has been identified when undertaking the ImageJ analysis is that the yellow cross-section lines are merely hand-drawn, and therefore may not be accurate on both samples.

4.2.1 Limestone: Closed-loop Experiment

The limestone CT scan images appear to show little detail. However, as the main focus is comparing the level of cementation in the fracture, they are deemed suitable to undergo ImageJ analysis. The following section will portray the CT scan images of the limestone core samples from the closed-loop experiment. Figures 4.31.1 and 4.31.2 portrays limestone sample B (ambient), using slide 28 (before the experiment) and slide 20 (after the experiment) from the sample B CT scan images. Figures 4.32.1 and 4.32.2 portrays limestone sample A (80°C), using slide 39 (before the experiment) and slide 40 (after the experiment) from the sample A CT scan images. Figures 4.33.1 and 4.33.2 portrays limestone sample D (40°C), using slide 43 (before the experiment) and slide 43 (after the experiment) from the sample D CT scan images.

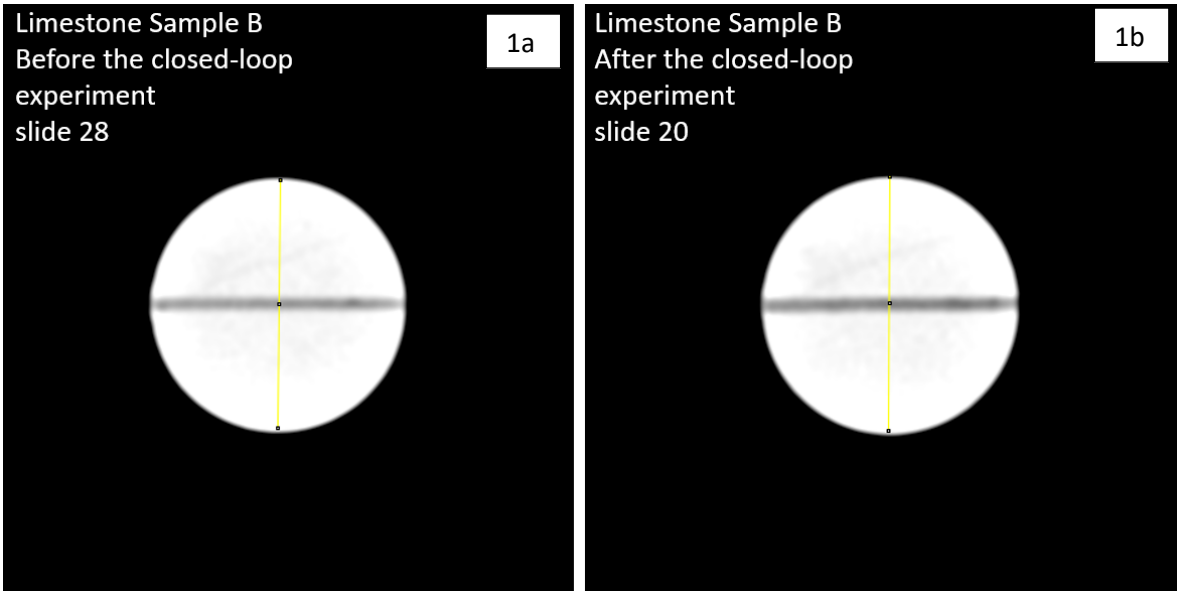

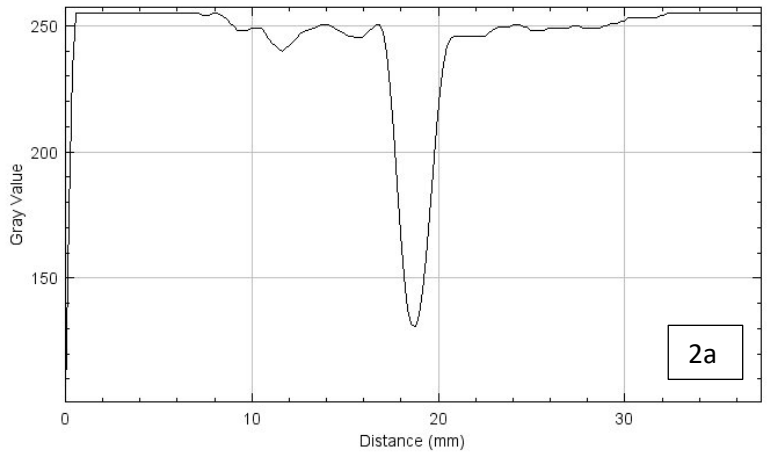

Graph to show the intensity of pixels in Limestone Sample B, from slide 28, before the closed-loop experiment

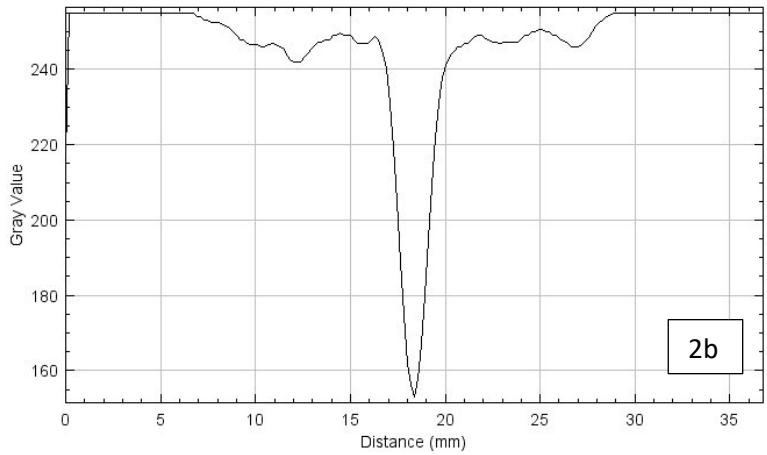

Graph to show the intensity of pixels in Limestone Sample B, from slide 20, after the closed-loop experiment

Figure 4.31.1a, 4.31.1b, 4.31.2a and 4.31.2b: (1 a-b) CT scan image of limestone sample B (ambient) showing an image slide, taken from approximately the centre of the core sample, before and after the closed-loop experiment. The yellow line on the CT scan image portrays the cross-section line used to produce the pixel intensity graph. (2 a-b) Two-dimensional graph to show the grey-scale intensity of the pixels in the CT scan image vs. the distance along the line. The x-axis represents the distance along the line and the y-axis represents the grey value, i.e., the pixel intensity.

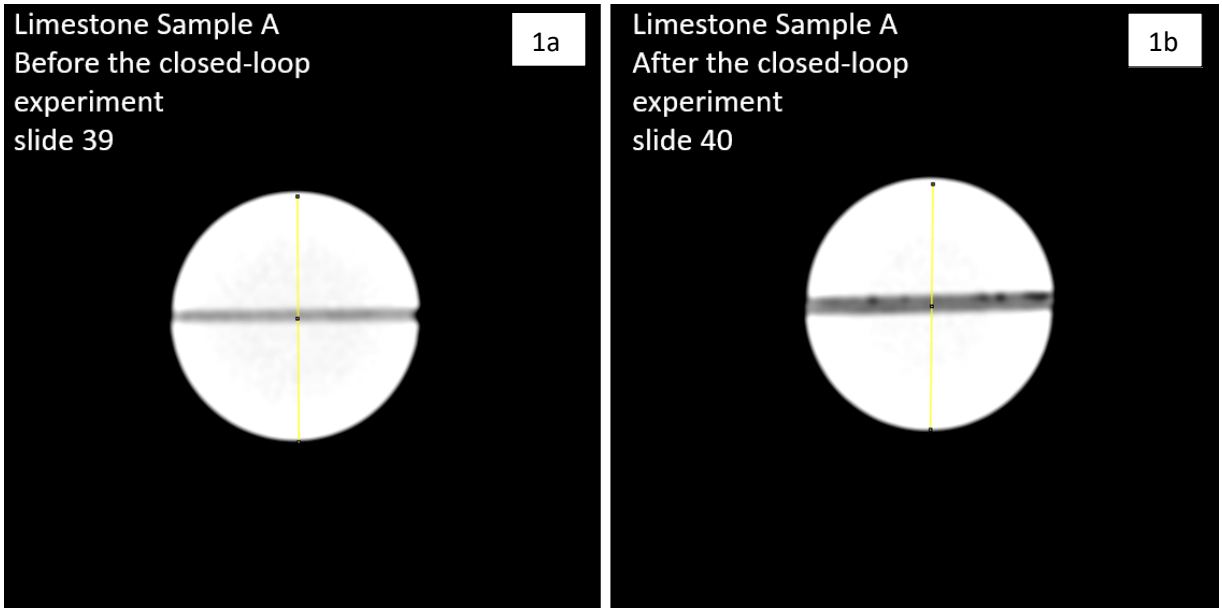

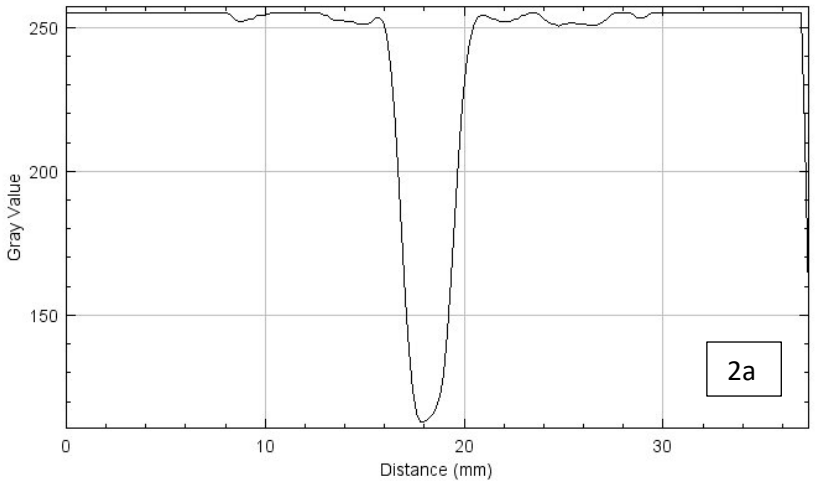

Graph to show the intensity of pixels in Limestone Sample A, from slide 39, before the closed-loop experiment

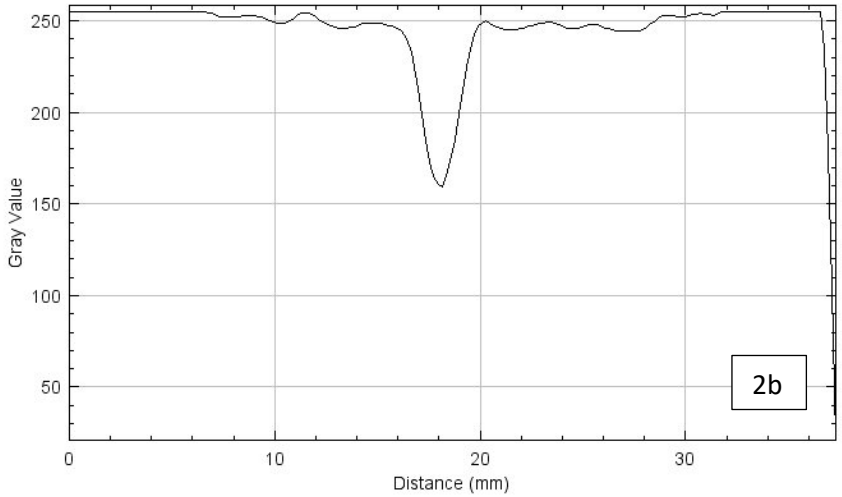

Graph to show the intensity of pixels in Limestone Sample A, from slide 40, after the closed-loop experiment

Figure 4.32.1a, 4.32.1b, 4.32.2a and 4.32.2b: (1 a-b) CT scan image of limestone sample A (80°C) showing an image slide, taken from approximately the centre of the core sample, before and after the closed-loop experiment. The yellow line on the CT scan image portrays the cross-section line used to produce the pixel intensity graph. (2 a-b) Two-dimensional graph to show the grey-scale intensity of the pixels in the CT scan image vs. the distance along the line. The x-axis represents the distance along the line and the y-axis represents the grey value, i.e., the pixel intensity.

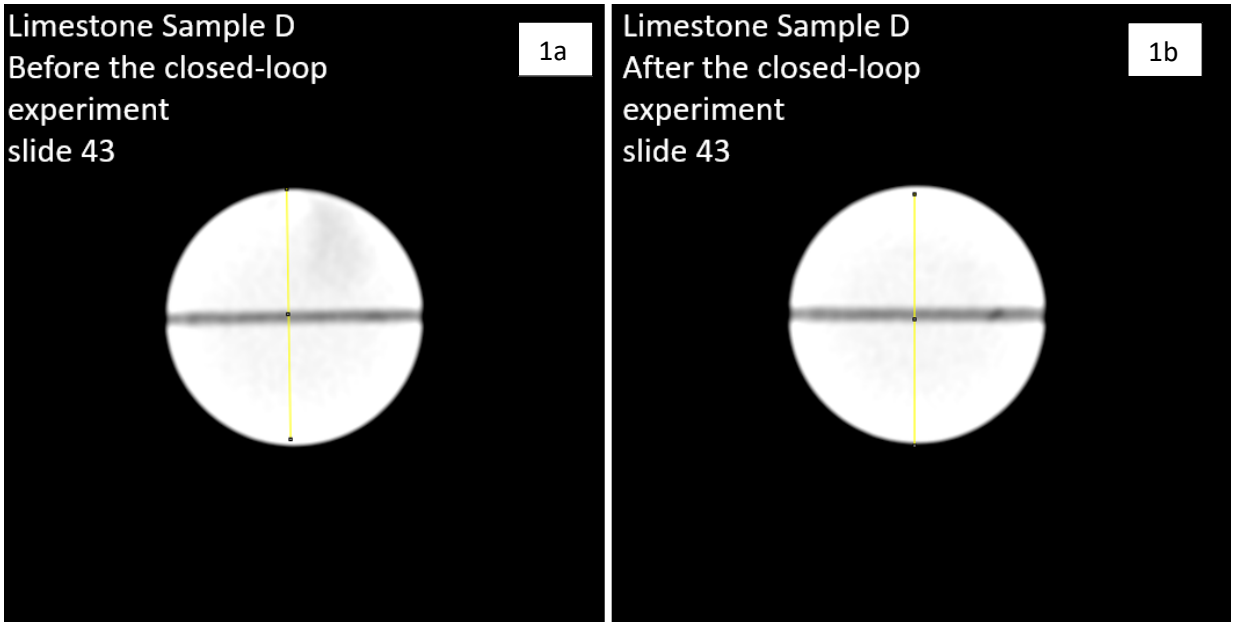

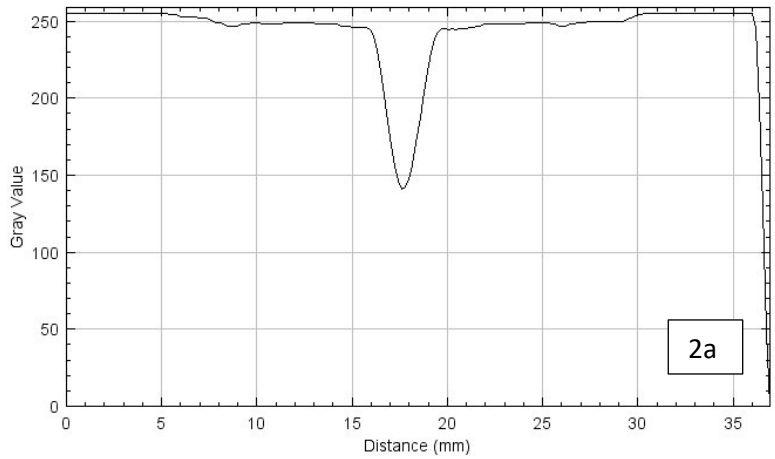

Graph to show the intensity of pixels in Limestone Sample D, from slide 43, before the closed-loop experiment

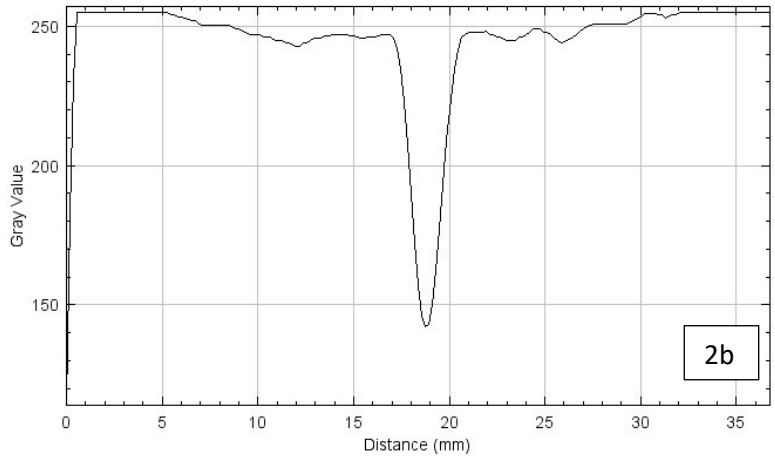

Graph to show the intensity of pixels in Limestone Sample D, from slide 43, after the closed-loop experiment

Figure 4.33.1a, 4.33.1b, 4.33.2a and 4.33.2b: (1 a-b) CT scan image of limestone sample D (40°C) showing an image slide, taken from approximately the centre of the core sample, before and after the closed-loop experiment. The yellow line on the CT scan image portrays the cross-section line used to produce the pixel intensity graph. (2 a-b) Two-dimensional graph to show the grey-scale intensity of the pixels in the CT scan image vs. the distance along the line. The x-axis represents the distance along the line and the y-axis represents the grey value, i.e., the pixel intensity.

4.2.2 Dolostone: Closed-loop Experiment

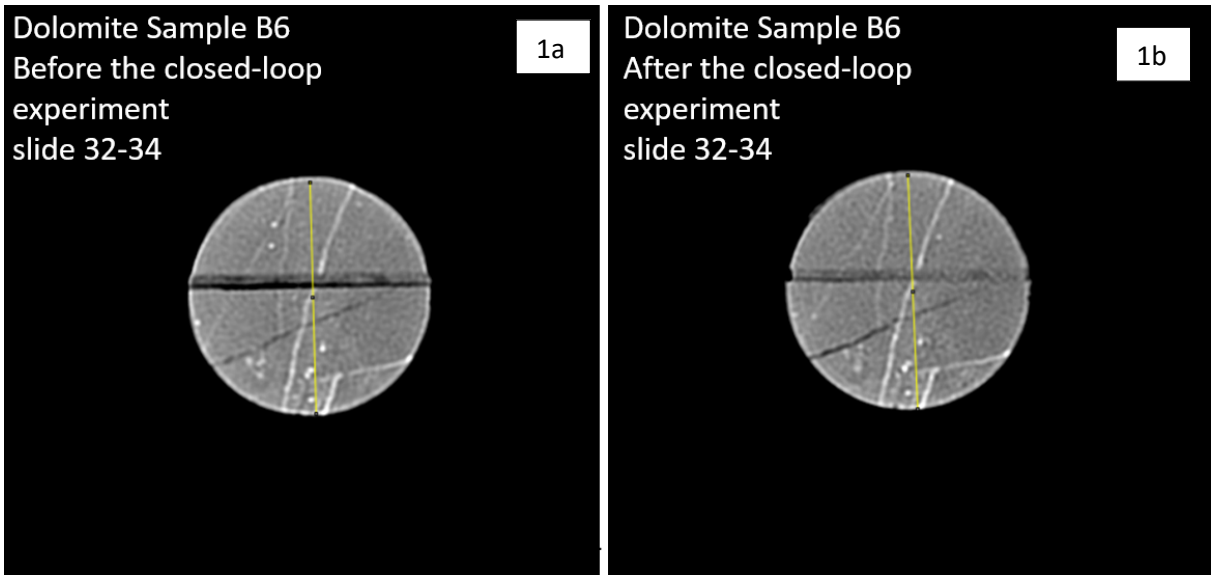

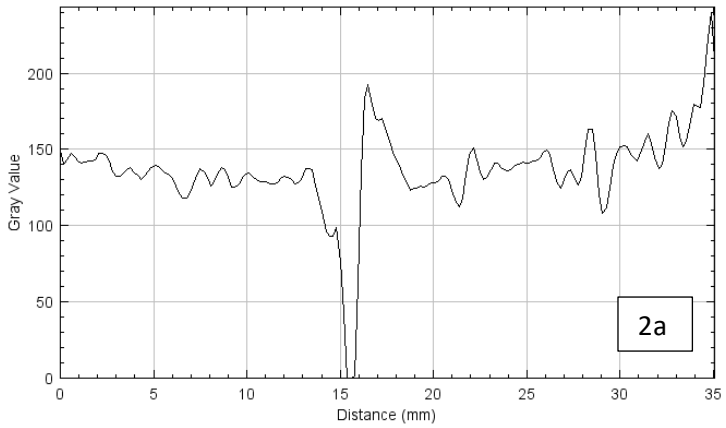

Graph to show the intensity of pixels in Dolostone Sample B6, from slide 32-34, before the closed-loop experiment

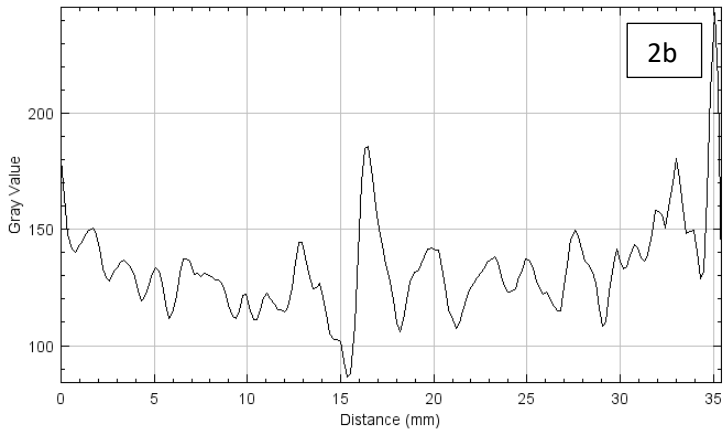

Graph to show the intensity of pixels in Dolostone Sample B6, from slide 32-34, after the closed-loop experiment

Figure 4.34.1a, 4.34.1b, 4.34.2a and 4.34.2b: (1 a-b) CT scan image of dolostone sample B6 (ambient) showing an image slide, taken from approximately the centre of the core sample, before and after the closed-loop experiment. The yellow line on the CT scan image portrays the cross-section line used to produce the pixel intensity graph. (2 a-b) Two-dimensional graph to show the grey-scale intensity of the pixels in the CT scan image vs. the distance along the line. The x-axis represents the distance along the line and the y-axis represents the grey value, i.e., the pixel intensity.

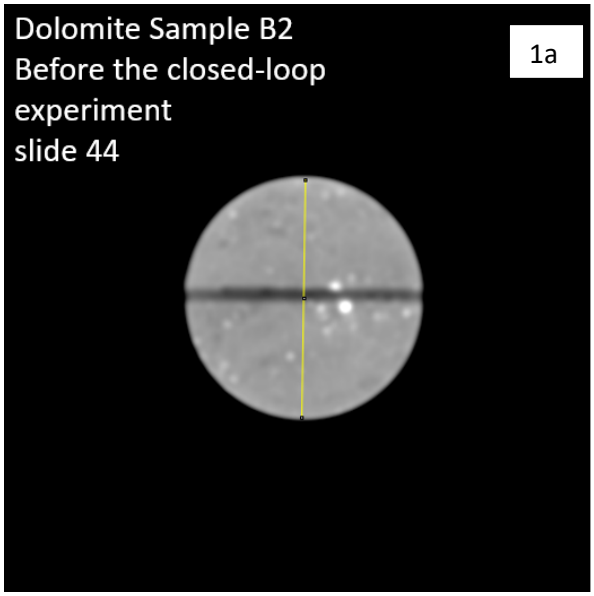

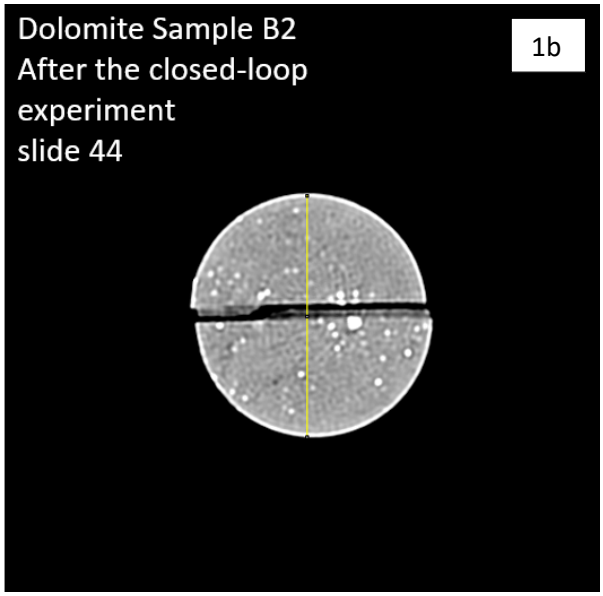

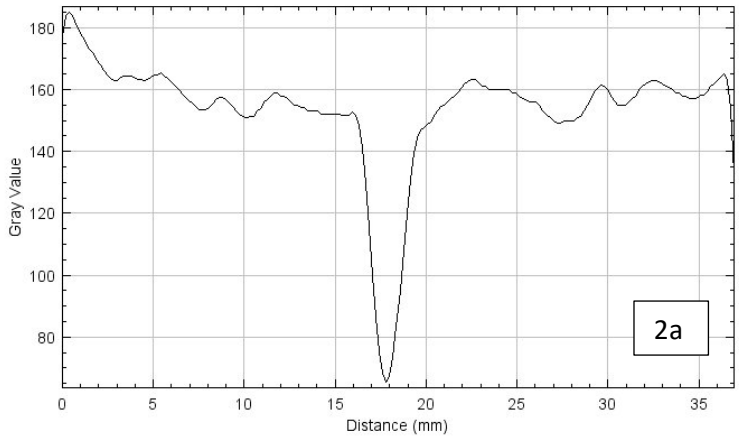

Graph to show the intensity of pixels in Dolostone Sample B2, from slide 44, before the closed-loop experiment

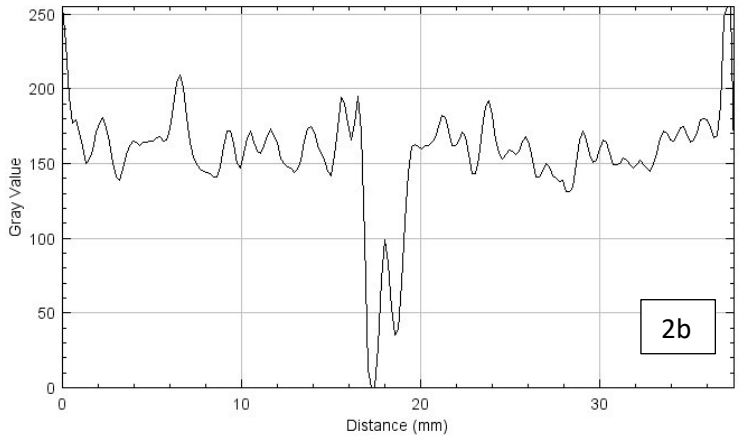

Graph to show the intensity of pixels in Dolostone Sample B2, from slide 44, after the closed-loop experiment

Figure 4.35.1a, 4.35.1b, 4.35.2a and 4.35.2b: (1 a-b) CT scan image of dolostone sample B2 (80°C) showing an image slide, taken from approximately the centre of the core sample, before and after the closed-loop experiment. The yellow line on the CT scan image portrays the cross-section line used to produce the pixel intensity graph. (2 a-b) Two-dimensional graph to show the grey-scale intensity of the pixels in the CT scan image vs. the distance along the line. The x-axis represents the distance along the line and the y-axis represents the grey value, i.e., the pixel intensity.

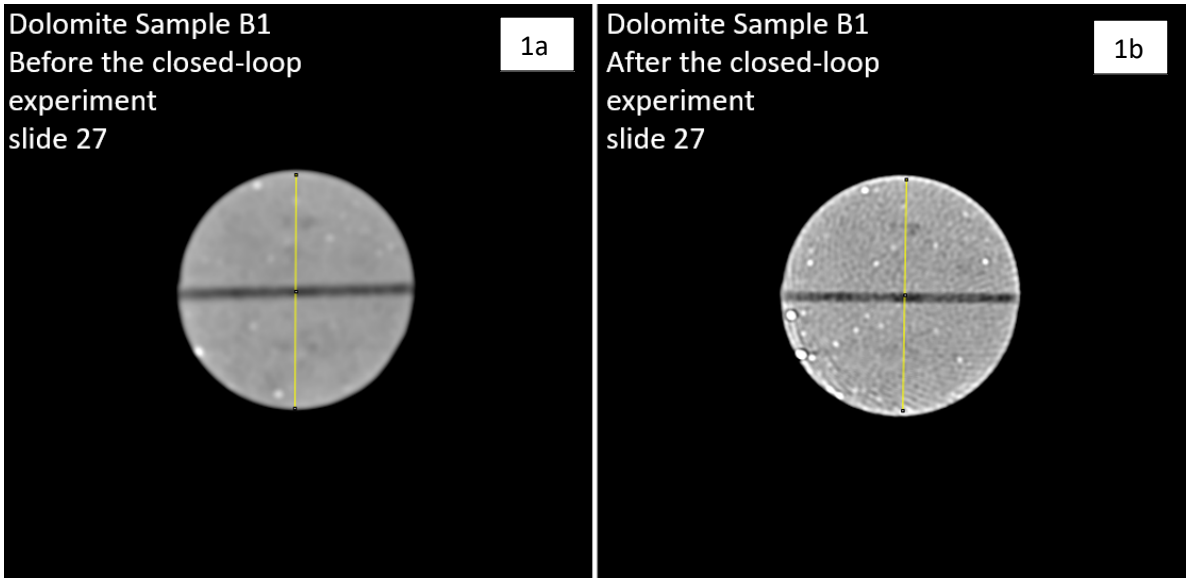

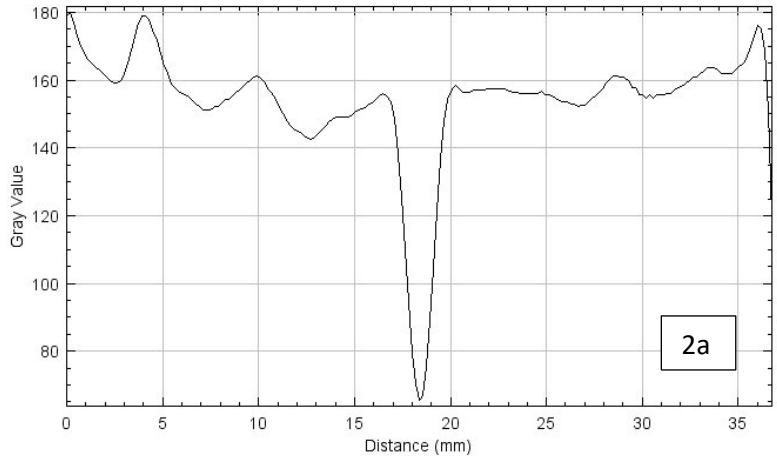

Graph to show the intensity of pixels in Dolostone Sample B1, from slide 27, before the closed-loop experiment

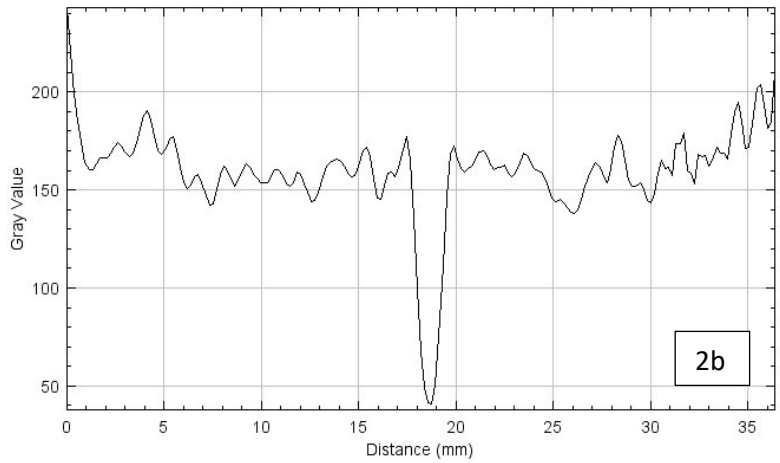

Graph to show the intensity of pixels in Dolostone Sample B1, from slide 27, after the closed-loop experiment

Figure 4.36.1a, 4.36.1b, 4.36.2a and 4.36.2b: (1 a-b) CT scan image of dolostone sample B1 (40°C) showing an image slide, taken from approximately the centre of the core sample, before and after the closed-loop experiment. The yellow line on the CT scan image portrays the cross-section line used to produce the pixel intensity graph. (2 a-b) Two-dimensional graph to show the grey-scale intensity of the pixels in the CT scan image vs. the distance along the line. The x-axis represents the distance along the line and the y-axis represents the grey value, i.e., the pixel intensity.

4.2.3 Limestone: Open-loop Experiment

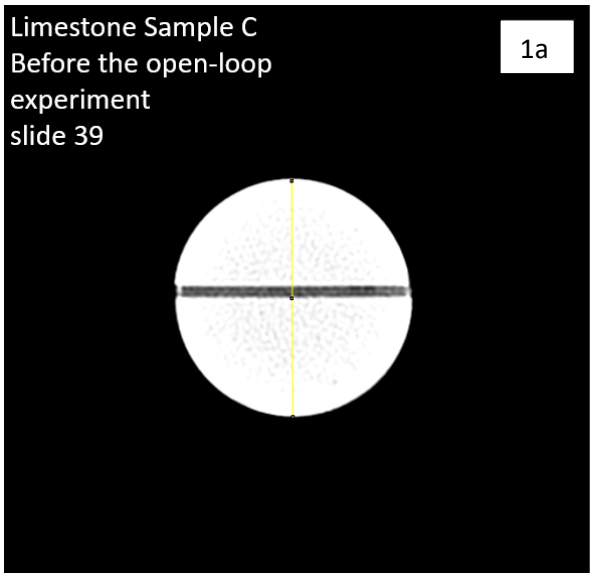

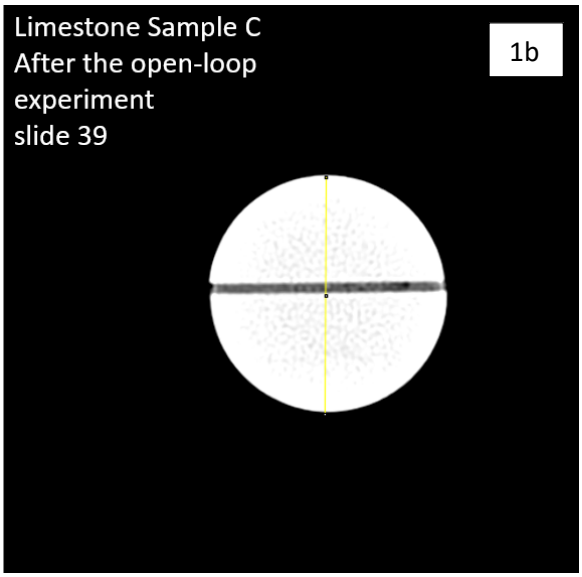

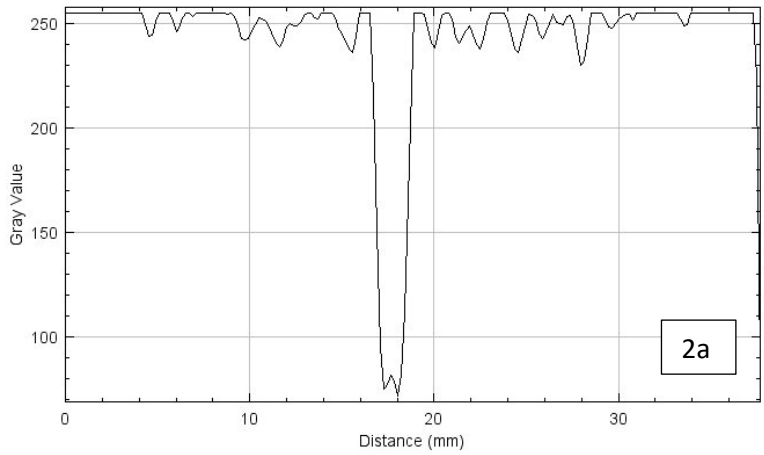

Graph to show the intensity of pixels in Limestone Sample C, from slide 39, before the open-loop experiment

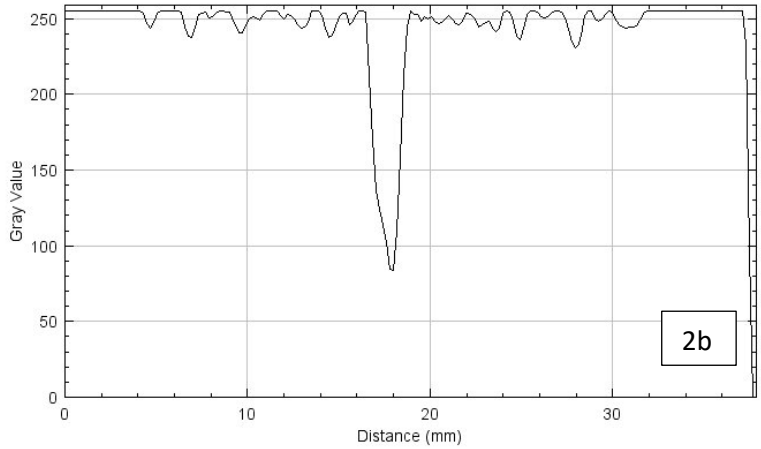

Graph to show the intensity of pixels in Limestone Sample C, from slide 39, after the open-loop experiment

Figure 4.37.1a, 4.37.1b, 4.37.2a and 4.37.2b: (1 a-b) CT scan image of limestone sample C (ambient) showing an image slide, taken from approximately the centre of the core sample, before and after the open-loop experiment. The yellow line on the CT scan image portrays the cross-section line used to produce the pixel intensity graph. (2 a-b) Two-dimensional graph to show the grey-scale intensity of the pixels in the CT scan image vs. the distance along the line. The x-axis represents the distance along the line and the y-axis represents the grey value, i.e., the pixel intensity.

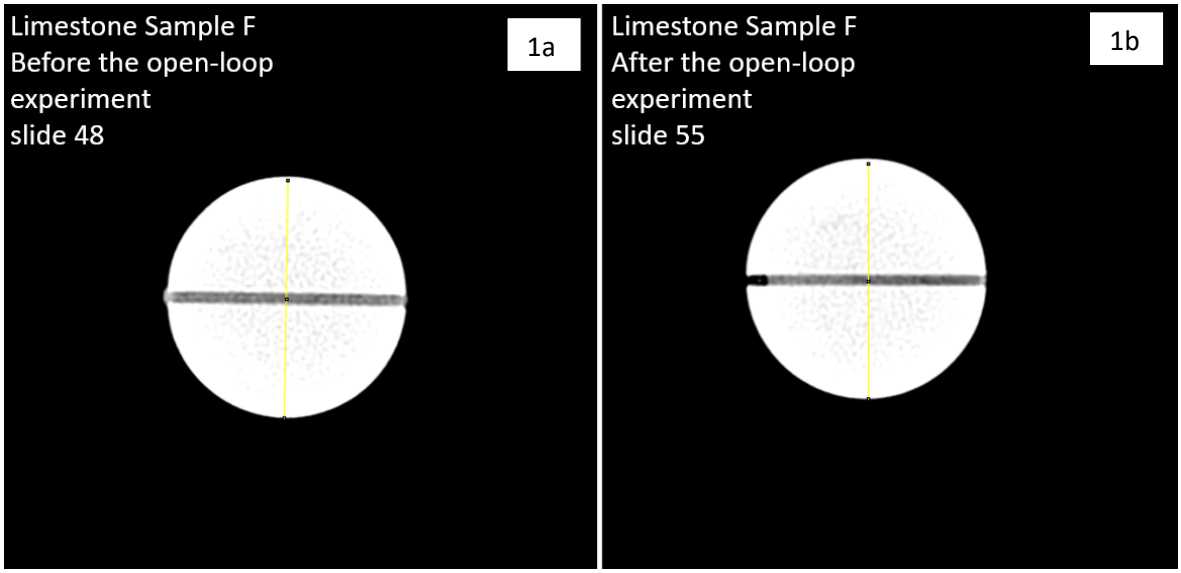

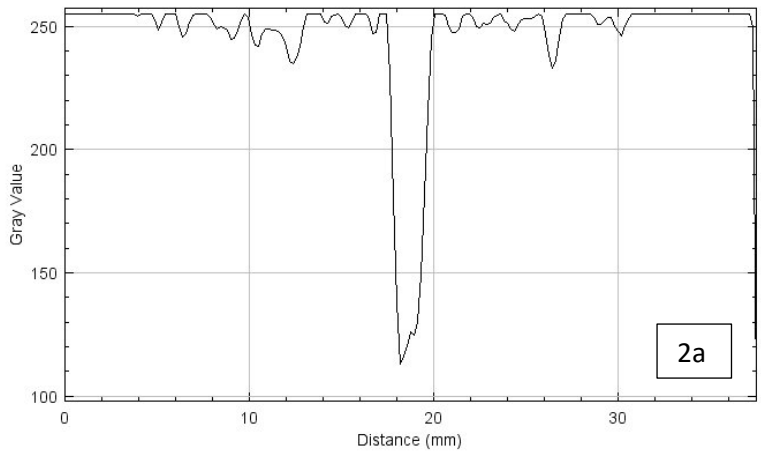

Graph to show the intensity of pixels in Limestone Sample F, from slide 48, before the open-loop experiment

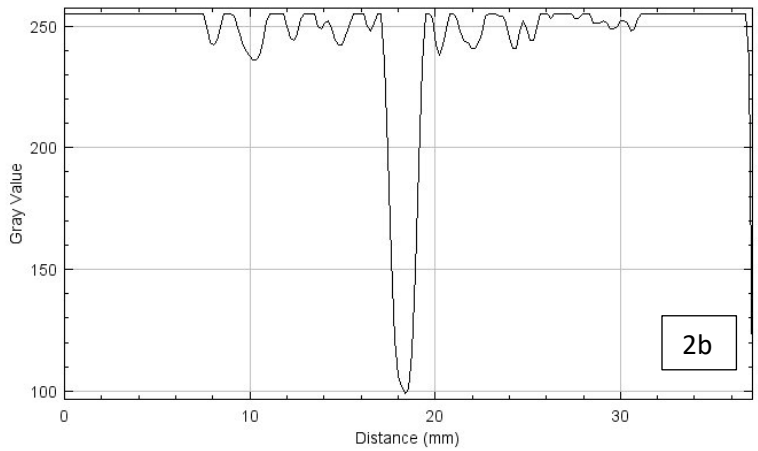

Graph to show the intensity of pixels in Limestone Sample F, from slide 55, after the open-loop experiment

Figure 4.38.1a, 4.38.1b, 4.38.2a and 4.38.2b: (1 a-b) CT scan image of limestone sample F (80°C) showing an image slide, taken from approximately the centre of the core sample, before and after the open-loop experiment. The yellow line on the CT scan image portrays the cross-section line used to produce the pixel intensity graph. (2 a-b) Two-dimensional graph to show the grey-scale intensity of the pixels in the CT scan image vs. the distance along the line. The x-axis represents the distance along the line and the y-axis represents the grey value, i.e., the pixel intensity.

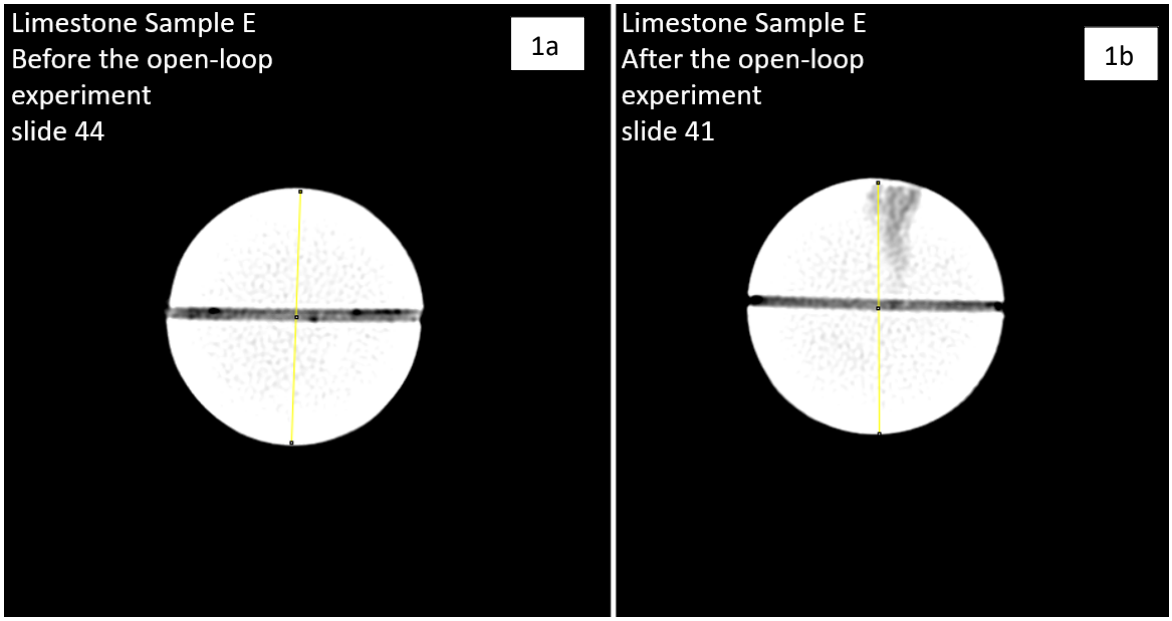

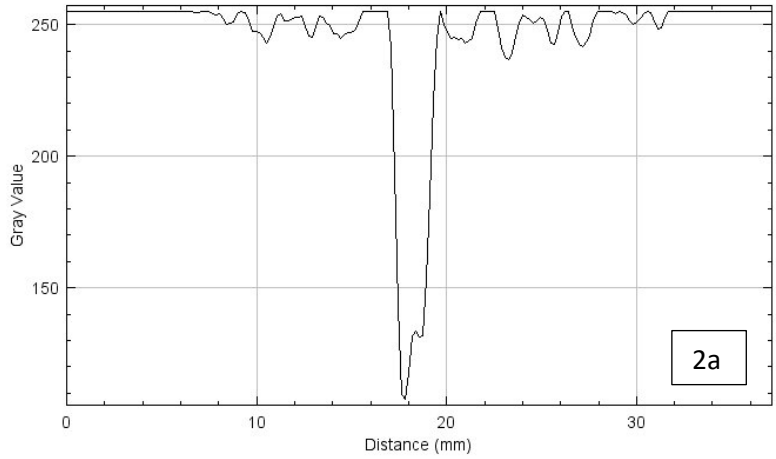

Graph to show the intensity of pixels in Limestone Sample E, from slide 44, before the open-loop experiment

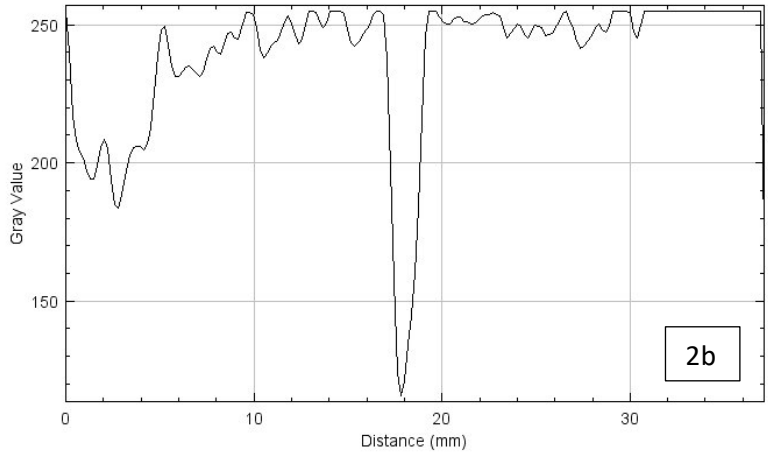

Graph to show the intensity of pixels in Limestone Sample E, from slide 41, after the open-loop experiment

Figure 4.39.1a, 4.39.1b, 4.39.2a and 4.39.2b: (1 a-b) CT scan image of limestone sample E (40°C) showing an image slide, taken from approximately the centre of the core sample, before and after the open-loop experiment. The yellow line on the CT scan image portrays the cross-section line used to produce the pixel intensity graph. (2 a-b) Two-dimensional graph to show the grey-scale intensity of the pixels in the CT scan image vs. the distance along the line. The x-axis represents the distance along the line and the y-axis represents the grey value, i.e., the pixel intensity.

4.2.4 Dolostone: Open-loop Experiment

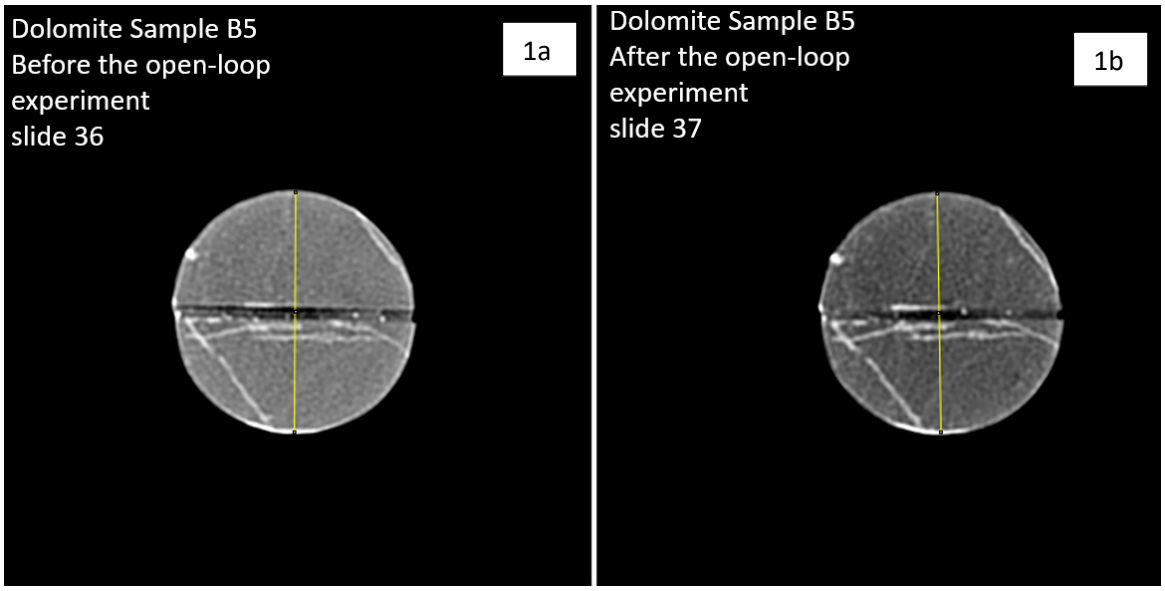

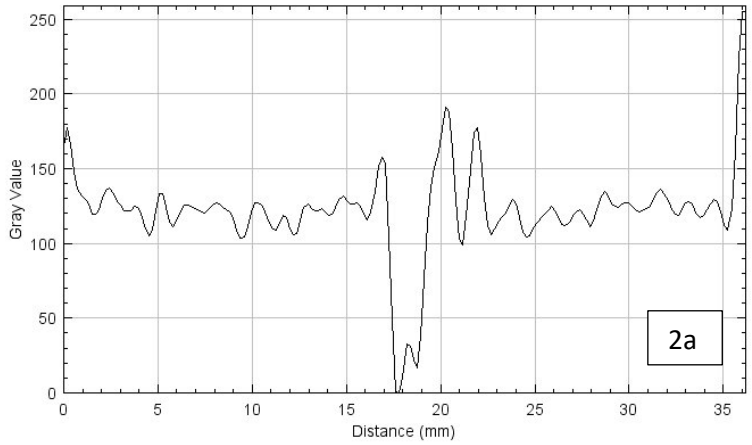

Graph to show the intensity of pixels in Dolostone Sample B5, from slide 36, before the open-loop experiment

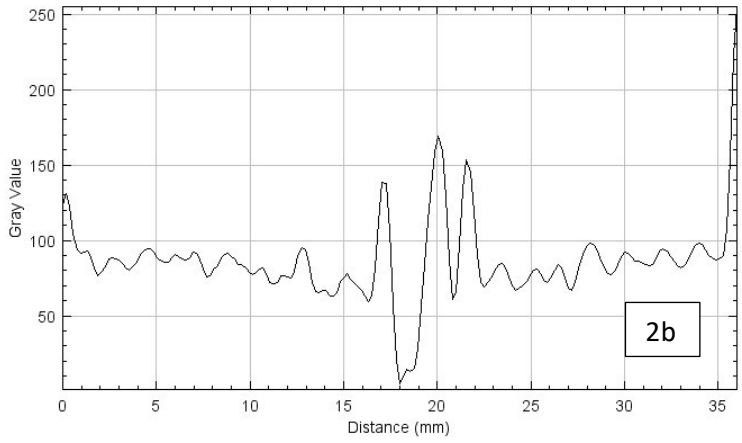

Graph to show the intensity of pixels in Dolostone Sample B5, from slide 37, after the open-loop experiment

Figure 4.40.1a, 4.40.1b, 4.40.2a and 4.40.2b: (1 a-b) CT scan image of dolostone sample B5 (ambient) showing an image slide, taken from approximately the centre of the core sample, before and after the open-loop experiment. The yellow line on the CT scan image portrays the cross-section line used to produce the pixel intensity graph. (2 a-b) Two-dimensional graph to show the grey-scale intensity of the pixels in the CT scan image vs. the distance along the line. The x-axis represents the distance along the line and the y-axis represents the grey value, i.e., the pixel intensity.

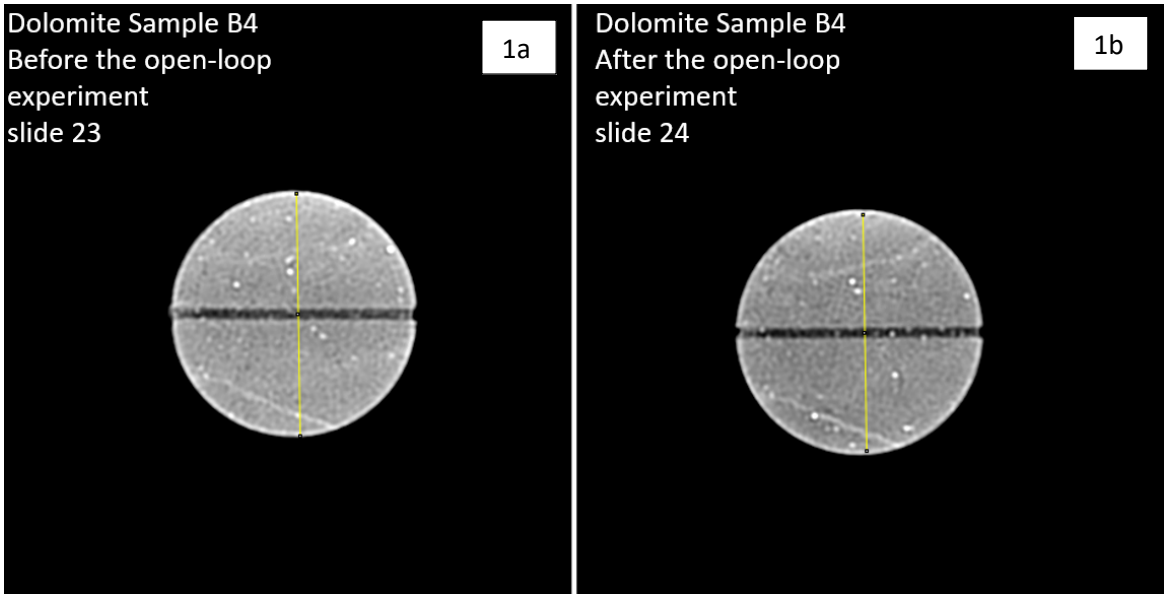

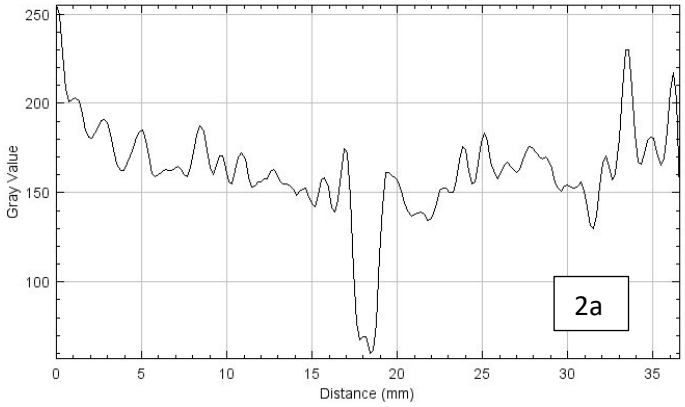

Graph to show the intensity of pixels in Dolostone Sample B4, from slide 23, before the open-loop experiment

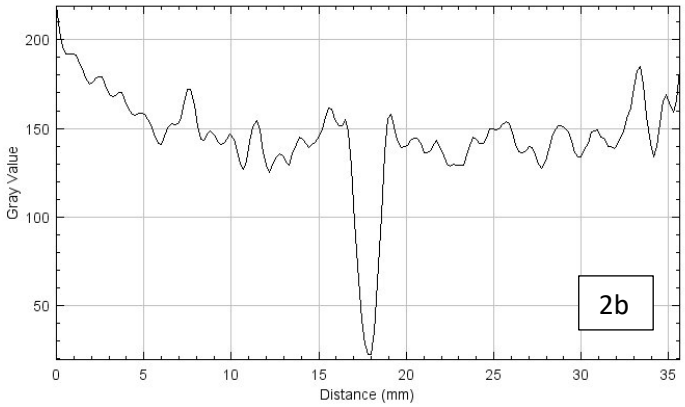

Graph to show the intensity of pixels in Dolostone Sample B4, from slide 24, after the open-loop experiment

Figure 4.41.1a, 4.41.1b, 4.41.2a and 4.41.2b: (1 a-b) CT scan image of dolostone sample B4 (80°C) showing an image slide, taken from approximately the centre of the core sample, before and after the open-loop experiment. The yellow line on the CT scan image portrays the cross-section line used to produce the pixel intensity graph. (2 a-b) Two-dimensional graph to show the grey-scale intensity of the pixels in the CT scan image vs. the distance along the line. The x-axis represents the distance along the line and the y-axis represents the grey value, i.e., the pixel intensity.

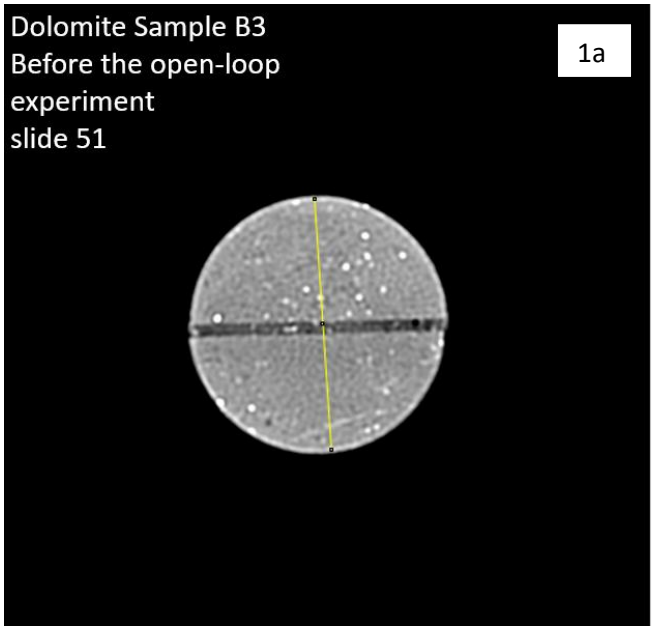

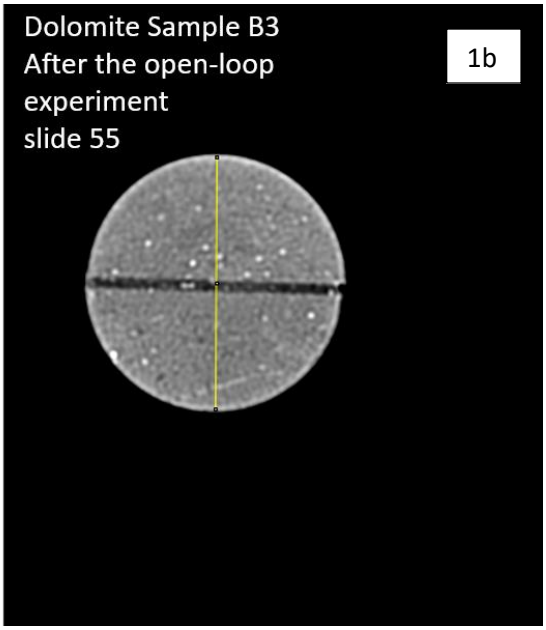

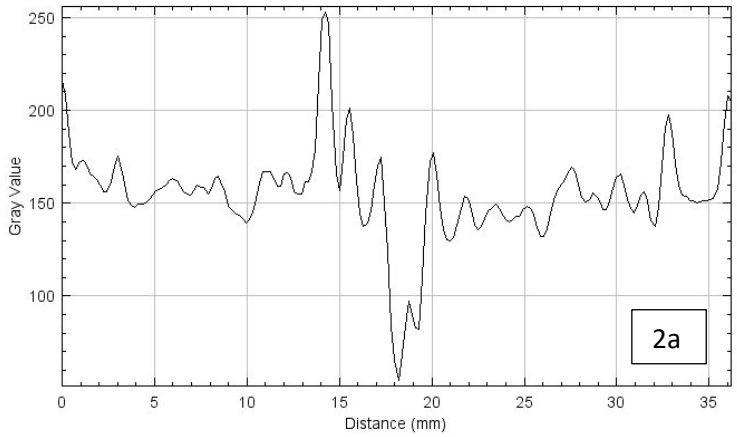

Graph to show the intensity of pixels in Dolostone Sample B3, from slide 51, before the open-loop experiment

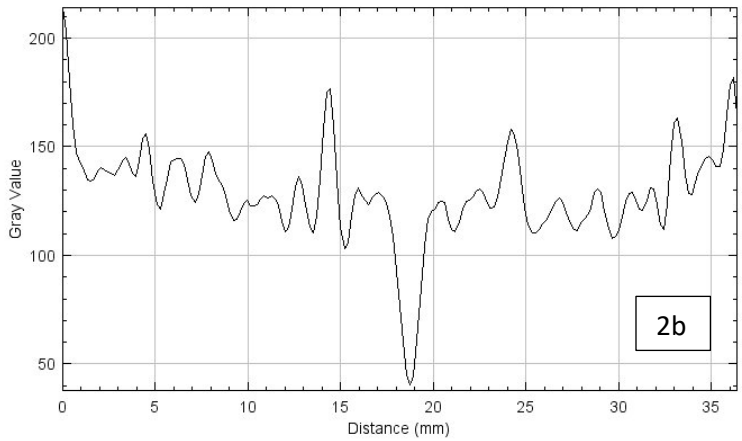

Graph to show the intensity of pixels in Dolostone Sample B3, from slide 55, after the open-loop experiment

Figure 4.42.1a, 4.42.1b, 4.42.2a and 4.42.2b: (1 a-b) CT scan image of dolostone sample B3 (40°C) showing an image slide, taken from approximately the centre of the core sample, before and after the open-loop experiment. The yellow line on the CT scan image portrays the cross-section line used to produce the pixel intensity graph. (2 a-b) Two-dimensional graph to show the grey-scale intensity of the pixels in the CT scan image vs. the distance along the line. The x-axis represents the distance along the line and the y-axis represents the grey value, i.e., the pixel intensity.

4.3 Water Sampling Results

Water sample measurements were taken throughout the experiment at three separate locations on both line one and line two (Fig. 3.1, 3.2, 3.3 and 3.3). Magnesium (Mg) and Calcium (Ca) concentrations were taken from the fluid travelling through both the limestone line and dolostone line. The water sample data has been split into three separate lines based on where the water sample was taken from, either the ambient core holder, the 80°C core holder or the 40°C core holder.

For limestone, Goldscheider et al. 2010, Morse et al. 2007, Plummer and Wigley (1976), Plummer et al. (1978) and Kirstein et al. 2016 argue that with the solubility of calcite decreases with increasing temperature. Wood (1986) suggests that at lower temperatures, in a closed system, calcite solubility increases with the increase in the temperature. However, in an open system Wood (1986) agrees with the aforementioned research which state that, with increasing temperature, calcite solubility will decrease. For dolostone, the same research applies due to a large portion of dolostone comprises of calcite. However, research undertaken by Zhang et al. (2007) suggests that dolomite dissolution increases with increasing temperature at lower temperatures and becomes retrograde at higher temperatures (>100 - 200°C). Morse et al. (2007) however disagree and argue the dissolution of dolomite appears to decrease as dolomite precipitation is evident with increasing temperature. The majority of the findings direct towards calcite solubility decreasing with increasing temperature. It is to be remembered that the majority of the research on the relationship between the solubility of calcite and temperature is undertaken on pure calcite and not limestone, therefore impurities in the limestone or dolostone may affect the results.

It would be expected that dolostone would show higher release of magnesium to solution values than the limestone samples due comprising of the mineral dolomite, which has a $MgCO_3$ – $CaCO_3$ composition. With calcium making up much of the chemical composition of calcium carbonate ($CaCO_3$) forming limestone and dolostone, it's expected to see a release of Ca to solution throughout the duration of the experiment in both the limestone and dolostone samples (Warren, 2000).

4.3.1 Limestone: Magnesium Concentration in the Fluid Percolating Through the Limestone

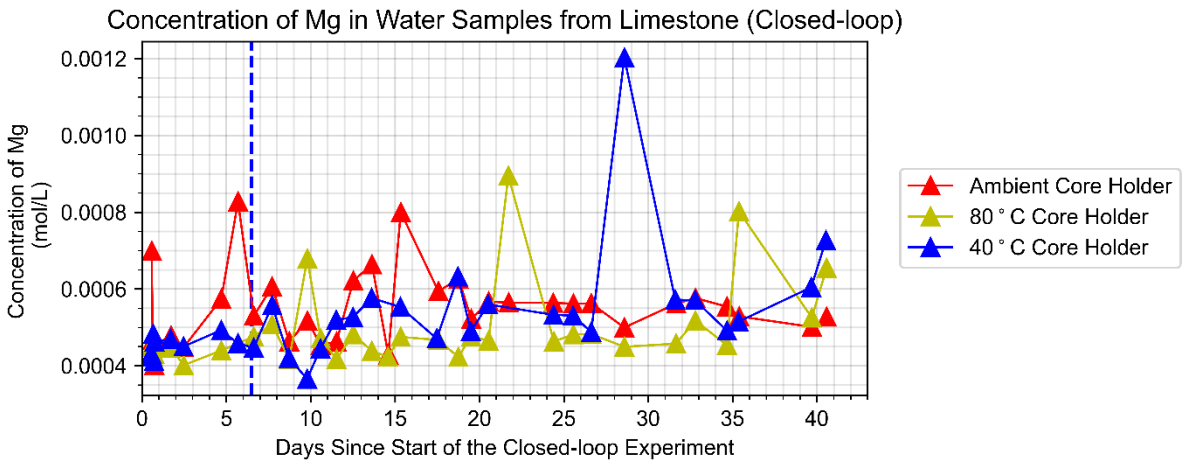

Figure 4.43: Graph to show the Mg-concentration of the fluid travelling through the Limestone core samples B (ambient), A (80°C) and D (40°C), respectively, throughout the closed-loop experiment (made using Python). The blue dashed line indicates the flow rate being reduced from 0.5rpm and 0.4rpm (discussed in section 4.5).

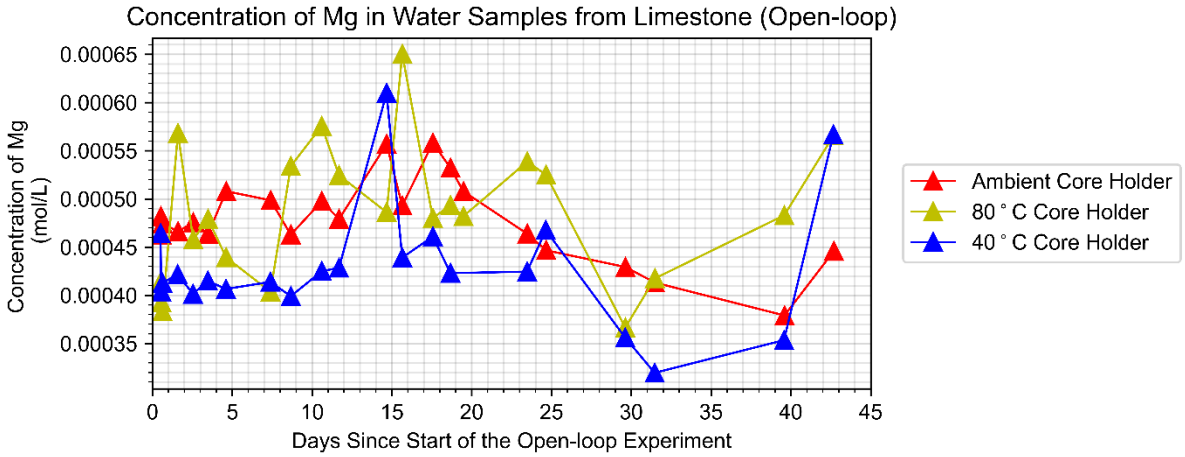

Figure 4.44: Graph to show the Mg-concentration of the fluid travelling through the Limestone core samples C (ambient), F (80°C) and E (40°C), respectively, throughout the open-loop experiment (made using Python).

Figure 4.43 shows the Mg-concentrations in the fluid percolating through the limestone during the closed-loop experiment. Figure 4.44 shows the Mg-concentrations in the fluid percolating through the limestone during the open-loop experiment. The concentration of magnesium recorded in the water sample taken from the water valves located after the ambient, the 80°C and the 40°C are recorded.

4.3.2 Limestone: Calcium Concentration in the Fluid Percolating through the Limestone

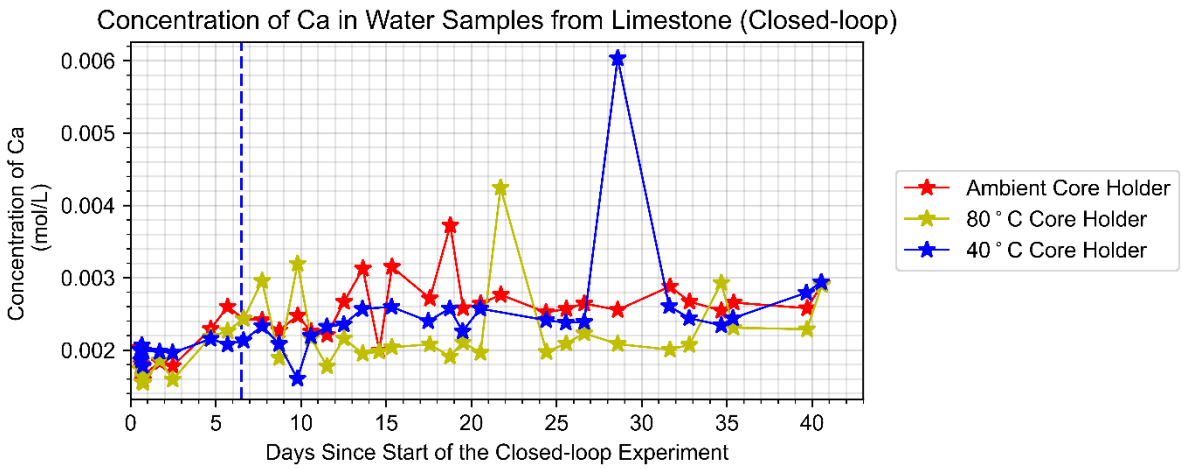

Figure 4.45: Graph to show the Ca-concentration of the fluid travelling through the Limestone core samples B (ambient), A (80°C) and D (40°C), respectively, throughout the closed-loop experiment (made using Python). The blue dashed line indicates the flow rate being reduced from 0.5rpm and 0.4rpm (discussed in section 4.5).

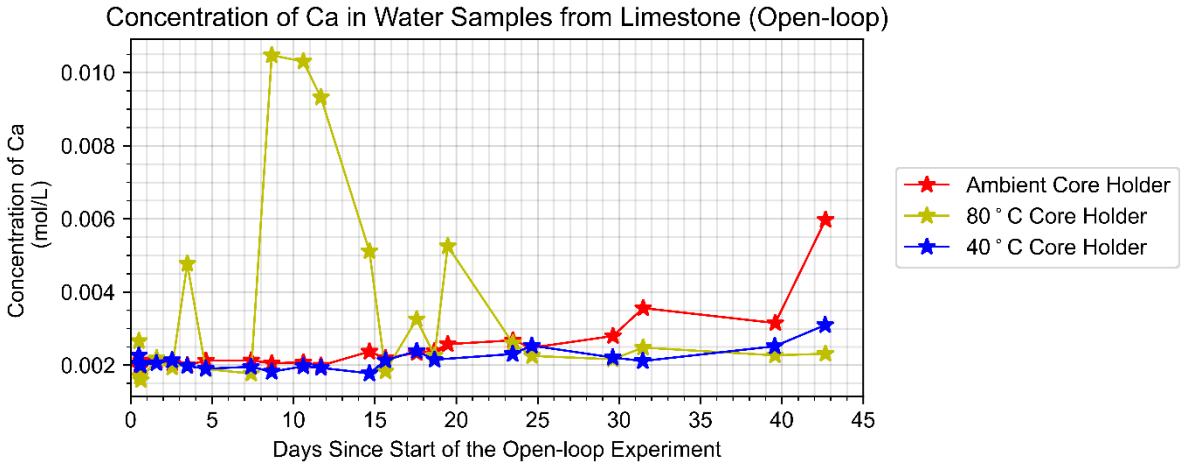

Figure 4.46: Graph to show the Ca-concentration of the fluid travelling through the Limestone core samples C (ambient), F (80°C) and E (40°C), respectively, throughout the open-loop experiment (made using Python).

In figure 4.45, looking at the Ca-concentrations in the fluid percolating through the limestone during the closed-loop experiment, the general trend appears to be a gentle increase in Ca-concentrations in the percolating fluid throughout the whole experiment.

Figure 4.46 shows the Ca-concentrations in the fluid percolating through the limestone during the open-loop experiment. Generally, the Ca-concentration in all three samples appears to show a slight increase in calcium concentration, albeit small, throughout the experiment. In the 80°C core holder,

approximately eight days after the experiment started, a large spike is evident with multiple results comprising the increase.

4.3.3 Dolostone: Magnesium Concentration in the Fluid Percolating through the Dolostone

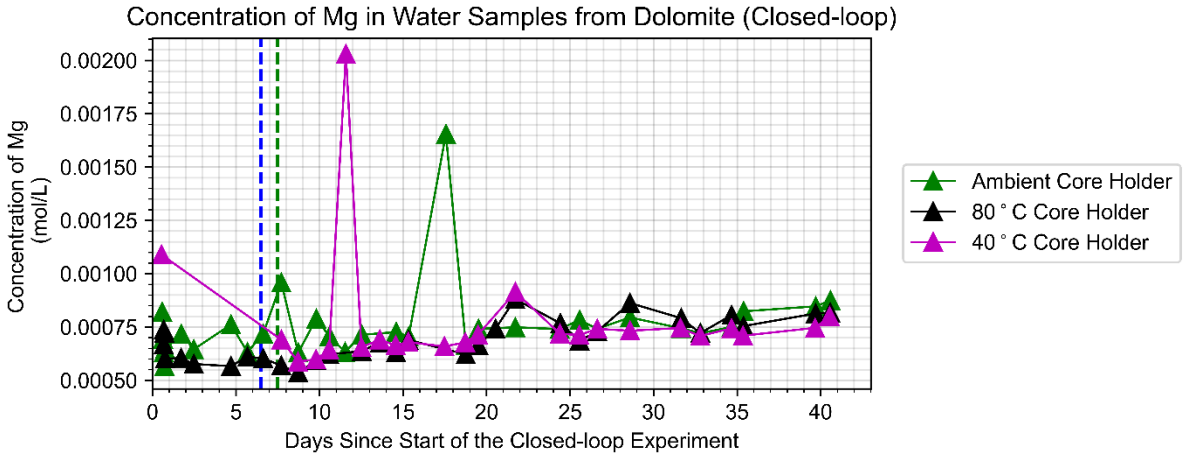

Figure 4.47: Graph to show the Mg-concentration of the fluid travelling through the Dolostone core samples B6 (ambient), B2 (80°C) and B1 (40°C), respectively, throughout the closed-loop experiment (made using Python). The blue dashed line indicates the flow rate being reduced from 0.5rpm and 0.4rpm and the green dashed line indicates when the leak was fixed (discussed in section 4.5).

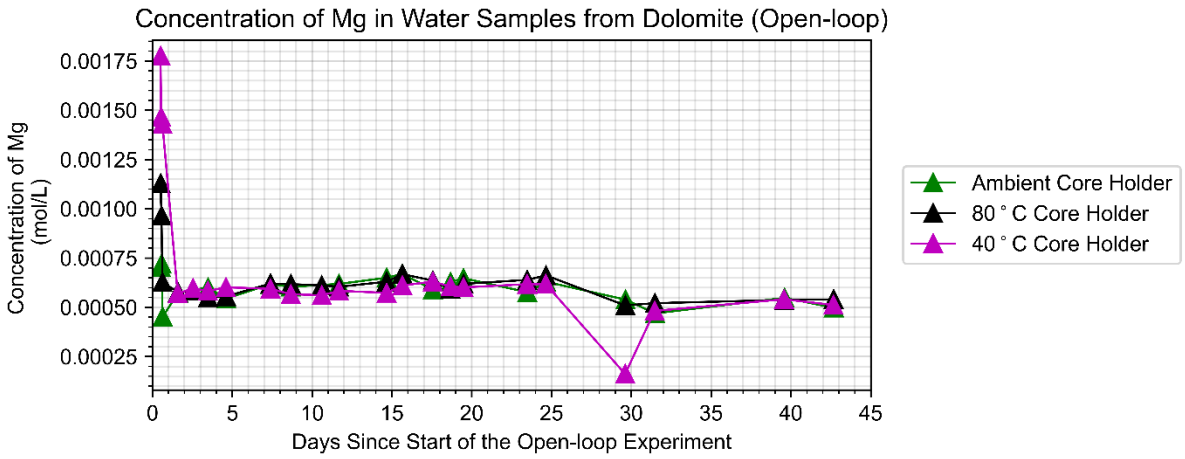

Figure 4.48: Graph to show the Mg-concentration of the fluid travelling through the Dolostone core samples B5 (ambient), B4 (80°C) and B3 (40°C), respectively, throughout the open-loop experiment (made using Python).

Figure 4.47 shows the magnesium concentrations of the fluid percolating through the dolostone samples throughout the closed-loop experiment. Overall, there appears to be little variation in magnesium in the fluid samples throughout the experiment. A steady, slow increase in magnesium is observed in the fluid throughout, generally showing all three water sample magnesium values remaining between 0.0006 mol/L and 0.0009 mol/L.

Figure 4.48 shows the magnesium concentrations of the fluid percolating through the dolostone samples throughout the open-loop experiment. There appears to be initial high magnesium values observed in the samples taken from the ambient and 80°C core holders. The observed magnesium values appear to drop after the first day, and show a slow, steady increase in magnesium until approximately 24 days after the experiment started, when values show a slight drop until the end of the experiment.

4.3.4 Dolostone: Calcium Concentration in the Fluid Percolating through the Dolostone

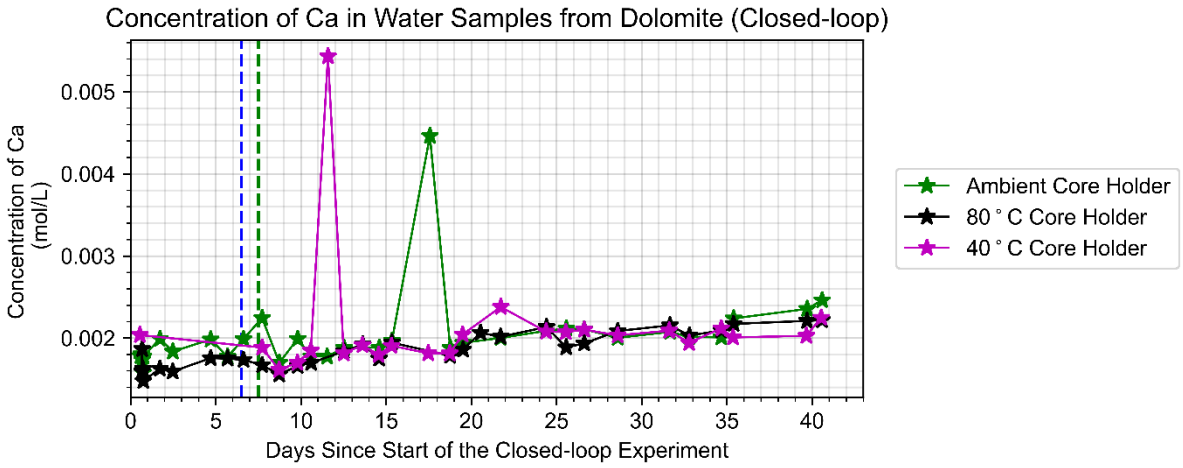

Figure 4.49: Graph to show the Ca-concentration of the fluid travelling through the Dolostone core samples B6 (ambient), B2 (80°C) and B1 (40°C), respectively, throughout the closed-loop experiment (made using Python). The blue dashed line indicates the flow rate being reduced from 0.5rpm and 0.4rpm and the green dashed line indicates when the leak was fixed (discussed in section 4.5).

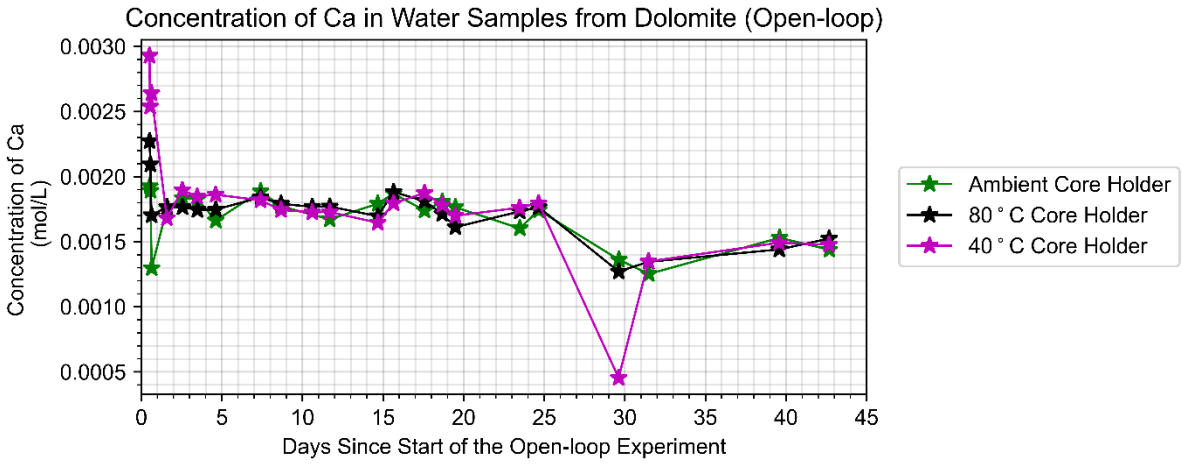

Figure 4.50: Graph to show the Ca-concentration of the fluid travelling through the Dolostone core samples B5 (ambient), B4 (80°C) and B3 (40°C), respectively, throughout the open-loop experiment (made using Python).

Figure 4.49 shows the calcium concentration in the fluid percolating through the dolostone, during the closed-loop experiment. The results show a slow and steady increase in calcium concentrations, in all three samples, throughout the closed-loop experiment. The majority of results lie between approximately 0.0014 mol/L and 0.0025 mol/L.

Figure 4.50 shows the calcium concentration in the fluid percolating through the dolostone, throughout the open-loop experiment. Similar to the magnesium results in the dolostone, throughout the open-loop experiment, the results portray initial high calcium concentrations in the fluid on the first day of the experiment. The high initial values are followed by a drop in calcium concentrations, whereby the results remain stable until approximately 24 days after the start of the experiment. Following this is a slight drop in calcium before a steady increase until the end of the open-loop experiment.

4.4 Core Sample Permeability Results

Below are the permeability results of the limestone and dolostone samples, during the closed-loop and open-loop experiment. Permeability measurements were taken throughout the experiment. The data to calculate permeability was taken from the water sample measurements, where amount of water in a recorded length of time was taken (see section 4.3).

4.4.1 Permeability of the Limestone Core Samples: Closed-loop Experiment

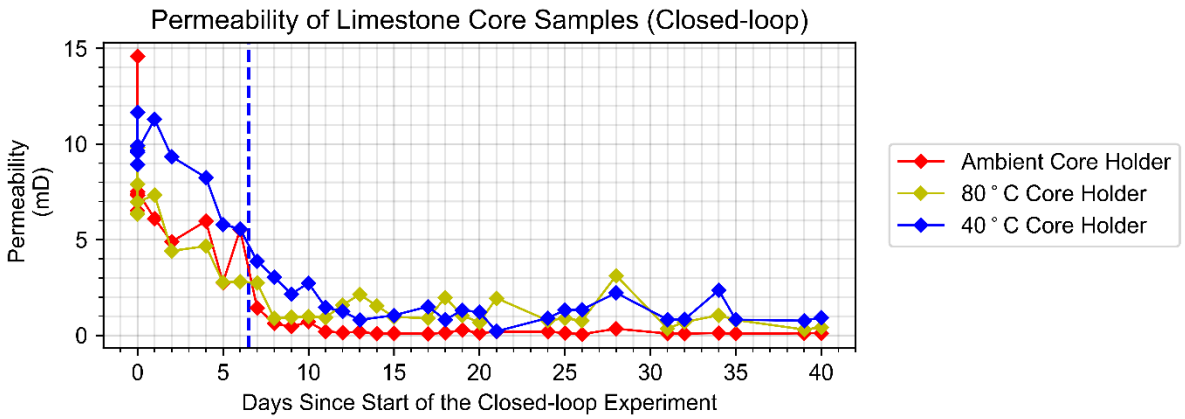

Figure 4.51: Graph to show the permeability of the limestone core samples B (ambient), A (80°C) and D (40°C), throughout the closed-loop experiment. The blue dashed line indicates the flow rate being reduced from 0.5rpm and 0.4rpm (discussed in section 4.5) (made using Python).

4.4.2 Permeability of the Limestone Core Samples: Open-loop Experiment

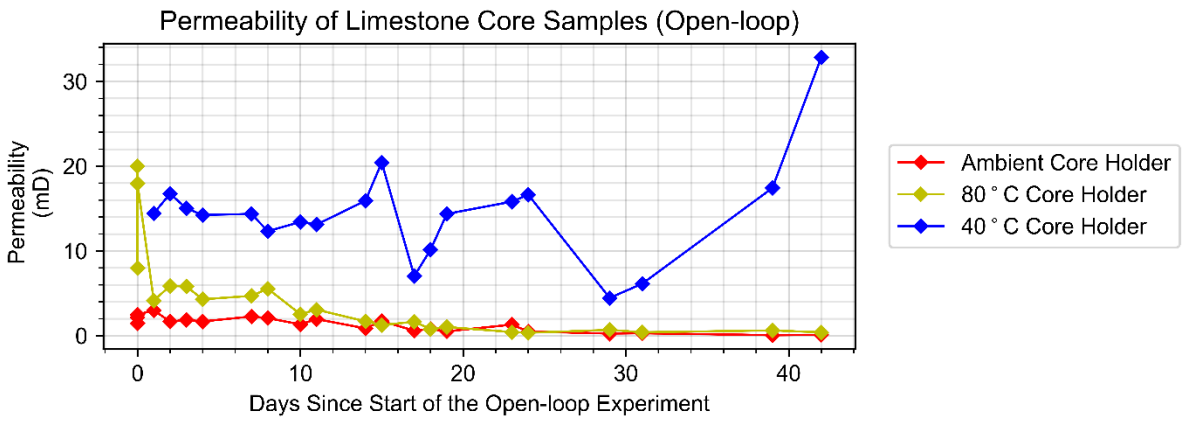

Figure 4.52: Graph to show the permeability of the limestone core samples C (ambient), F (80°C) and E (40°C), throughout the open-loop experiment (made using Python).

4.4.3 Permeability of the Dolostone Core Samples: Closed-loop Experiment

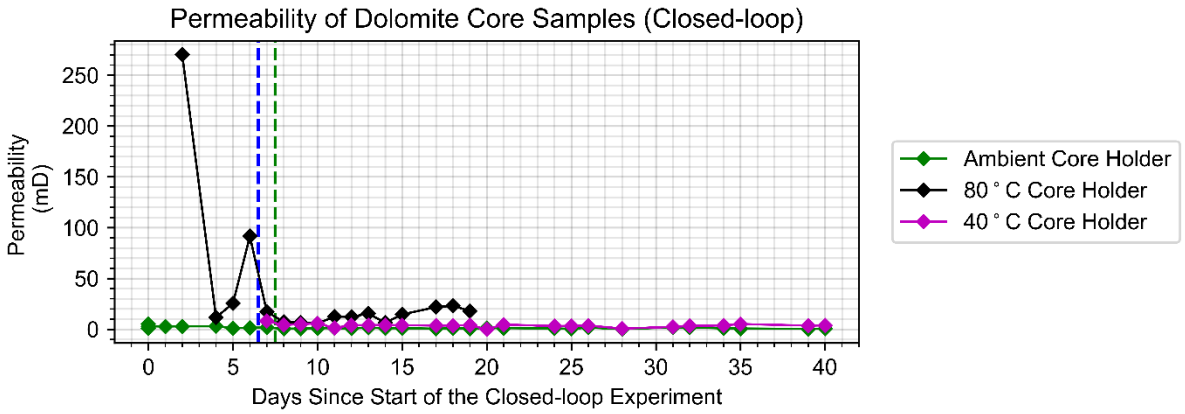

Figure 4.53: Graph to show the permeability of the dolostone core samples B6 (ambient), B2 (80°C) and B1 (40°C), throughout the closed-loop experiment. Gaps in the data are due to the removal of negative permeability values from sample B2 (80°C) and B1 (40°C). The blue dashed line indicates the flow rate being reduced from 0.5rpm and 0.4rpm and the green dashed line indicates when the leak was fixed (discussed in section 4.5) (made using Python).

4.4.4 Permeability of the Dolostone Core Samples: Open-loop Experiment

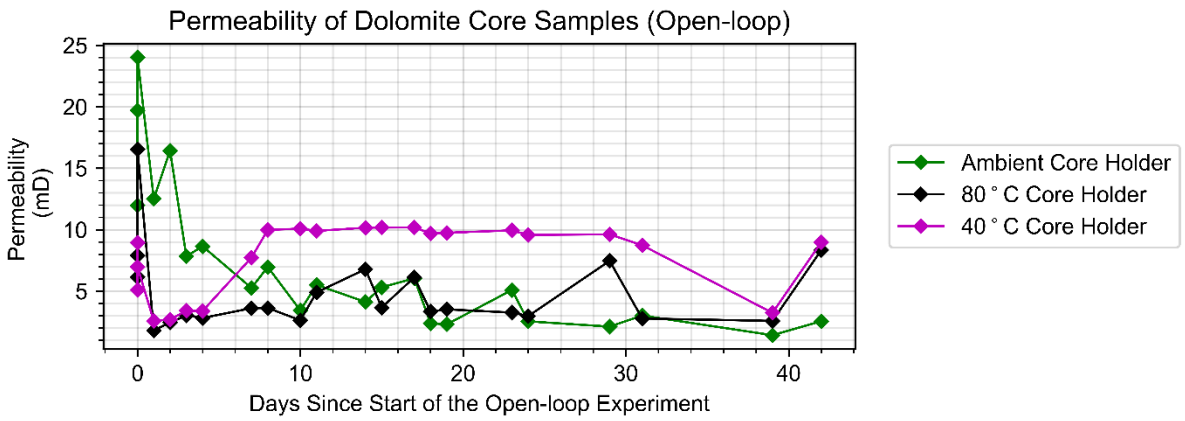

Figure 4.54: Graph to show the permeability of the dolostone core samples B5 (ambient), B4 (80°C) and B3 (40°C), throughout the open-loop experiment (made using Python).

Figures 4.51, 4.52, 4.53 and 4.44 portray the permeability results of the limestone and dolostone throughout the closed-loop and open-loop experiments. The permeability measurements were recorded throughout using steady-state liquid permeability measurements when the water samples were collected. The permeability results portray the change in permeability in all samples throughout the experiment. The permeability directly affects how much and how quickly fluid can flow through the system (Huenges, 2016). Therefore, making it important to consider in a real-life geothermal setting.

4.5 Pressure Results

Pressures results were recorded via gauges attached to the upstream and downstream of each core holder, therefore for three core holders there are six pressure results. The pressure gauges are labelled as such; for line one, pressure gauges 1A and 1B refer to the ambient core holder, 1C and 1D relate to the 80°C core holder and 1E and 1F relate to the 40°C core holder. Figures. 3.1, 3.2, 3.3 and 3.4, portray the position of the gauges in the experiment. The line one gauges are labelled as 1A – 1F and refer to the limestone line and the line two gauges are labelled as 2A – 2F and refer to the dolostone line. The compiled graphs have been included in the pressure results section, with some individual pressure graphs included if necessary.

The pressure results can be interpreted to further understand what was happening in the experiment system. If the pressures appear to stabilise and show equilibrium it may suggest that the system is flowing smoothly. However, if there appears to be large spikes or fluctuations in the pressure data it may represent a problem in the system, blockages or restrictions to fluid flow.

When plotting the pressure data for the closed-loop experiment there was a leak in line two (dolostone) which was only discovered on 30/07/2021, seven days since the start of the experiment. This resulted in the first 7 days of the dolostone line acting as an open-loop instead of a closed-loop system. A green dashed line has been plotted on the dolostone graphs to show when this occurred. Therefore, it is to be noted that a closed-loop system may only come into effect seven days after the experiment started, despite data being recorded before this. The water sample results taken from these initial days may similarly resemble an open-loop system, therefore the green dashed line has been plotted on the dolostone water sample graphs also (see section 4.3). The blue dashed line evident on both the limestone and dolostone pressure graphs represents the flow rate being reduced in the system from 0.5 rpm to 0.4 rpm. The flow was reduced at this point due to producing pressures too high for the core holders to manage without overloading.

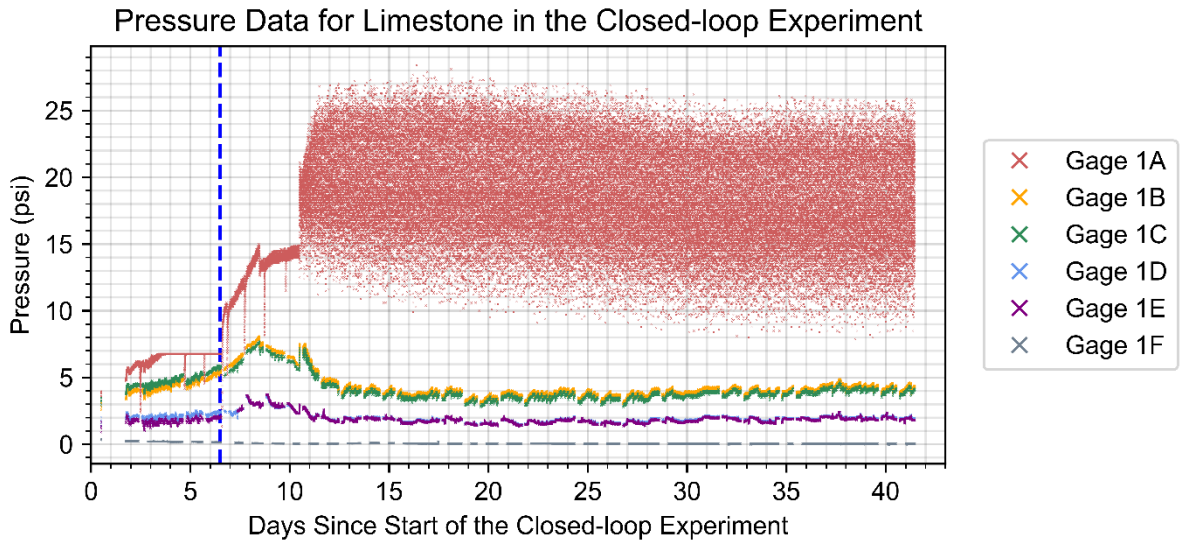

Fig 4.55: Graph to show the pressure changes for the Limestone (line 1), in pressure gauges 1A – 1F, throughout the duration of the closed-loop experiment. The blue dashed line, evident approximately 6 days after the experiment starts, represents the point the flow rate was reduced from 0.5 rpm to 0.4 rpm (made using Python).

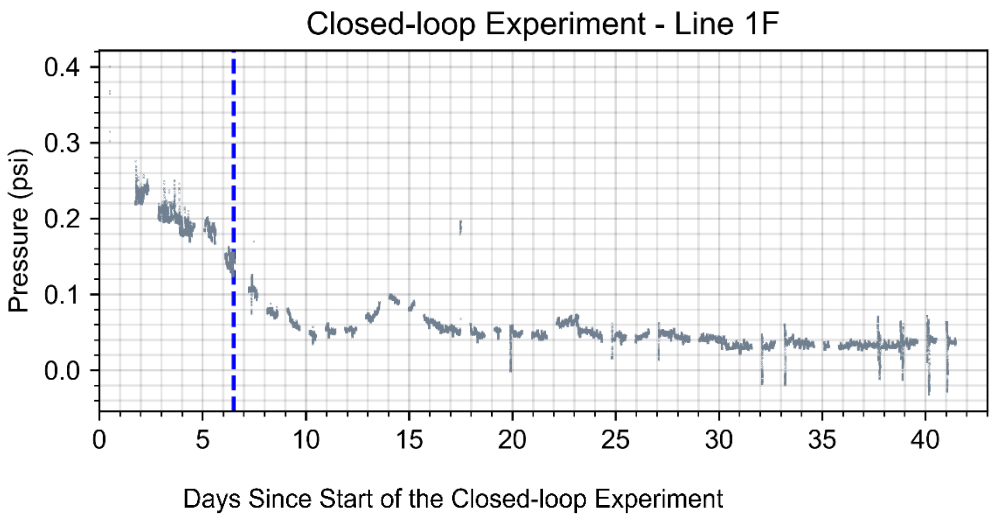

Fig 4.56: Graph to show the pressure changes for the Limestone (line 1), in pressure gauge 1F (the downstream of core holder three within the 40°C oven), throughout the duration of the closed-loop experiment (made using Python).

Figure 4.57: Residue left on the filter paper from the upstream (1A) of the first core holder in limestone (line one).

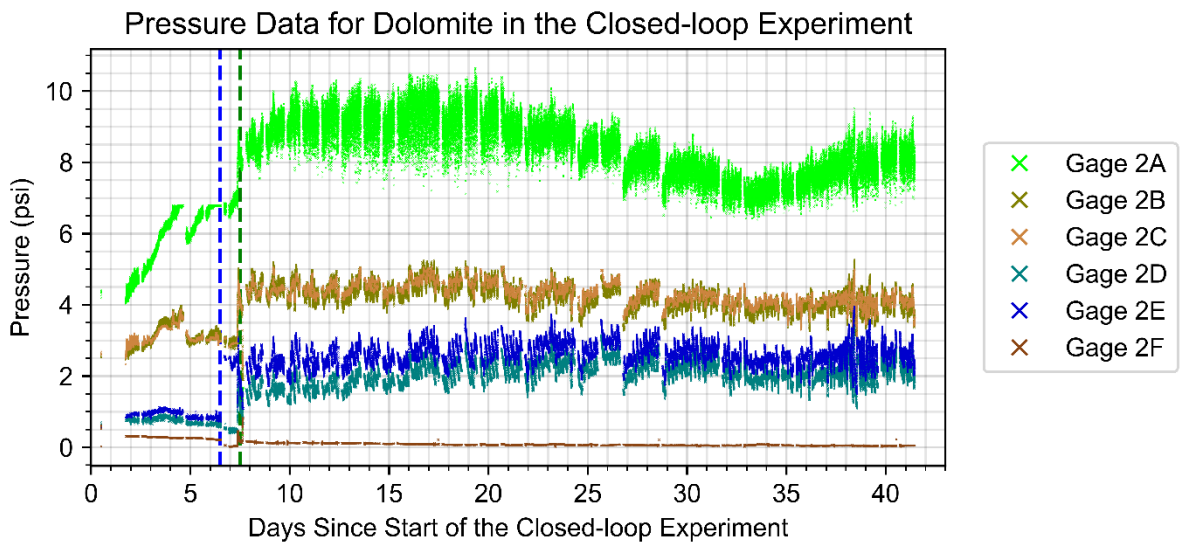

Fig 4.58: Graph to show the pressure changes for the Dolostone (line 2), in pressure gauges 2A – 2F, throughout the duration of the closed-loop experiment. The green dashed line represents the leak being fixed. The blue dashed line, evident approximately 6 days after the experiment starts, represents the point the flow rate was reduced from 0.5 rpm to 0.4 rpm (made using Python).

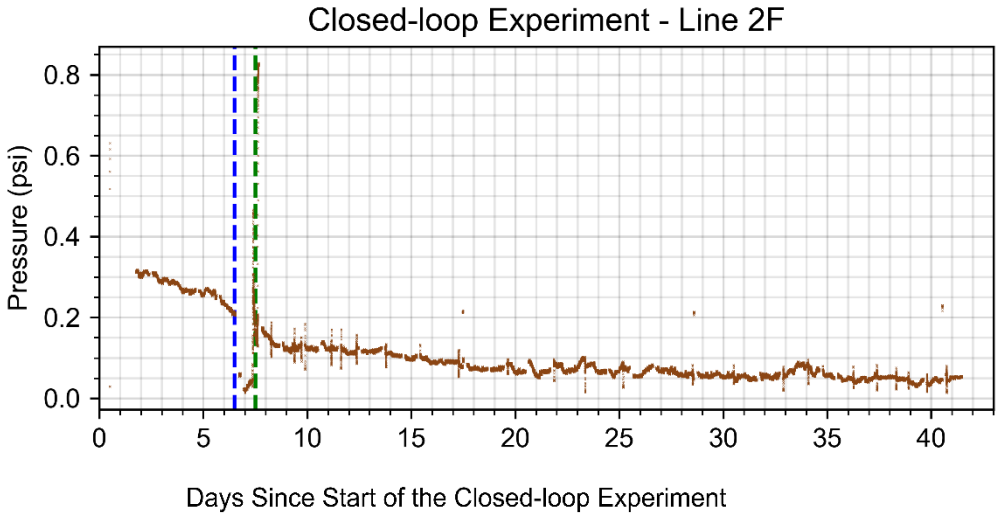

Fig 4.59: Graph to show the pressure changes for the Dolostone (line 2), in pressure gauge 2F (the downstream of core holder three within the 40°C oven), throughout the duration of the closed-loop experiment (made using Python).

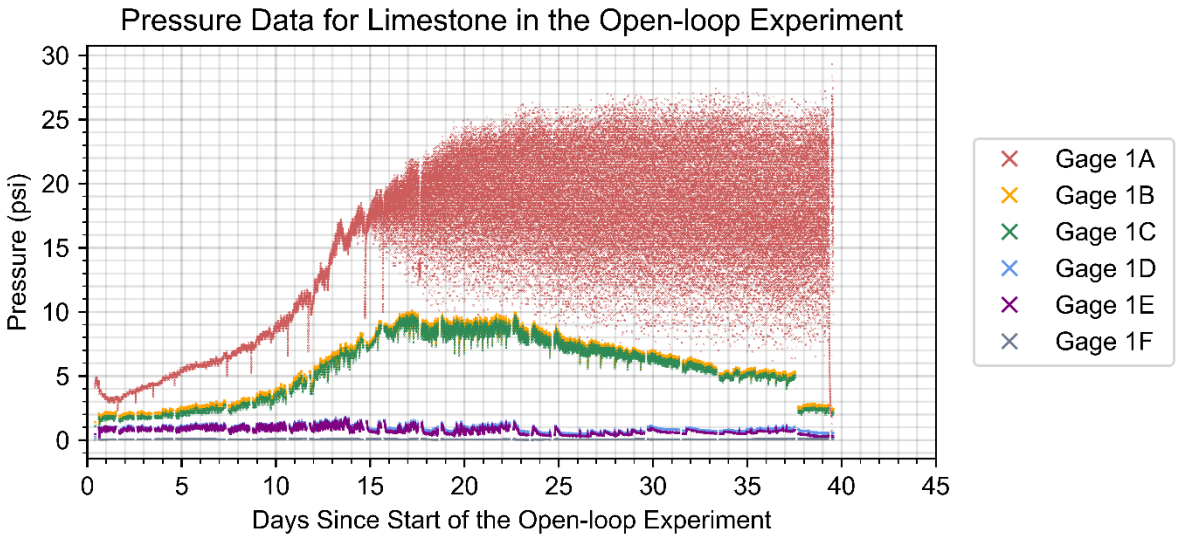

Fig 4.60: Graph to show the pressure changes for the Limestone (line 1), in pressure gauges 1A – 1F, throughout the duration of the open-loop experiment (made using Python).

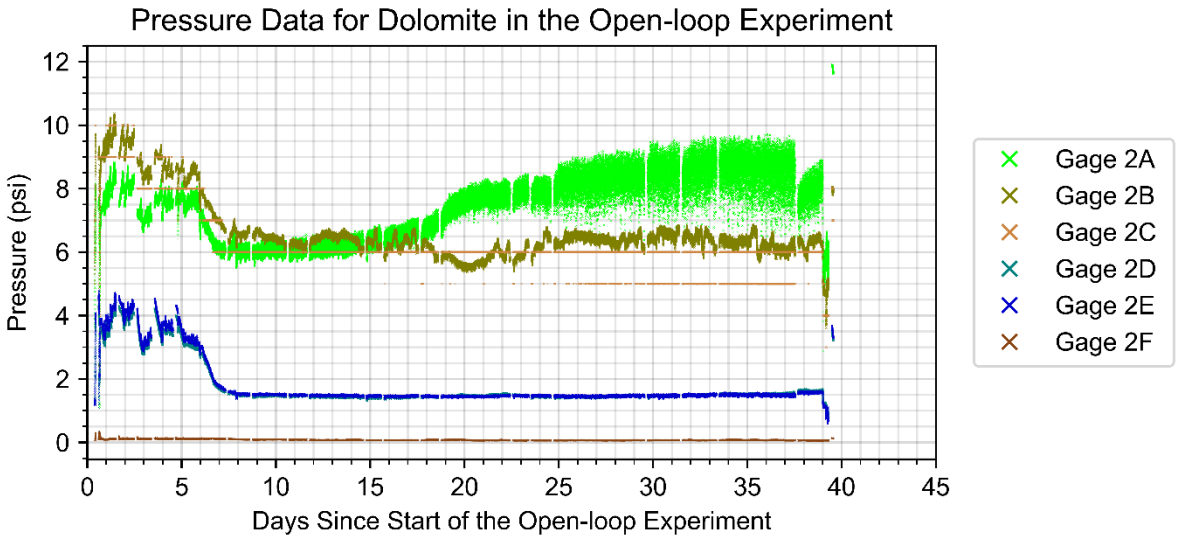

Fig 4.61: Graph to show the pressure changes for the Dolostone (line 2), in pressure gauges 2A – 2F, throughout the duration of the open-loop experiment (made using Python).

Figures 4.55, 4.58, 4.60 and 4.61 portray the pressure readings for the limestone and dolostone during both the closed-loop and open-loop experiments. Pressure drops were recorded when water sampling and have been removed to focus on the pressure results without data being affected by human interference. Figure 4.56 highlights that even when the pressure drops were removed, they remained evident on the pressure graph for gauge 1F (limestone) due to being delayed. The same is evident in figure 4.59 for gauge 2F (dolostone). Figure 4.57 highlights residue that was evident on the upstream

of the ambient core holder, which is the entry point to the system, in line one during the closed-loop experiment.

5. Discussion

5.1 Micro-structural Discussion

This section will refer back to the results from 'Section 4' to analyse the findings. It is worth remembering that the initial porosity of the samples will affect the final results and that comparisons of the post-experiment porosity are being made relative to each sample. Despite this, using ImageJ analysis alongside visual inspection of the SEM images provides an insight into the dissolution-precipitation reactions occurring in the limestone and dolostone samples.

For limestone, there are many studies which focus on the rate of calcite dissolution. From the literature review, studies from Goldscheider et al. 2010, Morse et al. 2007, Plummer and Wigley (1976), Plummer et al. (1978) and Kirstein et al. 2016 argue that the solubility of calcite decreases with increasing temperature. However, Wood (1986) argues that in a closed system, calcite solubility appears to increase with increasing temperature until 125°C when calcite solubility appears to decrease with an increase in temperatures. Wood (1986) suggests that in an open system the solubility of calcite appears to decrease with increasing temperature.

For dolostone, Zhang et al. (2007) suggest that dolomite dissolution also increases with increasing temperature at lower temperatures but then becomes retrograde at higher temperatures. The research suggests that the grain size plays a major role, showing that for smaller grain sizes (20-40 mesh), dolomite dissolution increases with increasing temperature between 0-200°C, yet between 0-100°C for the larger grain size samples (40-60 and 60-80 mesh). Morse et al. (2007) however disagree, arguing that the dissolution of dolomite appears to decrease with increasing temperature as increased dolomite precipitation is evident with increasing temperatures.

Due to the contradiction of the relationship between both limestone and dolostone and temperature appearing throughout the research, it is difficult to make assumptions on what is expected to see from the experiments undertaken. The research will be considered when analysing the findings. The majority of the findings direct towards calcite solubility decreasing with increasing temperature.

Kirstein et al. (2016)'s study identifies the dissolution of smaller grains within a calcite matrix compared to the larger calcite grains. This reinforces the likelihood of preferential dissolution of the

smaller grains (resultant from crushing due to the pressure), compared to the larger grains in the artificial fracture matrix of limestone and dolostone samples.

5.1.1 Limestone: Closed-loop Experiment

5.1.1.1 Limestone Fracture Analysis

Studying figures 4.6.1 – 4.6.3, a clear fracture is evident through the limestone core samples. The artificial fracture is filled with grains and pore spaces. The fracture contains considerably more and larger pores than the surrounding host rock, proving that the fracture is more permeable than the surrounding host rock and likely the preferential fluid pathway.

In figures 4.6.1 – 4.6.3 and 4.7.1 – 4.7.3, an evident, predominant grain size is established inside the limestone fractures. Inside the limestone fractures, surrounding the larger grains, there appears to be a number of small grains, smaller than the obvious and predominant grain-size. Due to the grains inside the fractures being sieved to between approximately 200-250 microns, it is clear the small grains have resulted from the experiment. One of the most likely scenarios for the presence of small grains in the fracture is due to the crushing of larger grains and/or the host, resulting from the pressure of the system, either from the fluid pressure or the imposed stress, which was at a constant of approximately 1500psi throughout the experiment. Evidence of grain crushing can be seen in figures 4.8.1 – 4.8.3 and 4.9.1 – 4.9.2. The larger, predominant grains within the fracture appear to be breaking down into smaller grains. Another contributor to the accumulation of small grains may have been the weathering and/or breakdown of larger grains from the constant exposure to fluid throughout the experiment.

In figures 4.6.1 – 4.6.3 and 4.7.1 – 4.7.3, there appears to be a larger number of small pockets of grains (the grains in-between the larger, pre-dominant grains inside the fracture) in sample B (ambient) compared to A (80°C) and D (40°C) (highlighted by red boxes in figure 4.7.1), albeit difficult to tell from studying the image alone. If this is the case, this may suggest that more dissolution of small grains was occurring in the 80°C and 40°C core holders. As the small grains likely resulted from the crushing of large grains due to the overriding pressure, it is likely the number of small grains produced in each sample was similar. Therefore, we would expect to see a similar number of small grains in each sample. If this isn't the case, it would suggest that more dissolution reactions have occurred to transport or dissolved the small grains in sample A (80°C) and sample D (40°C). An ImageJ analysis was undertaken

on figures 4.6.1, 4.6.2 and 4.6.3 to identify the amount of dark space in the fracture, which identifies the amount of porosity. The ImageJ analysis was undertaken on the fracture only, not the surrounding host rock. The results show the following porosity (%) in the fractures:

- sample B (figure 4.6.1) = 25.8% porosity in the fracture
- sample A (figure 4.6.2) = 25.9% porosity in the fracture
- sample D (figure 4.6.3) = 25.7% porosity in the fracture

The results show that sample A (80°C) has the largest porosity in the fracture compared to the other samples, as hypothesised from studying figures 4.6.1 – 4.6.3, however sample D (40°C) has the lowest porosity in the fracture. This analysis would suggest an increase in porosity, with the temperature increase to 80°C, followed by a slight decrease in porosity, with the decrease in temperature to 40°C. The initial porosity increase may indicate dissolution in the fracture, followed by the decrease in porosity, suggesting precipitation in the fracture. The fracture porosity difference between sample B (ambient) and sample D (40°C) appears small and potentially insignificant. The increase in fracture porosity between sample A and the other two samples suggest a more significant increase in porosity. This shows an increase in fracture porosity, likely related to an increase in limestone dissolution, with the increase in temperature.

The accumulation of small grains in 'pore throats' may result in the reduction of permeability throughout the sample, due to a lower connectivity of pore spaces (Garing et al. 2015). This increase in small grains, likely occurring from crushing of larger grains, may have helped to decrease the permeability throughout the experiment (Figure 4.7.1 – 4.7.3) (Garing et al. 2015). With increased dissolution of small grains, the permeability is likely to increase with more dissolution (Garing et al. 2015). Despite sample B (ambient) appearing to have a higher porosity than sample D (40°C), studying figures 4.7.1 – 4.7.3, if the small grains in sample B (ambient) were causing the blocking of pore throats between pores, it may decrease the permeability in sample B. In figures 4.7.1 – 4.7.3, sample A (80°C) visually appears to have fewer small grains in pore throats, which may suggest higher pore connectivity, and a higher permeability in sample A (80°C). This evidence corresponds to the permeability results for sample A (80°C) showing a higher permeability than sample B (ambient) and sample D (40°C) (figure 4.51). Sample A (80°C) having a higher porosity compared to limestone samples B and D may also suggest there has been an increase in dissolution with an increase in the temperature.

5.1.1.2 Limestone Host Rock Analysis

Studying figures 4.10.1 – 4.10.4 and figures 4.11.1 – 4.11.4, the host rock porosity is evident. The host rock porosity shows small pores, suggesting that the limestone samples have a low porosity. Overall, the porosity between the varying temperature core holders appears to show slight variation. When comparing all three samples B, A and D to the initial limestone sample taken pre-experiment, it is evident all three samples have undergone some change in their porosity throughout the duration of the experiment. When comparing between the images visually, it is evident more dark areas (relating to pore spaces) appear present in samples A and D taken post-experiment. This signifies that despite there being a main fluid flow pathway through the fracture, alteration has likely occurred inside the host throughout the experiment.

Sample A (80°C) shows a significantly larger number of pores in comparison to the ambient (sample B) and initial limestone sample (figures 4.10.1 – 4.10.4 and 4.11.1 – 4.11.4). This may signify more dissolution in the host rock in this sample, perhaps due to the higher temperature. The pores appear more abundant but also larger, meaning pre-existing pores have potentially increased in size and/or connected. An increase in pores and their connectivity may ultimately lead to an increase in porosity and permeability (Garing et al. 2015).

In Sample D (40°C) in figures 4.10.1 – 4.10.4 and 4.11.1 – 4.11.4, it could possibly be argued that there appears to be a higher porosity in this sample also, albeit difficult to see an obvious difference in the number of pores. It is difficult to determine this from the micro-structural images alone, due to there not being a significant change in sample D. It is difficult to accurately determine the porosity from the SEM images in the limestone, due to the pores being so small and varied throughout the samples. When compared alongside the permeability data however, sample A (80°C) and D (40°C) appear to have higher permeabilities than sample B (ambient) by the end of the experiment (figure 4.51). This aligns with the suggestion that more dissolution occurred in the host rock in sample A (80°C) and potentially in sample D (40°C) in the SEM images. The permeability data accounts for the fracture and the host rock, therefore sample D (40°C) appearing to have a slightly higher permeability than sample A (80°C) may be a result of the permeability of the fracture. An ImageJ analysis has been undertaken on figures 4.10.1 – 4.10.4, to try and quantify the porosity (%) in the host rock. The ImageJ analysis was undertaken on the entire host rock images. The results show the following porosity (%) in the host rock:

- initial limestone sample (figure 4.10.1) = 0.955% porosity in the host rock
- sample B (figure 4.10.2) = 0.9% porosity in the host rock
- sample A (figure 4.10.3) = 1.7% porosity in the host rock
- sample D (figure 4.10.4) = 1.1% porosity in the host rock

The results show that sample A (80°C) has the largest porosity in the host rock, as hypothesised from studying figures 4.10.1 – 4.10.4, whilst sample B (ambient) has the lowest porosity in the fracture. Sample B (ambient) portrays a lower porosity than the initial limestone sample. This may indicate that precipitation occurred in sample B at ambient temperatures, however, the difference between the initial porosity and the porosity recorded in sample B after the experiment is small. It's worth noting that the SEM images chosen for the ImageJ analysis may not be entirely representative of porosity throughout the entire samples. Sample D (40°C) portrays a higher porosity than sample B (ambient), followed by sample A (80°C) with the highest porosity of all three samples. This further adds to the results within the fracture, showing an increased porosity with increased temperature. Increased porosity suggests that increased limestone dissolution occurred in sample A, subject to 80°C.

It is difficult to identify where precipitation has potentially occurred in the samples when simply looking at the micro-structural images. If precipitation occurred, it would be presumed to have occurred in the place of the least resistance, most likely the fracture (Bai et al. 2019). If more precipitation was occurring inside the fracture compared to the host, perhaps the fluid flowed through the host to compensate for any cemented areas inside the fracture.

5.1.1.3 Summary of Limestone Analysis during the Closed-loop Experiment

- Small grains (surrounding the predominant grain-size) inside the fracture are likely resulting from the crushing of larger grains due to a pressure of approximately 1500psi throughout the experiment.
- ImageJ analysis indicates there is a higher porosity in the fracture in sample A (80°C) compared to samples B and D (40°C). Sample D (40°C) has the lowest porosity in the fracture of all the three samples. The results show an initial decrease in porosity from temperatures between approximately 25°C and 40°C, then an increase in porosity between temperatures 40°C and 80°C. The difference in porosity between sample B (ambient) and D (40°C) however is small, with a more significant difference in porosity between sample A (80°C) and samples B and D. The results suggest an increase in porosity with increasing temperature, suggesting increased

limestone dissolution with increasing temperature. The lack of small grains within the pore spaces in the fracture in sample A (80°C) further suggests increased dissolution in this sample.

- ImageJ analysis indicates there is a higher porosity in the host rock in sample A (80°C), with the second highest porosity in the host rock shown in sample D (40°C) and the lowest porosity evident in sample B (ambient). This evidence suggests that increased dissolution of limestone occurred with increasing temperature in the host rock.

5.1.2 Dolostone: Closed-loop Experiment

In section 4.5, a leak is mentioned, which occurred in the 40°C core holder in the closed-loop experiment. Before finding the leak, a lack of fluid was evident from the final water sampling valve located after the 40°C core holder (see figure 3.1 and figure 3.3). It was thought sample B1, located in the 40°C core holder, was restricting fluid flow, therefore, the sample was removed and cut in half to try and before being returned to the experiment. This is worth noting when analysing the results taken from sample B1 (40°C) throughout the discussion section.

On initial inspection of the SEM images in section 4.1, the dolostone samples (figures 4.12.1 – 4.12.3) appear to have a significantly higher number and larger pores than the limestone samples (figures 4.6.1 – 4.6.3).

5.1.2.1 Dolostone Fracture Analysis

Figures 4.12.1 – 4.12.3 portrays the fracture within the dolostone in samples B6 (ambient), B2 (80°C) and B1 (40°C). From visual inspection, sample B2 (80°C) (figure 4.12.2) portrays the highest porosity and permeability inside the fracture, showing larger and more inter-connected pore spaces throughout, in comparison to sample B6 (ambient) and sample B1 (40°C). Similar to the limestone, the smaller grains evident inside the dolostone fracture in all samples likely occurred from the pressure in the system remaining at 1500psi throughout, which potentially caused the breakdown of larger grains. Other contributors may also be weathering from the fluid resulting in the breakdown of larger grains (Ling et al. 2014). The same amount of pressure was applied throughout the system; therefore, it is presumed the number of small grains created from the crushing of the larger grains would have been the same throughout all samples. However, the evidence of larger and more interconnected pore spaces in sample B2 (80°C) suggests fewer small grains are evident in the fracture. One theory is the small grains in sample B2 (80°C) were dissolved. Wood (1986) suggests that at lower temperatures,

calcite dissolution increases with increasing temperatures until approximately 125°C. Zhang et al (2007) also argues that dolomite dissolution appears to increase with increasing temperature at lower temperatures between 0-200°C for small grain size particle and between 0-100°C for larger particles. More inter-connected pore spaces in sample B2 compared to samples B6 and B1 would suggest a higher permeability in the fracture of sample B2 (Huenges, 2016). This theory is also evident in the permeability data for the dolostone in the closed-loop experiment portrayed in figure 4.51. It is to be reminded that the development of a natural fracture in sample B2 likely affected the number of grains present post-experiment. It is impossible to say how many grains have potentially been lost out of the natural fracture (figure 4.14 and figure 4.15). The SEM image in figure 4.12.2 was taken away from the natural fracture, however it is still likely some grains may still have been lost from sample B2.

Figures 4.12.1 – 4.12.3 portrays dolostone (grey) with some limestone (white to pale grey) inclusions (figure 5.1.1). Studying the figures, the limestone inclusions are preferentially situated in the fracture compared to the dolostone host rock in samples B6, B2 and B1. The limestone inclusions appear in the initial dolostone sample pre-experiment, so it is known that the limestone was present pre-experiment (figure 4.17.1). The limestone being preferentially present inside of the fracture compared to the host rock, however, is unlikely a coincidence (figures 4.12.1 – 4.12.3). One theory is that the Mg has been preferentially released into solution inside the fracture, where more fluid is likely to be present in the samples. The abundance of more limestone inclusions within the fracture compared to the host rock suggests that more chemical reactions were potentially happening in the fracture, where it's assumed fluid would have been preferentially flowing. Therefore, leaving the pre-existing limestone inclusions inside the fracture in contrast to the Mg-rich dolostone. There is also the possibility that the Mg from the dolomite was preferentially released into solution, causing a compositional change in the dolostone and leaving a $CaCO_3$ composition of limestone (Warren, 2000).

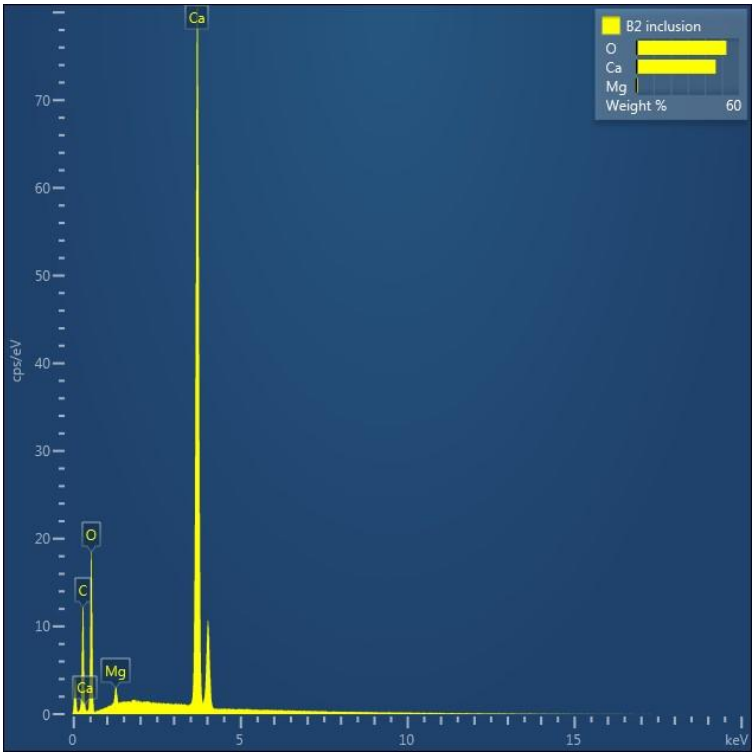

Figure 5.1.1: Graph to show the Aztec grain analysis undertaken on dolostone sample B2. The composition appears to consist of calcium carbonate, suggesting a limestone composition.

When studying the limestone inclusions in Figure 4.13.1 – 4.13.3, when compared to the dolostone, the limestone has little to no pores evident. The contrast in porosity continues to suggest that Mg-rich dolostone is potentially preferential to release into solution compared to the limestone. This is due to the limestone inclusions showing few or no pores, suggesting little dissolution as increased dissolution would likely increase the porosity.

Figure 4.13.1-4.13.2 shows the grains within the fracture in the dolostone samples, where it may be suggested the pores in samples B6 (ambient) and B1 (40°C) appear to be less connected compared to sample B2 (80°C). The pore spaces being less connected in these samples may suggest more difficult fluid flow through these samples. Some grains appear to be blocking pathways between the pore spaces in sample B6 and sample B1, therefore reducing permeability. Particularly, B1 (40°C) shows a lower connectivity between pore spaces in comparison to B2 (80°C). This may be due to either; (1) a lack in dissolution of small grains in samples B6 (ambient) and B1 (40°C) in comparison to sample B2 (80°C) or (2) more precipitation in samples B6 (ambient) and B1 (40°C) in comparison to sample B2 (80°C), or both options may have occurred. It is to be remembered that the natural fracture that occurred in sample B2 (80°C) may have resulted in the apparent loss of some grains. One theory could be that due to the 40°C core holder following on from the 80°C core holder, grains from sample B2

(80°C), where more dissolution appears to have occurred, may have been precipitated in sample B1 (40°C), where less dissolution and perhaps more precipitation appears to have occurred.

An ImageJ analysis was undertaken on figures 4.12.1, 4.12.2 and 4.12.3 to identify the amount of dark space in the fracture, which is the amount of porosity. The ImageJ analysis was undertaken on the fracture only, not the surrounding host rock. The results show the following porosity (%) in the fractures:

- sample B6 (figure 4.12.1) = 40.2% porosity in the fracture
- sample B2 (figure 4.12.2) = 51.0% porosity in the fracture
- sample B1 (figure 4.12.3) = 32.4% porosity in the fracture

The results show that sample B2 (80°C) portrays the highest porosity in the fracture, as hypothesised from studying figures 4.12.1 – 4.12.3, and sample B1 (40°C) has the lowest porosity in the fracture. The results appear similar to the porosity recorded in the limestone fractures in samples B, A and D from the closed-loop experiment, which also portrayed the sample subject to 80°C as having the highest porosity and the sample subject to 40°C as having the lowest porosity. This analysis shows there is an initial increase in dissolution in sample B2 (80°C) compared to sample B6 (ambient), when the fluid moves from an ambient temperature to 80°C, followed by a decrease in dissolution and potential precipitation in sample B1, subject to 40°C. This analyse shows that the most dissolution appears to be evident in sample B2, subject to 80°C. One theory why sample B1 (40°C) may show lower porosity compared to sample B6 (ambient) may be due to the increased porosity, and suggested dissolution, evident in sample B2 (80°C) (situated in the experiment before sample B1). Having potentially reacted with sample B2 (80°C) before reaching sample B1 (40°C), the fluid may be close to saturation and therefore, less dissolution can occur in sample B1 (Goldscheider et al. 2010).

5.1.2.2 Dolostone Fracture-Host Boundary

Figure 4.16.1 – 4.16.3 shows the fracture-host boundary in the dolostone samples (B6, B2 and B1) appearing more jagged in comparison to the limestone samples (B, A and D) fracture-host boundary (see previous figure 4.9.1 and 4.9.2). One reason for the difference in shape of the boundary may be due to the higher porosity of the dolostone host rock compared to the limestone. The pores in the dolostone appear more abundant and larger in size compared to the limestone. This may lead to instability in the dolostone and the potential breaking of grains from minerals being dissolved (Ling et

al. 2014). The breakdown of the dolostone fracture-host boundary has potentially resulted in the formation of evident small grains, which are easier to dissolve (Zhang et al. 2007).

Studying figures 4.12.1 – 4.12.3 and 4.16.1 – 4.16.3 and comparing the porosity of the grains (within the fracture) and porosity of the host rock in the dolostone samples, the host rock appears to have larger pores than that of the grains within the fracture. One theory is that there may be more dissolution required in the host rock to enable fluid flow, due to the host rock porosity appearing visually less connected, when analysing all the SEM images.

5.1.2.3 Dolostone Host Rock Analysis

Figures 4.17.1 – 4.17.4 portray the dolostone host rock at a magnitude of 1-2mm. Overall, all the dolostone samples portray obvious, large pores, proving a high porosity in the dolostone relative to the limestone samples previously analysed (figure 4.10.1 – 4.10.4).

When studying the SEM images, on initial inspection samples B2 (80°C) and B1 (40°C) appear to hold a higher number and also larger pore spaces in comparison to sample B6 (ambient) and the pre-experiment dolostone sample (figure 4.17.1 – 4.17.4). However, an ImageJ analysis revealed that sample B6 (ambient) actually has a higher porosity than samples B2 (80°C) and B1 (40°C). This higher porosity is likely due to the smaller pores within the matrix, evident in figures 4.18.1 – 4.18.4. In the initial dolostone sample (figure 4.18.1), there are obvious and predominant, larger pores throughout. In sample B6 (ambient) (figure 4.18.2), there appears to be potentially smaller and/or less of the predominant pores, however, interestingly, the host matrix appears to have a higher porosity, with multiple small pore spaces located in the matrix surrounding the main, predominant pores. It is interesting as to why there appears to be more dissolution of the matrix in sample B6 (ambient) compared to the other samples. Perhaps this is due to more dissolution occurring at lower temperatures as stated by Goldscheider et al. 2010, Morse et al. 2007, Plummer and Wigley (1976), Plummer et al. (1978) and Kirstein et al. 2016, who say that the solubility of calcite decreases with increasing temperature. However, this would conflict with the previous evidence seen so far throughout the limestone samples and dolostone fracture, which appears to show increasing dissolution with increasing temperature occurring in the results. The ImageJ analysis was undertaken on the entire host rock images portrayed in figures 4.17.1 – 4.17.4. The results show the following porosity (%) in the host rock:

- initial dolostone sample (figure 4.17.1) = 20.9% porosity in the host rock
- sample B6 (figure 4.17.2) = 27.9% porosity in the host rock
- sample B2 (figure 4.17.3) = 22.2% porosity in the host rock
- sample B1 (figure 4.17.4) = 17.2% porosity in the host rock

It is likely that the higher porosity in sample B6 (ambient) was created from increased dissolution of the dolostone host from the percolating fluid. Despite this, samples B2 (80°C) and B1 (40°C) portray obvious larger pores compared to sample B6, showing the potential breakdown of pore spaces. The results from the analysis of the porosity evident in the dolostone host rock, during the closed-loop experiment appear to support research from Goldscheider et al. 2010, Morse et al. 2007, Plummer and Wigley (1976), Plummer et al. (1978) and Kirstein et al. 2016, who say that the solubility of calcite decreases with increasing temperature. However, this counter-argues previous evidence from section 5.1.1 and 5.1.2, which suggested that there appeared to be increased dissolution at higher temperatures in the limestone and dolostone during the closed-loop experiment.

When studying the fracture in sample B1 (40°C), there appears to be less connected pore spaces and more cementation than the fracture porosity in sample B2 (80°C). However, when looking at the host rock porosity of sample B1 (40°C), it appears significantly altered, showing higher porosity and larger pore spaces than the initial dolostone porosity (figure 4.17.1 – 4.17.4). Therefore, perhaps there was precipitation or less dissolution within the fracture, whereby, this was compensated in the host rock and more dissolution occurred here.

In figures 4.18.1 – 4.18.4, sample B2 (80°C) and B1 (40°C) both portray sharp, angular and often right-angled edges along the pore spaces. The right-angled edges are called facets (Snyder and Doherty, 2007). Increased dissolution makes grains more angular, therefore further reinforcing that dissolution was occurring and the facets are particularly evident in samples B2 and B1, the higher temperature samples (Snyder and Doherty, 2007). This may suggest that more dissolution was occurring along pore boundary edges in both of these samples. These angular facets can also be seen in the initial dolostone sample taken pre-experiment, but not so much in sample B6 (ambient) (figure 4.18.1 – 4.18.4). The lack of facets in sample B6 (ambient) along the pore boundaries may reinforce that more precipitation was occurring inside the predominant pores than dissolution (as previously stated in the paragraph above) (figure 4.18.1 – 4.18.4).

5.1.2.4 Summary of Dolostone Analysis during the Closed-loop Experiment

- Similar to the limestone, the dolostone portrays small grains surrounding the large, predominant grains, which likely occurred from the crushing of these larger grains due to the constant pressure of approximately 1500psi throughout the experiment.
- ImageJ analysis indicates that sample B2 (80°C) portrays the highest porosity inside the fracture. This may identify increased dissolution with increased temperature or potentially due to the loss of grains from the evident natural fracture that occurred during the experiment.
- Limestone inclusions evident in all of the dolostone samples appear to be more concentrated in the fracture in comparison to the host rock. This suggests the release of more Mg into solution in comparison to the $CaCO_3$ inclusions. This also suggests more chemical reactions likely occurred in the fracture, where the fluid was likely preferentially flowing.
- The dolostone fracture-host boundary appears more jagged than the limestone boundary, suggesting instability along the boundary due to larger pores inside the dolostone.
- ImageJ analysis indicates that sample B6 (ambient) portrays a higher porosity in the host rock than sample B2 (80°C) and sample B1 (40°C). There appears to be increased porosity within the matrix of the host rock in sample B6 (ambient), however, not an increase in the large obvious pores that are evident in samples B2 and B1. This evidence suggests that there appears to be lower dissolution with the increase in temperature in the dolostone host rock, during the closed-loop experiment.
- Samples B2 (80°C) and B1 (40°C) show more jagged, angular and right-angles edges along their pores, known as facets. This may suggest that increased dissolution was occurring along the pore edges in samples B2 and B1, as more dissolution typically results in jagged edges.

5.1.3 Comparison Between the Limestone and Dolostone Analysis from the Closed-loop Experiment

Overall, the limestone host rock appears significantly less porous than the dolostone. The fracture-host boundary in the limestone appears to be more parallel compared to the jagged dolostone fracture-host boundary. This suggests less dissolution may have occurred in the limestone, as there appears to be less breakdown along the fracture-host boundary. However, it may also suggest that the dolostone was easier to break due to having an initial high porosity (Ling et al. 2014). Facets can be seen in the dolostone, which suggests dissolution due to the breakdown of the pore boundaries (however the limestone pores may be too small to determine facets along their pore boundaries) (Snyder and Doherty, 2007). The limestone fracture and host rock both portrayed the highest porosity, and therefore likelihood of increased dissolution, to occur at in the sample subject to the highest

temperature of 80°C. The same was evident within the dolostone fracture, however the opposite was evident in the host rock which portrayed a potential decrease in dissolution with an increase in temperature. Due to the conflicting results, it is difficult to determine whether less dissolution is definitely occurring with increased temperature.

The changes in porosity resulting from the relationship between temperature and dissolution are important when considering a geothermal setting (Huenges, 2016). With increased dissolution would likely become increased porosity. Increased porosity would help to maintain a viable geothermal system as the heated fluid would be able to flow through the surrounding dolostone host rock (Huenges, 2016).

5.1.4 Limestone: Open-loop Experiment

5.1.4.1 Limestone Fracture Analysis

Figures 4.19.1 – 4.19.3 portray the limestone samples C (ambient), F (80°C) and E (40°C) with the artificial fracture, infilled with grains. The dark spaces represent the pores spaces in the sample. In figures 4.19.1 – 4.19.3, the grains, within the fracture, appear to be angular to sub-rounded. Studying figures 4.19.1 – 4.19.3, there appears to be higher porosity and interconnected porosity, representing the permeability of the samples, within the fracture compared to the surrounding host rock. Therefore, suggesting the fracture will be the preferred area of fluid flow within the sample (there will still likely be fluid flowing through the host rock sample).

In figures 4.19.1 – 4.19.3, comparing the amount of the pore spaces in the fractures between core holders, it is difficult to tell which sample has the highest number of pore spaces within the fracture. As previously mentioned, the small, fine grains evident surrounding the large, pre-dominant grains have likely formed from the pressure in the system, resulting in evident crushed grains. Upon visual inspection of images 4.19.1 – 4.19.3 and 4.21.1 – 4.21.3, it may be argued that there appears to be a lack of small grains present in the fracture in sample F (80°C), compared to sample C (ambient). This may suggest that the smaller grains in sample F (80°C) have been removed via dissolution within the fluid. Sample E (40°C) has not been compared due to the presence of resin residue in the sample, resulting in the appearance of more pores in the sample. Also, the presence of the natural fracture in figure 4.20, along with the missing grains, suggest the number of grains evident in the SEM image may

not represent the true number of grains left in the artificial fracture before the natural fracture occurred.

An ImageJ analysis was undertaken on figures 4.19.1, 4.19.2 and 4.19.3 to identify the amount of dark space in the fracture, aka, the amount of porosity. The ImageJ analysis was undertaken on the fracture only, not the surrounding host rock. The results show the following porosity (%) in the fractures:

- sample C (figure 4.19.1) = 25.8% porosity in the fracture
- sample F (figure 4.19.2) = 24.5% porosity in the fracture
- sample E (figure 4.19.3) = 29.4% porosity in the fracture

Not factoring in sample E due to the presence of residue affecting the results, the ImageJ analysis results show that sample C (ambient) appears to have the largest porosity in the fracture compared to sample F (80°C), suggesting increased dissolution in sample C compared to sample F.

Figures 4.21.1 – 4.21.3 portray the grains within the fracture in the limestone during the open-loop experiment. The grains are evident at higher magnitude. Of the three samples, despite having a smaller porosity recorded from the ImageJ analysis in the fracture, sample F (80°C) appears to have the least number of small grains filling in the pore spaces and appearing the most inter-connected. In sample C (ambient), there appears to be several areas showing small-grain accumulation in pore spaces, which are highlighted by red boxes in figure 4.21.1. Sample E (40°C) appears to also show the accumulation of more small, fine grains in some pore spaces compared to sample F. This information suggests there may have been increased dissolution of finer material in sample F (80°C) compared to sample C (ambient) and sample E (80°C) as it is assumed a similar number of small grains would have been produced from crushing in all samples during the experiment (figures 4.21.1 – 4.21.3).

The blocking of pore throats with the fine material evident in figures 4.21.1 – 4.21.3 may reduce the interconnectivity of the pore spaces and thus, the permeability (Garing et al. 2015). In a geothermal system, the permeability enables fluid flow and therefore once this is reduced, it may affect the efficiency of a geothermal system reliant on natural fluid flow through the rock (Garing et al. 2015).

Figures 4.22.1 – 4.22.3 portray the fracture-host boundary in the limestone after the open-loop experiment. Evidence of crushing, likely due to the pressure in the system, is present along the boundary as the boundary appears to be 'breaking away' in certain areas. The red boxes in figures 4.22.1 – 4.22.3 highlight where crushing may be occurring. Figure 4.22.1 highlights a fracture within a grain, portraying the breakdown of grains in the fracture. Evident grain crushing and the breakdown of the fracture-host boundary is thought to have occurred due to pressure throughout the system, however, another reason to consider is that the constant fluid flow may have contributed to dissolution and breakdown of the rock.

5.1.4.2 Limestone Host Rock Analysis

Figures 4.23.1 – 4.23.4 and 4.24.1 – 4.24.4 portray the host rock of the limestone samples after the open-loop experiment, at magnitudes of 1-2mm and 500-600µm, respectively. It is difficult to compare between the limestone samples due to the initial porosity of the host rock being so low. It is to be reminded that many of the dark areas on sample E (40°C) have likely occurred due to resin residue within the sample. Studying figures 4.23.1 – 4.23.4, sample F (80°C) appears to comprise of a few areas of larger pore spaces in comparison to sample C (ambient) and sample E (40°C). The increased number of larger pore spaces suggest more dissolution may have occurred in sample F (80°C) in comparison to samples C and E. To further add to this evidence, figures 4.24.1 – 4.24.4 show a similar story, where sample F (80°C) appears to show a high porosity, with larger pore spaces, suggesting dissolution. An ImageJ analysis has been undertaken on figures 4.23.1 – 4.23.4, to try and quantify the porosity (%) in the host rock. The ImageJ analysis was undertaken on the entire host rock images. The results show the following porosity (%) in the host rock:

- initial limestone sample (figure 4.23.1) = 0.955% porosity in the host rock
- sample C (figure 4.23.2) = 2.1% porosity in the host rock
- sample F (figure 4.23.3) = 2.5% porosity in the host rock
- sample E (figure 4.23.4) = 3.3% porosity in the host rock

Not factoring in sample E due to the presence of residue affecting the results, the results show that sample F (80°C) appears to have a higher porosity in the host rock compared to sample C (ambient). This suggests increased dissolution appears in sample F (80°C) compared to sample C (ambient), alongside the evidence of visually larger pore spaces in sample F (80°C) in figures 4.23.1 – 4.23.4 and 4.24.1 – 4.24.4. Therefore, in the host rock the ImageJ analysis suggests that sample F (80°C) has a higher porosity, however, studying the fracture, the analysis suggests that sample C (ambient) has a higher porosity. The conflicting information in the analysis between the porosity in the fracture and

host rock may have occurred due to (1) differences in the initial porosity affecting the final porosity, (2) the SEM images chosen not representing the entire sample, (3) similar dissolution rates may have occurred throughout the samples, however, preferentially occurred in the fracture in sample C and in the host rock in sample F or (4) precipitation may have occurred, decreasing the porosity in the fracture in sample F (80°C). However, it is difficult to determine the relationship between the dissolution and temperature due to sample C (ambient) showing higher porosity in the fracture and sample F (80°C) showing higher porosity in the host rock.

5.1.4.3 Summary of Limestone Analysis during the Open-loop Experiment

- A natural fracture occurred in sample E. Therefore, the large gap in the fracture likely occurred from grain loss through the natural fracture. It is difficult to determine the number of grains lost through the fracture. Sample E also appears to portray dark areas of likely resin residue from analysis preparation, it is to be made sure that the dark areas are not to be confused with pores.
- Evidence of small grains, likely from crushing are evident in the samples. Sample C (ambient) appears to comprise the highest amount of fine material in the SEM images. Sample F (80°C) appears to show the least amount of fine material, suggesting increased dissolution and/or the movement of small grains in sample F.
- ImageJ analysis indicates there is a higher porosity in the fracture in sample C (ambient) compared to sample F (80°C), suggesting an increase in dissolution in the lower temperature sample.
- Sample F comprises of larger pore spaces in the host rock compared to samples C and E, suggesting increased dissolution was occurring in this higher temperature core holder.
- ImageJ analysis indicates there is a higher porosity in the host rock in sample F (80°C) compared to sample C (ambient), suggesting an increase in dissolution in the higher temperature sample.
- The conflicting results between the ImageJ analysis showing the porosity in the fracture compared to the host rock may have been determined by: (1) differences in initial porosity, (2) the SEM image chosen may not have been representative of the whole sample, (3) similar dissolution rates may have occurred throughout the samples but may have preferentially occurred in the fracture in sample C (ambient) and in the host in sample F (80°C) or (4) precipitation may have occurred and decreased porosity in the fracture in sample F (80°C).

5.1.5 Dolostone: Open-loop Experiment

5.1.5.1 Dolostone Fracture Analysis

Figure 4.25.1 – 4.25.3 portrays the SEM images of dolostone samples B5 (ambient), B4 (80°C) and B3 (40°C) taken after the open-loop experiment. The dolostone comprises of larger, more obvious pore spaces compared to the limestone. This reflects the higher porosity and permeability of the initial dolostone host rock taken pre-experiment (section 3.7 and section 3.8). The dolostone grains evident in the fracture appear to be angular to sub-rounded in shape. Studying the porosity in the fracture in sample B4 (80°C) compared to the samples B5 (ambient) and B3 (40°C), the gaps in the fracture in sample B4 appear visually larger and more connected, portraying larger gaps and likely representing higher porosity. An ImageJ analysis was undertaken on figures 4.25.1, 4.25.2 and 4.25.3 to identify the amount of dark space in the fracture, aka, the amount of porosity. The ImageJ analysis was undertaken on the fracture only, not the surrounding host rock. The results show the following porosity (%) in the fractures:

- sample B5 (figure 4.25.1) = 38.4% porosity in the fracture
- sample B4 (figure 4.25.2) = 39.0% porosity in the fracture
- sample B3 (figure 4.25.3) = 35.9% porosity in the fracture

The results show the lowest porosity between the dolostone samples is evident in sample B3 (40°C). Sample B4 (80°C) has the highest porosity in the fracture of all three samples after the experiment. This reinforces evidence from the limestone and dolostone from the closed-loop experiment, which showed the highest porosity was also in the sample subject to 80°C. This suggests that in the limestone and dolostone during the closed-loop experiment and the dolostone during the open-loop experiment, more dissolution is evident in samples subject to the higher temperature, 80°C core holder. Figures 4.27.1 – 4.27.3 portray the grains inside the fracture at a higher magnitude, whereby sample B4 (80°C) appears to have better connected pore spaces than samples B5 (ambient) and sample B3 (40°C). The connectivity of the pores likely results in a higher permeability in the fracture. This evidence reinforces the previously assumed likelihood that increased dissolution occurs within higher temperatures.

Figure 4.26 portrays the fracture in sample B5 (ambient) surrounded by a pale grey inclusion. A chemical composition analysis was undertaken on the pale grey mineral from both inside the fracture and outside the fracture (figure 5.1.2 and 5.1.3). The results show a calcium rich mineral, with a carbonate component, suggesting a calcium carbonate i.e., limestone inclusion. The inclusion surrounding the fracture appears to infill pre-existing pore spaces in the dolostone host rock (figure

4.26). It is difficult to determine whether the mineral was precipitated pre-experiment or during the experiment. An argument for the mineral occurring before the experiment is that the mineral inclusions in the host rock on either side of the fracture appears to fit well together. The mineral may have been precipitated into the dolostone in its natural setting and when fractured, the artificial fracture may have sliced pre-existing inclusions. However, an argument for the presence of the inclusion occurring as a result of the experiment is; the inclusion appears most abundant close to the fracture, the area with the most fluid flowing through. This high fluid flow may have resulted in the increase in the limestone inclusion by; (1) preferential release to solution of surrounding Mg in the dolostone sample, stripping the Mg and leaving the limestone and/or (2) precipitation of Ca into pre-existing dolostone pores due to high Ca-levels in the fluid, whereby calcium saturation levels are reached, resulting in precipitation. In the closed-loop experiment, there was evidence of preferential limestone inclusions inside the fracture. Therefore, providing evident that some of the limestone inclusions inside the fracture and surrounding the fracture may have occurred due to reactions during the experiment. However, due to the scale of the limestone inclusions surrounding the fracture in sample B5, along with the alignment of inclusions located either side of the fracture, a likely explanation is that most of the surrounding inclusions occurred pre-experiment.

Figures 4.27.2 portrays a higher magnitude SEM image of a limestone inclusion within a grain inside the dolostone fracture. The SEM image portrays the porosity difference in the limestone inclusion compared to the dolostone host. The limestone inclusion appears significantly less porous. More dissolution of the dolostone is likely to occur due to the high porosity dolostone being more unstable (Ling et al. 2014).

5.1.5.2 Dolostone Fracture-Host Boundary

Figures 4.28.1 – 4.28.3 portray SEM images of the fracture-host boundary, in the dolostone samples, located in the open-loop experiment. The dolostone boundary appears far more jagged and wavey in comparison to the limestone. Evidence of the dolostone breaking away from the host rock and entering the fracture can be seen in the images, portraying a dolostone fracture-host boundary that no longer appears clear-cut. The increased porosity evident in the dolostone potentially contributes to the dolostone being more unstable, therefore, being more susceptible to breaking along the pore boundaries and the disintegration of the breaking fracture-host boundary (Ling et al. 2014).

5.1.5.3 Dolostone Host Rock Analysis

Figures 4.29.1 – 4.29.4 and 4.30.1 – 4.30.4 portray the host rock of the dolostone samples after the open-loop experiment, at magnitudes of 1-2mm and 500-600µm, respectively. All three dolostone samples located in the open-loop experiment appear highly porous. The SEM image of sample B4 (80°C) portrays one large pore, suggesting the breaking of multiple smaller pores along the boundaries to produce one large pore space (figure 4.29.3). Comparing figures 4.29.1 – 4.29.4, showing the initial dolostone host rock and the three dolostone samples B5 (ambient), B4 (80°C) and B3 (40°C) taken after the open-loop experiment, all three samples appear to have been affected by dissolution, as the pore spaces, compared to the initial host rock, appear more abundant and larger in size. An ImageJ analysis was undertaken on the entire host rock images portrayed in figures 4.29.1 – 4.29.4. The results show the following porosity (%) in the host rock:

- initial dolostone sample (figure 4.29.1) = 20.9% porosity in the host rock
- sample B5 (figure 4.29.2) = 28.9% porosity in the host rock
- sample B4 (figure 4.29.3) = 21.0% porosity in the host rock
- sample B3 (figure 4.29.4) = 21.0% porosity in the host rock

The results show that sample B5 (ambient) has the highest porosity compared to the other samples, suggesting increased dissolution of dolostone by the percolating fluid. The porosity in samples B4 (80°C) and B3 (40°C) appear similar, however sample B4 (80°C) portrays the lowest porosity. This analysis shows the same pattern as the dolostone host rock porosity in the closed-loop experiment, which showed decreasing host rock porosity with increasing temperature. These results, which show less porosity with increasing temperature within the dolostone host rock during the open-loop experiment, supports research from Goldscheider et al. 2010, Morse et al. 2007, Plummer and Wigley (1976), Plummer et al. (1978) and Kirstein et al. 2016, who say that the solubility of calcite decreases with increasing temperature.

Figures 4.30.1 – 4.30.4 portray SEM images of the dolostone host rock samples at a higher magnitude. Evident facets can be seen along the pore space boundaries in all of the dolostone samples. The presence of facets become more right-angled and angular may suggest increased dissolution of the dolostone host rock (Snyder and Doherty, 2007). All of the samples appear to portray abundant jagged and right-angled pore space boundaries. Facets can also be seen in the initial dolostone sample, therefore it's hard to determine which facets existed in the host rock pre-experiment.

Comparing the SEM images of the dolostone samples between the closed-loop and open-loop experiments, the dolostone appears to show an interesting difference. Looking at the host rock in sample B6 (figures 4.17.1 – 4.17.4 and figures 4.18.1 – 4.18.4) (ambient), after the closed-loop experiments, compared to the host rock in sample B5 (figures 4.29.1 – 4.29.4 and figures 4.30.1 – 4.30.4) (ambient), after the open-loop experiment, sample B6 (ambient) appears to have significantly smaller pores. However, comparing the ImageJ porosity values showing sample B6 (ambient) with a host rock porosity of 27.972% and sample B5 (ambient) with a host rock porosity of 28.939%, the values appear similar. It is interesting as to why sample B6 (ambient), located in the closed-loop experiment, appears to comprise of a larger number small pores within the host rock matrix, compared to sample B5 (ambient), which still comprises of small pores in the matrix, however, alongside fewer but larger obvious pores.

5.1.5.4 Summary of Dolostone Analysis during the Open-loop Experiment

- Inclusions evident surrounding the fracture in sample B5 may have occurred pre-experiment. However, it is believed preferential release of Mg to solution and/or precipitation of Ca in some places may have occurred in the sample.
- ImageJ analysis indicates that sample B4 (80°C) portrays the highest porosity in the fracture, suggesting increased dissolution occurred in sample B4 compared to samples B5 (ambient) and B3 (40°C).
- The dolostone fracture-host boundary appears more wavey and jagged than the limestone. One theory is due to the high porosity of the initial dolostone, making the host rock more unstable and more likely to break along pores.
- ImageJ analysis indicates that sample B5 (ambient) has the highest porosity in the host rock, followed by sample B3 (40°C), which is followed by sample B4 (80°C). This suggests there is decreased dissolution with increased temperature in the dolostone host rock during the open-loop experiment.
- Facets are evident in the initial dolostone sample and in all the samples after the experiment, making it difficult to determine whether the facets occurred during the experiment. However, all the samples appear to show increased dissolution after the experiment. Sample B5 (ambient), in the open-loop experiment, appears to portray a higher porosity than sample B6 (ambient) located in the closed-loop experiment.

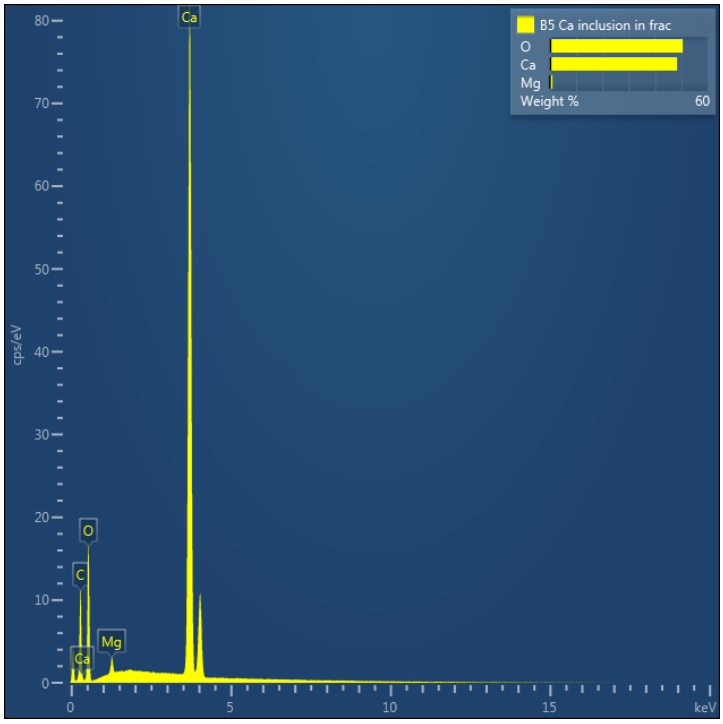

Figure 5.1.2: Chemical composition of the mineral evident in a grain, inside the fracture, in dolostone sample B5, located in the ambient core holder in the open-loop experiment.

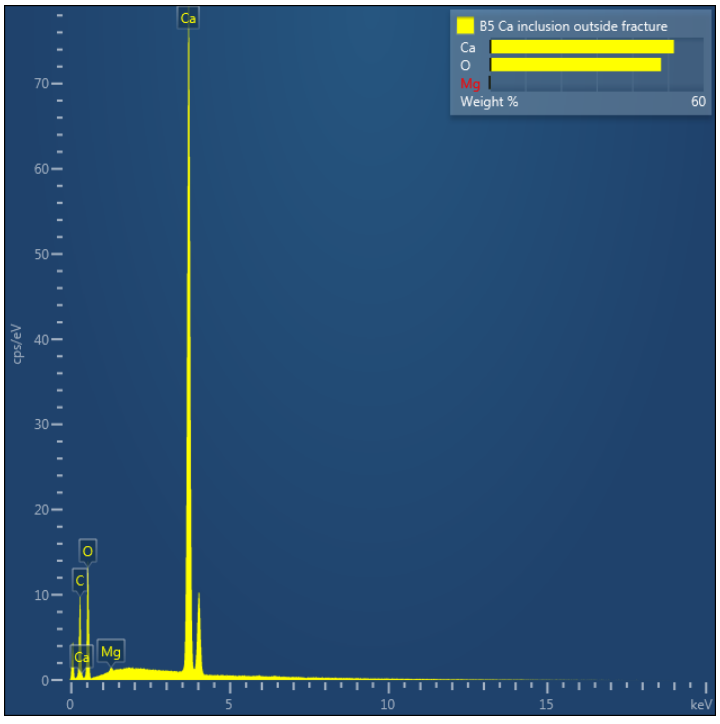

Figure 5.1.3: Chemical composition of the mineral evident outside the fracture in dolostone sample B5, located in the ambient core holder in the open-loop experiment.

5.2 CT Scan Discussion

5.2.1 CT Scan Analysis of the Limestone Core Samples

Figures 4.31.1 (a-b) – 3.31.2 (a-b), 4.32.1 (a-b) – 4.32.2 (a-b) and 4.33.1 (a-b) – 4.33.2 (a-b) portray CT scan images of the limestone core samples B (ambient), A (80°C) and D (40°C) before and after the closed-loop experiment. Comparing the CT scan images before and after the experiment, one can clearly see the fracture running through the centre of the core sample. The images are taken from the short axis of the core sample. The ImageJ analysis plots portray the grey-scale intensity of the pixels. The darker the pixel the lower the plot on the density graph. The black spaces represent pore spaces or gaps in the fracture, therefore suggesting lower porosity in these areas. Studying sample B (figure 4.31.1 (a-b) – 3.31.2 (a-b)), the fracture appears denser following the experiment due to showing fewer dark pixels and therefore, suggesting precipitation of grains within the fracture. This information suggests the fracture has become more cemented during the experiment, perhaps through precipitation or deposition of grains being transported by the fluid flow. Sample A (figure 4.32.1 (a-b) – 4.32.2 (a-b)) portrays the opposite, appearing to be less dense following the experiment, suggesting dissolution of grains during the experiment. Sample D (4.33.1 (a-b) – 4.33.2 (a-b)) portrays little to no change in the cementation of the fracture during the experiment; changes may still have occurred, however if they did occur, they have balanced one another out.

Figures 4.37.1 (a-b) – 3.37.2 (a-b), 4.38.1 (a-b) – 4.38.2 (a-b) and 4.39.1 (a-b) – 4.39.2 (a-b) portray CT scan images of the limestone core samples C (ambient), F (80°C) and E (40°C) before and after the open-loop experiment. Sample C (figure 4.37.1 (a-b) – 3.37.2 (a-b)) portrays little to no change in the cementation of the fracture. Sample F (4.38.1 (a-b) – 4.38.2 (a-b)) portrays less cementation of the fracture following the experiment, suggesting dissolution or movement of grains in the fracture. Sample E (4.39.1 (a-b) – 4.39.2 (a-b)) shows little to no change in the number of grains evident in the fracture following the experiment.

Comparing the results from the closed-loop and open-loop experiments, some conclusions can be drawn. The samples showing a reduction in the number of grains evident in the fracture after the experiment are samples A (closed-loop) and F (open-loop). Both of these samples were located in the 80°C core holder. This may be a coincidence, or it may suggest something is happening due to the higher temperature. The appearance of less grains in the fracture may have occurred from dissolution or the transportation of grains in the fluid. Due to only seeing less grains in the fractures in the 80°C core holder samples, it could be suggested that due to the increased temperature, more dissolution

was occurring within the samples and therefore, resulting in a loss of grains. This theory reinforces Wood (1986), showing that at lower temperatures, increased calcite dissolution would be expected with increased temperature. However, Wood (1986) suggests this is only the case in a closed system, yet the evidence portrays this occurring in both the closed-loop system and the open-loop system. This may be due to the fact the experiment focuses on limestone, with other minerals than calcite, and most of the research is undertaken on pure calcite not limestone.

Apart from samples B (ambient closed-loop), A (80°C closed-loop) and F (80°C open-loop), the other samples showed little to no change in the number of grains within the fracture pre- and post-experiment. This may suggest: (1) there has been little to no change or (2) any precipitation-dissolution reactions have cancelled one another out.

Sample B (ambient) showed an increase in the number of grains evident in the fracture following the closed-loop experiment. This may suggest precipitation was occurring within the fracture within this sample. Due to being in a closed-loop experiment, perhaps grains dissolved from the other samples were precipitated into the fracture inside sample B.

5.2.2 CT Scan Analysis of the Dolostone Core Samples

Figures 4.34.1 (a-b) – 3.34.2 (a-b), 4.35.1 (a-b) – 4.35.2 (a-b) and 4.36.1 (a-b) – 4.36.2 (a-b) portray CT scan images of the dolostone core samples B6 (ambient), B2 (80°C) and B1 (40°C) before and after the closed-loop experiment. The dolostone samples appear to show more detail than the limestone, with evident natural fractures and veins evident throughout all six of the dolostone core samples. Sample B6 (4.34.1 (a-b) – 3.34.2 (a-b)) appears to show an increase in the number of grains in the fracture post-experiment. Sample B2 (4.35.1 (a-b) – 4.35.2 (a-b)) shows less grains in the fracture after the experiment. Sample B1 (4.36.1 (a-b) – 4.36.2 (a-b)) portrays slightly less grains or little to no change in the number of grains evident in the fracture following the experiment.

Figures 4.40.1 (a-b) – 3.40.2 (a-b), 4.41.1 (a-b) – 4.41.2 (a-b) and 4.42.1 (a-b) – 4.42.2 (a-b) portray CT scan images of the dolostone core samples B5 (ambient), B4 (80°C) and B3 (40°C) before and after the open-loop experiment. Sample B5 (4.40.1 (a-b) – 3.40.2 (a-b)) appears to show little to no change in the number of grains evident in the fracture after the experiment. Sample B4 (4.41.1 (a-b) – 4.41.2 (a-

b)) appears to show less grains evident in the fracture, following the experiment. Sample B3 (4.42.1 (a-b) – 4.42.2 (a-b)) also shows a reduction in the number of grains in the fracture following the experiment.

The following theories are being put forward after comparing the results. Similar to the limestone, the samples located in the 80°C core holder, both samples B2 (closed-loop) and B4 (open-loop), appear to show a reduction in the number of grains in the fracture after the experiment. Also, both samples that were located in the 40°C core holder, samples B1 (closed-loop) and B3 (open-loop) from the change in density plot appear to show a reduction in the number of grains in the fracture, following the experiments. The reduction in grains within the fractures after the experiment is possibly due to dissolution of grains or the grains being transported by fluid. The reduction in grains evident in both the 80°C and 40°C core holders and not the ambient core holders, during the closed-loop and open-loop suggests that more dissolution may have been occurring in samples subject to the higher temperature core holders. The samples located in the ambient core holders appear to show either little to no change or an increase in grains in the fractures.

Sample B5 was located in the ambient core holder, during the open-loop experiment, and showed little to no change in the number of grains within the fracture. Similar to the limestone reasoning, this may show either little to no change in the number of grains being precipitated or dissolved in the sample or it may suggest any precipitation-dissolution reactions may be cancelling out one another, thus suggesting no change.

Sample B6 was located in the ambient core holder during the closed-loop experiment and shows an increase in the cementation of the fracture after the experiment, similar to limestone sample B, also located in the ambient core holder, during the closed-loop experiment. The increase in the number of grains in the fracture suggests there was increased precipitation or deposition of grains. The fact that both the limestone and dolostone samples, located in the same position, show an increase in the number of grains within the fracture, may be no coincidence. One theory is as follows; due to being located in the closed-loop experiment, there may have been a higher chance for the fluid to precipitate grains into sample B6 (ambient), which had been potentially dissolved from a high temperature sample. Sample B5, located in the ambient core holder in the open-loop experiment, shows little to no change in the number of grains. This may be due to the water in the open-loop experiment being

discarded, meaning the fluid can't interact with the sample in the ambient core holder following percolation through the heated samples. Therefore, if more dissolution is occurring within the heated samples, it would mean the fluid exits the open-loop experiment without having chance to precipitate grains into the ambient sample.

5.3 Water Sampling Discussion

5.3.1 Magnesium Concentration in the Fluid Percolating Through the Limestone: Closed-loop Experiment

Studying the Mg-concentrations in the fluid percolating through the limestone during the closed-loop experiment, there is an apparent slight increase in Mg-concentrations in the percolating fluid throughout the whole experiment (figure 4.43). This may be indicative of dissolution reactions occurring between the limestone sample and fluid. Due to an increase in Mg-concentrations in the water samples, it shows there is a release of Mg into solution from the core sample. This dissolution may result in the creation of new pores or widening or pre-existing pores (Ledésert et al. 2010). This dissolution will affect the porosity and permeability of the samples by creating a larger volume of pore space and likely interconnectivity of pores and an increase in permeability (Ledésert et al. 2010).

Continuing to study Fig. 4.43 above, all three core holders appear to show similar Mg-concentrations throughout the experiment. The fluid taken from the ambient core holder starts with the highest concentrations, followed by the fluid taken from the 40°C core holder and the 80°C core holder has the lowest. However, by the end of the experiment, the fluid taken from the 40°C core holder has the highest Mg-concentrations, followed by the 80°C core holder and the lowest is observed in the ambient core holder. When looking at the overall Mg-concentrations in the fluid taken from the 80°C core holder throughout the experiment and not just at the end, the release of Mg to solution remained the lowest in this sample. This portrays that the lowest release of Mg to solution occurred in the 80°C core holder, potentially showing that Mg solubility appeared lower at higher temperatures. Despite this, throughout the experiment the Mg-concentration in all three sample remains relatively similar, therefore, it is difficult to determine whether the temperature had a significant effect on the release of Mg to solution in the limestone during the closed-loop experiment.

Spikes appear to occur throughout the experiment at each sampling point. In figure 4.43, the largest spike appears to reach approximately 0.0012 mol/L in the 40°C oven. These spikes may be indicative

of high-levels of Mg being released to solution from the limestone sample. Due to the spikes occurring so randomly, it's hard to tell whether they show a significant trend. One theory as to why the spikes may occur may be small grains escaping the system and entering the water sample, therefore creating a false reading. This may not be the case in this instance, yet it is worth nothing.

Figure 4.43 Summary:

- Overall, the Mg-concentrations in the fluid percolating through the limestone in all three samples, during the closed-loop experiment, appear to show a slight constant rise in all samples throughout the whole experiment.
- Increased Mg-concentration in all three water samples throughout the experiment suggests release of Mg to solution occurred from all the samples.
- Spikes in the data may have occurred from small grains escaping the system and entering the water sample tube, potentially creating a false reading in the data, albeit difficult to confirm.

5.3.2 Magnesium Concentration in the Fluid Percolating Through the Limestone: Open-loop Experiment

Figure 4.44 shows the Mg-concentrations in the fluid percolating through the limestone during the open-loop experiment. The overall trend of all samples appears to be a slow increase in Mg-concentrations in the fluid until approximately 27 days after the start of the experiment, following this is a decline in Mg-concentration until another rise towards the end of the experiment. One theory is that dissolution-precipitation-dissolution cycles may have occurred, as seen in previous research findings (André et al. 2010). This theory means the fluid may have reacted with the limestone to release magnesium into solution, as the Mg-concentrations increase in the fluid. Due to this dissolution resulting in mineral breakdown, this can lead to new pores spaces being created or producing larger pre-existing pores (Min et al. 2016). With the new space creation inside the sample, a drop in pressure may cause precipitation to re-occur (Bai et al. 2019). This may explain why the results show a decrease in Mg-concentration in the percolating fluid and may suggest Mg precipitation has occurred.

In figure 4.44, similar to the closed-loop experiment, the open-loop experiment shows Mg-concentrations in all three fluid samples to be very similar throughout the experiment. At the end of the experiment, the fluid samples taken from the 80°C core holder and the 40°C core holder appear

to have higher Mg-concentrations than the fluid sample taken from the ambient core holder. However, throughout the experiment the sample taken from the 40°C core holder appears to have the lowest Mg-concentration. It is difficult to determine whether the temperature of each core holder had a significant effect due to the Mg-concentrations of all three samples being similar throughout the experiment.

Figure 4.44 Summary:

- Overall, the Mg-concentration in the fluid percolating through the limestone in all three samples, during the open-loop experiment, show a slow increase in Mg in the fluid until approximately 27 days after the experiment started, followed by a gentle decline until a final rise. This may represent a dissolution-precipitation-dissolution cycle.
- All three water sample results show similar Mg-concentrations throughout the experiment.

5.3.3 Magnesium Concentration in the Fluid Percolating Through the Limestone: Closed-loop Experiment vs. Open-loop Experiment

During the open-loop experiment, the valve at the end of the 40°C core holder was left open so fluid could leave the experiment. It would be interesting to know whether the effect of leaving the valve open at the end of the 40°C core holder had an effect on the pressure inside this core holder. If so, the difference in pressure may result in a change in the dissolution-precipitation reactions (Bai et al. 2019; André et al. 2010).

Observe figures 4.43 and 4.44 to compare the results of Mg-concentrations in the limestone during the closed-loop experiment and open-loop experiment. Generally, all three water samples from the closed-loop experiment portray a slow and steady increase in Mg throughout the experiment. In the open-loop experiment, all three water samples show a slow increase until approximately day 27 of the experiment, followed by a slow decline and a final rise towards the end of the experiment, albeit a slight change. Regardless of the subtle changes in both graphs, it could be argued that both results show dissolution is occurring within all three samples throughout the experiment. The dip in Mg-concentrations during the open-loop experiment may be the result of dissolution-precipitation-reactions within the rock (André et al. 2010).

Analysing figures 4.43 and 4.44, both the closed-loop and open-loop data showing Mg-concentrations in the fluid in the limestone show similar Mg values, approximately around 0.0004 to 0.0006 mol/L. In the closed-loop experiment, the values mainly stay within 0.0004 to 0.0008 mol/L, with only a few values reaching up to 0.0012 mol/L. In the open-loop experiment, most values are between 0.0004 to 0.0006 mol/L, with some dropping between 0.0003 to 0.0004 mol/L towards the end. The higher values seen during the closed-loop experiment suggests that more dissolution was occurring here. Theories as to why more dissolution may occur during the closed-loop experiment may be:

(1) As previously mentioned, the closed-loop experiment contained more pipe work, with previously mentioned evidence of precipitation inside the pipes. The pipes resulting in increased space to precipitate minerals, may have resulted a lower saturation in the fluid, and therefore space to increase the release of Ca and Mg to solution (André et al. 2010).
(2) If the fluid didn't reach saturation after one entire cycle of the experiment, the closed-loop experiment enables the fluid and rock to spend more time interacting with one another. Therefore, giving the fluid more chance to dissolve the limestone. This could potentially explain evident slightly higher Mg-values in the fluid samples from the closed-loop experiment.

5.3.4 Calcium Concentration in the Fluid Percolating Through the Limestone: Closed-loop Experiment

Figure 4.45 shows the Ca-concentration in the fluid percolating through the limestone in the closed-loop experiment. Initial Ca-concentrations in all three core holder samples show approximately 0.0015 – 0.002 mol/L of Ca in the fluid. By the end of the experiment all three core holder samples portray a Ca-concentration of approximately 0.0029 mol/L. Throughout the experiment there appears to be a subtle but steady increase in the release of calcium to solution in the water samples from all three core holders. This portrays that such chemical reactions were occurring between the fluid and limestone. With calcium making up much of the chemical composition of calcium carbonate ($CaCO_3$) forming limestone it is expected to see the release of calcium to solution throughout the duration of the experiment (Warren, 2000). Within the space of six weeks the Ca-concentration within the fluid increased by approximately 0.009 mol/L, which isn't a significantly large increase, albeit still an evident increase. The release of calcium to solution throughout the experiment was therefore happening. Due to the increase throughout the experiment only being slight, this could suggest the percolating fluid was near saturation levels of calcium (Goldscheider et al. 2010) or perhaps dissolution reactions were not occurring rapidly in the first place.

As previously mentioned, the obvious spike in the 40°C core holder, occurring approximately 28 days after the experiment started, may have been due to a small particle of limestone entering the sample. Further evidence to suggest the spike may have been caused by a particle inclusion is that the main spike in the calcium concentration in figure 4.45, aligns with the second spike in magnesium in figure 4.43, showing high values for both calcium and magnesium, which would be expected from an inclusion.

Spikes evident in figure 4.45 in all three water samples, may also suggest increased release of calcium into solution during that time period. Increased release of calcium to solution may occur in the closed-loop experiment, following precipitation of other minerals in the pipes. The release of calcium to solution may also have occurred in the samples if the saturation levels of the fluid have not been reached, enabling space for more calcium to be released to solution.

Figure 4.45 Summary:

- Slow, gentle increase in the release of calcium into solution is evident in the fluid percolating through the limestone, during the closed-loop experiment, throughout the experiment.
- The spike in the 40°C core holder at around 28 days after the experiment started may have been due to a particle inclusion.
- The other smaller spikes evident in all three water sample results show signs of increased dissolution periods throughout the closed-loop experiment.

5.3.5 Calcium Concentration in the Fluid Percolating Through the Limestone: Open-loop Experiment

Figure 4.46 portrays the calcium concentrations of the fluid percolating through the limestone samples, during the open-loop experiment. Generally, there appears to be a slight increase in calcium concentrations in the water samples taken throughout the experiment, although this increase is small and may be considered insignificant. Despite this, the evident increase still suggests the release of calcium into solution was occurring from all three limestone samples during the open-loop experiment.

Studying figure 4.46, in the 80°C core holder, approximately eight days after the experiment started, a large spike is evident with multiple results comprising the increase. The interesting thing to note

about this spike is that it comprises of multiple results taken across multiple days. This reinforces the legitimacy of this spike, as it is unlikely an increase in calcium concentration for several consecutive days occurred from a particle inclusion. The spike appears to reach over 0.01 mol/L in calcium concentration, showing almost a 10x increase from the initial approximate 0.002 mol/L values seen in the 80°C core holder. It is unclear as to why increased calcium released to solution during this time. The open-loop experiment constantly has fresh, unequilibrated water flowing through experiment. The fluid must have had enough space, alongside comprising of the right conditions so calcium can release to solution. The availability of calcium in the limestone sample likely contributed to the release of calcium to solution. Due to this spike occurring in the 80°C core holder, it may be plausible to suggest the increased heat contributed to increased dissolution, despite Wood (1986) arguing that calcite solubility increases with increasing temperature only in closed systems.

Figure 4.46 Summary:

- Increased calcium concentrations, despite being subtle, in the water samples throughout the experiment show increased release of calcium to solution in all three samples during the open-loop experiment.
- A large spike consisting of multiple water sample results occurred approximately eight days after the experiment started in the 80°C core holder. The increased temperature in this core holder may have been a contributing factor to increased release of calcium to solution, alongside calcium availability in the limestone core sample and the fluid being below calcium saturation levels (Goldscheider et al. 2010).

5.3.6 Calcium Concentration in the Fluid Percolating Through the Limestone: Closed-loop Experiment vs. Open-loop Experiment

Overall, both the closed-loop and open-loop experiments show a slight increase in calcium concentrations throughout the experiment. This increase appears gentle but constant. The increase in both experiments proves there was a release of calcium to solution within the limestone during both the closed-loop experiment and open-loop experiment (figures 4.45 and 4.46).

In figure 4.45 and figure 4.46, studying the calcium concentrations in both the closed-loop and the open-loop experiment, we see similar calcium values. The majority of the calcium results for both experiments fall between approximately 0.002 mol/L and 0.004 mol/L. Therefore, proving there was

no significant difference between the general trend of both results. The highest recorded calcium concentration was approximately 0.006 mol/L during the closed-loop experiment, and approximately 0.01 mol/L during the open-loop. Despite the general trends of both experiments showing similar calcium concentrations overall, the highest amount of calcium in the fluid was recorded during the open-loop experiment.

5.3.7 Summary of the Magnesium and Calcium Concentration Results in the Limestone Fluid: Closed-loop Experiment vs. Open-loop Experiment

Studying figure 4.43 (magnesium limestone closed-loop) and figure 4.45 (calcium limestone closed-loop), the concentration results for both magnesium and calcium in the limestone, during the closed-loop experiment, the results appear to show subtle, gentle, steady increases in concentration levels in the fluid throughout the experiment. Looking at figure 4.44 and figure 4.46, showing the magnesium and calcium levels in the limestone, during the open-loop experiment, the results appear to show more variation throughout the experiment, perhaps suggesting the fluid in the open-loop experiment didn't equilibrate as much as the fluid in the closed-loop experiment.

If water-limestone reactions were to occur in a natural setting over time, with a much larger water volume, it is plausible that a large amount of calcium could be released to solution until reaching equilibrium and if conditions allow it, potential precipitation (Ledésert et al. 2010). Increased dissolution will likely result in new pores and widening of pre-existing pore spaces, alongside connectivity of pores, therefore increased the host rock permeability (Garing et al. 2015). This increase in porosity and permeability will enable for the continuing of fluid flow throughout a geothermal system (Garing et al. 2015).

It is unclear as to how much exact precipitation occurred throughout the entire experiment. It would be useful to weigh the pipes before and after the experiment to determine the amount of precipitation that occurred within them, throughout the experiment. Although this won't entirely provide an accurate result, due to precipitation occurring inside the sample. Despite precipitation occurring inside the sample, across the entire length of both the closed-loop and open-loop experiments, not one out of the twelve samples produced precipitation high enough to prevent fluid flow through the samples. This provides useful evidence that in a geothermal system moving through the temperature gradients similar to those created in the experiment (approximately 20°C to 80°C), despite precipitation, fluid flow is still possible to be maintained overtime. It would be interesting to find out what would happen

over a longer period of time, would a geothermal system remain viable? Would the results shown across the period of approximately six weeks throughout the experiments be reflective of a real-life scenario, showing varying dissolution-precipitation cycles and constant fluid flow. Would there reach a point where precipitation would be too high, restricting flow? Or vice versa, where dissolution would become too high and would result in collapse of pore spaces? These factors would need to be considered specific to each geothermal system, due to changing compositions and temperature-pressure changes.

5.3.8 Magnesium Concentration in the Fluid Percolating Through the Dolostone: Closed-loop Experiment

Figure 4.47 portrays the magnesium concentrations in the fluid percolating through the dolostone samples, during the closed-loop experiment. As previously mentioned in the results, there appears to be little variation shown throughout the duration of the experiment. All three water samples appear to show a slow and steady increase in magnesium throughout. This identifies that the release of magnesium to solution occurs throughout the experiment at a slow and steady rate. Magnesium dissolution would be expected from the dolostone due to magnesium comprising a major component of dolomite ($MgCO3{\cdot}CaCO3$) (Warren, 2000).

As previously discussed, the spikes evident in the 40°C core holder and ambient core holder, occurring at approximately eleven and seventeen days after the experiment started respectively, are deemed insignificant (figure 4.47). This may be caused by potential particles entering the water samples, producing an inaccurate magnesium result.

All three samples, taken from the ambient, 80°C, and 40°C core holder show similar magnesium values in the water samples (figure 4.47). Due to the values appearing so close together, maybe the temperature difference does not have as significant effect as mentioned. However, this is just one graph, and the results must be compared alongside micro-structural and permeability data to determine the full picture.

Figure 4.47 Summary:

- A slow, steady increase in magnesium concentration in the fluid percolating through the dolostone is evident throughout the closed-loop experiment. This provides evidence that Mg is being released to solution from the dolostone core samples.
- Spikes evident in the 40°C and ambient core holders are deemed insignificant and may have occurred from particles entering the water sample, producing inaccurate readings.
- The magnesium results appear similar in all the samples throughout the experiment, despite being taken from three different temperature core holders.

5.3.9 Magnesium Concentration in the Fluid Percolating Through the Dolostone: Open-loop Experiment

Figure 4.48 portrays the magnesium concentrations of the fluid percolating through the dolostone samples, during the open-loop experiment. Overall, the general trend appears to be initial high magnesium values, immediately dropping on the first day of the experiment and followed by a slow, steady increase in magnesium concentrations in the water samples until approximately 24 days after the experiment started, when the concentration appears to drop, before slowly increasing again. The initial slight increase, evident from approximately day one to 24, portrays slow, steady and constant release of magnesium into solution occurred during the open-loop experiment. At approximately 24 days after the start of the experiment, the slight dip in magnesium concentration may have occurred as a result of multiple reasons. One theory may be that the water samples may have precipitated magnesium during the experiment, resulting in lower concentration values in the sample. A precipitation event may have occurred due to more space created in the samples (in the pore spaces or fracture), due to previous dissolution (Garing et al. 2015).

The initial high values of magnesium concentrations evident in the dolostone in the open-loop experiment appear to comprise of more than one datapoint, reinforcing the legitimacy of the result (figure 4.48). All the high magnesium concentration readings were recorded on the first day of the experiment. This trend can also be seen in the calcium results (figure 4.50) and a suggested theory is explained in the later section 4.3.16.

Figure 4.48 Summary:

- The release of magnesium to solution is evident in the dolostone throughout the open-loop experiment, due to slow and steady increases in magnesium concentrations in the water samples fluids. Approximately 24 days after the start of the experiment, the drop in magnesium concentration in the fluid may have occurred due to precipitation.
- Initial high magnesium values are evident on the first day of the experiment.

5.3.10 Magnesium Concentration in the Fluid Percolating Through the Dolostone: Closed-loop Experiment vs. Open-loop Experiment

Figures 4.47 and 4.48 show the magnesium concentration in the water samples from the dolostone, during the closed-loop experiment and open-loop experiment. Comparing the magnesium concentrations, most of the results during the closed-loop experiment portray magnesium values between 0.0006 mol/L and 0.0009 mol/L. Most of the results from the open-loop experiment are between 0.0005 mol/L and 0.0007 mol/L. Therefore, portraying slightly more release of magnesium to the fluid in the closed-loop experiment. A theory as to why slightly higher values were portrayed in the closed-loop experiment may be because the fluid spends longer in the system, perhaps giving the fluid more chance to release magnesium into solution than the open-loop fluid, which is discarded after the final core holder.

5.3.11 Magnesium Concentration in the Fluid Percolating: Limestone vs. Dolostone

Comparing figure 4.43 of Mg-concentrations in the limestone during the closed-loop experiment and 4.47 of Mg-concentrations in the dolostone during the closed-loop experiment, there appears to be higher release of magnesium to solution in the dolostone (the majority of values lie approximately between 0.0006 mol/L and 0.0009 mol/L) compared to the limestone (the majority of values lie approximately between 0.0004 mol/L and 0.0007 mol/L). The open-loop experiment portrays the same trend between the dolostone (approximately between 0.0005 mol/L and 0.0007 mol/L) and limestone (0.0004 mol/L and 0.0006 mol/L). This is to be expected as the dolostone naturally contains significant more magnesium.

During the closed-loop experiment (figures 4.43 and 4.47), both the limestone and dolostone portray similar dissolution patterns, whereby the magnesium concentrations in the water sample show a slow and steady rise throughout the experiment. During the open-loop experiment (figures 4.44 and 4.48),

the limestone and dolostone also portray similar patterns. Both results show a slight, steady increase until approximately 24 days after the experiment stated, when a slight dip in magnesium concentration values is evident. The fact that this is seen in both the limestone and dolostone samples, despite the lines remaining independent of each other, may suggest that the slight fluctuation in magnesium concentrations is due to a change happening within the entire system. For example, a pressure change in the system may affect both limestone and dolostone.

5.3.12 Calcium Concentration in the Fluid Percolating Through the Dolostone: Closed-loop Experiment

Figure 4.49 shows a slow, steady and constant increase in calcium concentrations in the dolostone fluid, during the closed-loop experiment. Therefore, suggesting a constant release of calcium into solution from the dolostone throughout the closed-loop experiment.

In figure 4.49, the spikes evident in the 40°C core holder and ambient core holder, occurring at approximately eleven and seventeen days after the experiment started respectively, are deemed anomalies. Due to these occurring at the same time as the spikes in figure 4.47, it is likely the increased calcium values are due to small particles entering the water samples, producing inaccurate results, as previously mentioned.

Figure 4.49 Summary:

- Slow, steady and constant increase in calcium in the water samples likely suggests the constant release of calcium into solution from the dolostone throughout the closed-loop experiment.
- Due to the spikes in calcium concentrations occurring at the same time as the magnesium concentrations in the dolostone (during the closed-loop experiment), the anomalies may have resulted from particles entering the water samples, as has been previously mentioned.

5.3.13 Calcium Concentration in the Fluid Percolating Through the Dolostone: Open-loop Experiment

Figure 4.50 portrays high initial calcium concentrations found in the water samples taken from the ambient and 40°C core holders from the dolostone, during the open-loop experiment. High initial values of calcium, that are evident on the first day of the experiment (figure 4.50), align with high

initial values of magnesium (figure 4.48) in the dolostone fluid during the open-loop experiment. The reason behind why this may have occurred is further discussed in section 4.3.16.

The high initial values are evident during the first day of the experiment and following this is a significant drop in calcium (figure 4.50). The calcium values appear to reach equilibrium, remaining stable, perhaps suggesting the fluid and rock appeared in steady state for a period of time. Approximately 24 days after the experiment started, there appears a slight decrease in calcium, followed by a gentle final rise. This slight drop in calcium may have been due to a possible change in the overall pressure, which was previously discussed in section 5.3.2. Another reason may be due to precipitation occurring within the system, due to either; (1) precipitation into space created from previous dissolution, i.e., pores or voids, or (2) fluid reaching calcium saturation levels (André et al. 2010).

In figure 4.50, a drop in calcium concentrations in a water sample which was taken from the 40°C core holder, occurring approximately 29 days after the start of the experiment, is likely an anomaly. Yet, despite the other anomalies this is unlikely due to a small particle entering the water sample, as that would result in an increase, not decrease in calcium.

Figure 4.50 Summary:

- On the first day of the open-loop experiment, high initial values of calcium align with high initial values of magnesium in the dolostone.
- The calcium concentrations appear to reach equilibrium in the first half of the open-loop experiment.
- The drop in calcium evident approximately 29 days after the start of the experiment in the dolostone is likely an anomaly.

5.3.14 Calcium Concentration in the Fluid Percolating Through the Dolostone: Closed-loop Experiment vs. Open-loop Experiment

Figures 4.49 and 4.50 show the calcium concentration in the water samples from the dolostone, during the closed-loop experiment and open-loop experiment. Comparing the calcium concentrations, most of the results during the closed-loop experiment portray results between 0.0014 mol/L and 0.0025

mol/L. Most of the results from the open-loop experiment are between 0.0013 mol/L and 0.002 mol/L. Therefore, portraying similar release of calcium into solution in the dolostone during the closed-loop and open-loop experiments.

5.3.15 Calcium Concentration in the Fluid Percolating: Limestone vs. Dolostone

Higher release of calcium to solution is evident in the limestone during the closed-loop experiment (average results between approximately 0.0015 mol/L – 0.003 mol/L) (figure 4.45) than the dolostone (average results between approximately 0.0014 mol/L – 0.0025 mol/L) (figure 4.49) during the closed-loop experiment. This would be expected due to the limestone comprising of calcium carbonate ($CaCO_3$) and dolostone comprising of a magnesium component ($CaMg(CO_3)_2$). The same is seen in the open-loop experiment, where the limestone (average results between approximately 0.0015 mol/L – 0.0036 mol/L) (figure 4.46) portrays higher calcium than the dolostone (average results between approximately 0.0013 mol/L – 0.002 mol/L) (figure 4.50).

During the closed-loop experiment (figures 4.45 and 4.49), the limestone and dolostone portray similar release of calcium to solution patterns. Both graphs show a slow, constant increase in calcium concentrations in the water samples, throughout the experiment, suggesting constant release of calcium into solution from both the limestone and dolostone samples.

During the open-loop experiment (figures 4.46 and 4.50), the limestone and dolostone appear to show more variation in the release of calcium into solution. The limestone portrays a slow, steady and constant increase in calcium throughout (figure 4.46). Despite the slight drop in calcium concentration that appears to occur in the dolostone approximately 24 days after the start of the experiment, the dolostone appears to show equilibrium during the first half of the experiment and gentle increase towards the end. The drop may relate to a pressure change in the system as discussed earlier, or perhaps precipitation leading to an evident drop in calcium concentrations in the water sample. Despite these details, generally, both the limestone and dolostone portray dissolution is occurring and some form of equilibrium is reached between the host rock and fluid.

5.3.16 Summary of the Magnesium and Calcium Concentration Results in the Limestone and Dolostone Fluid: Closed-loop Experiment vs. Open-loop Experiment

The steady, constant rise in magnesium and calcium concentrations often found throughout the closed-loop experiment results suggests an equilibrium was reached during the closed-loop experiment. The open-loop results appear more variable. However, the closed-loop results typically show a slow, steady increase in either magnesium or calcium concentrations in both the limestone and dolostone, suggesting constant dissolution from the samples.

Figure 4.50 portrays high initial calcium concentrations found in the water samples taken from the ambient and 40°C core holders from the dolostone, during the open-loop experiment. High initial values of calcium, that are evident on the first day of the experiment (figure 4.50), align with high initial values of magnesium (figure 4.48) in the dolostone fluid during the open-loop experiment. One theory is that the lines were not flushed between experiments, therefore the high initial values may be a remnant reading. One suggestion for future experiments of a similar nature is to flush the lines between experiments to remove any leftover artefacts.

Overall, all the limestone and dolostone samples, in both the closed-loop and open-loop experiments, portray evidence of dissolution throughout the experiment.

5.4 Core Sample Permeability Discussion

5.4.1 Permeability of the Limestone Core Samples: Closed-loop Experiment

Figure 4.51 shows the permeability results of the entire core sample of the limestone samples B (ambient), A (80°C) and D (40°C) during the closed-loop experiment. The overall permeability trend of all three limestone samples shows a significant decreasing curve until approximately 10 days after the start of the experiment, when the curve begins to flatten out. Following the decrease, the results begin to stabilise and appear to reach equilibrium. The initial drop, showing a decrease in permeability, evident in all three limestone samples may be a result of the system settling and trying to reach equilibrium. The drops in permeability appear to align approximately around the time the limestone pressure data results show a significant drop in pressures (figure 4.51 and figure 4.55), showing a pressure decrease around approximately 10 days after the start of the experiment, after reaching a peak (see section 4.5). One theory, explained in section 4.5, as to why the high-pressure recordings may have occurred was due to the reduction of flow rate approximately six days after the start of the

experiment. The reduction was made from 0.5rpm to 0.4rpm due to overriding pressure readings. Around approximately eight days after the start of the experiment, the pressure readings in the limestone (closed-loop) reached a pressure peak, followed by a decline (figure 4.55). Perhaps these high readings in the pressures align with the high permeability results in the limestone evident in figure 4.51 at the start of the closed-loop experiment. Therefore, the high initial flow rate may have altered the permeability results, due to using the pressure data to calculate permeability, producing an inaccurate high permeability result in the limestone or making it too difficult for the flow to stabilise, therefore provide inaccurate limestone permeability readings.

Figure 4.51 Summary:

- The permeability results, during the closed-loop experiment, in all three limestone samples shows a decreasing curve before appearing to reach equilibrium.

5.4.2 Permeability of the Limestone Core Samples: Open-loop Experiment

Figure 4.52 portrays the limestone samples C (ambient), F (80°C) and E (40°C) during the open-loop experiment. Studying the permeability results of samples C (ambient) and F (80°C), the results appear similar to that of the closed-loop experiment. Showing initial higher permeability values in both sample before falling to a steady-state and appearing to reach an equilibrium in the system. The drop in permeability results before reaching a steady-state may also be due to the pressures in the system trying to reach equilibrium. Similar to the closed-loop experiment, the pressure results show an increase in pressures until approximately 15 days after the experiment started, before peaking and dropping. This approximately aligns with the permeability results in samples C (ambient) and F (80°C) appearing to reach steady-state.

Sample E (40°C) shows permeability results largely different, in that the results don't appear to reach a steady-state and show constant fluctuations throughout the experiment, followed by a final increase at the end (figure 4.52). One theory could be design of the experiment has produced large fluctuations in the 40°C core holder. The water sample valve remained open throughout the open-loop experiment, due to allowing the percolating water to be discarded after one cycle through the system. Perhaps leaving the water valve open affected the pressures recorded in the 40°C core holder, affecting the final permeability calculations. Perhaps if a future attempt was to try and mitigate this, it might be worth putting the water valve further away from the final core holder (although placing

the water sample valve further away may affect the Mg and Ca concentrations in the water samples as minerals may precipitate in the pipes).

Figure 4.52 Summary:

- Samples C (ambient) and F (80°C) portray a similar trend to the closed-loop experiment, whereby the permeability results appear to drop until reaching a steady-state in the experiment.
- A possible reason why sample E (40°C) shows fluctuations in the permeability results is due to the open water valve (in the open-loop experiment) affecting the pressure.
- One way to mitigate fluctuations in the 40°C core holder in the future may be to place the water valve further away from the core holder, despite this potentially affecting the Mg and Ca water sample data.

5.4.3 Limestone Permeability Discussion: Closed-loop Experiment vs. Open-loop Experiment

The initial drop evident in all three samples in figure 4.51 and samples C (ambient) and F (80°C) in figure 4.5.2 are believed to be a result of the pressures in the system. Due to the pressures taking a while to equilibrate, the differential pressure used to calculate permeability will change throughout the experiment.

When studying both figures 4.51 and 4.52, it may be worth noting that the permeability data for sample B (closed-loop) and sample C (open-loop), located in the ambient core holder for their respective experiment, appear to show the lowest permeabilities throughout most of the experiment. Samples located in the 80°C and 40°C core holders appear to have higher permeability values than the samples located in the ambient. This may suggest that more dissolution occurred in the 80°C and 40°C core holders, due to increased dissolution resulting in the likely increase and largening of pores, thus increasing the permeability. This reinforces Wood (1986) who states that calcite solubility increases with increasing temperature at low temperatures below 125°C. However, Wood (1986) states this occurs in a closed system and the results show the dissolution and temperature trend is occurring in both the closed-loop and open-loop experiment.

5.4.4 Permeability of the Dolostone Core Samples: Closed-loop Experiment

Figure 4.53 portrays the permeability results in the dolostone samples B6 (ambient), B2 (80°C) and B1 (40°C), throughout the closed-loop experiment. Gaps in the permeability data are due to the negative permeability values being removed from sample B2 (80°C) and B1 (40°C). The negative permeability values occurred due to the differential pressure values (upstream – downstream) being negative. It is unclear as to why this occurred, it suggests the problem lies with the pressure readings.

From the data recorded in figure 4.53, both sample B6 (ambient) and sample B1 (40°C) show constant and steady permeabilities throughout the experiment. However, sample B2 (80°C) shows an initial high value, followed by a second peak, before appearing to flatten-out. The initial fluctuation is likely due to pressures in the system starting to settle. The overall permeability values evident in sample B2 (80°C) stay above that of the other two samples. Higher permeability suggests potential dissolution of grains to produce more pore spaces and/or increase the inter-connectivity of pore spaces. This suggests that more dissolution may have happened within the higher temperature core holders. The lowest of permeability evident in the dolostone during the closed-loop experiment is found in sample B6, located in the ambient core holder, suggesting less dissolution.

Figure 4.53 Summary:

- Gaps in the data are the result of negative differential permeability samples which have been removed.
- The highest values appear to be from sample B2 (80°C).

5.4.5 Permeability of the Dolostone Core Samples: Open-loop Experiment

Figure 4.54 portrays the permeability results of the dolostone samples B5 (ambient), B4 (80°C) and B3 (40°C), throughout the open-loop experiment. Samples B5 (ambient) and B4 (80°C) appear to show a similar trend of a decreasing curve, showing high initial permeability values, which decline and appear to reach a steady state. As previously described, this declining curve is likely an effect of pressures in the experiment.

Similar to the limestone in the open-loop experiment, the permeability results measured for sample B3, located in the 40°C core holder, appears to act differently to the other two dolostone samples

(figure 4.52 and 4.54). However, different to the limestone, the dolostone sample B3 (40°C) permeability results appear to flatten, whereas the limestone sample E (40°C) showed to fluctuations. The permeability results for this sample may be an effect of pressure (figure 4.62). The pressure readings may have been affected by the water sample valve being left open during the open-loop experiment, located at the end of the experiment, after the 40°C core holder containing sample B3. The water sample valve was required to be left open to enable the percolating fluid to be discarded. This likely resulted in a pressure difference that affected the 40°C core holder and thus producing permeability results in sample B3 that have been affected.

Figure 4.54 Summary:

- Sample B5 (ambient) and sample B4 (80°C) portray a declining curve which appears to flatten.
- Sample B3 (40°C) permeability results appear to act differently to the other two dolostone samples B5 and B4, located in the open-loop experiment. The permeability results in the dolostone, during the open-loop experiment, appear to flatten out during the middle of the experiment. The permeability results from sample B3 (40°C) are perhaps an effect of the water valve, located at the end of the 40°C core holder, remaining open during the open-loop experiment and affecting the pressures in the 40°C core holder.

5.4.6 Permeability Changes Throughout the Experiment

Initial permeability ranges were measured of the limestone and dolostone core samples pre-experiment, comprising of permeability measurements pre-fracturing and post-fracturing of the samples (Table 6 in section 3.8). Due to high variability, and recorded pressure data that may not have been fully equilibrated, the permeability results in the limestone and dolostone taken post-fracturing appeared particular varied.

The initial limestone permeability range, taken post-fracturing was measured as 3.04 – 23.80 mD. This appears to be a particularly large range in limestone permeability measurements. Therefore, it's difficult to compare permeability results throughout both experiments, due to being such a large range. Despite this, studying figures 4.51 (closed-loop) and 4.52 (open-loop) of the entire limestone core sample, once the permeability results appear to flatten and reach an equilibration throughout the experiment, the lowest initial permeability value of 3.04 mD still lies above the equilibrated line

for both experiments. This perhaps suggests that there has been an overall decrease in permeability throughout the experiment. Reasons as to why this occurred may be as follows:

(1) The pressure in the system resulted in the crushing of grains and producing of small grains, clogging pore throats and reducing the connectivity of pores, therefore reducing permeability (Garing et al. 2015).
(2) Precipitation happening from the percolating fluid into pre-existing pore spaces or voids. Goldscheider et al. (2010), Morse et al. (2007), Plummer and Wigley (1976), Plummer et al. (1978) and Kirstein et al. (2016) state that calcite solubility decreases with increasing temperature, therefore calcite may have precipitated throughout the experiment.

The initial dolostone permeability range, taken post-fracturing was measured as 1.68 – 14.31mD. The range in permeability results is slightly smaller than the limestone, perhaps proving more accurate, albeit still a large range and, therefore, difficult to compare with the permeability data throughout the experiments. Studying figure 4.53 (closed-loop), the permeability results shown for sample B6 (ambient) and sample B1 (40°C) appear to equilibrate between approximately 0.4 – 5.2mD (data is missing for sample B2). Studying figure 4.54 (open-loop), the permeabilities shown for sample B5 (ambient) and sample B4 (80°C) appear to equilibrate between approximately 2 – 7.5mD and around approximately 10mD for sample B3 (40°C). The initial dolostone permeability range taken post-fracturing and pre-experiment of 1.68 – 14.31mD appears to cross the aforementioned ranges from the closed-loop and open-loop experiment in the dolostone. Therefore, it is difficult to tell whether the dolostone permeability has reduced overall. Despite this, the initial dolostone permeability range (1.68 – 14.31mD) is on the upper end of the permeability results, therefore it may be assumed than on average the permeability may have decreased, particular for the closed-loop experiment where the permeabilities equilibrated between 0.4 – 5.2mD. It is difficult to determine whether the permeability has actually decreased in the dolostone, throughout the experiment, however, it is possible to assume this by looking at the results. Reasons for the dolostone permeability reducing may be the same as for the limestone. When studying these permeability ranges, it should be noted that there may be some error in the results, due to the recorded pressures in the system perhaps not being fully equilibrated.

5.5 Pressure Discussion

5.5.1 Limestone Pressure Data Discussion: Closed-loop Experiment

Analysing the pressure data in the limestone for the closed-loop experiment, all of the pressure gauges, 1A – 1F (figure 4.55), appear to stabilise throughout the experiment.

The pressures recorded by pressure gauge 1F (figure 4.56) appear to act slightly different to the other pressure recordings, due to there not being an initial increase in pressure. This is also seen in pressure gauge 2F (see later). The constant fall in pressure may relate to line 1F and 2F being located at the end of the experiment. One theory is that due to these being located at the end, there is no backlog of built-up pressures from further down the system. The vacuum created in the long pipe may also contribute to the lower pressures here (explained later).

From the closed-loop experiment, the data from gauge 1A is particularly interesting (Fig. 4.55). The data appears completely scattered and alternating between high and low pressures. The pressure gauge for 1A is located at the start of the experiment, between the pump and the first limestone sample. The alternating, scattered data is indicative of a pressure build-up at the entry point of the experiment. The fluid may not be able to percolate the limestone sample fast enough due to having such a low permeability. This data can be analysed alongside the image of the filter paper located on the upstream of the first limestone core holder, which portrays significant residue build-up (Fig. 4.57). It is hypothesised that the growth of material on the filter paper is from precipitation of limestone grains or anaerobic bacteria. The latter is hypothesised from a pungent smell of the filter paper upon its removal.

When comparing between the graphs 1A to 1F, the point where the build-up of pressure in Line 1A begins, approximately day 10, appears to correlate with a significant decrease in pressure, following a major spike in graphs 1B – 1E (figure 4.55). Graph 1F shows initial high pressures that continuously fall until the pressure readings level out. The previously mentioned residue, alongside the low permeability of the limestone, may have resulted in the build-up of fluid at the entry point into the system and therefore resulting in such increase pressures evident in gauge 1A. The significant drop in pressures in 1B – 1E may be the result of accommodating high pressure build-up of fluid at the upstream of 1A. Therefore, the sudden decrease after the spike in the aforementioned graphs is presumed to be a result of a blockage at 1A. Despite this, fluid was still able to pass through the system,

albeit at a slower flow rate than would have occurred without the filter paper. To re-design the experiment without using filter paper would be tricky, due to the paper proving practical by keeping the in-filled fracture grains in place throughout the experiment.

If the blockage is the reason for such high pressures at the point of 1A in the experiment, it is assumed that the differential pressure will be higher than it would be without the blockage (figure 4.55). This would lead to higher permeability calculations of the sample located in core holder one (line one), which is limestone sample B, in the closed-loop experiment. This may be avoided in the future by applying the differential pressure from core holder three (line one) to give a more accurate permeability, although still not completely accurate.

On 29/07/2021, six days since the start of the closed-loop experiment, the flow rate was reduced from 0.5 rpm to 0.4 rpm, due to several overriding pressure readings and the pressures reaching levels too high to be recorded by the pressure gauges available. The blue dashed line, evident on the pressure and water sample graphs from the closed-loop experiment, indicates when the flow rate was reduced. The initial increase in pressures occurring for the first six days may have something to do with the initial high flow rate of 0.5 rpm. However, it is difficult to determine how much, if any, this initial high flow rate contributed to the increase in pressures seen in the first six days, due to the pressure continuing to increase after the flow rate was reduced. It could be argued there may have been a lag in the system before the pressures were re-stabilised after the reduction in flow rate. It is worth bearing this in mind as a reason for the obvious high peak in the limestone (line one) during the closed-loop experiment. The dolostone pressures appear to remain high throughout, however the dolostone perhaps responded less significantly to the reduction in flow rate due to being more permeable (see later for the dolostone pressure graphs for the closed-loop experiment).

The raw pressure data shows significant spike decreases in pressure throughout the experiment, relating to regular water sampling and thus a decrease in pressures. Due to this change in pressure resulting from human activity, the spikes have been removed. When inspecting information from gauge 1F (limestone) and gauge 2F (dolostone), it appears that the water sample spikes at both these points are delayed compared to graphs 1A – 1E and 2A – 2E (figures 4.55, 4.56, 4.58 and 4.59). This may be due to the closed-loop system having a delayed pressure drop due to creating a head in the system. In the closed-loop system a long pipe connects the end of the experiment (1F and 2F) to the

start, therefore creating a pressure drop and/or suction from the end of the long pipe (beginning of the experiment) to the point where the 1F and 2F sample is taken. When the tap is opened to collect the water sample, this may result in the break in the head and loss of suction. After the sampling tap is closed, there may be a delay in fluid flow as the other samples have to be collected. Once all of the samples have been collected, the system resumes fluid flow and suction in the pipe can be re-gained.

The general trend of the pressure data in the Limestone (line one) from the closed-loop experiment, can be summarised as such:

- In graph 1A, there appears to be an initial rapid increase in pressure at approximately day 10, followed by a gentle decline throughout the experiment until approximately day 33. After day 33, there appears to be a gentle increase in the pressure readings at this pressure gauge.
- In graphs 1B – 1E, there appears to be an initial spike, followed by a rapid decline in pressure until approximately day 15, where the pressure begins to become more level. The data continues to show a gentle, slow increase in pressure until approximately day 38, when the pressure begins to slowly decline until the end of the experiment.
- Graph 1F shows initial high-pressure readings, followed by a rapid decline until approximately 10 days after the experiment began, when the pressure becomes more stable and the curve flattens.
- In all of the Limestone graphs, 1A – 1F, it appears that the pressures become stable throughout the experiment and therefore indicating the experiment reaches a potential pressure equilibrium.
- Potential blockage due to residue and/or low permeability of limestone at point 1A may be the cause for high, fluctuating pressures shown here.

5.5.2 Dolostone Pressure Data Discussion: Closed-loop Experiment

Figure 4.58 portrays the pressure data for the dolostone during the closed-loop experiment. The pressures recorded in gauge 2A are higher than 2B – 2F, similar to the limestone results. This may be also due to the build-up of pressure at the upstream of the first pressure gauge, due to being the entry point into the system. Comparing the pressure values for the limestone gauge 1A and dolostone gauge 2A during the closed-loop experiment, the limestone values appear much higher. This may reflect the lower permeability of the limestone compared to the dolostone, making it harder for fluid to percolate. The dolostone appears to have experienced some blockage and pressure build-up,

however, the dolostones lower permeability likely meant the pressure values (recorded in the upstream of the first core holder) appear lower than the limestone pressure values.

Following the fixed leak in the dolostone line, the pressures appear to stabilise, suggesting equilibrium reached in the dolostone line (figure 4.58). There appears to be an initial increase in pressure following the leak being fixed. The general trend shows the pressures in gauges 2A – 2C show a slow rise in pressures until approximately 18 days after the experiment started. Around this point in the experiment, the pressures start to slowly fall until approximately 33 days after starting. Following this, the pressures steadily start to rise once more until the end of the experiment, with a slight peak in pressures at around day 39 after starting. Graphs 2D and 2E show a similar trend. When the leak is fixed there is an initial rise in pressure. This pressure continues to slowly increase until approximately 24 days after the experiment started. The pressure then stabilises and begins to slowly fall until approximately 35 days after the experiment started. The pressures continue to rise until a slight peak is evident at 39 days after starting. There appears to be pressure spike in graphs 2A – 2E approximately 39 days after the experiment starts. Graphs 2B – 2E all show a slight decline in pressure after the peak. The changes evident throughout the system appear small and pressure changes would be expected.

The pressure results from gauge 2F appear somewhat different to the other pressure gauge data (figure 4.58). Following the leak being fixed, the pressures appear to gently fall until approximately 21 days after the experiment starts, when the pressures equilibrate. The fall in pressures recorded at gauge 2F may be a result of being located at the end of the experiment, similar to the limestone (figure 4.59). It Is hypothesised in the limestone section that due to both gauges 1F and 2F being located at the end, there is no backlog of built-up pressures from further down the system. The vacuum created in the long pipe may also contribute to the lower pressures here. Similar to the limestone, the dolostone pressure readings also show a delay in pressure decreases in pressure gauge 2F when undertaking the water sampling, therefore the same reasoning, which was explained in section 5.5.1, has been applied to the dolostone. The theory mentions that a delayed pressure drop may have resulted from the long pipe in the closed-loop experiment that connects the end core holder back to the first core holder may have created a head in the system, thus creating a pressure drop from the end of the long pipe, where samples 1F and 2F are collected, to the beginning of the experiment.

The general trend of the pressure data in the limestone (line one) during the closed-loop experiment, can be summarised as such:

- The pressures recorded in gauge 2A are higher than 2B – 2F and are similar to the limestone results, this may be due to a pressure build-up and/or blockage.
- Following the pressure reduction, alongside the fixed leak, the pressures appear to stabilise, suggesting equilibrium reached in the dolostone line.
- Gauge 2F portrays delayed spike decreases compared to gauges 2A – 2E, thought to occur when the valves were opened to take the water samples, therefore leading to a pressure drop in the pipe.
- The results from gauge 2F appear to fall until appearing to reach an equilibrium. This is thought to occur due to the position of the gauge, meaning there is no backlog of built-up pressures from further down the system, alongside a potential vacuum in the pipe at the end of the closed-loop experiment which may have resulted in pressure differences.

5.5.3 Limestone Pressure Data Discussion: Open-loop Experiment

Analysing the pressure data in the limestone (line one) for the open-loop experiment, all of the pressure gauges, 1A – 1F (figure 4.60), appear to act differently to the pressures that have been recorded in the limestone in the closed-loop experiment.

The pressures recorded by pressure gauge 1A (figure 4.60) appear to show a constant increase in pressure until the pressure readings appear to become completely scattered, approximately 15 days after the experiment started, until the end of the experiment. A similar situation is evident in the limestone in the closed-loop experiment, showing a similar fluctuation of pressures appear in gauge 1A. Therefore, the same may be hypothesised for the open-loop experiment as the closed-loop experiment. The pressure gauge for 1A is located at the start of the experiment, between the pump and the first limestone sample. This may indicate a pressure build-up or blockage occurring at the entry point into the experiment. The fluid may not be able to percolate the limestone fast enough due to having such a low permeability.

Pressure gauges 1B and 1C (figure 4.60) appear to also show a steady increase in pressure until approximately 15 days after the experiment started. The pressures then appear to flatten until approximately 22 days after the experiment started and following this, the pressures show a gentle,

steady decrease until the end of the experiment. The rise and fall of pressures in both gauges 1B and 1C correspond with the scattered data from pressure gauge 1A. The pressure build-up at the entry point of gauge 1A may have affected the pressures further down the system, including pressure gauges 1B and 1C to level out and decrease. Pressure gauges 1B and 1C appear to show an abrupt decrease in pressure around approximately 37 days after the experiment started. It is unclear as to why this sudden decrease happens, however, it may be due to a sudden release of pressure that had built-up.

Pressure gauges 1D, 1E and 1F (figure 4.60) appear to show relatively equilibrated pressure readings, despite expected fluctuations in pressure, throughout the experiment. This may be due to no pressure building up further down the system. Also, water valve 1E, located at the end of the experiment (figure 3.1 and figure 3.3), remained open to replicate an open-loop system, therefore, this may have prevented pressure from building up around these gauges.

The pressures recorded in pressure gauge 1F (figure 4.60), during the open-loop experiment, appear to show no spikes from human activity when taking water samples throughout the experiment (the spikes are not evident on the graph due to being removed so the data is easier to interpret). This is due to the water sample valves being constantly left open, to discard of water throughout and maintain an open-loop system throughout the experiment.

The general trend of the pressure data in the Limestone (line one) from the open-loop experiment, can be summarised as such:

- In pressure gauge 1A, there appears to be an initial pressure increase until approximately 15 days after the experiment started. Following this, the pressure data appears completely scattered, which may represent a blockage at the entry point (figure 4.60).
- Pressure gauges 1B and 1C (figure 4.60) appear to show a slow increase until approximately 15 days after the start of the experiment, when the pressure flattens out, before decreasing. This may align with the pressure blockage in gauge 1A which may have resulted in a decrease in pressure further down the system.
- Pressure gauges 1D, 1E and 1F (figure 4.60) appear to be relatively equilibrised throughout the experiment.

- Pressure gauge 1F (figure 4.60) shows no spike decreases from water valve sampling due to water valve 1E, located at the end of the experiment remaining open to replicate an open-loop system, and therefore, resulting in the lack of spikes shown in pressure gauge 1F.

5.5.4 Dolostone Pressure Data Discussion: Open-loop Experiment

Analysing the pressure data in the dolostone (line two) for the open-loop experiment, all of the pressure gauges, 2A – 2F (figure 4.61), appear to act differently to the pressures that have been recorded in the dolostone in the closed-loop experiment.

The pressures recorded in gauge 2A (figure 4.61) appear to show a decrease approximately seven days after the experiment started. Following this, the pressure appears to slightly increase throughout the experiment, apart from an abrupt dip approximately 37 days after the experiment started. This drop correlates with the pressure drop seen in gauges 1B and 1C, in the limestone, in the open-loop experiment. This indicates that the drop is likely to be caused by something that affected the whole system, such as changes in the overriding pressure. The pressure results appear to alternate and show more variation approximately 25 days after the experiment started, which may represent a build-up of pressure in gauge 2A. Comparing the pressure values for the limestone gauge 1A and dolostone gauge 2A during the open-loop experiment, the limestone values appear much higher, reflecting the lower permeability of the limestone, therefore, making it harder for the fluid to percolate.

Pressure gauge 2B (figure 4.61) shows pressure readings at the start of the experiment to be higher than 2A. This suggests there may have been a pressure build-up in the downstream of the ambient core holder or a backlog of pressure from the upstream of the 80°C core holder (figures 3.1 and 3.3). The pressures in gauge 2B appear to fall below that of 2A approximately 16 days after the experiment started.

Pressure gauges 2B, 2C and 2D appear to show a similar trend in pressure data, whereby there appears to be an initial decrease approximately seven days after the experiment started, until the pressures appear to equilibrate until the end of the experiment, suggesting equilibrium of the pressures occurred. The results evident from pressure gauge 2C appear to plot straight lines. This is due to pressure gauge 2C only recording data to whole decimal places and may be mitigated in the future by making sure the pressure gauge records to more than one decimal place.

Similar to pressure gauge 1F seen in the limestone in the open-loop system, gauge 2F (figure 4.61), compared to the other samples, showed no spike decreases from water sampling due to water valve 2E remaining open to replicate an open-loop system during the experiment (the spikes are not evident on the graph due to being removed so the data is easier to interpret). The variation in gauges 2A – 2F at the very end of the experiment is likely an effect of turning the experiment off.

The general trends of the pressure data in the dolostone (line two) during the open-loop experiment, can be summarised as such:

- The pressures recorded in gauge 2A appear to show more variation approximately 25 days after the experiment started, suggesting a build-up of pressure.
- Pressure gauges 2B – 2F appear to flatten, suggesting equilibration of pressure.
- Pressure gauge 2F appeared to show no spike decreases from water sampling due to water valve 2E remaining open to replicate an open-loop system during the experiment.

5.6 Discussion Summary

This section will aim to bring together and summarise the findings made throughout the results and discussion sections (sections 4 and 5), including the micro-structural results, CT scan images, water sample, permeability and pressure results. Three major comparisons will be drawn upon to summarise the analysis, comprising the difference between:

5.6.1 The Limestone and Dolostone Results
5.6.2 The Effects of the Differing Temperature Core Holders including the Ambient, the 80°C and the 40°C Core Holders
5.6.3 The Effects Between Both the Closed-loop Experiment and the Open-loop Experiment

5.6.1 The Comparison of the Limestone and Dolostone Results

5.6.1.1 Micro-structural Results

Studying the microstructural results comprising of SEM images (section 4.1) from the experiments, there is a significant difference in the initial porosity of the limestone and dolostone. Compared to the limestone, the dolostone has a significantly higher initial porosity and permeability. The high initial

porosity and permeability of the dolostone is reflected in the SEM images portraying larger pore spaces in the dolostone compared to the limestone.

From the ImageJ analysis undertaken on the SEM images to determine the porosity after the experiments, the limestone and dolostone relative porosities can be compared (section 4.1). During the closed-loop experiment, both the limestone and dolostone samples subject to temperatures of 80°C (sample A and sample B2, respectively) portrayed the highest porosity inside the fracture, compared to the other limestone and dolostone samples in the same experiment. During the open-loop experiment, the limestone and dolostone portray the opposite. Limestone sample, which was subject to 80°C, showed to have the lowest porosity in the fracture, compared to the other limestone samples in the open-loop experiment. Dolostone sample B4, which was subject to 80°C, showed to have the highest porosity inside the fracture, compared to the other dolostone samples in the open-loop experiment. The contrasting views may be due to grain loss through the occurrence of natural fractures. Also, the ImageJ analysis only portrays the porosity relative to one other and because we don't have the initial porosity of the in-filled fracture, it is uncertain whether the samples showing higher porosity were subject to more dissolution or simply started with a higher porosity.

Studying the host rock ImageJ analysis results, the limestone and dolostone show contrasting data (section 4.1). For the limestone host rock, during both the closed-loop and open-loop experiments, the samples subject to 80°C (sample A and sample F, respectively) portrayed the highest porosity and the samples subject to ambient temperatures (sample B and sample C, respectively) portrayed the lowest porosity. For the dolostone, during both the closed-loop and open-loop experiments, the samples subject to 80°C (sample B6 and sample B5, respectively) portrayed the lowest porosity and the samples subject to ambient temperatures (sample B1 and sample B3, respectively) portrayed the highest porosity. A possible explanation may be that due to the limestone having such an initial low porosity and permeability, perhaps more dissolution needed to occur in the host rock to enable fluid flow. In the dolostone, the host rock had an initial high porosity and therefore, perhaps flow was able to percolate the dolostone quicker than the limestone, leaving less time to dissolve the host.

5.6.1.2 CT Scan Results

In the CT scan images, the limestone and dolostone portray very similar results (section 4.2). The limestone and dolostone both portray an increase in fracture grains in the samples (limestone B/dolostone B6) located in the ambient core holder, during the closed-loop experiment. All limestone

and dolostone samples (limestone A and F/dolostone B2 and B4) located in the 80°C core holder, during both the closed-loop and open-loop experiments, shows a decrease in the number of grains in the fractures. Almost, all the limestone and dolostone samples (limestone D and E/dolostone B1 and B3) located in the 40°C core holder, during both the closed-loop and open-loop experiment, portray little to no change in the number of grains evident inside the fractures, apart from dolostone sample B3, which showed a decrease in the number of grains evident inside the fracture, following the open-loop experiment. This similarity in the number of grains evident in the fracture between the limestone and dolostone samples suggests that this is likely a factor of the temperature in the core holders, not composition. The dolostone CT scan images appeared more detailed than the limestone, showing evident natural fractures.

5.6.1.3 Water Sample Results

In section 4.3, studying Mg-concentrations in the fluid percolating through the limestone and dolostone during the closed-loop experiment, there appears to be more release of magnesium to solution in the dolostone (the majority of values lie approximately between 0.0006 mol/L and 0.0009 mol/L) compared to the limestone (the majority of values lie approximately between 0.0004 mol/L and 0.0007 mol/L). The open-loop experiment portrays the same trend between the dolostone (approximately between 0.0005 mol/L and 0.0007 mol/L) and limestone (0.0004 mol/L and 0.0006 mol/L). This is expected as the chemical formula for dolomite is MgCO3-CaCO3 and thus, naturally contains significant more magnesium.

The results show that magnesium concentrations were increasing in the fluid percolating through both the limestone and dolostone throughout the closed-loop and open-loop experiments, indicating a release of magnesium to solution occurred throughout the experiments.

Higher release of calcium into solution is evident in the limestone (average results between approximately 0.0015 mol/L – 0.003 mol/L) compared to the dolostone (average results between approximately 0.0014 mol/L – 0.0025 mol/L) during the closed-loop experiment. The same is seen throughout the open-loop experiment. This would be expected due to the limestone comprising of calcium carbonate ($CaCO_3$) and dolostone comprising of dolomite and consequently, consisting of magnesium (Warren, 2000).

5.6.1.4 Permeability Results

The permeability results suggest that the limestone samples decreased in permeability throughout the experiment (see previous section 5.4.6 which discusses permeability changes throughout the experiment). For the dolostone, it is more difficult to tell due to there being an overlap between the pre-permeability values and the permeability measurements recorded throughout the experiment. However, the initial dolostone permeability range (1.68 – 14.31mD) is on the upper end of the permeability results for the dolostone measured during the experiment, therefore it may be assumed that the permeability of the dolostone likely decreased during the experiment. Previously discussed theories as to the limestone and dolostone permeabilities decreased are:

(1) The pressure in the system resulted in the crushing of grains and producing of small grains, clogging pore throats and reducing the connectivity of pores, therefore reducing permeability.
(2) Precipitation happening from the percolating fluid into pre-existing pore spaces or voids (Garing et al. 2015). Goldscheider et al. (2010), Morse et al. (2007), Plummer and Wigley (1976), Plummer et al. (1978) and Kirstein et al. (2016) state that calcite solubility decreases with increasing temperature, therefore calcite may have precipitated throughout the experiment.

5.6.1.5 Pressure Results

During the closed-loop experiment and comparing the pressure values for the limestone gauge 1A and dolostone gauge 2A during the closed-loop experiment, the limestone values appear much higher (section 4.5). This may reflect the lower permeability of the limestone compared to the dolostone, making it harder for fluid to percolate. The same is seen in the limestone gauge 1A and dolostone gauge 2A during the open-loop experiment.

5.6.1.6 Comparison Between the Limestone and Dolostone Summary

The limestone and dolostone appear to act very similarly throughout the closed-loop and open-loop experiments. They both show similar release of calcium and magnesium into solution patterns (albeit at different values), particularly during the closed-loop experiment, alongside a general decrease in the permeability results in both experiments. The CT scan results show the samples subject 80°C showed a decrease in the number of grains evident in the fracture in both the limestone and dolostone, during both experiments. A major difference between the limestone and dolostone is that

dissolution evident in the host rock. In the limestone host rock, the samples subject to temperatures of 80°C showed to have the highest porosity (compared to the other samples) in both experiments. In the dolostone host rock, the samples subject to temperatures of 80°C showed to have the lowest porosity (compared to the other samples) in both experiments.

5.6.2 The Effects of the Differing Temperatures Between the Ambient, the 80°C and the 40°C Core Holders

5.6.2.1 Micro-structural Results

The ImageJ analysis portrays the sample porosity relative to one another. Higher porosities can be seen with increasing temperature in the limestone fracture (only in the closed-loop experiment), and in the host rock during both the closed-loop and open-loop experiments (section 4.1). The same can be seen in the dolostone fracture during both the closed-loop and open-loop experiments. However, decreasing porosity with increasing temperature is evident in the limestone fracture during the open-loop experiment and in the dolostone host rock during both experiments. However, these results are only increasing and decreasing relative to one another in the same line. Studying the SEM image visual analysis alongside the ImageJ analysis, the data generally appears to suggest increasing dissolution with increasing temperature when comparing between samples.

5.6.2.2 CT Scan Results

The CT-scan results portray evidence for increasing dissolution with increasing temperature in both the limestone and dolostone during the closed-loop and open-loop experiment (section 4.2). This is due to the ImageJ analysis portraying a decrease in the grains present inside the fracture after the experiment compared to before. This analysis compares CT-scan images from before and after the experiment and therefore, is not relative to other samples in the experiment. This reinforces what is seen in the SEM images. In some limestone and dolostone samples subject to ambient temperatures, there appeared to be an increase in grains present in the fracture after the experiment, suggesting precipitation at lower temperatures.

5.6.2.3 Water Sample Results

In general, the limestone and dolostone samples subject to different temperatures both showed similar trends in the release of magnesium and calcium to solution throughout the closed-loop and open-loop experiment (section 4.3).

5.6.2.4 Permeability Results

Studying the permeability results, despite all of the permeability of all of the samples appearing to decrease, the highest permeability values were evident in the samples subject to the 80°C and 40°C core holders and the lowest permeability values were evident in the samples subject to ambient temperatures (section 4.4). Therefore, suggesting that relative to one another, more dissolution may have occurred in the samples subject to increased temperatures.

5.6.3 The Comparison Between the Closed-loop Experiment and the Open-loop Experiment

5.6.3.1 Micro-structural and CT Scan Results

Comparing the ImageJ analysis of the micro-structural images, from both the closed-loop and open-loop experiments, the relationship between sample porosity and temperature appears to show a similar pattern after both the experiments (section 4.1 and 4.2). Studying at the limestone, samples A (closed-loop) and F (open-loop), both subject to 80°C, show increased porosity in the host rock with increased temperature. Studying the dolostone, samples B2 (closed-loop) and B4 (open-loop), both subject to 80°C, show the same trends of increased dissolution in the fracture and decreased dissolution in the host rock relative to the other samples. Studying the CT scan images, the limestone and dolostone both show relatively similar patterns that occur throughout the closed-loop and open-loop experiments.

Studying the magnesium levels in the fluid percolating through the limestone, there appeared to be an increase in the release of magnesium to solution during the closed-loop experiment due to portraying higher magnesium values in the water sample. Reasons as to why this may have occurred were previously discussed in section 5.3.3. Studying the calcium levels in the fluid percolating through the limestone, the pattern and levels of calcium remain similar in both of the experiments.

5.6.3.2 Water Sample Results

Studying the magnesium levels in the fluid percolating through the dolostone, the concentration levels appear similar, albeit slightly higher during the closed-loop experiment (section 4.3). Similar values for calcium concentration are seen in the dolostone during both the closed-loop and open-loop experiment.

Despite these similarities, the patterns evident between the closed-loop and open-loop experiment appear to act quite differently. During the closed-loop experiment, the results show a steady and constant rise in magnesium and calcium in both limestone and dolostone. During the open-loop experiments the magnesium and calcium results appear more variable. This is further discussed in section 5.3.16.

5.6.3.3 Permeability Results

One of the main differences between the closed-loop and open-loop experiment was that water valves 1E and 2E, located after the 40°C core holder, remained open in the open-loop experiment to enable the fluid to be discarded after one cycle of the experiment (section 4.4). It is thought that the open valve affected the permeability results evident in samples subject to 40°C throughout the open-loop experiments, due to showing variable values compared to other samples in the same line.

5.6.4 Summary of the Experiment Results

Overall, the data shows conflicting information throughout due to, for example, one set of experimental data suggesting a permeability decrease and one set of data suggesting a permeability increase in the same sample. This may be due to the chosen methods of analysis discussed further in-detail below. Despite this, it's evident that the permeability of the limestone and dolostone samples, throughout both the closed-loop and open-loop experiments, is constantly changing.

When analysing the SEM images, it is to be remembered that the ImageJ analysis only portrays the porosity relative to the other samples in the same line and same experiment. It would be useful to know the initial porosity of the fracture before the experiment and due to not knowing this, it is unclear whether the samples that show a higher fracture porosity were actually subject to high

dissolution rates or simply started with a higher porosity than the other samples. Despite this, the ImageJ analysis is useful to compare between the samples. Visual inspection of the SEM images also enables an insight into what happened during the experiment.

The CT scan results differ from the ImageJ analysis due to comparing images from before and after the experiment. Similarly, the water sample and permeability results portray changes occurring throughout the experiments. The pressure results provide an insight into the state and stability of the experiment.

The main takeaway from the CT scan images is that in both the limestone and dolostone samples, during both the closed-loop and open-loop experiments, however, with the exception of limestone sample A in the closed-loop experiment, the samples subject to temperatures of 80°C portray a decrease in the number of grains present in the fracture compared to before the experiment from the density plot. This suggests that more dissolution was occurring in the samples subject to higher temperatures. This analysis disagrees with Goldscheider et al. (2010), Morse et al. (2007), Plummer and Wigley (1976), Plummer et al. (1978) and Kirstein et al. (2016), who state that the solubility of calcite will decrease with increasing temperature. This may be due to the fact that limestone and dolostone contains other minerals, resulting in dissolution rates that react differently to those of pure calcite. A disadvantage of the CT scan images is that the results are entirely dependent on where the cross-section line is drawn. It is difficult to align the cross-section line on every single sample, therefore, debating the accuracy of the analysis.

Generally, the water sample results suggest the release of magnesium and calcium to solution from the limestone and dolostone samples, particularly during the closed-loop experiment. It is difficult to determine the amount of precipitation occurring due to this information not being recorded in the water sample results. For example, it is unclear whether the increase in dissolution is being counter-acted by an even larger increase in precipitation. The only evidence is that from the micro-structural, CT scan and permeability results. As previously mentioned, it'd be useful to weigh the pipework before and after the experiments to determine how much precipitation occurred outside of the samples.

The permeability results generally show an overall decrease in permeability in the limestone and dolostone samples from both the experiments. This may be due to the presence of crushed grains blocking pore throats and making it harder for fluid to percolate (Garing et al. 2015). Also, precipitation may have occurred, decreasing the connectivity of pore spaces and thus, permeability.

The following theory has been put forward in an attempt to conclude the results. Overall, most of the micro-structural results suggest increased dissolution in the limestone and dolostone samples with increased temperature during the experiment, when comparing the samples against each other. Comparing the SEM images from before and after the experiment, there appears to be clear differences and changes in the porosity of the samples. There appears to be an increase in dissolution in the samples subject to higher temperatures of 80°C in the dolostone fracture and in the limestone, both inside the fracture and the host rock during both experiments. An exception is the dolostone host rock portrays a lower porosity at the higher temperature of 80°C, as does the limestone inside the fracture, during both the closed-loop and open-loop experiment. The CT scan results also portray that with increased temperature there appears to be more dissolution of the fracture grains. Evident magnesium and calcium appearing to be released into solution throughout the experiments reinforces the increase in dissolution and consequently, porosity.

Research undertaken by Wood (1986) argues that retrograde solubility in calcite only occurs after 125°C is reached, between the temperature of 0 – 125°C the solubility of calcite appears to increase with increasing temperatures. Therefore, due to this experiment focusing on the 0 – 80°C temperature range, it would be expected to see increasing solubility of calcite, therefore, increased calcite dissolution with increasing temperature in a closed system. This aligns with the majority of the ImageJ analysis, CT scan images and water sample results, which shows evidence of increased dissolution with increased temperature (minus the ImageJ analysis from dolostone host rock, which shows lower porosity with higher temperature, in the closed-loop experiment). However, Wood (1986) suggests that in an open system the solubility of calcite is entirely retrograde between the temperatures of 0-200°C. However, the experiment concentrated on temperature and CO_2 variables and imposed high CO_2 values on the system. Therefore, it is unclear how applicable these results are to the open system experiment undertaken in this paper, due to not imposing high levels of CO_2 on the system. The micro-structural results appear torn as to whether to agree with this statement. The limestone fracture and dolostone host rock portraying lower porosity with increasing temperature, reinforcing Wood (1986), however, porosity in the dolostone fracture and limestone host rock portray increasing dissolution

with increasing temperature in the open-loop experiment. The CT scan image analysis appears to disagree that calcite solubility decreases with increasing temperature in an open system due to showing evidence for increasing dissolution with increasing temperature. Zhang et al. (2007)'s study suggests similar to Wood (1986) but with reference to dolomite and mentions no difference between closed-loop or open-loop experiments. The research argues that dolomite solubility appears to increase with increasing temperature at lower temperatures between 0-200°C for small grain size particle and between 0-100°C for larger particles. Following these temperatures, the dissolution of dolomite appears to decrease with increasing temperatures. The study suggests that the grain size determines the temperature at which the dissolution of dolomite switches from increasing with increasing temperatures to decreasing with increasing temperatures. Therefore, most of the micro-structural analysis, the CT scan analysis and water sample analysis is reinforced by the research that increased dissolution can be seen in limestone and dolostone with increasing temperature.

However, the permeability results generally suggest that the limestone and dolostone samples decreased in permeability throughout the experiment. Due to the micro-structural, CT scan and water sample results generally showing an increase and dissolution, it would be expected to see an increase in permeability and not the evident decrease in permeability portrayed. Reasons for the lower permeability of the samples after the experiment may be due to the blocking of pore throats from grain crushing (Garing et al. 2015). The SEM images in many samples portray evidence of crushed grains which may contribute to low permeability. This would still enable for a high porosity but low permeability. Another suggestion would be that precipitation led to the decrease in permeability. Even though, the rest of the results point to increased dissolution, increased dissolution may still have occurred alongside precipitation which would decrease the permeability. It is difficult to determine precisely how much precipitation occurred during the experiment without pre-experiment SEM images of the exact sample.

Despite the permeability values appearing to all decrease throughout the experiment, comparing between the samples subject to ambient temperatures, 80°C and 40°C the samples subject to higher temperatures generally showed higher permeabilities and the samples subject to ambient temperatures generally showed the lowest permeability. Therefore, it may be plausible to suggest that all the samples decreased in permeability throughout the experiment, however there is evidence to suggest from the collective analysis that increased dissolution occurred at higher temperatures relative to the other samples in the same line in the same experiment.

6. Conclusion

Overall, a long-term geothermal simulation experiment has been presented, with the aim to explore how fluid flow changes the porosity and permeability in limestone and dolostone core samples. Significant attention has been drawn towards any porosity and permeability changes resulting from precipitation-dissolution reactions. The carbonate samples have been subject to variable conditions, of which are characteristic of a natural geothermal setting, to determine how these affect porosity and permeability changes. These variables included comparing limestone and dolostone host rocks, analysing the effects of temperature changes up to 80°C and comparing the effects between a closed-loop and open-loop system.

Analysing the results, the changes in permeability indicate an overall decrease in permeability throughout the experiments in both the limestone and dolomite samples. Studying the micro-structural, CT scan and water sample analysis, however, the data indicates an increase in dissolution and consequently, porosity, has occurred throughout the experiment, particularly increasing with increasing temperature. Micro-structural evidence suggests the presence of small grains, thought to have formed from the crushing of larger grains due to fluid pressure or imposed stress in the system and cumulating in 'pore throats' between grains, led to an overall decrease in permeability but an increase in porosity. These smaller grains are evident in the SEM images and were thought to have been suspended by the percolating fluid before they were deposited in pore throats. Therefore, the overall results show a decrease in permeability but an increase in porosity occurring throughout the duration of the experiment. Huenges (2016) highlighted the importance of adequate porosity and permeability in a geothermal system to allow fluid to percolate through the host rock. For a geothermal energy plant, if a slow, steady decrease in permeability was to occur over-time, as suggested by the experiment results, this could reduce the long-term efficiency of a system due to the restriction of fluid flow.

6.1 Suggestions for Future Work

The work carried out throughout this dissertation has enabled for many faults to be highlighted in the experimental design and analysis, with the aim to improve future research (highlighted in the previous section 3.10). Due to the vast amount of data throughout the dissertation, much of the discussion is over-simplified and therefore, it would be interesting to focus more on specific area. For example, it would be interesting to use the pore boundaries in the SEM images to determine the dissolution

history. Focusing on the facets and the grain micro-structures will likely identify a detailed story of the dissolution-precipitation history.

7. References

Amini, H.R., Reinhart, D.R. (2011), Regional prediction of long-term landfill gas to energy potential. Waste Management, 31(9-10), 2020-2026.

André, L., Rabemanana, V. and Vuataz, F.D., 2006. Influence of water–rock interactions on fracture permeability of the deep reservoir at Soultz-sous-Forêts, France. *Geothermics*, *35*(5-6), pp.507-531.

Antonellini, M., Petracchini, L., Billi, A. and Scrocca, D., 2014. First reported occurrence of deformation bands in a platform limestone, the Jurassic Calcare Massiccio Fm., northern Apennines, Italy. *Tectonophysics*, 628, pp.85-104.

Bai, Y. Bai, Q. (2019) 17 – Subsea Corrosion and Scale. *Subsea Engineering Handbook (Second Edition),* pp. 455 – 487.

Ballas, G., Fossen, H. and Soliva, R., 2015. Factors controlling permeability of cataclastic deformation bands and faults in porous sandstone reservoirs. *Journal of Structural Geology*, 76, pp.1-21.

Ballas, G., Soliva, R., Sizun, J., Benedicto, A., Cavailhes, T. and Raynaud, S., 2012. The importance of the degree of cataclasis in shear bands for fluid flow in porous sandstone, Provence, France. *AAPG Bulletin*, 96(11), pp.2167-2186.

Bansal, A., Illukpitiya, P., Singh, S.P., Tegegne, F. (2013), Economic competitiveness of ethanol production from cellulosic feedstock in Tennessee. Renewable Energy, 59, 53-57

Boden, D. (2017). Geologic Fundamentals of Geothermal Energy. In *Geologic Fundamentals of Geothermal Energy*. CRC Press. https://doi.org/10.1201/9781315371436

British Geological Survey (2021) BGS Lexicon of Named Rock Units - Result Details. *Webapps.bgs.ac.uk*. [Online]. [Accessed 9 September 2021]. Available from: https://webapps.bgs.ac.uk/lexicon/lexicon.cfm?pub=MO.

Caine, J., Evans, J. and Forster, C., 1996. Fault zone architecture and permeability structure. *Geology*, 24(11), p.1025.

Christopher, H., and Armstead, H., 1978, *Geothermal Energy,* E and EN Spon, London

Cooke, A.P., Fisher, Q.J., Michie, E.A. and Yielding, G., 2018. Investigating the controls on fault rock distribution in normal faulted shallow burial limestones, Malta, and the implications for fluid flow. *Journal of Structural Geology*, *114*, pp.22-42.

Cooke, A.P., Fisher, Q.J., Michie, E.A. and Yielding, G., 2020. Permeability of carbonate fault rocks: a case study from Malta. *Petroleum Geoscience*, *26*(3), pp.418-433.

Ferreira, T. Rasband, W. (2012) ImageJ User Guide. Accessed: 19/01/2022. Available from: https://imagej.nih.gov/ij/docs/guide/user-guide.pdf

Fisher, Q.J., Casey, M., Harris, S.D. and Knipe, R.J., 2003. Fluid-flow properties of faults in sandstone: The importance of temperature history. *Geology*, *31*(11), pp.965-968.

Fisher, Q.J. and Knipe, R.J., 2001. The permeability of faults within siliciclastic petroleum reservoirs of the North Sea and Norwegian Continental Shelf. *Marine and Petroleum Geology*, *18*(10), pp.1063-1081.

Fossen, H., Schultz, R., Shipton, Z. and Mair, K., 2007. Deformation bands in sandstone: a review. *Journal of the Geological Society*, 164(4), pp.755-769.

Fridleifsson, I.B., Bertani, R., Huenges, E., Lund, J.W., Ragnarsson, A. and Rybach, L., 2008, January. The possible role and contribution of geothermal energy to the mitigation of climate change. In *IPCC scoping meeting on renewable energy sources, proceedings, Luebeck, Germany* (Vol. 20, No. 25, pp. 59-80). Citeseer.

Garing, C., Gouze, P., Kassab, M., Riva, M. and Guadagnini, A., 2015. Anti-correlated porosity–permeability changes during the dissolution of carbonate rocks: experimental evidences and modeling. *Transport in Porous Media*, *107*(2), pp.595-621.

Glassley, W.E., 2014. *Geothermal energy: renewable energy and the environment*. CRC press.

Goldscheider, N., Mádl-Szőnyi, J., Erőss, A. and Schill, E., 2010. Thermal water resources in carbonate rock aquifers. *Hydrogeology Journal*, *18*(6), pp.1303-1318.

Huenges, E. (2016) 25 - *Enhanced geothermal systems: Review and status of research and development*, Geothermal Power Generation, Editor: Ronald DiPippo, Woodhead Publishing, pg 743-761.

Johnston, I.W., Narsilio, G.A. and Colls, S., 2011. Emerging geothermal energy technologies. *KSCE Journal of Civil Engineering*, *15*(4), pp.643-653.

Johri, M., Zoback, M. and Hennings, P., 2014. A scaling law to characterize fault-damage zones at reservoir depths. *AAPG Bulletin*, 98(10), pp.2057-2079.

Kaminskaite, I., Fisher, Q. and Michie, E., 2019. Microstructure and petrophysical properties of deformation bands in high porosity carbonates. *Journal of Structural Geology*, 119, pp.61-80.

Kirstein, J., Hellevang, H., Haile, B.G., Gleixner, G. and Gaupp, R., 2016. Experimental determination of natural carbonate rock dissolution rates with a focus on temperature dependency. *Geomorphology*, *261*, pp.30-40.

Ledésert, B., Hebert, R., Genter, A., Bartier, D., Clauer, N. and Grall, C., 2010. Fractures, hydrothermal alterations and permeability in the Soultz Enhanced Geothermal System. *Comptes Rendus Geoscience*, *342*(7-8), pp.607-615.

Ling, H.E., Lun, Z., Jianxin, L.I., Ji, M.A., Ruilin, L.U.I., Shuqin, W.A.N.G. and Wenqi, Z.H.A.O., 2014. Complex relationship between porosity and permeability of carbonate reservoirs and its controlling factors: A case study of platform facies in Pre-Caspian Basin. *Petroleum Exploration and Development*, *41*(2), pp.225-234.

Lubiniecki, D., White, S., King, R., Holford, S., Bunch, M. and Hill, S., 2019. Structural evolution of carbonate-hosted cataclastic bands adjacent to a major neotectonic fault, Sellicks Beach, South Australia. *Journal of Structural Geology*, 126, pp.11-24.

Mburu, M., 2009. Geothermal energy utilisation. *Exploration for Geothermal Resources*, pp.1-11.

McPhee, C., Reed, J. and Zubizarreta, I., 2015. *Core analysis: a best practice guide*. Elsevier.

Micarelli, L., Benedicto, A. and Wibberley, C., 2006. Structural evolution and permeability of normal fault zones in highly porous carbonate rocks. *Journal of Structural Geology*, 28(7), pp.1214-1227.

Michie, E., Kaminskaite, I., Cooke, A., Fisher, Q., Yielding, G. and Tobiss, S., 2021. Along-strike permeability variation in carbonate-hosted fault zones. *Journal of Structural Geology*, 142, p.104236.

Michie, E.A.H., Yielding, G. and Fisher, Q.J., 2018. Predicting transmissibilities of carbonate-hosted fault zones. *Geological Society, London, Special Publications*, *459*(1), pp.121-137.

Mikhaylov, A., 2020. Geothermal energy development in Iceland. *International Journal of Energy Economics and Policy*, *10*(4), p.31.

Min, S.H.E., Jianfeng, S.H.O.U., Anjiang, S.H.E.N., Liyin, P., Anping, H. and Yuanyuan, H., 2016. Experimental simulation of dissolution law and porosity evolution of carbonate rock. *Petroleum Exploration and Development*, *43*(4), pp.616-625.

Mohais, R., Xu, C. and Dowd, P., 2011. Fluid flow and heat transfer within a single horizontal fracture in an enhanced geothermal system. *Journal of heat transfer*, *133*(11)

Morse, J.W., 2018. The kinetics of calcium carbonate dissolution and precipitation. In *Carbonates* (pp. 227-264). De Gruyter.

Morse, J.W., Arvidson, R.S. and Lüttge, A., 2007. Calcium carbonate formation and dissolution. *Chemical reviews*, *107*(2), pp.342-381.

National Geographic, 2021. Geothermal Energy. *National Geographic Society*. [Online]. [Accessed 15 February 2021]. Available from: https://www.nationalgeographic.org/encyclopedia/geothermal-energy/

Phillips, O.M., 1991. *Flow and reactions in permeable rocks*. Cambridge University Press

Plummer, L.N. and Wigley, T.M.L., 1976. The dissolution of calcite in CO2-saturated solutions at 25 C and 1 atmosphere total pressure. *Geochimica et Cosmochimica Acta*, *40*(2), pp.191-202.

Plummer, L.N., Wigley, T.M.L. and Parkhurst, D.L., 1978. The kinetics of calcite dissolution in CO 2-water systems at 5 degrees to 60 degrees C and 0.0 to 1.0 atm CO 2. *American journal of science*, *278*(2), pp.179-216.

Rohde, R., Muller, R.A., Jacobsen, R., Muller, E., Perlmutter, S., Rosenfeld, A., Wurtele, J., Groom, D. and Wickham, C., 2013. A New Estimate of the Average Earth Surface Land Temperature Spanning 1753 to 2011, Geoinfor Geostat: An Overview 1: 1. *of*, *7*, p.2.

Romanov, D., Gabrovsek, F. and Dreybrodt, W., 2003. The impact of hydrochemical boundary conditions on the evolution of limestone karst aquifers. *Journal of Hydrology*, *276*(1-4), pp.240-253.

Rybach, L., 2003. Geothermal energy: sustainability and the environment. *Geothermics*, *32*(4-6), pp.463-470.

Rybach, L., 2007, September. Geothermal sustainability. In *Proceedings European Geothermal Congress* (Vol. 5).

Schneider, C. A., Rasband, W. S., & Eliceiri, K. W. (2012). NIH Image to ImageJ: 25 years of image analysis. *Nature Methods*, *9*(7), 671–675. doi:10.1038/nmeth.2089

Shih, S.M., Lin, J.P. and Shiau, G.Y., 2000. Dissolution rates of limestones of different sources. *Journal of Hazardous materials*, *79*(1-2), pp.159-171.

Singurindy, O., Berkowitz, B. and Lowell, R.P., 2004. Carbonate dissolution and precipitation in coastal environments: Laboratory analysis and theoretical consideration. *Water Resources Research*, *40*(4).

Snyder, R.C. and Doherty, M.F., 2007. Faceted crystal shape evolution during dissolution or growth. *AIChE journal*, *53*(5), pp.1337-1348.

Solomon, S., Qin, D., Manning, M., Chen, Z., Marquis, M., Averyt, K.B., Tignor, M., and Miller, H.L. (eds), 2007. *Climate Change 2007: The Physical Science Basis*. Contribution of Working Group I to the Fourth Assessment Report of the Intergovernmental Panel on Climate Change. Cambridge University Press, Cambridge; New York, NY, 996 pp.

Stefansson, V., 2000. The Renewability of Geothermal Energy. Proceedings World Geothermal Congress, Japan, 2, pp. 883–888.

Tondi, E., Antonellini, M., Aydin, A., Marchegiani, L. and Cello, G., 2006. The role of deformation bands, stylolites and sheared stylolites in fault development in carbonate grainstones of Majella Mountain, Italy. *Journal of Structural Geology*, 28(3), pp.376-391.

United Nations Environment Programme UNEP (2018) *Emissions Gap Report 2018.*

United Nations, 2012. World population prospects: The 2012 revision. United Nations Department of Economic and Social Affairs, Population Division. http://esa.un.org/wpp/.

Van Oversteeg, K., Lipsey, L., Pluymaekers, M., Van Wees, J.D., Fokker, P.A. and Spiers, C., 2014, February. Fracture permeability assessment in deeply buried carbonates and implications for enhanced geothermal systems: inferences from a detailed well study at luttelgeest-01, the Netherlands. In *Proceedings Thirty-Eighth Workshop on Geothermal Reservoir Engineering, Stanford University, Stanford, California*.

Zambrano, M., Pitts, A.D., Salama, A., Volatili, T., Salama, A., Giorgioni, M. and Tondi, E., 2019. Analysis of fracture roughness control on permeability using SfM and fluid flow simulations: implications for carbonate reservoir characterization. *Geofluids*, *2019*.

Zambrano, M., Tondi, E., Mancini, L., Lanzafame, G., Trias, F.X., Arzilli, F., Materazzi, M. and Torrieri, S., 2018. Fluid flow simulation and permeability computation in deformed porous carbonate grainstones. *Advances in water resources*, *115*, pp.95-111.

Zhang, R., Hu, S., Zhang, X. and Yu, W., 2007. Dissolution kinetics of dolomite in water at elevated temperatures. *Aquatic Geochemistry*, *13*(4), pp.309-338.

Ziagos, J.P. and Blackwell, D.D., 1986. A model for the transient temperature effects of horizontal fluid flow in geothermal systems. *Journal of Volcanology and Geothermal Research*, *27*(3-4), pp.371-397.